Assessment of Geomorphic Processes for the Upper Santa Clara River Watershed

Los Angeles County, California

FINAL REPORT
May 2011

Prepared for
Ventura County Watershed Protection District
Planning and Regulatory Division
800 S. Victoria Avenue
Ventura, CA 93009

Los Angeles County Department of Public Works
900 S. Fremont Avenue
Alhambra, CA 91803

U.S. Army Corps of Engineers
Los Angeles District
915 Wilshire Boulevard, Suite 1101
Los Angeles, CA 90017

Prepared by
Stillwater Sciences
2855 Telegraph Avenue, Suite 400
Berkeley, CA 94705

Stillwater Sciences

Contact:

Derek Booth, Ph.D., P.E., P.G.
Senior Geomorphologist
Stillwater Sciences
2855 Telegraph Avenue, Suite 400
Berkeley, CA 94705
(510) 848-8098
dbooth@stillwatersci.com
www.stillwatersci.com

Sergio Vargas, P.E.
Deputy Director
Ventura County Watershed Protection District
800 S. Victoria Avenue
Ventura, CA 93009
(805) 650-4077
sergio.vargas@ventura.org
www.vcwatershed.org

Cover photography (from top to bottom):

1. Eastward (upstream-facing) view of the Upper Santa Clara River channel in the Acton basin, with the San Gabriel Mountains viewed in the distance, November 2009.
2. Southwestward (downstream-facing) view into Haskell Canyon where vegetation has started to recover following the 2007 Buckweed Fire, December 2009. The Santa Clarita basin is viewed in the distance.
3. Channelized reach of lower South Fork SCR, view north (upstream), March 2010.
4. Santa Clara River downstream of the Interstate 5 crossing and upstream of the Castaic Creek confluence, view south toward meander bend in channel, March 2010.

Acknowledgements:

We appreciate the support and direction we have received from the Feasibility Study participating agencies (listed alphabetically): Los Angeles County Department of Public Works, U.S. Army Corps of Engineers–Los Angeles District, and Ventura County Watershed Protection District. The key individuals from these agencies who have worked closely with us during the course of this study include: Martin Araiza (LADPW), Long Thang (LADPW), Darrell Buxton (USACE-LA), Jody Fischer (USACE-LA), Jim Hutchison (USACE-LA), Zia Hosseinipour (VCWPD), Iraj Nasseri (LADPW), Yunsheng Su (VCWPD), and Sergio Vargas (VCWPD). RBF Consulting played a key role in facilitating the contracting of this project.

We would like to thank the contributions made by individuals from other organizations who provided background information and data: Aaron Allen (USACE), Angelique Carreon-Quion (LA Dept. of Regional Planning), Toby Minear (U.C. Berkeley), Minas Sirakie (LA Dept. of Water and Power), and Gloria Wu (LA Dept. of Water and Power). Much appreciation is given to Dr. Cliff Riebe of the University of Wyoming who performed the sediment dating analysis and to Dr. Jonathan Warrick of the U.S. Geological Survey who conducted an external scientific review of the draft version of this report.

Project team:

The project team was led by Drs. Peter Downs and Derek Booth as principal investigators. Technical analysis and written synthesis were provided by geomorphologists Glen Leverich (Project Manager), Scott Dusterhoff, and John Wooster. Sediment transport capacity modeling was performed by Dr. Yantao Cui. Additional analyses and written materials were prepared by Zooey Diggory and Krista Orr. GIS analyses were performed by Sebastian Araya, Rafeal Real de Asua, and Eric Panzer. Field surveys were assisted by Mike Reyman.

Suggested citation:

Stillwater Sciences. 2011. Assessment of geomorphic processes for the upper Santa Clara River watershed, Los Angeles County, California. Final Report. Prepared by Stillwater Sciences, Berkeley, California for Ventura County Watershed Protection District, Los Angeles County Department of Public Works, and the U.S. Army Corps of Engineers-L.A. District.

Assessment of Geomorphic Processes for the Upper Santa Clara River Watershed, Los Angeles County, California

Executive Summary

This report presents a geomorphic assessment of key natural and anthropogenically driven processes that have physically shaped and continue to influence the USCR watershed. The overlying forces controlling geomorphic processes and resulting conditions in the watershed are examined over past, present, and future time frames, and at watershed-wide through sub-reach spatial scales. Detailed assessments of sediment sources and tributary sediment yields based on review of scientific literature and analyses of field data collected for this study are presented, with an emphasis on the primary controls that have shaped the watershed and drainage network over time. We note how these controls (e.g., wildfire, land-cover/-use) themselves vary through time (Chapter 3 and Section 4.2.4.2). An evaluation of mainstem river processes is presented that considered sediment sources, transport capacity, and morphological changes (since the late 1920s) that will assist watershed managers with critical information when planning future management, development, and restoration actions (Chapter 4).

Key Findings of the Watershed Geomorphic Assessment

The USCR watershed lies in the tectonically active, semi-arid Transverse Mountain ranges of southern California. As part of this setting, the 1,680 km^2 USCR watershed is host to a diverse patchwork of landscape types, each composed of a unique suite of geomorphic processes controlled by regional and local forces—tectonics, climate, geology, topography, wildfires, and land use. Where rapid uplift rates, weak lithologies, extreme yet episodic rainfall, steep slopes, and intensive land practices coincide, sediment-production rates can be dramatically high. The variability in sediment-production rates across the watershed has a pronounced effect on the river morphology, which, at the reach scale, is further influenced by the degree of sediment connectivity with specific sediment sources and by the transport capacity along the channel. In general, the highest elevation areas of the watershed are host to the densest vegetation cover (mix of scrub/shrub and forest), receive the most rainfall (greatest average annual precipitation), and are composed of the oldest, most erosion-resistant bedrock lithologies (igneous, meta-igneous rocks [gneiss, granites]). In contrast, the lowland and foothill areas, typically those within and surrounding the Santa Clarita basin, are much drier, host a sparse vegetation cover (mix of grassland and scrub/shrub), and are composed of the youngest, weakest rock types. Wildfire frequency is greater in the hillslopes immediately surrounding the Santa Clarita basin, which can further increase hillslope erosion rates especially when followed closely by large storm events.

Overall, the watershed sediment-production rate is approximately 2.9 million metric tonnes per year ($t\ yr^{-1}$), or 1,700 tonnes per square kilometer per year ($t\ km^{-2}\ yr^{-1}$) averaged across the entire USCR watershed area. Because Castaic and Bouquet Canyon dams intercept water and sediment from approximately one-third of the watershed area, the predicted watershed sediment-production rate is only 2.3 million $t\ yr^{-1}$, but accounting for dams increases the calculated production rate per unit area to 1,900 $t\ km^{-2}\ yr^{-1}$. This value compares well to production rates estimated independently from rock uplift rates, landscape denudation rates, and our sediment dating analysis. The average annual watershed sediment yield estimated using flow and sediment discharge records at the County line gauges (USGS 11108500 and 11109000) is less than half of the calculated production rate, which is understandable given the substantial volumes of stored sediment in the lower reaches of the major tributaries and in the mainstem itself, particularly in the Acton and Santa Clarita basins. Sediment storage in the mainstem USCR and downstream reaches of the major coarse sediment-delivering tributaries is also expressed by the results of the bed level change analysis, which demonstrates long-term aggradation throughout much of the Santa Clarita basin. Our sediment transport capacity analysis similarly predicted reach-scale aggradation along the river in the Upper and Lower regions (Acton and Santa Clarita basins).

Sediment delivery from hillslopes and tributaries to the mainstem USCR are dominated by extreme events associated with large, infrequent storms. The episodic and extreme nature of discharge in the USCR watershed results in the majority of sediment transport occurring in very short periods of time. For example, annual sediment discharge over the past 57 years is estimated to have varied by a factor of more than 50,000—from a low of approximately 410 tonnes (WY 1961) to more than 22 million tonnes (WY 1969, which contains the flood of record). The two water years that contain the highest annual maximum instantaneous discharge account for over half of the total sediment yield out of the USCR. In contrast, over one-half of all years have an annual total sediment yield less than 10% of the average annual total sediment yield. Unlike humid-region rivers, moderate discharges of intermediate recurrence thus do not carry the majority of the sediment load—the “dominant discharge” for the USCR is the largest discharge on record.

Due to the episodic nature of the system, the active channel of the USCR has adjusted primarily in response to the largest flood events (as observed over the past century). Channel boundaries have only significantly expanded during the three largest flows on record (e.g., 1928 St. Francis Dam failure and the 1969 and 2005 floods). Of these events, the dam-break flood caused a massive scouring of the river and valley floor and, therefore, this event represents the most recent and significant channel-forming flow in those impacted reaches.

Throughout much of the USCR, active channel widths have been further reduced by floodplain encroachment and even river channel encroachment over the past several decades. These developments have stabilized channel boundaries along most of the lower channel reaches, which are most prevalent through the more urbanized areas of Santa Clarita. The flow constrictions associated with the width reductions have the potential to create an unstable condition in the river’s morphology, which could result in accelerated channel bed level changes and/or bank failure and create additional hazards to the population and infrastructure. Partly in response to this dynamic, some lower tributary reaches have now been completely lined with concrete, essentially locking those channels in place but impacting a range of natural geomorphic and ecological processes.

The long-term trends in the level of the channel bed indicate a general aggradational pattern in the Santa Clarita basin, punctuated by notable occurrences of localized incision at the major tributary confluences (Castaic Creek, San Francisquito Canyon, South Fork SCR, and Bouquet Canyon). The overall aggradational and narrowing trends observed in the river’s morphology suggest four possible influences: (1) recovery following the scouring flows released during the St. Francis Dam failure event (i.e., recovery to a quasi-equilibrium condition); (2) flow reductions from dam-regulated subwatersheds; (3) increased sediment yields from past land-use activities, such as early settlement and ranching/agriculture activities, but not related to the urban developments that pave over land surfaces and intercept water and sediment delivered from upstream sources; and (4) floodplain and active channel encroachments by the growing urban footprint. Due to their spatial and temporal overlap, attributing specific changes in the river’s morphology to one of these major influences with any confidence is not possible.

In the Middle and Upper regions, significant occurrences of river incision have been identified at the Lang Station Road crossing near the mouth of Soledad Canyon and at the Arastre Road crossing near Acton. Considerable channel incision has occurred on the downstream sides of these two crossings, and coarse sediment (sand and gravels) aggradation has periodically occurred on their upstream sides. The highest degree of channel incision is located below the Lang Station Road crossing, which also lies immediately downstream of the only active instream aggregate mining operation along the USCR. Instream aggregate extraction here is estimated at about 200,000–500,000 t yr^{-1} over the last several decades, representing about one-quarter to one-half of the total sediment load passing the County line gauge.

The growing urban footprint in Santa Clarita and Acton basins is projected to further reduce sediment-production rates (and associated tributary sediment yields to the river channel) in the watershed by a similar magnitude to that of instream aggregate mining. However, this result does not indicate that continued development in the watershed will lessen the likelihood of geomorphic hazards from occurring (e.g., debris flows, landslides, flash floods). These events have widely distributed sources, commonly with a watershed or subwatershed extent, that are unlikely to be significantly affected by human development in the USCR watershed for the foreseeable future. However, further expansion of the urban footprint (particularly in steep upland areas) will place a greater proportion of the population and infrastructure closer to the sources and consequences of these hazards. Further, continued expansion and construction of hazard-mitigating infrastructure have the potential to result in understandable but largely unpredictable responses by the river and tributary morphology during large flood events.

Table of Contents

List of Tables

List of Figures

List of Appendices

LIST OF ACRONYMS AND ABBREVIATIONS

Acronym or abbreviation	Definition
ac	acres
AMS	accelerator mass spectrometer
CDF FRAP	California Department of Forestry and Fire Protection – Fire and Resource Assessment Program
CDFG	California Department of Fish and Game
CDP	Census Designated Place
CDWR	California Department of Water Resources
cfs	cubic feet per second
CGS	California Geological Survey
cm	centimeter
CNRA	California Natural Resources Agency
D_{50}	grain diameter at which 50% of the particle size distribution lies above and below
DDE	Debris Design Event
DEM	digital elevation model
DP	Debris Production
DPA	Debris Potential Area
DRI	debris retention inlet
ENSO	El Niño–Southern Oscillation
est.	established
FEMA	Federal Emergency Management Agency
ft	feet
g	grams
GIS	geographic information system
GLU	Geomorphic Landscape Unit
HEC-RAS	Hydrologic Engineering Center's River Analysis System
HSPF	Hydrologic Simulation Program-Fortran
I-5	Interstate 5
IfSAR	Interferometric Synthetic Aperture Radar
in	inch
kg	kilogram
km	kilometer
LADPW	Los Angeles County Department of Public Works
LADWP	Los Angeles Department of Water and Power
LiDAR	Light Detection and Ranging
LSCR	Lower Santa Clara River
m	meter
M	(earthquake) Magnitude
mi	mile

Acronym or abbreviation	Definition
mm	millimeter
O	oxygen
NAIP	National Agriculture Imagery Program
PRIME	Purdue Rare Isotope Measurement Laboratory
Q_2	2-year flow
Q_{100}	100-year flow
$Q_{sed\ cap}$	average annual bedload transport capacity
RI	Recurrence Interval
s	second
SAF	San Andreas Fault
SCR	Santa Clara River
Si	silica
SNPCR	Saugus-Newhall Production-Consumption Region
t	tonnes (metric)
UCSB	University of California at Santa Barbara
USACE (Corps)	United States Army Corps of Engineers
USCR	Upper Santa Clara River
USFS	United States Forest Service
USGS	United States Geological Survey
VCWPD	Ventura County Watershed Protection District
WY	water year
yd	yard
yr	year

Notes:
[1] Geologic rock unit symbology is defined in Appendix A.
[2] Symbology used in mathematical equations is defined in the text adjacent to the associated equation(s).
[3] Bed sediment facies notation defined in Table 4-4, footnote c.

GLOSSARY OF KEY TERMS

Keyword	Definition
abrasion	The process of mechanical wearing, grinding, scraping, or rubbing away of rock (or sediment) surfaces by friction or impact, typically in a stream channel as sediment transport is occurring.
aggradation	The process involving the deposition of sediment on the landscape, but most commonly in a stream channel.
alluvial	Having originated through the transport by and deposition from running water.
bedload	Sediment transporting along the streambed by rolling, sliding, and saltating (jumping). Includes coarser grains larger than 0.0625 mm in diameter, such as sand, gravel, cobbles, and boulders; however, sand can often be transported as suspended bed material load in higher energy flows, thus making them part of the bed material load.
bed material load	Composed of sediments transporting as bedload and suspended load.
boulders	Substrate particles greater than 256 mm in diameter. Often subclassified as small (256-1,024 mm) and large (>1,024 mm) boulders.
bulk density	The mass of a material (rock or sediments) divided by the total volume they occupy [M/L^3].
channel	Natural or artificial waterway of perceptible extent that periodically or continuously contains moving water.
channel migration	Lateral movement of the active channel, usually in response to large flow events.
bankfull discharge	Discharge that just overtops a river or stream channel banks onto the adjacent floodplain. Bankfull discharge occurs approximately every 1 to 2 years, with a median recurrence interval of 1.5 years (~Q_2) and is generally considered to be the primary channel-forming discharge in humid environments, but not in the semi-arid USCR watershed.
cobble	Substrate particles 64-256 mm in diameter. Often subclassified as small (64-128 mm) and large (128-256 mm) cobble.
cosmogenic nuclides	Produced in the minerals (i.e., quartz) of soil and rock materials at the landscape's surface and can be measured to estimate landscape erosion rates.
denudation	The sum of the processes that result in the wearing away or the progressive lowering of the Earth's surface by various natural agencies, including weathering, erosion, mass wasting, and transportation.
deposition	The process whereby Earth materials accumulate, which is commonly achieved by the mechanical settling of sediment from suspension in water or the accumulation of coarse materials as delivered by ice, water, or wind.
discharge (stream)	The volume of flow passing a stream cross section in a unit of time [L^3/T].
erosion	The process whereby Earth materials are loosened, dissolved, or worn away, and simultaneously transported away from the material source by natural agencies, such as abrasion, solution, transportation, and weathering, but is most commonly achieved mechanically by ice, water, or wind, or even biogenic agents (e.g., tree throw, gopher burrowing).
geographic information system (GIS)	A computer system capable of storing and manipulating spatial data. A geographic information system has four major components: a data input subsystem, a data storage and retrieval subsystem, a data manipulation and analysis subsystem, and a data reporting subsystem.
gravel	Substrate particles between 2 and 64 mm in diameter.
incision	The process whereby a channel (stream or trench) vertically erodes downward resulting in a lower bed elevation.

Keyword	Definition
recurrence interval (R.I.)	The interval, or duration, of time between flow events of a particular magnitude (e.g., the January 25, 1969 flood event with a peak discharge of 4,670 $m^3 s^{-1}$ [165,000 cfs] recorded at the USGS County line stream gauge is calculated to have a recurrence interval, R.I., of 54 years, based on consideration of all annual peak discharges recorded at this gauge between water years 1938 and 2009).
riparian vegetation	Vegetation growing on or near the banks of a stream or other body of water in soils that exhibit some wetness characteristics during some portion of the growing season.
sand	Substrate particles 0.062-2 mm in diameter.
sediment	Fragments of rock, soil, and organic material transported and deposited in beds by wind, water, or other natural phenomena.
sediment delivery	The process whereby sediment is transported from a production source to a given location in the drainage network.
sediment delivery ratio	Ratio of sediment production rate to sediment delivery rate. High delivery ratios indicate that production closely equals delivery, and low delivery ratios indicate that production is much lower than delivery, usually due to storage.
sediment discharge	The quantity of sediment passing a stream cross section in a unit of time (i.e., volume or mass per unit of time).
sediment production rate	The total amount of sediment eroded from the landscape surface over a given time period; usually reported in mass per year [*M/T*].
sediment storage	The process by which sediment is delivered to a location and is then stored there for a period of time (e.g., days to millennium, or even beyond).
sediment transport	The process involving the movement of sediment.
sediment transport capacity	The maximum load a stream channel can transport.
sediment yield	The total amount of sediment transported past a point over a given time period; usually reported in mass per year [*M/T*].
silt	Substrate particles 0.004-0.062 mm in diameter.
suspended load	Sediment that transports continuously in suspension within the water column. Includes particles finer than 0.0625 mm (i.e., wash load), but can include bed material load (e.g., sand) in higher energy flows.
thalweg	A longitudinal line following the deepest points along the steambed.
water surface slope	Approximate indication of water velocity as the ratio of vertical drop per unit distance as measured along the thalweg at various river or stream discharges.
water year (WY)	A 12-month period for any given year from October 1 through September 30.

General information sources used here:
MacArthur and Hall 2008
Neuendorf et al. 2005
Ritter et al. 2002
Selby 1993

UNIT CONVERSION FACTORS

Most values presented in this report are reported in the metric system. This table presents conversion factors of the commonly used metric units to English system units.

Metric	Multiply by	English
mm (millimeters)	3.937×10^{-2}	in (inches)
m (meters)	3.281	ft (feet)
km (kilometers)	6.214×10^{-1}	mi (mile)
km^2 (square kilometers)	3.861×10^{-1}	mi^2 (square miles)
m^3 (cubic meters)	3.531×10^{1}	ft^3 (cubic feet)
t (tonnes)	1.102	tn (tons)
t km^{-2} (tonnes per square kilometer)	2.855	tn mi^{-2} (tons per square mile)

1 INTRODUCTION

Geomorphology is the study of landforms and the processes that modify them over time, encompassing spatial and temporal scales that range from the instantaneous motion of individual sand grains in rivers during floods to the uplift of entire mountain ranges over millions of years. It synthesizes information about the internal geologic processes that create topography and the external surface processes that erode and move material incrementally across the landscape.

The goals and objectives of this project, and the background conditions of the Upper Santa Clara River watershed, are presented in this chapter as an introduction to this watershed assessment of geomorphic processes.

1.1 Project Goals and Objectives

This geomorphic assessment investigates the key natural and anthropogenically driven processes that have physically shaped and continue to influence the eastern half of the Santa Clara River watershed that is almost entirely contained within Los Angeles County, commonly referred to as the Upper Santa Clara River (USCR) watershed (Figure 1-1). The USCR watershed geomorphology assessment is designed to assist the Ventura County Watershed Protection District (VCWPD), Los Angeles County Department of Public Works (LADPW), and the U. S. Army Corps of Engineers–Los Angeles District (USACE-LA) in identifying opportunities and constraints associated with protecting, managing, and restoring lands as part of the Santa Clara River USACE Feasibility Study efforts. The assessment builds upon an extensive set of previous studies of geomorphic processes in the watershed and vicinity, including a geomorphic assessment of the Lower Santa Clara River (LSCR) watershed (Stillwater Sciences 2007a). This assessment augments the existing studies by providing a comprehensive overview of current and historical watershed-wide geomorphic processes, both natural and anthropogenically altered, and their links to in-channel and floodplain factors. The assessment additionally evaluates future geomorphology conditions within the developed and currently undeveloped areas of the watershed.

The goals of a watershed assessment of physical processes is to identify the existing geomorphic assets of the watershed, the potential hazards to floodplain infrastructure resulting from river instability, and the challenges and opportunities for enhancement of geomorphic processes that benefit natural ecologic function through river management. “Geomorphic hazards” can be defined as a potential threat to humans and their welfare; they are frequently associated with the magnitude, frequency, duration, and spatial extent of instability (or adjustment) of the river channel. “Geomorphic assets” are defined as features, sites or catchments of great habitat or other environmental value, based on rarity, uniqueness, critical place or function in the ecosystem, scenic attraction, or heritage value—the basis for river preservation and enhancement. Geomorphic assets are the antithesis of geomorphic hazards but they usually result from the same geomorphic processes as the hazards, thereby introducing a source both of conflict and potential opportunity for river channel management.

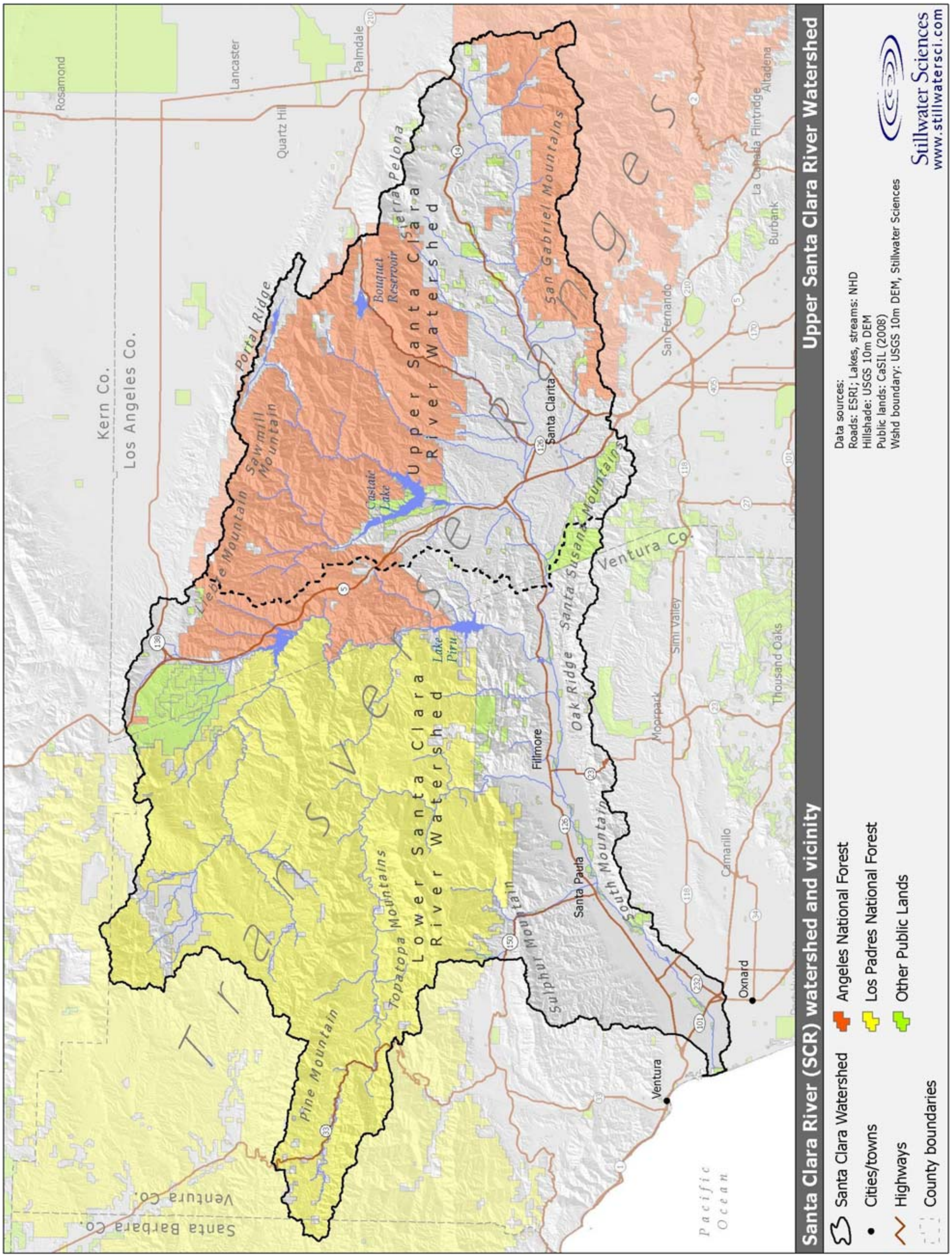

Figure 1-1. The Santa Clara River watershed and vicinity.

Derived from this understanding, the objectives for this geomorphic assessment of the USCR watershed are:

1. Characterization of geomorphic processes and channel response along the USCR, relating observations to the dynamics of channel change in a dryland river setting, including the impact of tectonic activity, storm events, and wildfire;
2. Characterization of sediment delivery and channel adjustment attributable to past and present human activities, including channel modification associated with urban development;
3. Assessment of probable future hazards and assets related to geomorphology in the USCR watershed, to better understand the challenges and opportunities facing sustainable approaches to river management.

The approach employed to achieve the goals and objectives of this assessment has been based on:

1. providing a synthesis of existing and newly collected data to describe channel morphologic change and watershed sediment transport dynamics under current conditions, driven by both natural and anthropogenic controls (e.g., storm events and land-use change, respectively); and
2. forecasting probable future geomorphic conditions within the mainstem and tributary channels throughout the USCR watershed to the extent permitted by available data.

Watershed geomorphic processes in tributaries and along the mainstem of the USCR have been examined from both a current and a historic perspective, to produce a comprehensive understanding of the geomorphic processes controlling channel migration, sediment production, delivery, storage, and transport within the watershed. Ultimately this work will help the Feasibility Study project partners to identify management strategies that meet the goal of maintaining and restoring geomorphic processes so as to protect vulnerable floodplain infrastructure and sustain desired ecologic function throughout the watershed.

In geographic scope, the assessment encompasses:

1. the river and floodplain areas of the mainstem Santa Clara River through Los Angeles County, and
2. the developed, downstream reaches of major tributaries designated by the USACE and Federal Emergency Management Agency (FEMA) as part of the Feasibility Study.

The downstream extent of this assessment generally coincides with the USGS's "Los Angeles-Ventura County line gauge" (USGS 11108500 and 11109000). The assessment area focuses particularly on streams and reaches downstream of dams where they occur, because the dams act to sever the longitudinal connectivity of upstream geomorphic processes. Along with the entire length of the mainstem USCR, all Feasibility Study-identified tributaries have been considered in this geomorphology assessment (Table 1-1, Figure 1-2).

The USCR assessment area therefore spatially complements the completed LSCR geomorphic study (Stillwater Sciences 2007a) resulting in a geomorphic assessment that encompasses the entire Santa Clara River watershed. The two assessments are not completely identical due to differences in data availability and study goals, but the results are comparable in terms of characterizing sediment delivery, magnitude and frequency of sediment transport events, and historical and future channel adjustments. In anticipation of merging the findings of the LSCR and USCR assessments into a single document for the entire watershed, this report follows a structure similar to that used in the LSCR report.

Table 1-1. Feasibility Study and other major streams of the Upper Santa Clara River (USCR) watershed. [a]

Major stream name [a]	Feasibility Study reach system [b]		Total drainage area (total area below dams) [c]		Total stream length (total length below dams, if present) [d]	
	USACE study reach	FEMA study reach	km^2	mi^2	km	mi
Soledad Canyon	X		23.2	9.0	8.8	5.5
Kentucky Springs	X		23.5	9.1	11.6	7.3
Aliso Canyon	X		63.2	24.4	15.5	9.7
Gleason Canyon			15.5	6.0	9.5	5.9
Trade Post Canyon	X		6.7	2.6	5.0	3.6
Acton Canyon	X	X	54.4	21.0	9.3	5.8
Escondido Creek	X	X	24.6	9.5	10.2	6.4
Red Rover Mine	X		5.7	2.2	5.7	3.5
Acton Canyon 2	X		6.5	2.5	5.0	3.1
Hughes Canyon			8.0	3.1	4.2	2.7
Young Canyon			7.3	2.8	5.1	3.2
Agua Dulce Canyon	X	X	76.1	29.4	12.4	7.7
Bear Canyon			15.1	5.8	8.0	5.0
Tick Canyon	X		14.8	5.7	8.8	5.5
Oak Springs Canyon	X		14.6	5.7	8.7	5.4
Sand Canyon	X		33.0	12.7	13.8	8.6
Iron Canyon	X		6.9	2.7	7.9	4.9
Mint Canyon	X		75.8	29.3	22.4	14.0
Bouquet Canyon	X	X	180.4 (145.2)	69.7 (56.0)	34.6 (26.1)	21.6 (16.3)
Dry Canyon	X		19.7	7.6	16.5	10.3
Haskell Canyon	X	X	28.4	11.0	14.4	9.0
Plum Canyon	X		8.2	3.2	6.5	4.1
Vasquez Canyon	X		11.1	4.3	7.9	4.9
Texas Canyon	X		28.2	10.9	12.8	8.0
So. Fork SCR	X	X	116.2	44.9	7.3	4.6
Pico Canyon	X	X	17.6	6.8	8.4	5.3
Lyon Canyon	X		3.6	1.4	5.3	3.3
Gavin Canyon	X		29.4	11.4	5.5	3.5
Towsley Canyon	X		14.9	5.8	5.8	3.6
Placerita Creek	X		23.1	8.9	11.8	7.4
Newhall Creek		X	21.3	8.2	4.8	3.0
San Francisquito Cyn	X	X	134.6	52.0	34.9	21.8
Lion Canyon	X		2.2	0.8	2.5	1.5
Castaic Creek	X		524.6 (122.6)	202.5 (47.3)	39.5 (12.5)	24.7 (7.8)
Hasley Canyon	X		20.7	8.0	9.4	5.9
Violin Canyon 1	X		15.1	5.8	14.2	8.9

Major stream name [a]	**Feasibility Study reach system** [b]		**Total drainage area (total area below dams)** [c]		**Total stream length (total length below dams, if present)** [d]	
	USACE study reach	**FEMA study reach**	**km²**	**mi²**	**km**	**mi**
Violin Canyon 2 (Marple Canyon)	X		9.6	3.7	8.3	5.2
Long Canyon	X		4.0	1.5	5.9	3.7
S. M. Chiquito Cyn	X		12.4	4.8	7.9	5.0
S. M. Grande Canyon	X		8.6	3.3	4.6	2.9
Potrero Canyon	X		11.6	4.5	8.6	5.4
Upper Santa Clara River [e]	X	X	**1,679 (1,242)**	**648 (479)**	**62.4**	**39.1**

[a] Streams listed in order of upstream to downstream position along the USCR starting at the headwaters in the eastern end of the watershed. Stream names that are indented and printed in italics are tributaries to the stream listed above (e.g., Gleason Canyon is a tributary to Aliso Canyon). "S.M." is abbreviated for San Martinez.

[b] Checkmark indicates that the stream is part of the respective USACE and/or FEMA Feasibility Study reach system.

[c] Drainage area derived in a GIS using a USGS 10m Digital Elevation Model (DEM). Area includes the total drainage area of any listed stream watershed.

[d] Stream length derived in a GIS using a USGS 10m DEM-generated stream network with a contributing area threshold of 0.04 km^2.

[e] As measured along the river course between the retired USGS stream gauge station (11108500) at the Los Angeles-Ventura County line and the confluence with Kentucky Springs Canyon.

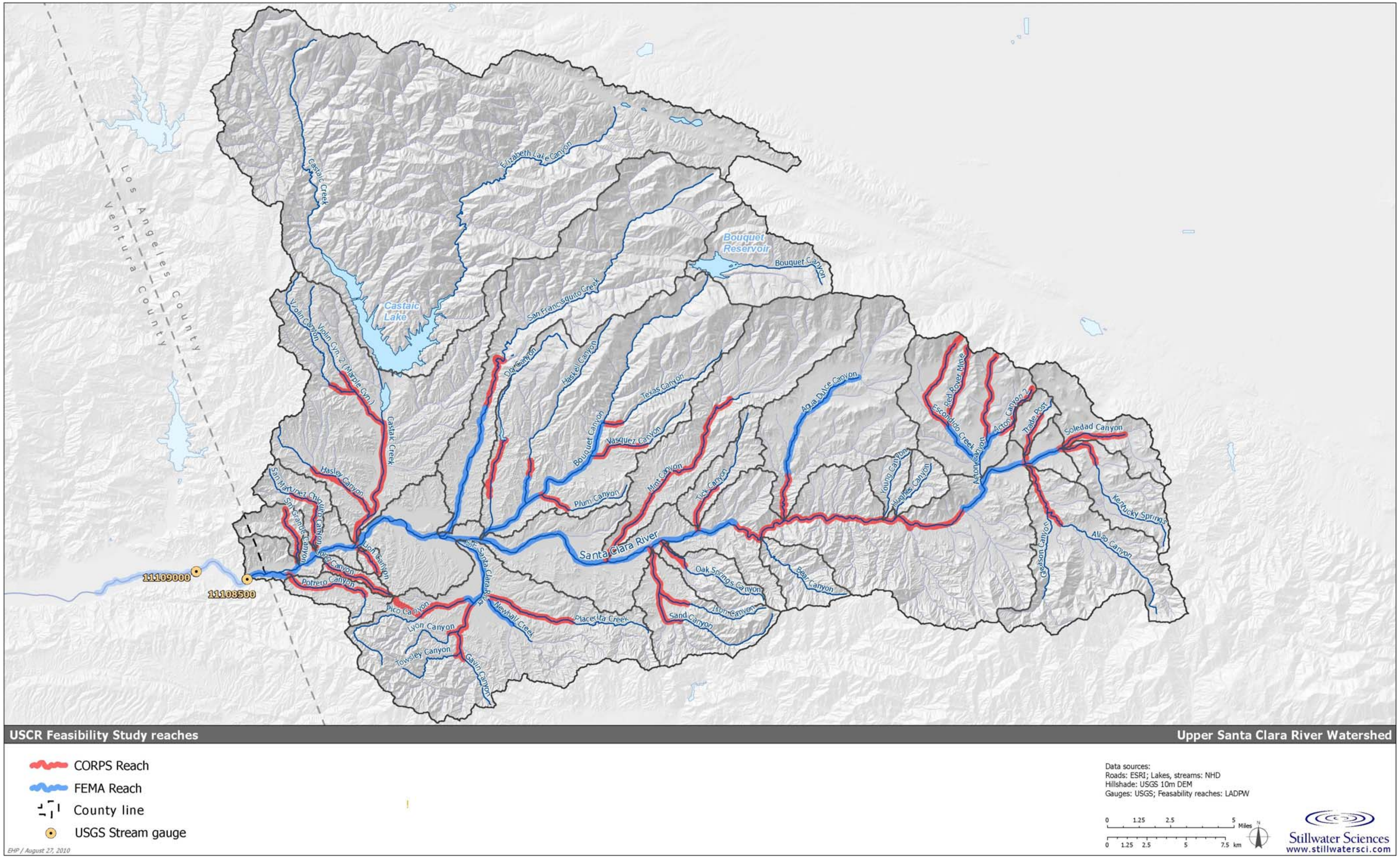

Figure 1-2. Feasibility Study and other mainstem river and tributary reaches and their contributing areas considered in the USCR watershed geomorphic assessment.

1.2 Regional Setting and Watershed Characteristics

Flowing 186 km (116 mi) from the northwestern San Gabriel Mountains to the coast, the entire Santa Clara River drains approximately 4,212 km^2 (1,626 mi^2)—one of the largest watersheds on the southern California coast. Within the confines of the assessment area, the USCR drains 1,679 km^2 (648 mi^2) and runs a distance of 62 km (39 mi) (Figure 1-2). Elevations here range from about 240 to 2,070 m (800–6,770 ft) (Figure 1-3). The river is fed by numerous named stream tributaries as it flows westward from the broad Acton basin, through a confined canyon (Soledad Canyon), and through the expansive Santa Clarita Valley (the Santa Clarita basin).

The Santa Clara River as a whole is relatively pristine in comparison with other large, coastal southern California rivers (e.g., Simons, Li & Associates 1983 and 1987, AMEC 2005, Kennedy/Jenks 2008). For example, on the Los Angeles, Santa Ana, and San Gabriel rivers, flood protection and urban development modifications have been so extensive that natural physical processes have become largely ineffective at maintaining a dynamic river system. Although recent urban developments in the Santa Clarita and Acton basins of the USCR watershed have encroached upon the river's floodplain, and even on the active channel bed in some instances, the mainstem USCR retains many of the attributes of more natural coastal southern California rivers, including a sand-bedded, braided channel, and broad floodplain terraces. The downstream reaches of several major tributaries, however, have been highly modified by channelization efforts where these water courses flow through the urban areas (e.g., South Fork SCR, and Bouquet and Mint canyons). The river and its tributaries experience high annual flow variability, multi-year droughts, and extreme seasonal flooding, which together result in a highly dynamic alluvial system.

For this assessment, the USCR watershed is divided into three morphologically similar areas (Figure 1-3). The geomorphic regions are distinguished primarily by valley width and, accordingly, general sediment delivery and transport characteristics inherent within. The *Upper Region* encompasses the Acton depositional basin and includes all areas of the upper watershed draining to the river downstream to a point just above the river's transition to the canyon reaches. This region includes the tributary streams of Acton and Aliso canyons. The *Middle Region* is essentially defined by those areas of the watershed that drain to the highly confined canyon reaches, or Soledad Canyon. Agua Dulce Canyon is the primary tributary flowing to the river in this region. The *Lower Region* is relatively large as it includes the drainages of all tributaries feeding the river in the Santa Clarita Valley, or Santa Clarita basin as is referred to herein. The watershed's largest tributaries, including Castaic Creek, South Fork Santa Clara River (South Fork SCR), and San Franciscquito, Bouquet, and Mint canyons, all join the river in this broad depositional basin.

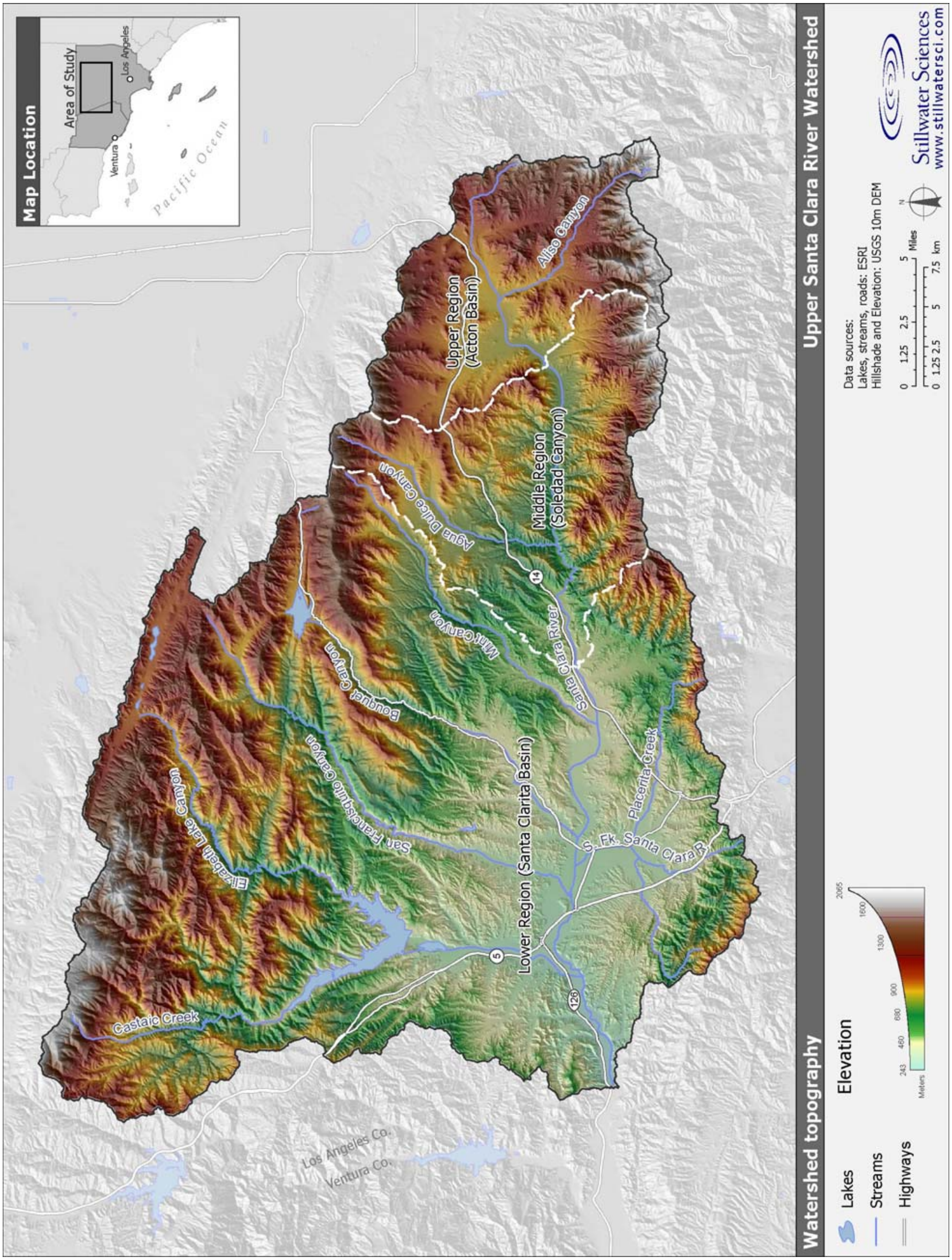

Figure 1-3. Topography and geomorphic regions of the USCR watershed.

1.2.1 Geology and tectonic setting

The USCR watershed is located within a distinctive geologic province of California known as the Transverse Ranges. Unlike the Coast Ranges to the north and the Peninsular Ranges to the south, both of whose major ridges and intervening valleys trend generally northwest–southeast, the Transverse Ranges are oriented almost exactly east–west and form a marked disruption to the overall grain of California topography. The USCR flows between the east–west-trending mountains of this province: the Transverse Mountains on the north and San Gabriel and Santa Susana mountains on the south.

The regional tectonic activity of California over the last 6 million years has created this unusual topographic and tectonic setting. Positioned immediately adjacent to the northeastern boundary of the watershed (and slightly near Lake Hughes and Elizabeth Lake), the 1,000-km-long (600-mi-long) San Andreas Fault (SAF) separates the northwest-moving Pacific plate from the (relatively) stationary North American plate (Figure 1-4). Where the SAF is straight, these plates slide past each other as a “transform plate boundary,” with either continuous motion (at rates of a few centimeters per year) or stick–slip motion where movement is episodic (and often expressed as earthquakes when it occurs) (Shen et al. 1996). The SAF is deflected from its straight trend, however, at its intersection with a northeast–southwest trending cross-cutting fault—the Garlock Fault—about 50 km south of Bakersfield. Where the SAF is bent, the Pacific and North American plates cannot simply slip past each other. Because the underlying plate motion continues, the north-migrating rocks of the Pacific plate (which include those of the USCR watershed) “pile up” in the region south of the San Andreas Fault’s bend. The crustal shortening that results from this underlying plate movement provides an ideal setting for rapid rates of landscape uplift.

The drainage network pattern exhibited in the watershed is strongly influenced by geologic structure and the location of active faults. Through the reaches of Soledad Canyon, the river follows the axis of the west-trending Soledad Fault before eventually following the San Gabriel (in part) and Holser faults in the Santa Clarita basin. Several of the watershed’s major tributaries follow (and were likely formed by) significant faults, such as Mint, Pelona (Bouquet), and San Francisquito (not shown in Figure 1-4, but this fault is mapped by Dibblee [1997: Green Valley quadrangle] as following middle San Francisquito Canyon along the north side of the Pelona Schist unit). One exception is the Clearwater Fault, which cuts across upper Castaic Creek and Elizabeth Lake and San Francisquito canyons, but several of their major tributaries do follow (and were likely formed by) this fault (listed from east to west: Cherry, Clearwater, Ruby, Warm Springs, and Fish canyons).

Persistent regional geologic instability over the last 28 million years has exposed a wide variety of highly deformed, fractured, and faulted rock types across the entire Santa Clara River watershed (Yeats 1981, Rockwell et al. 1984, Rockwell 1988). The USCR watershed is dominated by a mixture of geologically old igneous and metamorphic rocks, including gneiss (unit “gn” in Figure 1-4), schist (“ps”), granite (“gr”), and granodiorite (e.g., “lgd”), and younger sedimentary rocks, ranging from claystone to sandstone and conglomerate. The former (older) bedrock group is primarily situated in the high-relief uplands of the northern and eastern portions of the watershed, while the latter (younger) group is concentrated in and around the Santa Clarita basin, which is understandable considering that several of these sedimentary units have recently formed in this depositional basin over the past several million years.

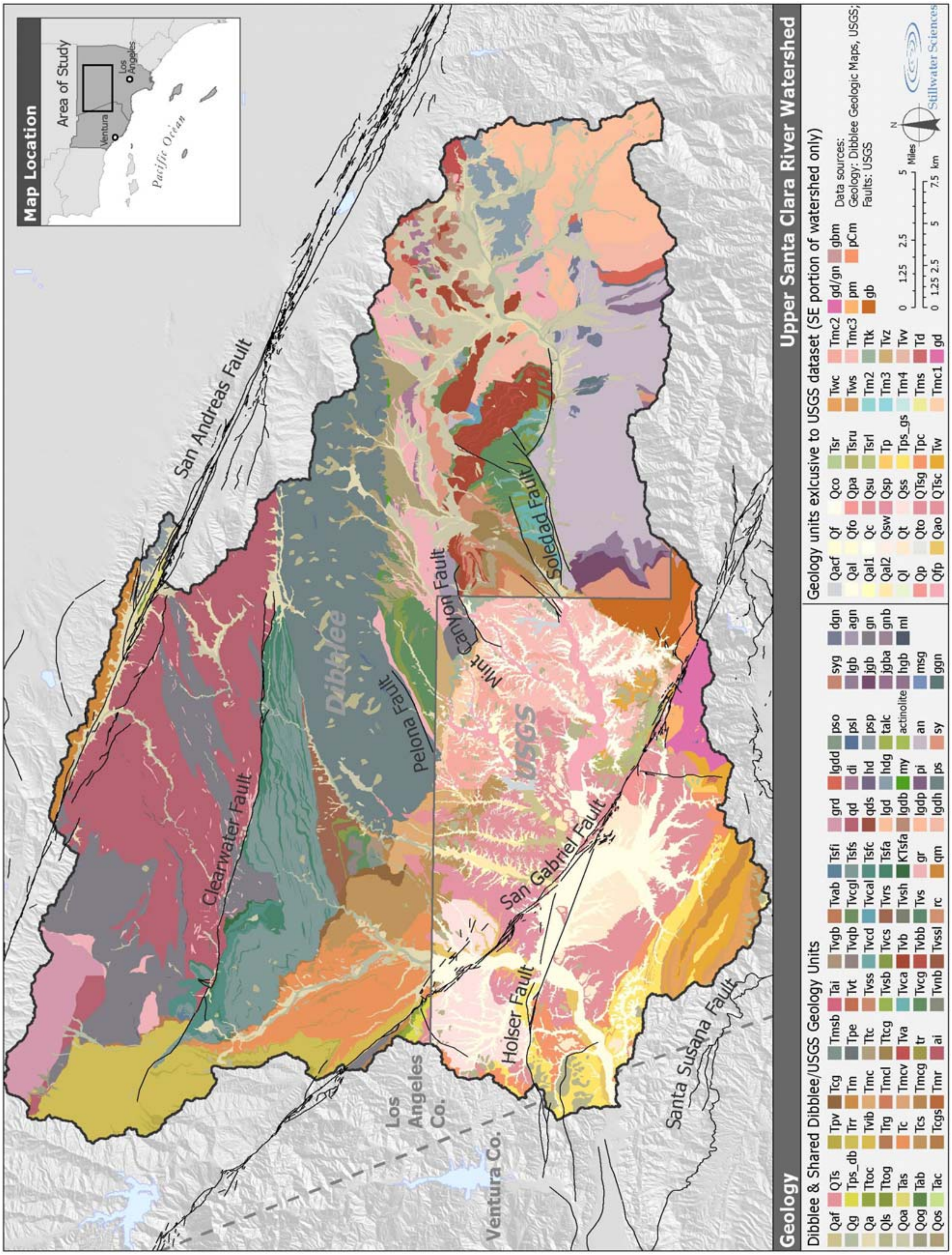

Figure 1-4. Generalized geologic map showing rock units and major fault traces in the USCR watershed.
See Appendix A for description of rock units. Color scheme used here based on source maps (Dibblee and USGS, various dates).

Fractures, deformation, and faulting contribute to high bedrock erodibility throughout the USCR watershed. For example, the sedimentary bedrock units (e.g., Castaic ["Tc" and "Tcs"], Mint Canyon [e.g., "Tmc"], Pico ["Tp" and "Tps_gs"], and Saugus ["QTs", "Qsu", "Qsp", "Qss"] formations) in the Santa Clarita basin are often poorly consolidated, intensely folded, and have steeply tilted beds, making them susceptible to landsliding (e.g., Harp and Jibson 1996) and erosion by dry raveling (Scott and Williams 1978). Even areas underlain by granite, gneiss, and schist (which are normally relatively resistant to erosion) have been described as being highly erodible (e.g., Scott and Williams 1978, Wells et al. 1987) due to extensive deformation and fracturing, which is especially true of the Pelona Schist bedrock unit ("ps") that trends across much of the watershed (Spotila et al. 2002).

Additional explanation of tectonic activity and uplift rates are presented in Section 3.3.1. A brief explanation of the geologic units shown in Figure 1-4 is presented in Appendix A.

1.2.2 Climate and hydrology

Coastal watersheds of southern California function according to a semi-arid, two-season Mediterranean-type climate, with cool wet winters and dry warm-to-hot summers. Rainfall and air moisture both tend to decrease with increasing distance from the coast. Within the USCR watershed, proximity to the Pacific Ocean moderates both seasonal and diurnal temperatures. Most precipitation occurs between November and March, with precipitation varying significantly throughout the USCR watershed and appears to be most strongly influenced by elevation and distance from the Pacific Ocean (Figure 1-5). That is, the wettest areas are found along the high relief mountain ranges on the north and south sides of the watershed, while the driest areas are found in the lowlands of the Santa Clarita and Acton basins, with the easterly Acton basin experiencing considerably drier conditions as a consequence of being located much farther inland. Overall, average annual precipitation in the watershed ranges between 23 and 84 cm (9–33 in) during the years 1971–2000. At higher elevations, some winter precipitation occasionally falls as snow.

Periodicity in the pattern of the wet/dry years in southern California is correlated to the El Niño–Southern Oscillation (ENSO) climatic phenomenon. ENSO is characterized by warming and cooling cycles in the waters of the eastern equatorial Pacific Ocean, which typically have a 1–1.5 year duration and a 3–8 year recurrence interval (NWS CPC 2010). In southern California, ENSO years are characterized by relatively high rainfall intensities, with rivers and streams (such as those in the USCR watershed) exhibiting higher annual peak flow magnitudes than they do in non-ENSO years. The most recent ENSO event occurred in water year (WY) 2010 (NWS CPC 2010). Additional details on the effects of ENSO events on flow magnitude and sediment delivery rates are discussed in Section 4.1.3.

The climatic and hydrologic characteristics of the USCR watershed generally produce an intermittent flow regime along the majority of the mainstem USCR and its tributaries; ephemeral streams are also common throughout the drainage network. Reaches of lower Castaic Creek and Bouquet Canyon typically support a low flow even during dry summer months as they receive flow from their respective water storage reservoirs upstream. The watershed also hosts a highly developed groundwater pumping infrastructure used to supply water for agricultural, domestic, and industrial purposes, primarily in the Santa Clarita basin. As a consequence, summer baseflow in certain river and lower tributary reaches through the Santa Clarita basin is undoubtedly diminished as compared to historical, pre-pumping conditions (see Chapter 2). A detailed account of the groundwater-surface water interactions in the USCR watershed is presented in the *Upper Santa Clara River Integrated Regional Water Management Plan* report (Kennedy/Jenks 2008).

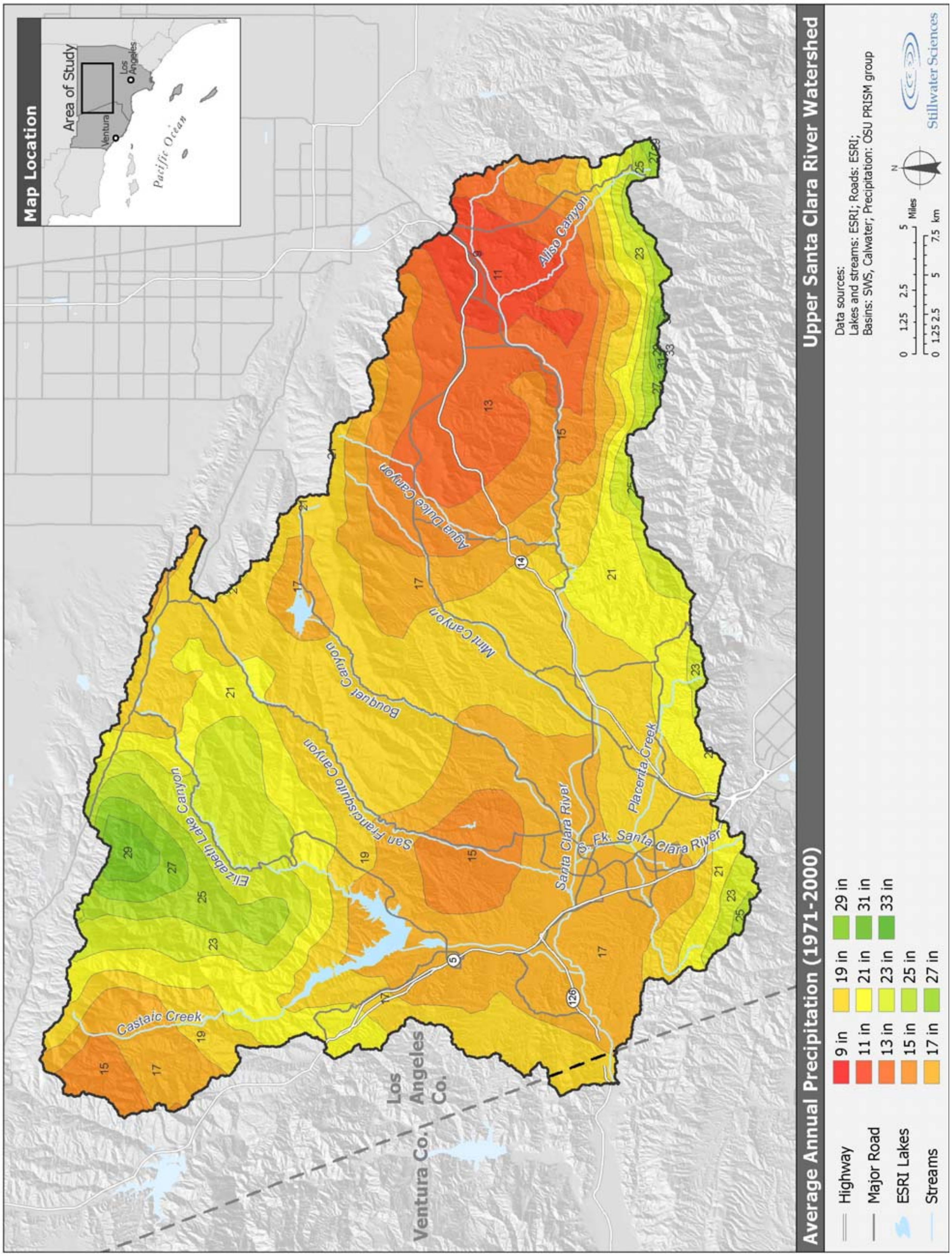

Figure 1-5. Distribution of average annual precipitation across the USCR watershed based on data from the period 1971-2000.

Similar to other southern California river systems, the USCR watershed experiences highly variable annual rainfall and peak flows. Typical of semi-arid to arid watersheds, flood flows in the USCR typically increase, peak, and subside rapidly in response to high-intensity rainfall. This hydrologic attribute is characteristic of a "flashy" hydrograph shaped by a rapid increase in discharge over a short time period with a quickly developed peak discharge in relation to normal baseflow (Ward 1978). The five largest natural floods on record at the County line stream gauge (USGS 11108500 and 11109000: 1953–present) were in 1969 (1,948 $m^3 s^{-1}$ [68,800 cfs]), 1966 (906 $m^3 s^{-1}$ [32,000 cfs]), 2005 (906 $m^3 s^{-1}$ [32,000 cfs]), 1983 (866 $m^3 s^{-1}$ [30,600 cfs]), and 1978 (646 $m^3 s^{-1}$ [22,800 cfs]) which all occurred during ENSO years (see Table 4-1 for a complete record of recorded flows in excess of 283 $m^3 s^{-1}$ [10,000 cfs]). The largest actual flood in the watershed was the 1928 failure of the St. Francis Dam, with an estimated peak discharge between the dam site on San Francisquito Canyon down to the County line of 14,000 to 28,000 $m^3 s^{-1}$ (500,000–1,000,000 cfs) (Begnudelli and Sanders 2007). The effects of this event on lower San Francisquito Canyon and the SCR below this confluence are discussed in Section 4.2.1.3.

1.2.3 Land use/Land cover

The USCR watershed remains relatively undeveloped when compared with many of the coastal watersheds to the south, such as the Los Angeles, Santa Ana, and San Gabriel rivers. The Angeles National Forest accounts for approximately 51% (858 km^2) of the total USCR watershed area (Figure 1-1). Land development is generally concentrated within the lowlands and surrounding foothills on the Santa Clarita and Acton basins, with several other unincorporated towns and low density settlements scattered throughout. Infrastructure in support of water supply storage and conveyance, power transmission, natural resource extraction and distribution (e.g., oil and natural gas), and transportation (e.g., highways) is present throughout much of the watershed, except in the more remote, higher elevation areas. Additional details on historic and present-day land use activities and their effects on the watershed's geomorphic processes are presented in Chapter 2 and Section 4.2.

Land cover in the upland areas predominantly comprises scrub/shrub (chaparral) vegetation, accounting for nearly two-thirds of the total USCR watershed area (Figure 1-6, see Table A-4 in Appendix A). Higher density vegetation cover and larger trees generally concentrate on north-facing slopes, but particularly so in the wetter and higher elevation areas of the watershed (e.g., Castaic Creek/Elizabeth Lake Canyon headwaters and the north side of the San Gabriel Mountains). Despite the mostly semi-arid climate, the vegetation cover in the USCR watershed effectively hinders erosion of land surfaces by providing: (1) a continuous surface cover that intercepts rainfall and prevents rainsplash erosion, and (2) roughness to the landscape surface that divide and slow sheetwash upon the land surface (see Section 3.2.1). Conversely, regular burning of the watershed's vegetation cover by frequent wildfires often results in increased surface erosion and pulses of fine sediment into the drainage network (see Section 3.2.3.3).

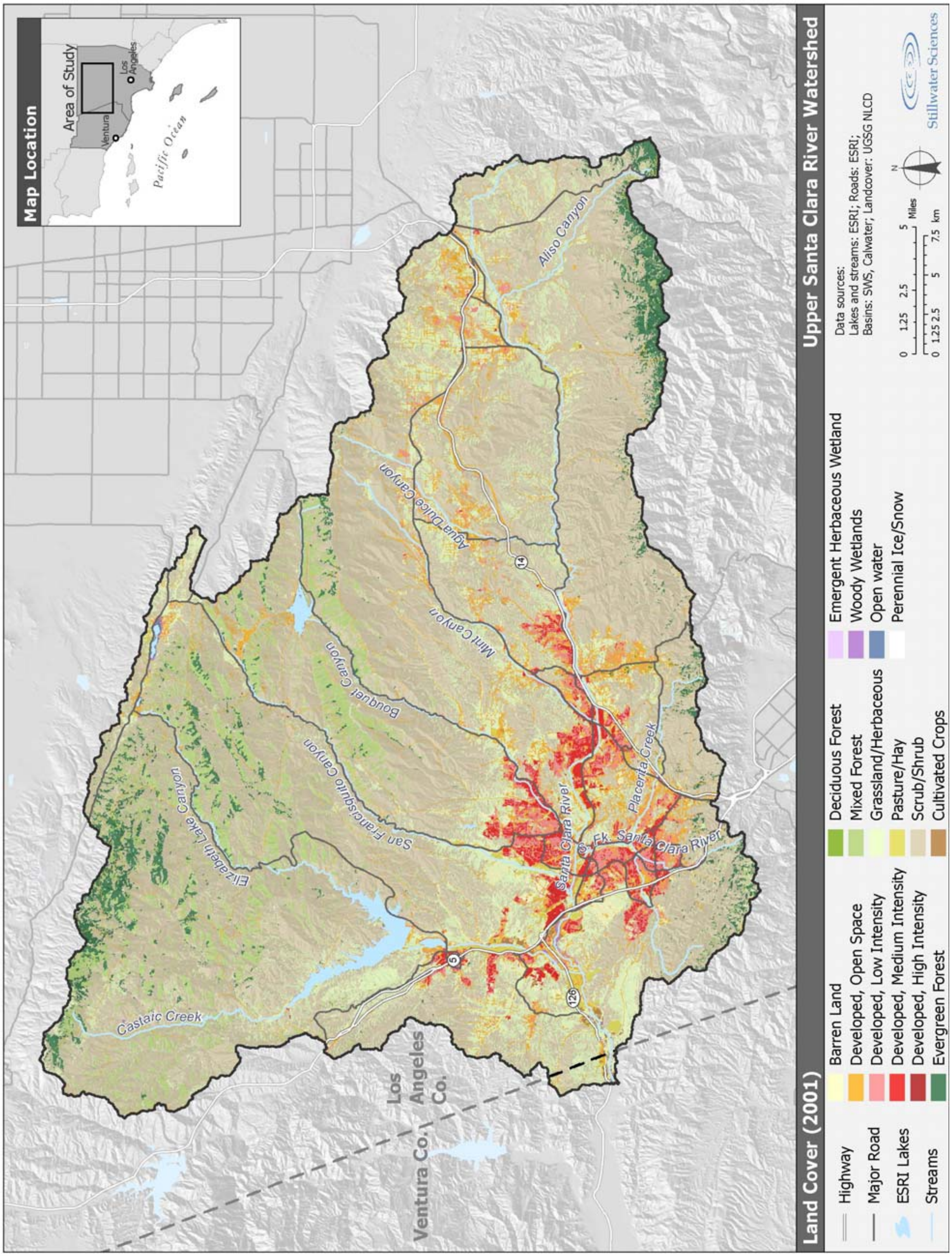

Figure 1-6. Land cover (2001) within the USCR watershed.

2 HISTORICAL PERIODS OF CHANGES TO WATERSHED GEOMORPHIC PROCESSES

A conceptual understanding of past periods is critical in determining how the physical watershed and river corridor used to function, and it helps form the foundation for determining how changes in watershed and river function have occurred. Understanding these elements makes it possible to hypothesize the potential future trajectory of channel conditions and thus helps to guide sustainable river management strategies. Information from a variety of sources (Table 2-1) has been distilled into a time chart of historical events that may have had an effect on water and sediment discharge in the USCR watershed, and have, therefore, influenced geomorphic processes and channel morphological responses within the river corridor (Figure 2-1 and Appendix B). Much, but not all, of this historical information was initially compiled for the Lower Santa Clara River geomorphology study (Stillwater Sciences 2007a) but has been tailored here specifically for the USCR watershed.

The history of land-use changes and the evolution of water and river management practices within the entire Santa Clara River watershed have been comprehensively documented by Schwartzberg and Moore (1995) and AMEC (2005). These authors subdivided the history of the entire watershed into four distinct phases based primarily upon cultural and land developmental considerations: pre-European settlement (pre-1872), the Agrarian Era (1782–1870), the Commercial Era (1870–1920), and the Industrial Era (1920–present).

From a geomorphological perspective, the data in Figure 2-1 and Appendix B suggest, however, that there may be five historical periods that have likely altered the response of channel morphology to natural extremes in water and sediment discharge. These periods are as follows:

- Pre-1760: “Pre-European Colonization”
- 1760–1820: “European Arrival”
- 1820–1910: “Settlement & Ranching”
- 1910–1980: “Irrigation, Diversions, Dams, & River Modifications”
- 1980–2010 (present): “Urbanization”

This section provides a broad overview of the anthropogenic activities associated with these five periods and discusses their potential influence on geomorphologic processes in the USCR watershed over time. Expected future conditions for many, but not all, of the watershed impacts considered in Figure 2-1 have been included based upon forecasts made by others (e.g., AMEC 2005, Kennedy/Jenks 2008). This time period is simply referred to as “future” here and extends out to the year 2050, which was selected because minimal information was available beyond this year. Additional details regarding specific events that occurred during these historical periods and regarding expected future conditions beyond 2010 are presented in Section 4.2 and Appendix B. A description of the method utilized to determine “wet” and “dry” periods in the watershed, which follows the method initially developed by Freeman (1968) for use with the long-term Santa Paula precipitation data, are also described in this appendix. A detailed discussion on wildfires and their effects is presented in Section 3.2.3.3.

Table 2-1. Historical sources for the USCR watershed.

Data	Source	Dates	Notes
Aerial photography	LADPW, UCSB, USGS	1928 to present	Excellent photo coverage in 1928, the oldest known aerial photographs of the USCR watershed; likely commissioned in response to the 1928 St. Francis Dam failure. Photo coverage and availability is sparse until the 1960s; much improved after 1980.
Topographic maps and digital data	Intermap, LADPW, USGS	1930s, 1964, 2001, 2005	Excellent topographic coverage from historical 24:000 scale USGS maps (1930s; 5-ft contour spacing along river channel), 1:1200 scale LADPW maps (1964; 2-ft contour spacing), high resolution Intermap IfSAR data (2001; 5-m resolution), and high resolution LADPW LiDAR data (2005; 5-ft resolution).
Precipitation and streamflow	LADPW, LADWP, USGS, VCWPD	various	Historical precipitation data from Santa Paula in the LSCR watershed extended back in time by Freeman (1968). Various rain and stream gauge records throughout the USCR watershed with varying durations, dating back to 1918 (precipitation at LADWP's Powerhouse #1—San Francisquito Canyon).
Wildfires	CDF FRAP	1878 to present	Comprehensive database of documented wildfire events throughout California, including the USCR watershed.
Miscellaneous ground-based photography	LADPW, VCWPD	1928 and 1969	Excellent panoramic photos of the river following the 1928 St. Francis Dam failure and low-elevation, oblique-angle aerial photographs of the river during the 1969 floods.
Textual accounts	Report: Schwartzberg and Moore (1995), *Santa Clara River Enhancement and Management Plan: A History of the Santa Clara River*	1700s and later	Excellent summary of the history of the entire Santa Clara River Valley (Ventura and Los Angeles counties). Includes some accounts of the river's historical condition.
Textual accounts and ground-based photography	Santa Clarita Valley Historical Socity website: http://www.scvhistory.com/scvhistory/index2.htm	Pre-history and later	Compilation of newspaper articles, research, photographs, and accounts of historical conditions in the USCR Valley.

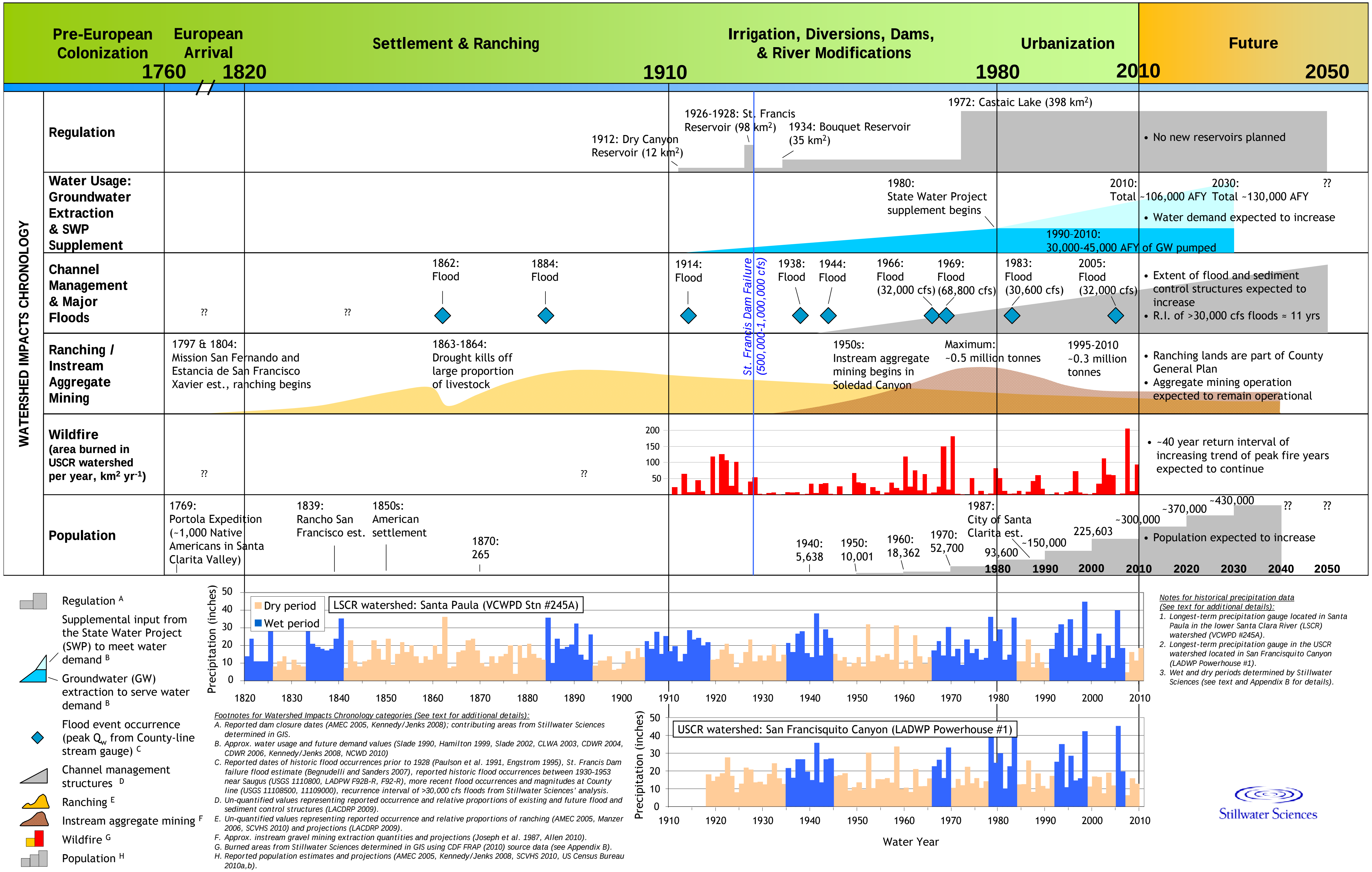

Figure 2-1. Chronology of potential watershed impacts and events. Precipitation records indicate periods of cumulatively wetter and drier periods in the watershed. See text and Appendix B for additional details.

2.1 Pre-European Colonization (pre-1760) and European Arrival (1760-1820)

In the period prior to widespread European ranching and colonization (approximately prior to 1820, following establishment of Mission San Fernando in 1797), the USCR watershed presumably was in a relatively pristine state, responding only to fluctuating flood, drought, and fire sequences with relatively minor impacts associated with the agricultural practices of the indigenous Tataviam peoples, which were culturally similar to the Chumash peoples to the west (Schwartzberg and Moore 1995, W&S Consultants 1995 as cited by USACE and CDFG 2009, Szabolcsi 2000). There are historical reports that describe perennial stream flow for several southern California rivers, including the Santa Ana, Santa Margarita, and San Luis Rey, that are now intermittent largely as a result of water impoundment, diversion, and groundwater pumping (Boughten et al. 2006). As summarized by Schwartzberg and Moore 1995, Father Juan Crespi (of the Portola Expedition that traveled along the California coast) noted a mature riparian forest along the USCR near Castaic Creek in 1769: “tall thick cottonwoods and oaks” and an “arroyo with a great deal of water which runs in a moderately wide valley, well grown with willows and cottonwoods”. It is therefore likely that the USCR (and the entire SCR course through Ventura County, as well) experienced perennial stream flow and supported a more-or-less continuous and broad riparian forest in all reaches, with the possible exception of those located farther upstream in the Acton basin which ran through (and continue to run through) a considerably more arid terrain.

2.2 Settlement & Ranching (1820–1910)

Beginning in the 1820s, establishment of large-scale ranching activity throughout the SCR watershed and other coastal California watersheds (including much of the USCR watershed (e.g., Santa Clarita and Acton basins) is likely to have caused significant changes to rainfall-runoff relationships as deep-rooted native perennial grasses in the valleys and foothills were degraded and replaced by shallow-rooted non-native annual grass species, which are less able to resist soil erosion (Rice and Foggin 1971, Gabet and Dunne 2002). Drought in the mid-1860s caused a shift from traditional cattle grazing to sheep, potentially accelerating the removal of vegetation and subsequent erosion (Freeman 1968, Manzer 2006). Timber-harvesting activities were generally limited in the USCR watershed due to the lack of easily accessible conifer stands; however, logging activities did occur in the region including the upland areas of the watershed (Blakley and Barnette 1985, USFS 2010). Overall, it is likely that greater volumes of hillslope runoff were generated per unit rainfall as a result of land-use change during this period, with far greater volumes of fine sediment production throughout the watershed and increased shallow landslide potential on the hillslopes (Rice and Foggin 1971, Gabet and Dunne 2002). Historical accounts describe the extensive effort undertaken to clear riparian forests throughout central and southern California watersheds (Gordan 1996, as cited in Boughton et al. 2006). Floodplain forests were first cleared for fuel supply, then to prepare the land for grazing and farming, and finally to increase flood conveyance.

By the end of this period, public concern over land-use effects on the region’s landscape fueled the creation of the Angeles National Forest in 1892 (originally designated as the San Gabriel Timberland Reserve) (USFS 2010). Presently, the national forest includes just over one-half of the USCR watershed’s total area.

2.3 Irrigation, Diversions, Dams, & River Modifications (1910–1980)

The period starting in the 1910s is characterized primarily by large-scape development of water supply infrastructure to serve the growing demand for water with the increase in agricultural use and settlement along the entire SCR valley (including the Santa Clarita basin, particularly on the Newhall Ranch property which was formerly part of the immense Rancho San Francisco) (Freeman 1968, Schwartzberg and Moore 1995). Other land uses that became established in the USCR watershed during this time period included mining and oil drilling, both of which involved land clearing, road and railway construction, town establishment, and water use. During this timeframe, irrigation using surface flow from the river and its tributaries began to be supplemented by pumped groundwater supplies. The first public water utility in the Santa Clarita Valley, the Newhall Water System (now the Newhall County Water District), was formed in 1913 and provided groundwater to 125 connections; by 1953 this had expanded to six wells serving 870 connections with a combined production of 725 gallons per minute (Hamilton 1999). Presently, there are several other water providers in Santa Clarita and Acton basins obtaining mostly groundwater for their supply, which is now augmented by water supplied from the State Water Project (via Castaic Lake), which began in 1980 (CLWA 2003, AMEC 2005, Kennedy/Jenks 2008). A 1933 map prepared by the California Department of Water Resources (CDWR) depicting land use types in the Santa Clarita basin shows that much of the river valley up to Soledad Canyon in the east, including the lower reaches of the major tributaries (e.g., South Fork SCR, Castaic Creek, and San Francisquito and Bouquet canyons), was supporting the production of some water-intensive crops (e.g., citrus and alfalfa) but most farmed lands were unirrigated (see Figure 3-1 in Schwartzberg and Moore 1985). Impacts of groundwater extraction in the USCR watershed, specifically the Santa Clarita basin, likely included an initial reduction in baseflow within the river followed by a lowering of the groundwater table due to pumping, albeit at minor amounts when considering that dryland agriculture dominated in this area. Nearly all of these lands have since been developed during the recent urban growth period (see below).

By 1912, the first large dam in the watershed had been constructed in Dry Canyon, a tributary to lower Bouquet Canyon (the dam was subsequently decommissioned in the 1960s due to leakage); in 1913 the Owens Valley–Los Angeles aqueduct, which cut through Soledad, Bouquet, and San Francisquito canyons, was completed. In 1926, St. Francis Dam was completed on San Francisquito Creek; however, the dam failed catastrophically in March 1928, resulting in one of the largest and most tragic dam failures in United States history. The long-term effects of the St. Francis Dam disaster on the morphology of the entire Santa Clara River are unknown but are potentially significant and ongoing (see Section 4.2 and Stillwater Sciences 2007a). Bouquet Dam was completed in 1934 to impound imported water in Bouquet Reservoir, in the relatively dry northeastern corner of the watershed. Castaic Dam, completed in 1972, retains water imported from northern California. Today, these two dams intercept runoff and sediment from 26% of the USCR watershed area (see Sections 3.4 and 4.2).

2.4 Urbanization (1980–2010)

More recent, and perhaps the most significant, influences on the evolutionary history of the USCR are associated with the increasing rate of urban development in Los Angeles County. After purchasing Rancho San Francisco (now known as Newhall Ranch) in 1875, Henry Mayo Newhall sold a right-of-way to the Southern Pacific Railroad, and the towns of Newhall and Saugus were established shortly thereafter (Massie 1989). Population growth for the next 60 years was steady but relatively slow, with occasional spikes in population as a result of new mining claims. Although only recently incorporated in 1987, the City of Santa Clarita (which includes Canyon Country, Newhall, Saugus, and Valencia) is now the second-largest city in Los Angeles County based on size (approximately 170 km^2) and the fourth-largest based on population (CDF 2010, as cited by City of Santa Clarita 2010). Between 2000 and 2008 the City of Santa Clarita's population growth was almost twice the growth of all of Los Angeles County (see Section 4.2).

During this growth period, the USCR floodplain and channel were increasingly modified for the purpose of providing for urban development, along with associated flood control and debris flow protection infrastructure. Urban growth throughout the watershed, and southern California as a whole, is also linked to demand for aggregate materials needed to improve and expand existing infrastructure. Thus during the 1970s and 1980s, the pace of mining activity in the watershed escalated dramatically (Joseph et al. 1987). However, compared with the LSCR closer to Ventura, instream aggregate mining (as opposed to off-channel mining and hillside quarries) has been limited to a single operation along the USCR, situated near the downstream end of Soledad Canyon (see Section 4.2).

Increased rates of channel incision downstream of aggregate mining pits have been documented worldwide, and so the overall geomorphic impacts of such direct modifications to water and sediment discharge is likely to have been significant in the USCR. They are difficult to discriminate, however, from impacts resulting from previous watershed land-use changes and natural flood events (Simons, Li & Associates 1987, Chang 1990). For example, the reduction in sediment discharge caused by dam construction may have reversed some of the increase in sediment load that likely followed ranching and subsequent changes in upland vegetation. Clear-water discharge from dams may have also led to channel incision, such as below Castaic Dam on lower Castaic Creek (Simons, Li & Associates 1987). Bank protection in the Santa Clarita basin may have changed instream flow patterns, deflecting erosional energy to new locations. Levees and hardened banks may also be increasing rates of channel incision by confining flood events to the floodway and thus increasing flow depths rather than allowing overbank flooding to occur (Simons, Li & Associates 1987) (see Section 4.2).

2.5 Future (2010-2050)

Beyond present day, it is predicted that the county's population will continue to increase at current growth rates, particularly within the Santa Clarita basin and surrounding areas, such as in Acton (Kennedy/Jenks 2008). As such, the urban footprint will continue to expand within the watershed, resulting in an increased demand for water, flood and debris protection, and construction materials (i.e., aggregate) (see Section 4.2.5).

The subsequent sections in this report further investigate the geomorphic conditions and processes in the USCR mainstem following almost two centuries of European colonization, land-use changes, and direct modification of water and sediment discharges and channel morphology in the watershed. It is important to note that, first, the periods outlined above are separated for convenience and that their impacts on the watershed are both gradational and cumulative over time. Because the cumulative impact is difficult to quantify, however, this report has compiled a large number of both quantitative and qualitative studies as the basis for a preliminary understanding of the evolutionary trajectory of the river channel. Second, sediment transport and morphological changes in the entire Santa Clara River occur only in brief periods during flood events, and especially when flood events follow large fires (Lavé and Burbank 2004, Warrick et al. in prep). As such, both a natural component to channel morphology changes and a confounding factor of human impacts in the watershed are expressed during major flood (and especially fire-flood) events. This makes disentangling comprehensive human impacts from natural events one of the most challenging arenas in geomorphology (Downs and Gregory 2004).

3 HILLSLOPE AND TRIBUTARY SEDIMENT PRODUCTION AND DELIVERY

3.1 Overview

This chapter evaluates the hillslope processes that control the production of sediment across the watershed, and the subsequent delivery of that sediment into the channel network. Overall, rates of hillslope sediment production in the USCR watershed are driven by tectonics, geology, climate, and land uses. In detail, sediment is released from hillsides via several discrete processes, including dry ravel, soil creep, gullying, and landsliding.

Representative rates of soil production and hillslope sediment transport are difficult to quantify because they are driven by the episodic and commonly transient effects of rainstorms, windstorms, fires, earthquakes, and human and other disturbances (Benda and Dunne 1997, Gabet and Dunne 2003). The inherently episodic nature of erosional processes results in substantial year-to-year variability and makes any assessment of sediment-production and transport rates sensitive to the timescales over which they are averaged (Kirchner et al. 2001). For example, if the basin-wide erosion rate is averaged over a relatively dry 10-year period it will be considerably lower than if it were averaged over a 10-year period that included several wet years. Although long-term averages cannot predict the sediment load for any given year, they nevertheless are useful in assessing the long-term consequences of alternative management actions.

As the first step in understanding and quantifying the magnitude of sediment flux down the channel of the USCR, this section evaluates the production of hillslope sediment across the watershed and the delivery of that sediment into the channel network. These rates have been estimated using a variety of techniques, over a variety of temporal and spatial scales, because multiple scales of analysis can provide more robust and reliable estimates than any single method alone. Over a millennial timeframe, long-term erosion rates can be estimated using sediment dating techniques (i.e., measurement of cosmogenic nuclide concentrations in eroded sediments), which we have employed as part of this study. Over the longest time scales, best represented by the geologic record of the past several million years, the likely magnitude of sediment production should approximate the rate of overall landscape uplift (Burbank et al. 1996). This provides a coarse indication of the likely range of average sediment-delivery rates across the watershed as a whole, and one that is completely independent of other methods.

Over shorter, more human timescales, rates of sediment production can be assessed using a "geomorphic landscape unit" (GLU) approach, in which different parts of the watershed are recognized to erode at different rates due to differences in their physical characteristics, and to which representative erosion rates can be assigned and then summed over the watershed area as a whole. The degree to which these long-term and short-term estimates agree, not only with each other but also with additional data on the rate of in-channel sediment transport directly, provides a measure of the reliability of these GLU-derived results. Finding agreement within an order of magnitude between sediment-production rates derived from these various approaches is ideal.

3.2 Dominant Sediment Production and Delivery Processes

Upland topography reflects the interplay of uplift due to tectonic processes and the wearing away of slopes by erosion. In general, high, steep mountains occur in areas that have been subjected to sustained, rapid uplift, whereas low, gently sloping mountains occur in areas where uplift is slow or has been followed by long periods of denudation. Steeper areas generally have higher erosion rates (e.g., Ahnert 1970), because erosion is typically more effective on steeper slopes and because steep slopes are prone to mass movement, which can enhance erosion. Hence, faster tectonic uplift rates are generally associated with steeper mountains and faster erosion rates. In general, the linkages between uplift, slope steepness, and erosion imply that slopes should tend to contribute sediment in proportion to their uplift rates over the long term.

Slopes throughout the Santa Clara River watershed are steep (see Figure 3-11 in Section 3.3.4.1), with long-term uplift rates that are among the fastest in the continental United States (see Section 3.3.1). Erosion rates are likewise rapid but are not so fast that soils are completely stripped everywhere from slopes.

Soil moves downslope toward channels and unchanneled valleys, transported incrementally by hillslope sediment transport processes, such as mass wasting, overland flow, and biogenic disturbances. These processes deliver sediment directly to channels from slopes, or bring it to unchanneled valleys where it may first collect before being delivered to channels by channel-head erosion and landsliding. After entering channels, sediment is transported downstream by stream flow or in concentrated debris flows. Sediment transport by the USCR and its major tributaries is discussed in Chapter 4. In this chapter, the focus is on the upslope processes that ultimately deliver that sediment to the drainage network.

3.2.1 Discrete hillslope processes

Evaluation of active hillslope processes in the watershed was accomplished by reviewing other geology and geomorphology studies previously conducted in the watershed, and then performing ground-based field surveys. These field surveys served to identify and characterize active geomorphic processes in viewable and/or accessible areas, with a focus on areas representative of general landscape types (e.g., consisting of distinct combinations of geology, land cover, and hillslope gradient) (see Section 3.3.3). Active hillslope processes in the watershed, as identified during the field surveys and supported by information presented in other published accounts, are summarized in Table 3-1. Examples of observed, active hillslope processes in the watershed are shown in photographs presented in Figure 3-12 of Section 3.3.4.1.

Table 3-1. Active hillslope processes in the USCR watershed.

Category	Hillslope process	Process description [A]
Natural processes		
Sediment production	Conversion of bedrock to soil mantle	Physical, chemical, and biotic-breakdown of bedrock material into friable weathered rock and then physically disrupted into soil. [a]
	Rockfall	Mass failure of mostly rock that has separated from its parent bedrock surface (typically along vertical cliff). [a]
Mass-wasting processes	Soil creep	Slow, often indiscernible downslope movement of surface soils or rock debris. [a]
	Dry ravel	Downslope transport of individual particles under power of gravity (or bioturbation) rather than water; mostly occurring where vegetation cover is non-existent. [b]
	Rain impact	Erosion of soil surface through the impact of rain drops that effectively detach and transport sediment particles; rain impact energy diffused or altogether blocked by ground cover vegetation. [a]

Category	Hillslope process	Process description [A]
Mass-wasting processes (cont.)	Biogenic transport	Exhumation and down-slope transport of soil and rock fragments by biological forces, including tree-throw and burrowing animals. [a]
Mass-wasting processes (cont.)	Shallow landsliding	Mass failures that have a composition mostly of colluvial sediments, a failure plane above the soil-bedrock interface, and a relatively long travel distance through the low order channel network. [c]
Mass-wasting processes (cont.)	Deep-seated landsliding	Mass failures that have a composition mostly of bedrock (parent material), a failure plane below the soil-bedrock interface, and a surface area >0.1 km^2. [d]
Overland flow erosion	Sheetwash	Downslope transport of fine particles (<2 mm) driven by concentrated surface runoff. [a]
Overland flow erosion	Rilling	Formation of generally discontinuous, small channels less than several cm deep and wide that develop on slopes composed of fine-grained sediments where surface runoff has concentrated. Typically occurs in areas of land disturbance and/or vegetation clearing. [a]
Tributary connection with hillslope processes	Gullying	Formation often driven by the coalescence of several rills into an enlarged master rill, which can further extend the drainage network upslope. Often occurs in areas of land disturbance and/or vegetation clearing. [a]
Tributary connection with hillslope processes	Channel head advance	Upslope migration of a stream channel into hillslope colluvium, usually due to gully incision and/or channel head-cutting. [a]
Human disturbances		
Agriculture and rangeland	Surface wash, rilling, and gullying	(see description above)
Agriculture and rangeland	Shallow landsliding	(see description above)
Road-related	Cut and fill failures	Erosion by sheetwash, rilling, gullying, or shallow landslides into road cuts or road fill material. [e]
Road-related	Surface erosion	Erosion of fine sediments from unpaved road surfaces. [e]
Road-related	Gully formation associated with inboard ditch relief	Occurs when road runoff concentrates into an inboard ditch that then incises the ditch and/or adjacent surfaces where the routed flows have been discharged. [e]
Road-related	Gully formation and mass failure on the outboard side	Occurs when road runoff concentrates on the outboard side of the road and erodes/destabilizes road fill material and/or hillside soils. [e]
Urban	Construction phase sediment pulse	Release of fine sediment downslope and into the drainage network during the disturbance of the landscape.
Urban	Slope destabilization	Surface erosion and mass failures can occur on slopes that have been over steepened and/or undercut.

[A] Sources: [a] Selby 1993; [b] Gabet 2003; Roering et al. 2003; [d] Roering et al. 2005; [e] Reid and Dunne 1984

3.2.1.1 Soil creep and dry ravel

In the entire SCR watershed, the lateral supply of sediment to channels is thought to be fairly continuous (Scott and Williams 1978), with wet-season contributions from overland flow, landslides, and soil slumps; and dry-season contributions from dry ravel. Although the intuitive correlation between sediment delivery and rainfall applies in this region (see, for example, Stillwater Sciences 2010), non-rainfall-driven processes are also important. Hillslope soils within the USCR watershed are typically thin and coarse-textured, with steep slopes that often exceed the angle of repose of the unconsolidated material. These conditions, along with the semi-arid, Mediterranean-type climate, make slopes especially prone to dry raveling. High rates of dry raveling have been documented in the San Gabriel Mountains (Anderson et al., 1959, Krammes 1960, Krammes and Rice 1963, Krammes 1965, Wells 1981, Wells 1985), a portion of which feed the river from the south; as much as half or more of the total sediment movement on slopes in the San Gabriel Mountains is argued to be by dry raveling (Anderson et al. 1959, Krammes 1965). Evidence from sediment traps on hillslopes in nearby Santa Barbara County indicates that dry raveling is also an important process in other coastal southern California watersheds (Gabet 2003). Dry ravel appears to be especially pronounced after fires, because the sediment that has accumulated behind vegetation is free to travel downslope when the supporting vegetation is burned away (Gabet 2003, Schmidt et al. 2008). Taken together, available data and field observations indicate that dry raveling is significant throughout the entire Santa Clara River watershed.

3.2.1.2 Rain impact

The impact of rain on slope surfaces can be an effective sediment transport mechanism (see Gabet and Dunne 2003, and references therein), depending on drop size, velocity, and rainfall intensity, which together regulate "rain power" (i.e., the rate of transfer of energy to the surface). Larger drops and higher velocities generally lead to more efficient sediment detachment and transport. Vegetation can effectively armor surfaces against rain-induced erosion, intercepting drops and absorbing their energy before they hit the surface. Hence, erosion by rain impact can be enhanced after fires that eliminate protective vegetative cover. In general, coarser particles are harder to detach. Higher rainfall intensities should lead to more effective transport, but only up to a point; if rainfall rates are extremely high, such that overland flow is significant, the water on the surface may actually attenuate the effect of rain impact, reducing its ability to detach sediment.

Sediment transport by rain impact has been shown to be significant on steep experimental plots in the northern Transverse Ranges at Sedgwick Reserve above the Santa Ynez Valley near Santa Barbara (Gabet and Dunne 2003), which experiences the same semi-arid Mediterranean climate that prevails in the nearby Santa Clara River watershed. Land-use history and vegetation types are similar as well. Hence, it seems reasonable to presume that sediment transport by rain impact is significant in the USCR watershed, especially after vegetation-destroying fires (e.g., Wells 1981).

3.2.1.3 Biotic processes

Biotic processes stir soil and transport sediment downslope (Roering et al. 2002). In mountainous watersheds, biotic sediment transport processes include animal burrowing and tree throw (which causes upheaval and downslope transport of sediment from root wads). Although tree throw is unlikely to be effective in the USCR watershed due to its paucity of forest cover (see Figure 1-6), significant transport by burrowing of pocket gophers (*Thomomys bottae*) has been observed in Sedgwick Reserve (Gabet 2000, Seabloom et al. 2000), with transport rates increasing as a function of increasing hillslope gradient. Given Sedgwick's proximity and similarity, it seems reasonable to assume that burrowing by pocket gophers is an important sediment transport process in the USCR watershed as well.

3.2.1.4 Shallow landslides

In many soil-mantled, mountainous landscapes, shallow landsliding is an important sediment transport mechanism. Shallow landsliding links hillslopes, where sediment is produced as soil, to stream channels, where landslide material either remains in storage until it is scoured away by flood flow. These landslides also have the potential to mobilize into high-energy debris flows, which may travel far down-channel, scouring and depositing sediment along the way (*e.g.*, Dietrich and Dunne, 1978; Benda and Dunne, 1997).

A shallow landslide or soil slip occurs when sediment is destabilized on a steep hillslope or in an unchanneled valley. Such instability is affected by many factors including slope steepness, soil thickness and cohesion, and the presence or absence of tree roots and hydrologic flowpaths (e.g., Iverson et al. 1997, Roering et al. 2003). Many of these factors are directly affected by human activity. For example, the change in land cover from native scrub/shrub to exotic grasses has been shown to lead to an increase in landslide frequency in coastal southern California watersheds (Corbett and Rice 1966, Orme and Bailey 1971, Rice and Foggin 1971, Gabet and Dunne 2002). Shallow landslide scars are ubiquitous on soil mantled, steep slopes in the USCR watershed (see Figure 3-7 below).

Quantifying the relative importance of landsliding as a sediment transport mechanism is difficult without extensive field studies, but insight can be gained from recent research in the southern San Gabriel Mountains. Analysis of aerial photographs and field reconnaissance suggest that landsliding has contributed only about 10% of the material that has collected over the last 70 years in debris basins at the base of a series of small watersheds draining the San Gabriels (Lavé and Burbank 2004). The other 90% of the debris-basin sedimentation is presumably due to fluvial transport of material that has sloughed into channels by dry raveling and other slope processes. Long-term, however, the contribution from landsliding has been estimated to be substantially higher than the 10% inferred from short-term rates (Lavé and Burbank 2004). This is more consistent with previous studies, which also report proportionally large sediment contributions from landslides (Rice et al. 1969; Rice and Foggin 1971), and is probably because the 70-year sampling interval is too short to include large but infrequent slides that would substantially increase the sediment contribution from slope failures.

3.2.1.5 Deep-seated landslides

Deep-seated landslides incorporate mostly bedrock in the slide mass and do not travel long distances from their source areas. They are large (area >0.1 km^2) and generally occur on slopes that are conditioned for failure over the long term by factors such as channel incision, slope morphology, geologic structure, shear strength loss due to weathering, and lithologic variation (e.g., Miller and Sias 1998). Human activities that contribute to initiation of deep-seated landslides include mining and dam building (e.g., Voight 1978), and possibly also timber harvesting, road building, and changes in surface hydrology. Because they are large and relatively long-lived in the landscape, deep-seated landslides may persistently contribute sediment to streams at accelerated rates (e.g., Densmore and Hovius 2000, Mather et al. 2003). Numerous deep-seated landslides have occurred in the USCR watershed, as visible in published geologic maps of the watershed (Dibblee and USGS, various dates [see Appendix A]). Construction of the St. Francis Dam's left-side abutment in a paleo-landslide (formed in the highly sheared Pelona Schist bedrock unit) ultimately re-initiated mass movement of the slide materials, resulting in the catastrophic failure of the dam. A complete inventory of deep-seated landslides within the watershed is not currently available, but the San Martinez Grande landslide—located in the San Martinez Grande watershed and triggered by the Northridge Earthquake along with several other hillslope failures—is perhaps the biggest in the USCR watershed at 8,000,000 m^3 (Harp and Jibson 1996) (see Figure 3-2 below).

3.2.1.6 Sheetwash and rilling

Overland flow on slopes will occur if soils become saturated or if the rainfall rate exceeds the infiltration capacity of the soil (Horton 1945). Overland flow may sometimes be promoted by sparse vegetation and can occur either as a sheet of running water (called "sheetwash" or "sheet flow"), if areas of saturation and low infiltration are extensive, or in concentrated flow in shallow (1–10 cm deep) channels or "rills". Sheetwash and rilling can entrain soil particles and deliver them rapidily down slopes, leading to significant hillslope erosion.

Soil particles that are entrained in sheet flow move down the slope as "slope wash". The effectiveness of sheetwash as a sediment transport process depends on particle size and cohesion and on the extent and nature of vegetative cover. On hillslopes, such as those in the USCR watershed, sheetwash is most effective at moving particles that have already been detached by other processes, such as rainsplash and biotic activity, and/or in areas where vegetation cover has been denuded by natural or man-made disturbances (e.g., wildfires) (Wells 1981).

Concentrated overland flow in shallow rills continues the sediment detachment process on its own and, thus, substantially enhances sediment transport on slopes. Concentrated flow in rills can also increase runoff to channels during periods of intense rainfall (e.g., Wells 1981) by focusing water downslope before it has a chance to infiltrate into soils. Rills characteristically appear on many southern California slopes after fires, due to the development of water-repellant soil horizons (as discussed further in Section 3.2.3.3 below).

3.2.1.7 Gullying and channel head advance

Gullying on steep slopes, such as those in the USCR watershed, will occur under two scenarios: (1) rills previously formed on surfaces experiencing excessive overland flow concentration coalesce into a dominant, master rill, incising into the surface material; or (2) the upstream end of a tributary channel advances up-gradient (i.e., "channel head advance"; Selby 1993). Although some gullies can exist in isolation (i.e., situated upon a hillside with no connection with a stream channel), most do exhibit hydrologic connectivity with the drainage network. An increased occurrence of gullies in a given landscape is typically induced by land-cover changes, such as vegetation removal or other factors that alter drainage patterns and overland flow patterns in the watershed (e.g., ranching, urbanization, road construction).

3.2.2 Production and delivery of fine and coarse sediment

With continuous landscape uplift to drive hillslope processes and large areas of highly sheared and/or fractured igneous, metamorphic, and sedimentary rock units now hundreds of meters above the valley bottoms, the USCR watershed's geologic characteristics have a strong influence on erosion rates and spatial distribution. The eroded sediment is derived from four distinct sources (Figure 3-1), categorized as follows:

1. Competent crystalline and sandstones – Relatively durable and moderately fractured igneous (e.g., granite), meta-igneous (e.g., gneiss), and sandstone, chiefly found in the higher elevation and headwater areas of the watershed and primary producer of coarse-grained materials (Figure 1-4);
2. Weak metamorphics and sandstones – Moderately erodible and highly sheared/fractured rocks that erode into abundant sand, gravel, and cobble-sized clasts, primarily the Pelona Schist traversing San Francisquito, Bouquet, upper Mint, and upper Aqua Dulce canyons; and the geologically young, poorly consolidated sandstones/conglomerates flanking the Santa Clarita basin;

3. Siltstones – Easily erodible, fine-grained siltstone, mudstone, and claystone of the geologically young Pico and Castaic formations, primarily found interbedded with sandstone units in the western portions of the watershed (e.g., Pico Canyon and lower Castaic Creek); and
4. Unconsolidated – Easily erodible, mostly coarse-grained alluvial and colluvial material that deposited relatively recently along river valleys and as part of large paleo-landslides.

This four-part division into relative grain size and erodibility components is central in understanding the present behavior, and predicting the future behavior, of river channels such as the USCR. By analogy to other rivers world-wide, the fine-grained sediment load (i.e., with particle diameters <0.0625 mm) represents the majority of sediment that is delivered by hillslopes into the channel, and that is subsequently transported by the channel to the ocean. Field observations indicate that areas displaying relatively high hillslope erosion are chiefly underlain by the geologically younger sandstone/conglomerate and shale units, along with the highly sheared/fractured Pelona Schist. Although coarse-grained sediments are produced in much less voluminous quantities by the other geologic source terrains, these larger particles are particularly important to stabilizing channel bed morphology and, thus, supporting favorable aquatic habitat conditions and minimizing the need for channel management.

The processes and rates by which sediment is eroded off of hillslopes, and subsequently delivered to the channel network, vary substantially across the watershed. All rock units in the watershed produce some fraction of fine-grained sediments, although their relative proportion of fine to coarse particle sizes depend on the specific material properties and the local conditions (e.g., vegetation cover, land uses, and hillslope gradient). Coarse-bearing bedrock can produce fine-grained sediments when the rock already contains a fine matrix component or when biotic (e.g., tree throw or gopher burrowing) or abiotic (e.g., bedrock dissolution or abrasion during transport) processes occur. Fine sediment production from predominately coarse-bearing bedrock is evident by the presence of a mixed-size soil mantle throughout the watershed, not just in those areas underlain by fine-grained rock units.

Overall, the fine-grained rocks are generally very susceptible to erosion, especially in the absence of vegetation, whereas the coarse-grained rocks are generally less so. By analogy to other studies, rates of sediment delivery from the fine-grained rocks (and rocks having a mix of grain sizes) should vary most directly with hillslope gradient and vegetation cover (Reid and Dunne 1996). Observations throughout the USCR watershed affirm this principle, recognizing that vegetation cover is both a cause and an effect of relative hillslope stability. Lack of vegetation cover enhances the rate of sediment delivery; but where the ground is unstable or eroding rapidly, vegetation does not grow well.

Further discussion on fine and coarse-sediment producing areas of the watershed is presented below in Section 3.3.4.

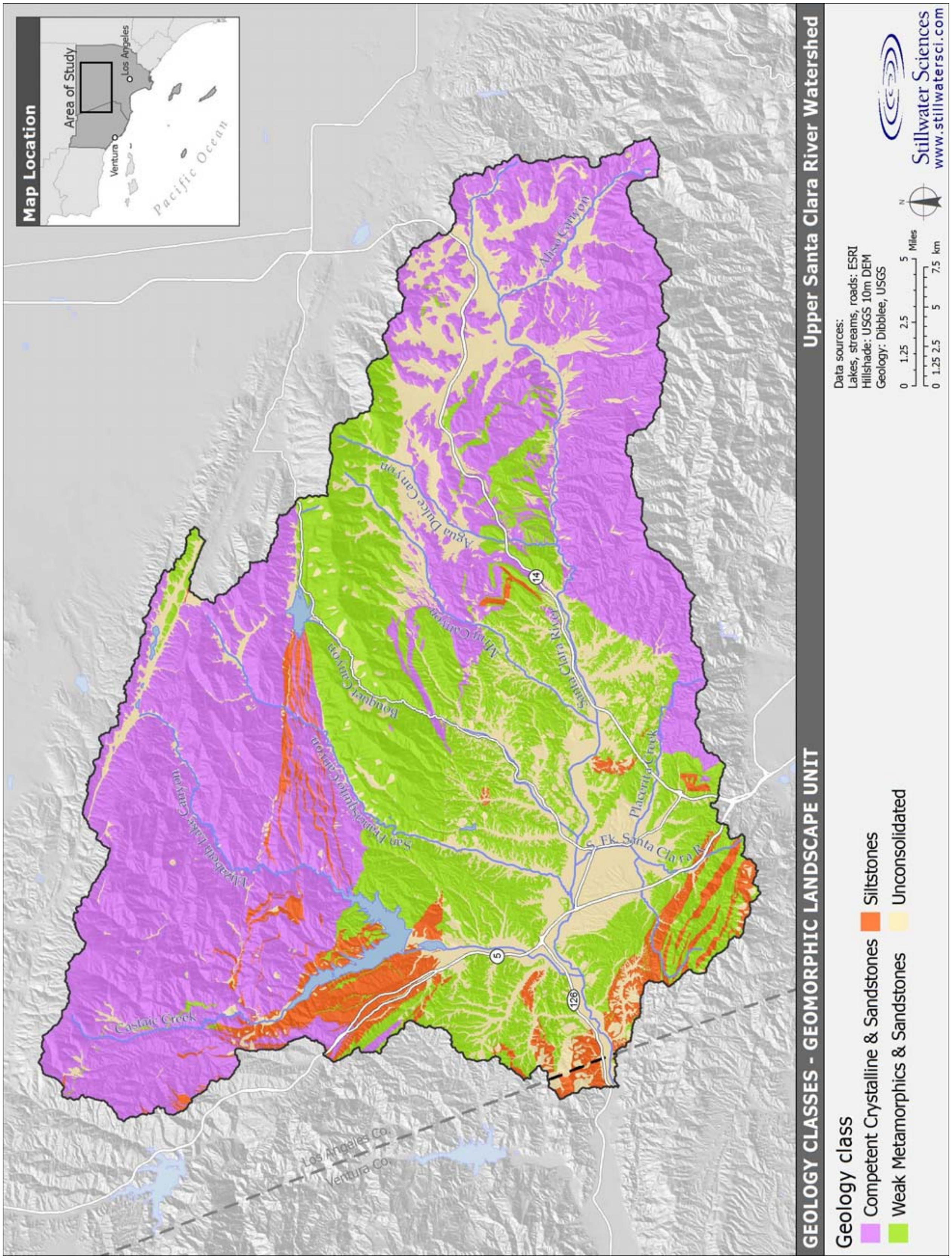

Figure 3-1. Generalized geologic rock unit categories used for analysis of watershed-scale sediment production.

3.2.3 Factors affecting hillslope sediment production

In the USCR watershed and elsewhere in southern California, there are several dominant forces that directly affect hillslope sediment production and, thus, sediment delivery to the drainage network. This section discusses these natural and man-made forces: storms, earthquakes, wildfire, and human-induced land cover change.

3.2.3.1 Large storms

Slope failures, whether shallow or deep-seated, are usually associated with a triggering event, particularly a storm of prolonged duration or high intensity. Heavy rains brought by the El Niño event of 1997–1998 triggered thousands of shallow landslides throughout California; in nearby Sedgwick Reserve, for example, more than 150 slides occurred in a scant 9.5 km^2 (Gabet and Dunne 2002). Slope failures are more likely to be triggered in areas that have recently been destabilized by human or natural disturbances, such as fire, which destroys vegetation and roots and thus reduces soil cohesion. A discussion on El Niño events as they relate to peak streamflow events in the USCR is presented below in Section 4.1.3.

3.2.3.2 Earthquakes

Ground motions during earthquakes can also trigger landslides. The USCR's location within the seismically-active San Andreas Fault system (Figure 1-4), makes its slopes especially prone to earthquake-induced landsliding—a potentially significant source of both coarse and fine sediment for the river corridor. The low tensile strength and high relief of bedrock in the watershed generally results in steep, easily eroded canyon walls that are susceptible to failure during seismic events.

In 1994, a Magnitude 6.7 earthquake triggered nearly 7,400 landslides across the entire Santa Clara River watershed (Figure 3-2) (Harp and Jibson 1996). The most intense area of landslide activity occurred in the Santa Susana Mountains bordering the southwestern portion of the USCR watershed, in deformed siltstone and sandstone of the Pico and Castaic formations having little cementation and thus low tensile strength. Most of the earthquake-induced slides were shallow, with depths less than 5 m and an average volume of less than 1,000 m^3. However, some individual slides had volumes exceeding 100,000 m^3. Several tens to possibly hundreds of slides were deep (>5 m) slumps, including the previously noted San Martinez Grande deep-seated slide (Harp and Jibson 1996).

Although the shallow landslides typically traveled considerable distances (>50 m) downslope from their source areas (Harp and Jibson 1996), not all of the material that was mobilized during the Northridge earthquake was immediately transported downstream to the mainstem river. Numerous landslide deposits remained intact in tributary channels where they came to rest immediately after being triggered by the earthquake (A. Orme, pers. comm., 2005). Examination of recent aerial photographs taken at the location of the large San Martinez Grande landslide show that this large deposit has remained largely intact since 1994. Even so, subsequent storms have likely led to the erosion of stored materials at most or all of the landslide locations; exactly how much of the sediment remains in the watershed is unknown. Transport of that material could be reactivated by future earthquakes or intense storms and thus add significantly to the sediment load of the USCR. Given that the majority of these landslides were located at the west side of the USCR watershed (i.e., downstream end), any increase in sediment delivery from the continued erosion of these features would result primarily in increased sediment delivery to the mainstem LSCR, rather than the USCR.

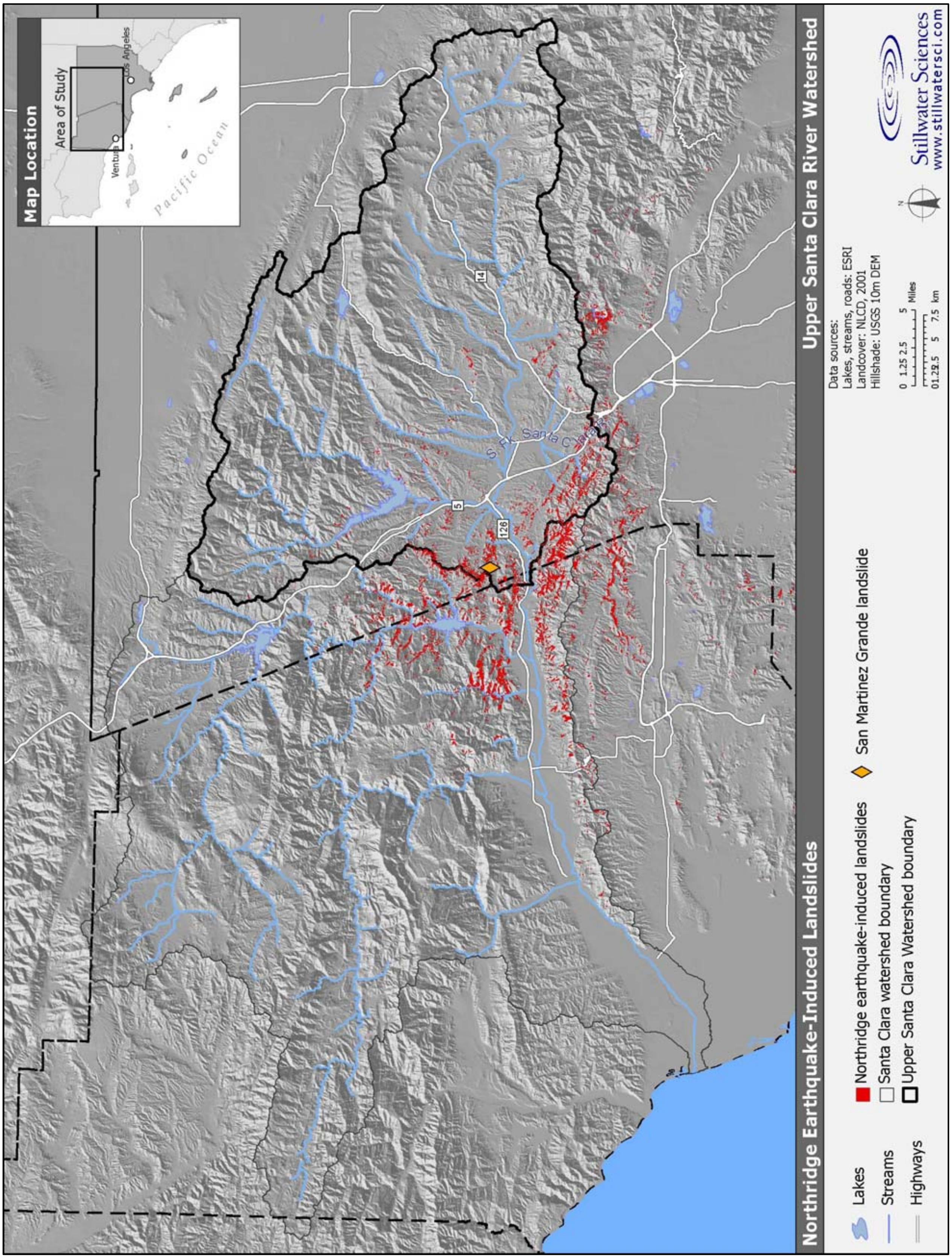

Figure 3-2. Landslides triggered by the 1994 Northridge earthquake (*M*=6.7). Hundreds of landslides occurred in the USCR watershed.

3.2.3.3 Wildfire

Wildfires have always been a significant contributor to hillslope erosion throughout the entire SCR watershed. Wildfires often contribute to drastically accelerated rates of sediment supply in subsequent years: hillslopes in steep, semi-arid to arid lands during the post-fire period can respond to winter rains with increased runoff and accelerated erosion, which results in debris flows, landslides, and floods—thus completing what has been dubbed the “fire–flood” sequence (USFS 1954).

In the USCR watershed, the landscape is dominated by large areas of contiguous chaparral vegetation, which is fire-dependent for germination and regeneration and thus has a proclivity to burn (Keeley et al. 1981, Keeley 1987). In addition to the type of vegetation, climate, soil type, and fire history patterns all play a primary role in controlling fuel conditions for fires within the watershed. Currently, most of the USCR watershed is designated as open space, much of it within (and surrounded by) the Angeles National Forest (Figure 1-1). As these areas are generally undeveloped with nominal fuel-control efforts and large stands of older chaparral vegetation, wildfires continue to control vegetation generation as well as affect hydrologic and geomorphic dynamics within the watershed at varying spatial and temporal scales (Bendix and Cowell 2010).

Historical trends in the USCR watershed

Over the past century, the majority of the USCR watershed has been burned by wildfire (Figure 3-3). Most of the watershed has been burned at least twice in the last century, with many areas of the watershed that are characterized by supporting mostly scrub/shrub vegetation burning up to 9 times since 1878 (CDF FRAP 2010). Fire frequency is highest in the areas surrounding the Santa Clarita basin, with the highest burn frequency occurring along lower Castaic Creek near Hasley Canyon—an area also heavily impacted by landslides triggered during the 1994 Northridge earthquake (see above). Further, the areas burned more frequently also overlie the generally weaker rock units that are more prone to erosion compared with the more competent rock units located in the headwaters of most of the major tributaries (see Figure 3-1 and Section 3.3).

Examination of the historical wildfire records (CDF FRAP 2010) reveals that, between the years of 1911 and 2009[1], the average annual burned area within the USCR watershed is approximately 30 km^2 (7,340 ac), with a slight increase in the average amount of burned watershed area over this duration. As Figure 3-4 shows, a cyclical pattern emerges that is characterized by an approximate 40-year return period of peak maximum burned areas. Studies in the surrounding region have found similar patterns and return intervals in peak events (e.g., Mensing et al. 1999). For the USCR-specific data, there are three periods represented—pre-1911–1928, 1929–1970, and 1971 to approximately present day—each with similar trends whereby the peak events progressively increase over the period and then re-sets to much lower magnitudes, upon which a new period has been initiated. Also observable in this plot is that the three largest peaks in the data closely follow three of the largest flood seasons during this timeframe, with the exception of the 1938 and 1983 flood seasons (see Figure 2-1). That is, the peak burn years of 1921, 1970, and 2007 respectively follow the flood seasons of 1914[2], 1969, and 2005. Mensing et al. (1999) and Kelley and Zedler (2009) found that large fires in the region consistently occur at the end of wet periods and the beginning of droughts, which is consistent with our findings for the USCR watershed (see Figure 2-1). Wildfire occurrence, intensity, and areal extent in any given year, however, are locally influenced by summer/fall temperatures, presence and strength of Santa Ana winds, available fuel supply, natural fire ignition events (e.g., lightning), and human actions

[1] There is a continuous series of wildfire event records between these years.
[2] Although the 1914 floods were not measured, this flood season was reported in numerous anecdotal accounts to have been very significant throughout the entire SCR watershed (Freeman 1968).

(Keeley and Zedler 2009). This indicates that small and large fires in the future have the potential to occur during any given year in the USCR watershed, but that the largest ones (in terms of most watershed area burned in a given year) will likely continue to follow the flood-drought climatic cycle of the region. Additional discussion on fire management effects is presented below.

The ten largest fires, in terms of areal extent, are summarized in Table 3-2 and shown in Figure 3-5; the largest of these fires—the Buckweed Fire of 2007—burned nearly one-tenth of the USCR watershed area. The most recent significant event was the 2009 Station Fire, which burned a substantial portion of the Angeles National Forest in the San Gabriel Mountains, extending northward into the USCR watershed. The headwaters of Aliso Canyon were observed during our field surveys to have experienced considerable burn damage (e.g., vegetation denudation and charred soils). Photographs taken of the recently burned landscape in Aliso Canyon (2009 Station Fire) and of recovering hillslopes in Haskell Canyon (2007 Buckweed Fire) show examples of how hillslopes physically change in response to and recover following large wildfires (Figure 3-6).

Table 3-2. Ten largest documented fires in the USCR watershed for the period (1878-2009) in rank order of their area of influence across the watershed.

Fire name [a]	Portion of watershed	Year [a]	Total burn area [a]		Burn area within USCR watershed [b]		% of USCR watershed burned [b]
			km^2	ac	km^2	ac	
Buckweed	Bouquet, Mint, and San Francisquito canyons	2007	155	38,347	155	38,347	9.2
Liebre	Upper Castaic Creek	1968	197	48,564	130	32,190	7.8
Unnamed	Soledad Canyon reach of USCR	1960	115	28,393	110	27,177	6.6
Station	Upper Aliso Canyon	2009	644	159,158	93	22,932	5.5
Ravenna	Ravenna and into Soledad Canyon reach of USCR	1919	289	71,373	89	21,904	5.3
Agua Dulce	Lower Bouquet and Mint canyons	1970	88	21,756	88	21,756	5.2
Unnamed	Elizabeth Lake Canyon	1924	98	24,239	78	19,189	4.6
Copper	San Francisquito Canyon	2002	77	19,102	77	19,102	4.6
Mint Canyon	Upper Mint Canyon	1922	83	20,512	71	17,637	4.3
Marple	Upper Castaic Creek	1996	80	19,860	66	16,303	3.9

[a] Source: CDF FRAP (2010).
[b] Proportion of fire extent within the total watershed area determined in GIS.

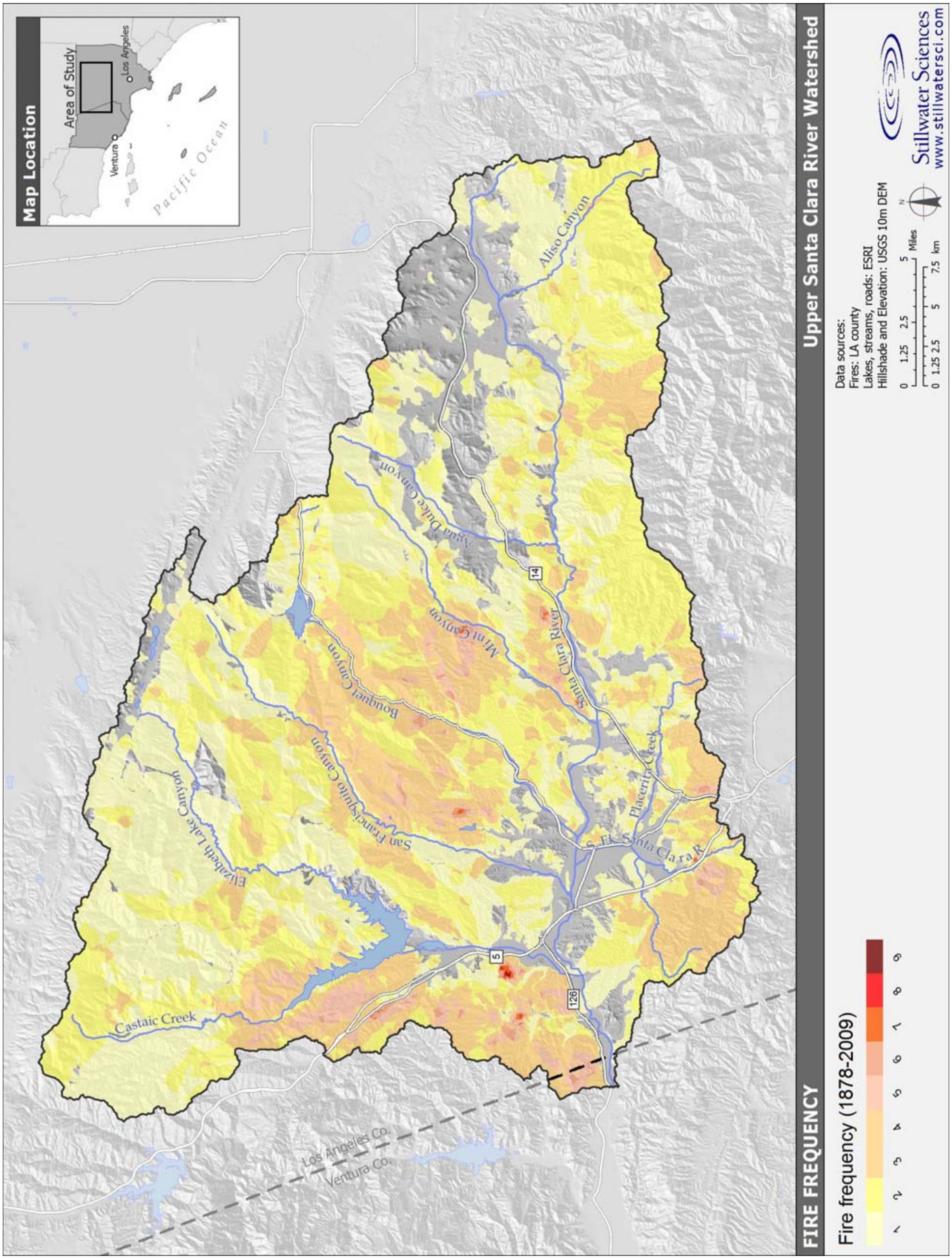

Figure 3-3. Frequency of burn events in the USCR watershed (1878–2009).

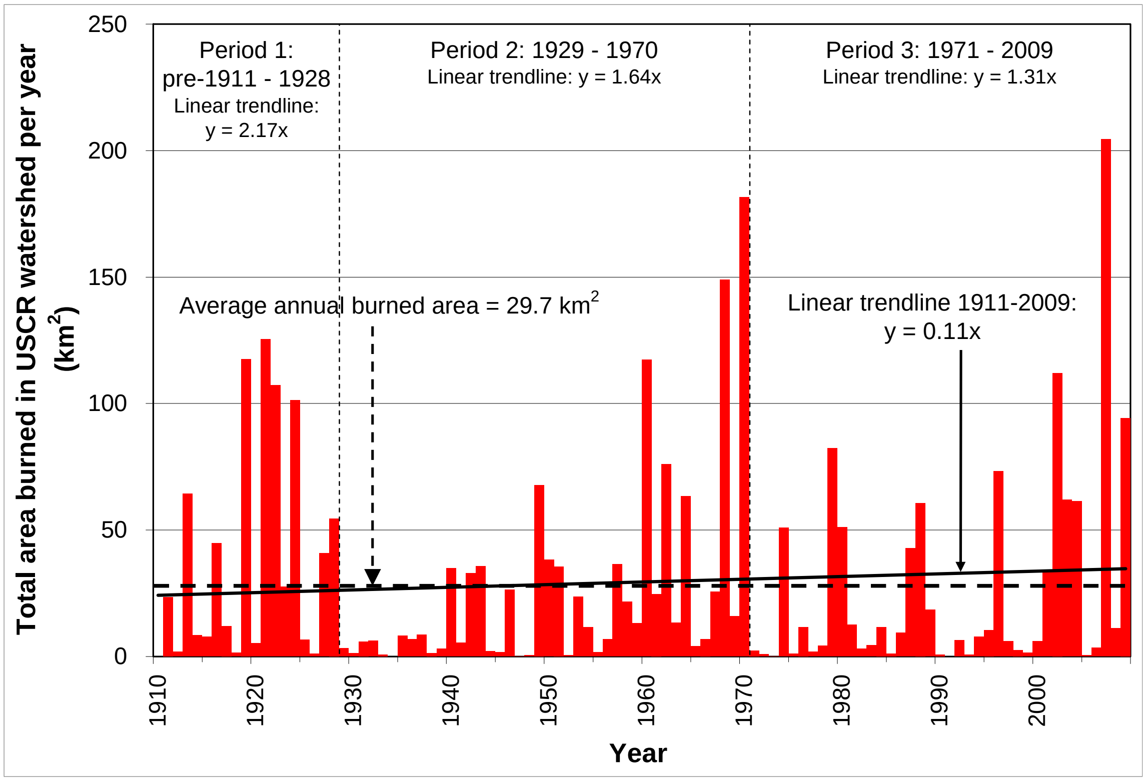

Figure 3-4. Total area of the USCR watershed burned annually from 1911–2009 and the three periods of increasing peak magnitudes contained therein (source: CDF FRAP 2010).

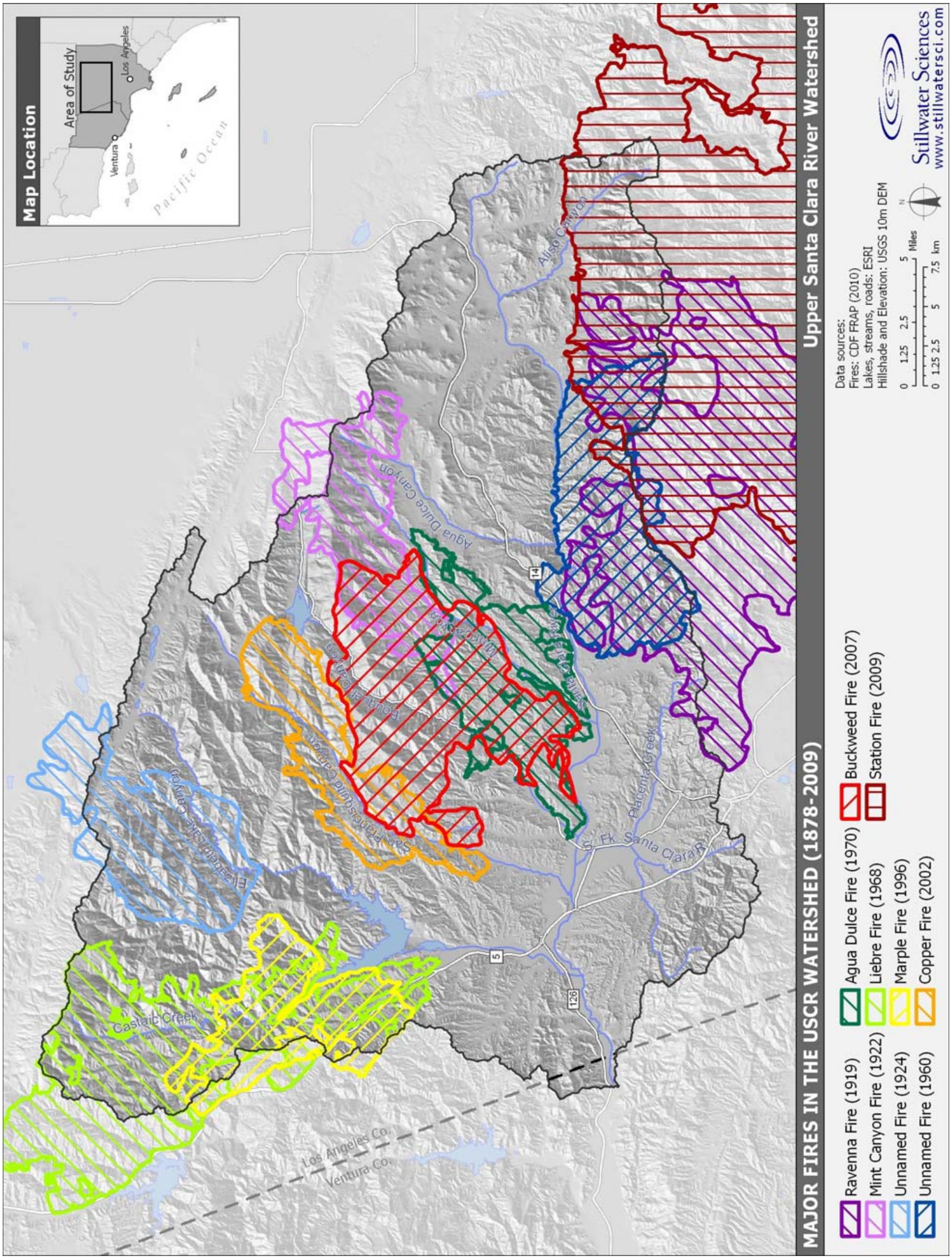

Figure 3-5. The ten largest fires in the USCR watershed (1878-2009).

Figure 3-6. Fall 2009 views of two recently burned landscapes in the USCR watershed: the denuded hillsides in upper Aliso Canyon recently burned by the 2009 Station Fire (upper); and vegetation regrowth two years after the 2007 Buckweed Fire in upper Haskell Canyon (lower).

Impacts of wildfire on sediment dynamics in chaparral environments

Wildfire can cause significant physical changes to watershed ground surfaces, thereby affecting geomorphic and hydrologic processes responsible for the production and delivery of sediment to adjacent channels. Impacts include both direct changes to the physical properties of rocks and soil, and changes to geomorphic and hydrologic process rates until pre-fire conditions are reestablished (Shakesby and Doerr 2006). These changes can reduce the infiltration rate by an order of magnitude, shift the dominant runoff process from subsurface storm flow to overland flow, and increase peak flows and sediment yield by more than two orders of magnitude (see Larsen and MacDonald 2007 and citations therein). The primary changes to watershed ground surfaces induced by wildfires include removal of vegetation, alteration to soil physical and chemical structure, and changes to rates of bedrock and *in situ* coarse sediment erosion. The specific geomorphic and hydrologic impacts associated with these wildfire-induced changes are described below.

Vegetation and runoff

Removal of vegetation by wildfire increases overland flow and soil losses relative to undisturbed watersheds (see Shakesby and Doerr 2006 and the citations therein), and in general these changes tend to be directly related to fire severity (a function of fire duration and intensity; Prosser and Williams 1998). Vegetation removal can be important in post-fire hydrologic response as it temporarily reduces or stops transpiration, interception, and surface storage of precipitation, thereby increasing the relative percentage of post-fire precipitation that results in overland flow (Tiedemann et al. 1979, Loaiciga et al. 2001). Within chaparral environments, changes to vegetation cover from wildfire have been shown to increase the amount of post-fire overland flow by over 7 times the values on unburned hillslopes (Wells 1981), and vegetation re-growth 3 years after a wildfire has been shown to decrease overland flow by almost 80% of the value immediately after the fire (Cerdà and Doerr 2005). With respect to soil loss, fire-induced vegetation removal can cause both a loss of natural check dams of coarse organic material that act to store sediment on hillslopes, and an increase in the bare surface area available for erosion, thereby increasing the overall amount of post-fire sediment delivered to channels (Wells 1981). Fire-induced reduction in vegetation cover can also increase soil erosion by direct rainsplash, causing erosion by subsequent overland flow to occur more readily compared to pre-fire conditions (Shakesby and Doerr 2006).

Soil properties

Many researchers consider the effects of rainsplash as one of the most important factors leading to increased post-fire soil erosion (Shakesby and Doerr 2006). High temperatures can cause hydrophobic organic substances in topsoil to become volatile and attach to soil particles in the soil subsurface, thereby making the subsurface soil more hydrophobic and causing the infiltration to decrease (Doerr et al. 2005). Terry and Shakesby (1993) have shown that post-fire water-repellent soils can remain non-cohesive during precipitation events, thereby making soil particles more easily detached by rainsplash. For example, fire-induced soil water repellency has been shown to increase overland flow by 1.5 to 3 times over values in un-burned areas (Prosser 1990). High temperatures associated with wildfires have also been shown to decrease the relative distribution of clay particles in a soil, thereby decreasing the soil cohesion and increasing the soil's erosion potential (Duriscoe and Wells 1981). Recent laboratory studies by Moody and Smith (2005) show that unburned cohesive forest soils can have critical shear stresses for erosion initiation that are over five times greater than those for the same soils rendered non-cohesive by wildfire. These studies have also shown a similarity in the temperature thresholds for changes to soil water repellency and the critical shear stress for soil erosion initiation, suggesting an inherent link between the two soil properties (Moody and Smith 2005).

Other physical changes to the soil induced by wildfires include removal of the top organic litter layer and changes to the particle-size distribution (i.e., amount of sand, silt, and clay) of the soil. The differences in the amount of organic litter removed by fire can have a significant impact on the amount of precipitation that infiltrates. Copeland (1965) showed that for a litter cover of 60 to 75% essentially all of the simulated precipitation was infiltrated, whereas for a 10% litter cover only 27% of precipitation was infiltrated. Burning of soil during wildfires thus typically results in soil that is more friable, less cohesive, more water-repellent, and more erodible (DeBano et al. 1998, Scott et al. 1998, Neary et al. 1999, Doerr et al. 2005), although the specific fire-induced changes to the soil physical properties depend largely on soil type and the soil temperature reached during the fire (DeBano et al. 1998).

Rock weathering

Fire effects on rock erosion rates are primarily a function of fire temperature and rock physical properties, which include lithology, surface area, and water content, and are manifested through two dominant processes: spalling (detachment of lensoid-shaped fragments up to 3 cm in length) and actual rock fracture. In general, fire temperature and rock properties act to decrease the rock strength, thereby making the rock more susceptible to subsequent erosion. A laboratory analysis by Goudie et al. (1992) showed that igneous rocks have a relatively larger decrease in rock strength associated with increasing temperature than sedimentary rocks, and at temperatures indicative of chaparral wildfires (685°C, as reported in Wright and Bailey 1982), the granite tested had an 80-90% decrease in rock strength, whereas the sandstone tested had only a 20% decrease in rock strength. Specifically, spalling associated with wildfires can result in the erosion of several centimeters from a rock surface (Dorn 2003) and has been shown to be influenced strongly by lithologic characteristics. For instance, Ballais and Bosc (1994) noted post-fire spalling on sedimentary rock (limestones and sandstones), but observed no post-fire spalling on metamorphics (gneisses and schists). In the USCR watershed, we observed spalling on charred granitic (Lowe Granodiorites [igneous rock]) river cobbles and boulders in the recently burned areas of Aliso Canyon (Figure 3-7). Rock fracture of large boulders on hillslopes following wildfires has been shown to be an important agent in creating smaller, more mobile clasts. In those arid and semi-arid environments where chemical weathering of rock surfaces can be slow and depth-limited, it has been suggested to be a key mechanism for landscape evolution (Dragovich 1993, Dorn 2003).

Figure 3-7. Photographic example of observed spalling of a granodiorite boulder burned in upper Aliso Canyon during the 2009 Station Fire.

Impacts on rates of sediment production and delivery

Most studies of fire effects cannot directly calculate increase in sediment production because data on pre-fire sediment rates are typically lacking, but they can quantify post-fire rates in detail. From a compilation of 25 measured post-fire rates (Shakesby and Doerr 2006, their Table 3), first-year post-fire erosion measurements for watersheds ranging in size from <0.001 km^2 to >5 km^2 range between 0–41,400 tonnes per square kilometer (t km^{-2}) with a median value of about 6,000 t km^{-2}. The lone San Gabriel Mountain study reported in this compilation (from Krammes and Osborne 1969) measured 19,700 t km^{-2} from three small plots with a combined area of less than 100 m^2.

Those studies that do quantify the changes in runoff and sediment yield following fire have been concentrated in semi-arid regions of the world with vegetative and climatic characteristics similar to southern California, and so many of the results should have broad applicability to the USCR watershed. From local studies, De Koff et al. (2006) measured a 6.6-fold increase in sediment yield from a prescribed burn in chaparral-covered southern California; Wells (1981) documented up to ten- to hundred-fold increases in sediment transport rates in woodlands of the San Gabriel Mountains. Other short-term increases in erosion rates following wildfires in chaparral-dominated southern California watersheds include factors ranging between 18-fold (Wohlgemuth 2003) and 35-fold (Rowe et al. 1954) increases over long-term pre-fire values. Most of these increases can be attributed to increases in dry raveling rates, both during and immediately after fires, and increases in sediment delivery along post-fire rills (Wells et al. 1987, Wells 1987).

Reported rates tend to decline rapidly following the first year of post-fire rains, which leads to a so-called “window of disturbance” (Prosser and Williams 1998) that begins immediately after a wildfire and can vary in length from several seconds to a decade, depending on fire and watershed characteristics (Figure 3-8). For instance, Doerr et al. (2000) showed that wildfire can affect soil infiltration characteristics and sediment production and delivery dynamics for periods ranging up to several months, depending on fire duration and intensity. Other research has shown that the overall cumulative impact of fire on sediment production and delivery dynamics can be on the order of years, with impact durations ranging from 2–4 years (Wohlgemuth et al. 1998) to up to 10 years after the fire (LACFCD 1959, USFS 1997). One study that specifically assessed coarse sediment production separately found elevated rates for at least five years following a burn (Reneau et al. 2007). The 5 years following a fire has been suggested to be the most critical for fire-induced sediment production (Lavé and Burbank 2004). Because of very high rates immediately post-fire, however, wildfire still may account for 50% (Davis et al. 1989) to 80% (Lavé and Burbank 2004) of the total long-term sediment production and subsequent delivery within chaparral-dominated southern California watersheds.

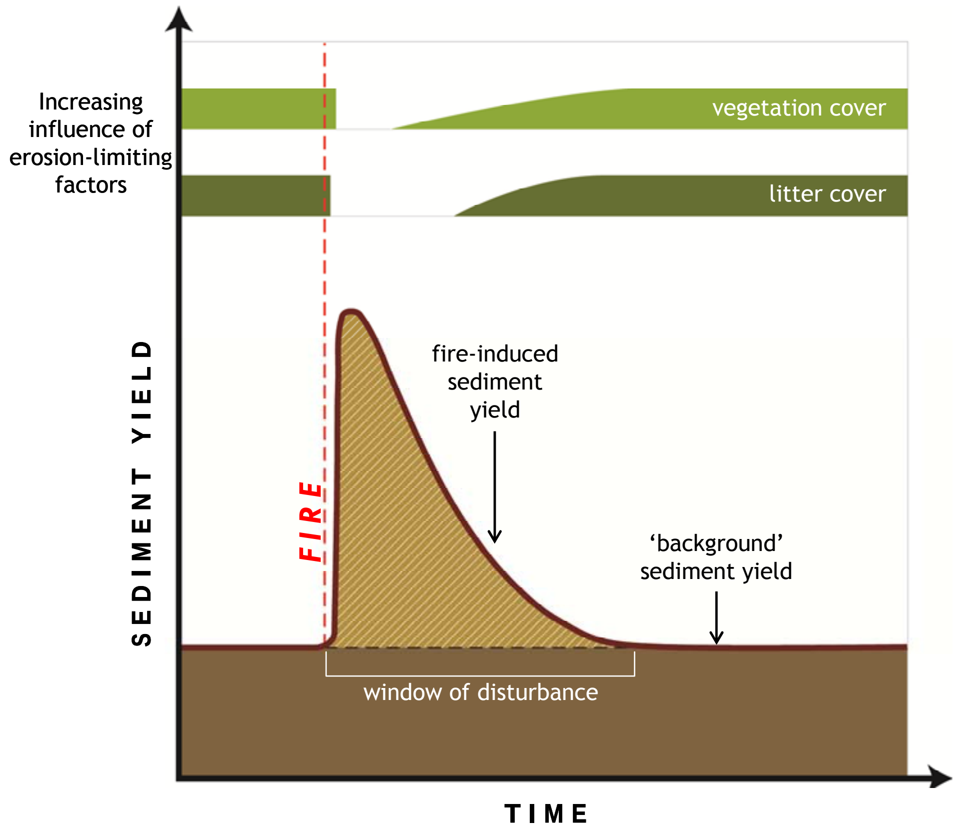

Figure 3-8. Conceptualization of sediment yield and associated vegetation and litter recovery during the fire-induced "window of disturbance" (based on Shakesby and Doerr 2006).

3.2.3.4 Human-induced land cover change

Rates of sediment production and transport on slopes can be significantly altered by human disturbance and changes in land management practices. This most certainly has been the case in the USCR watershed as a whole.

Today, significant changes in the watershed are due to expanding urbanization and changes in the way lands are managed for fire suppression. Historically, major changes followed the arrival of Europeans, the onset of extensive grazing, the California Gold Rush (which accelerated range degradation), agricultural development in the early 1900s, and the population boom that followed World War II (Willis and Griggs 2003).

Effects of European settlement on sediment transport rates

Records indicate that European settlement of coastal southern California led to the degradation of native grasses on slopes starting in the early 1800s, the appearance of widespread barren lands by the mid- to late 1800s, and domination by non-native animals of rangelands by the late 1800s (Pulling 1944). This has led to significant increases in sediment yields in modern times; rates of offshore sedimentation along coastal southern California during the 20th century are many times more than they were in pre-colonial times (Sommerfield and Lee 2003). Moreover, peak rates of sedimentation in estuaries along the California coast appear to have occurred in mid- to late 19th century, coinciding with the peak degradation of rangelands (Willis and Griggs 2003, Warrick and Farnsworth 2009). Conversely, the construction of dams has served to reduce the accentuated sediment yields. In the entire SCR watershed, it has been estimated that dams have reduced the suspended-sediment flux by about 45% since the construction of the watershed's dams (Warrick and Farnsworth 2009).

Effects of conversion to non-native grasses on landslide frequency

The non-native annual grasslands of the Transverse Ranges have been shown to be three times more susceptible to mass wasting than native brush and chaparral (Rice and Foggin 1971). Analysis of 150 landslides at Sedgwick Ranch, north of Santa Barbara, confirms that conversion of native scrub/shrub to exotic-dominated grassland can lead to an increase in landsliding frequency (Gabet and Dunne 2002) and, presumably, sediment yield. When scrub/shrub cover was converted to grassland, soils became unstable (Rice et al. 1969, Orme and Bailey 1971) because the effective cohesion imparted by the shallow-rooted grass was lower than it had been for the deeper-rooted scrub. This instability led to progressive thinning of soils over time by landsliding, which will presumably continue until soils become thin enough that the shallow-rooted grass can stabilize them against failure. There is some indication that slopes may never stabilize under the new land cover, due to the high moisture-holding capacity of root masses (A. Orme, pers. comm., 2005). In any case, sediment yields under non-native grasses are likely to stay higher than they were under natural conditions (unless soil depth eventually adjusts to the new root cohesion). This is an example of a land-use "legacy" on geomorphic processes: the conversion to grassland from native scrub/shrub continues to affect sediment yields long after the land-use change was initiated. Such legacies are important throughout the USCR watershed.

Fire management

Given the dramatic, accelerating effects of fire on hillslope sediment transport (discussed above), it is worth considering whether land management practices have affected fire frequency and thus contributed indirectly to increased sediment production in the watershed.

These considerations were the focus of a recent study of the frequency of big fires in the Los Padres National Forest (Santa Barbara and Ventura counties) area (Mensing et al. 1999). Charcoal layers in sediment from the offshore Santa Barbara Basin, fed predominately by the SCR (51%), were used to derive a 560-year record of fires with area greater than 200 km^2, revealing that the recurrence interval has remained constant at 20–30 years over the period of record, despite substantial changes in management practice. Historical records indicate that the Chumash (coastal) and Tantaviam (Santa Clarita Valley) Indians managed vegetation for thousands of years by burning slopes until the late 1700s, when European settlers began practicing fire prevention by, for example, outlawing fires in wildfire-prone areas (Mensing et al. 1999). A more active approach, emphasizing quick-response fire suppression, was adopted in about 1900 and continues to be used today. The unchanging frequency of big fires over a 560-year period that was marked by changing fire management suggests that big fires are a natural part of the environment, occurring regardless of what coastal residents have been doing to suppress or prevent them (Mensing et al. 1999; Keeley and Zedler 2009). This challenges previous indications, from analysis of a time series of LANDSAT imagery (Minnich 1983), that big fires are an artifact of changes in vegetation distributions due to increased fire suppression.

Conversely, smaller fires, which may affect sediment yields locally, may be much more closely related to changes in land management practices and the growing urban footprint that has effectively placed people closer to fire-susceptible landscapes. Analysis of data from the Los Angeles County debris basins suggests that encroaching urbanization in southern California wilderness has increased overall fire frequency (Lavé and Burbank 2004), a finding supported regionally by Keeley and Zedler (2009) who concluded that the frequency (not areal extent) of small fires has increased in recent years due to human ignitions. Sediment yields and fire history from the small watersheds that feed the debris basins, considered together, suggest that anthropogenic fires (i.e., fires caused by human inhabitants rather than natural causes) have augmented sediment yields by as much as 400% in particular watersheds, with an average of all data equal to 60% (Lavé and Burbank 2004). An earlier analysis of the same debris basin data, however, yielded inclusive results about the effects of fire frequency on sediment yield (Brozovic et al. 1997, Booker 1998), which is consistent with the findings of Mensing et al. (1999) and Keeley and Zedler (2009) that both found that the incidence of large fires in the region has not increased over time.

Taken together, these disparate results suggest that although the frequency of fire may have increased with human encroachment into fire-susceptible regions, their effects on long-term sediment yield are difficult to quantify precisely. Discussion on sediment yields measured in the debris basins of the USCR watershed is presented below in Section 3.3.3.

3.3 Rates of Hillslope Processes

Watershed topography reflects the interplay between uplift (if any) due to tectonic processes and the sculpting and wearing away of slopes by erosion. In general, high steep mountains occur in areas that have been subjected to sustained rapid uplift, whereas gently sloping terrain is found where uplift is slow or has been followed by long periods of denudation. The linkages between uplift, slope steepness, and erosion imply that slopes should tend to contribute sediment in proportion to their uplift rates over the long term (Burbank et al. 1996). Uplift rates, in turn, are directly related to the tectonic setting and deformation history of the landscape (see Section 1-3).

3.3.1 Rates of rock uplift

The mountains of the region have been uplifted over millions of years by a complex series of processes at the boundary between two tectonic plates (Blythe et al. 2000, Meigs et al. 2003). Long-term average uplift rates from the region's mountain ranges are among the fastest on record for the continental United States. In the San Gabriel Mountains, Blythe et al. (2000) looked at the cooling history of mineral grains, which can indicate the age at which rocks now at the surface were buried at least several kilometers deep in the crust. The younger that age, the more rapid has been the exhumation of the overlying material. Based on such data, Blythe et al. (2000) determined likely uplift rates averaging as high as about 1 millimeter per year (mm yr^{-1}) in the eastern San Gabriel Mountains, with less well-determined but significantly lower rates in the western San Gabriel Mountains. These rates are somewhat lower than the 0.75 to >5 mm yr^{-1} range of uplift rates that has been reported for the Santa Ynez Mountains, which rise along the coast northwest of the SCR watershed (Metcalf 1994, Trecker et al. 1998, Duvall et al. 2004). A recent summary of coastal uplift rates for the Transverse Ranges region reports an even broader range of 0.05 to 9 mm yr^{-1} (Orme 1998).

Within the boundaries of the USCR watershed, the Holser Fault—a reverse fault that follows a trace that closely aligns with the San Cayetano Fault to the west (see Figure 1-4)—has been estimated to have experienced displacement rates of up to 0.4 mm yr^{-1} (Peterson et al., 1996). Another thrust fault with reported dip-slip estimates is the Santa Susana Fault, which parallels the Holser Fault to the south and trends close to the southwest corner of the USCR watershed. Peterson and Wesnousky (1994) and Wills et al. (2008) predicted a relatively high slip rate of up to 5 and 8 mm yr^{-1}, respectively, along this thrust fault, which is in the same order of magnitude of estimates along the San Cayetano Fault to the west. There are no known estimates of dip-displacement rates along the other major faults in the USCR watershed—Clearwater, Pelona, Mint Canyon, and Soledad—as these faults do not exhibit significant vertical movement.

Rates of bedrock denudation from granitic slopes in the San Dimas Experimental Forest (southern San Gabriel Mountains) have been reported to range from 0.05 to 0.46 mm yr^{-1} (average = 0.29 mm yr^{-1}), based on methods that average denudation rates over 1,000-year time scales (Heimsath 1998). These averages are at the low end of the range of rates implied by the long-term, million-year average uplift rates of the San Gabriel Mountains. Assuming a bedrock density of 2.6 tonnes per cubic meter (t m^{-3}) (typical for granite, which underlies much of the USCR watershed), the average bedrock denudation rate corresponds to equivalent soil production rate of 750 tonnes per square kilometer per year (t km^{-2} yr^{-1}).

Table 3-3. Summary of rates of uplift, displacement, sediment production, and sediment yield.

Location	Rate expressed as landscape denudation rate (mm yr^{-1})			Rate expressed in sediment production units (t km^{-2} yr^{-1}) [a]			Reference
	Low	High	Average	Low	High	Average	
Rates of Uplift and Dip-displacement							
San Gabriel Mts.	<0.1	1.0	—	<260	2,600	—	Blythe et al. 2000
Santa Ynez Mts.	0.75	>5.0	—	1,950	13,000	—	Metcalf 1994, Trecker et al. 1998, Duvall et al. 2004
Transverse Ranges (all)	0.05	9.0	—	130	23,400	—	Orme 1998
San Cayetano Fault	1.1	8.8	—	2,900	22,900	—	Rockwell 1988
Holser Fault	>0	0.4	—	>0	1,040	—	Peterson et al. 1996
Santa Susana Fault	>2	>8	—	>5,200	>20,800	—	Peterson and Wesnousky 1994, Wills et al. 2008
Regional Rates of Sediment Production from the Transverse Ranges							
San Gabriel Granite	0.05	0.46	0.29	130	1,200	750	Heimsath 1998, Appendix 2

[a] Uplift rates are converted to sediment production units under the hypothetical assumption that rates of mountain uplift are roughly balanced by rates of hillslope erosion (such that topography does not change over time); conversions from length per unit time into sediment production rate units use bedrock density = 2.6 tonnes m^{-3}. Blank entries indicate rates were not reported or are not applicable.

In summary, published rates of crustal uplift surrounding and within the USCR watershed range from about 0.1 mm yr^{-1} up to 9 mm yr^{-1}, with the fastest rates to the west along the Transverse Mountains and the slowest rates to the south along the San Gabriel Mountains. Based on overall watershed physiography and the limited degree of deformation observed in the sedimentary rocks here, with some notable exceptions in the Pico Formation (near the active Santa Susana Fault), we infer that uplift rates in the watershed are at most one to a few mm per year. "Uplift rates," however, do not directly translate into erosion rates or sediment production rates, particularly in still-active mountain belts, and so long-term sediment production averaged across the USCR watershed is probably somewhat less than this range.

To move beyond this broad constraint on predicted sediment production using evidence from tectonic uplift, however, requires a more refined assessment. This geologic-based assessment, however, provides a useful constraint for evaluating the predicted magnitude of sediment production derived using other, independent approaches.

3.3.2 Rates from cosmogenic nuclide sediment dating

As a refinement on the estimates of erosion rates and sediment yields outlined above, a complementary analysis was conducted involving cosmogenic nuclide dating of sediments. This data also serves as an independent check on the watershed-wide and tributary-scale sediment yield estimates derived from our geomorphic landscape unit (GLU) production method (see Section 3.3.4). Cosmogenic nuclide concentrations were measured in sediment samples collected in select locations throughout the USCR watershed, generally at the downstream ends of tributary channels, in order to quantify landscape erosion rates within those contributing areas (Figure 3-9). A brief description of this methodology and the results of this analysis are provided below (greater detail is contained in specialist published accounts, e.g., Lal 1991, Granger et al. 1996, Granger and Riebe 2007).

Cosmic rays traveling from outer space constantly bombard the Earth's surface, penetrating up to several meters into soil and rock. When these particles occasionally collide with the atomic nuclei of certain minerals in soil and rock, cosmogenic nuclides are produced (also referred to as *in-situ* produced cosmogenic nuclides) (Granger and Riebe 2007). In essence, the amount of nuclides accumulated within a mineral grain is a function of the time that grain has resided at or near the ground surface (Lal 1991). Therefore, cosmogenic nuclide concentrations increase in grains of rock or soil that have been exposed for long periods of time at the land surface, inferring a relatively slow erosion rate for that portion of the landscape. In contrast, a grain of rock or soil containing a low cosmogenic nuclide concentration indicates that that portion of the landscape has experienced a relatively high erosion rate because the grain has resided there for a relatively short time. Ultimately a rock fragment or soil particle eventually detaches from the surface, transports down-gradient, is delivered to the stream network, and resides on the streambed for some indeterminate time period. That sediment particle, along with others on the streambed, can be collected as a bulk sample and analyzed by an accelerator mass spectrometer (AMS) to determine the cosmogenic nuclide concentration of the sample. Because the bulk sample contains numerous grains originating from different parts of the contributing drainage area, and representing different erosion rates, the AMS analysis represents an integrated erosion rate for the contributing landscape. This concept of spatially-averaged denudation rates, $\langle D \rangle$, using cosmogenic dating techniques may be represented mathematically as follows:

$$N_{stream} = \frac{\int \left\{ \sum P_i(0) L_i \right\} * dA}{\int D * dA} = \frac{\sum P_i(0) L_i}{\langle D \rangle} \tag{3.1}$$

where N_{stream} denotes the average cosmogenic nuclide concentration in stream sediment, P_i denotes cosmogenic nuclide production rate, L_i denotes the effective penetration length, A denotes the sediment contributing area, and D denotes the total denudation rate (Granger and Riebe 2007). The erosion rate results are reported in mass per area per year, or grams per square centimeter per year (g cm^{-2} yr^{-1}).

There are several major *in-situ* produced cosmogenic nuclides in terrestrial materials, but the two of interest in this study are aluminum 26 (^{26}Al) and beryllium 10 (^{10}Be). These two nuclides are produced, respectively, from silica (Si) and oxygen (O), and have half lives on the order of 0.7 and 1.3 million years, which enables us to quantify erosion rates of landscapes over very long time periods (Granger and Riebe 2007). The ideal "target" mineral for analysis is quartz because it is composed of these two elements ($Si0_2$) and is found in abundance in the USCR watershed as it is a key mineral found in many of the rock units present here.

For this study, we collected sediment samples from several locations in the watershed [3](Figure 3-9). Because bedrock lithology is considered to be a major control on erosion rates in this region (e.g., Scott and Williams 1978, Warrick and Mertes 2009, and this study), the sample sites chosen were ultimately based on: (1) sampling of a dominant geologic unit; (2) sampling the largest contributing area composed almost wholly of a single geologic unit; and (3) accessibility to the location. Two additional samples were collected from the mainstem USCR in order to obtain a watershed-wide measurement of larger-scale erosion rates across numerous terrain types. One of these was at the downstream end of Soledad Canyon, to represent the geologically older and climatically drier terrains, and the other at the downstream end of the USCR watershed at the County line stream gauge (USGS 11108500), to integrate across all terrain types across the entire watershed. A summary of the samples, their locations, and their dominant bedrock lithology is presented in Table 3-4.

Our sampling methods involved collecting streambed sediments from the sample location, which included all grain sizes that could be extracted by hand with a shovel (i.e., <256 mm [smaller than boulders]). In order to collect a representative sample of streambed sediments eroded from throughout the contributing drainage, sediments were initially extracted from the streambed in three locations spaced about 10 m apart along the length of the channel and down to a maximum depth of 1 m. The extracted sediments, amounting to about 15-gallons, were mixed on site and then split into thirds so that the final sample was contained within a single, sealed 5-gallon bucket. The samples were shipped to Dr. Cliff Riebe at the University of Wyoming to prepare them for eventual analysis with an AMS and measurement of cosmogenic nuclide concentration. Sample preparation is time-intensive and involves reducing the sediments into very fine-grained particles and separating, concentrating, and purifying the target mineral (quartz) before isolating the isotopes from the minerals and separating them from non *in-situ* cosmogenic isotopes. The prepared samples were analyzed using an AMS at the Purdue Rare Isotope Measurement Laboratory (PRIME Lab; http://www.physics.purdue.edu/primelab/). The results were reviewed by Dr. Riebe and corrected for local conditions in the USCR watershed, such as altitude, latitude, hypsometry (relationship of elevation and drainage area), and bedrock density, which influence cosmogenic nuclide concentrations. The results of the analysis are summarized in Table 3-4. Laboratory reports are presented in Appendix C.

Results of the sediment dating analysis provide real confirmation of the relative erodibility of certain rock types present in the USCR watershed, where the youngest rock types exhibited the highest erosion rates and the oldest exhibited the lowest rates. For example, the Pico Canyon sample, which receives sediment exclusively from the Pliocene siltstones (and some sandstones) of the Pico Formation, was determined through the sediment dating analysis to have the highest erosion rates, at approximately 6,000 t km^{-2} yr^{-1}. These rates were at least a factor of six greater than the other samples collected in lithologically-homogenous drainages (i.e., not including the samples from the mainstem USCR). This result is consistent with qualified assessments of this rock unit exhibiting relatively high erosion rates (e.g., USGS 1997: Santa Susana quadrangle; this study). The samples exhibiting the next highest erosion rates (~1,000 t km^{-2} yr^{-1}) were from Grasshopper and Hasley canyons, which receive sediments derived from the young Castaic

[3] A total of 12 samples were collected; however, the samples from Aliso Canyon (granodiorite rock unit) and an unnamed tributary in Soledad Canyon (Vasquez Formation sandstone) yielded an insufficient concentration of quartz thereby precluding their further analyses.

Formation siltstones and Saugus Formation sandstones, respectively. Both of these units, along with the Mint Canyon Formation sandstones contributing to the Plum Canyon sample, are also considered by field geologists to be prone to high erosion rates (e.g., USGS 1997: Mint Canyon and Val Verde quadrangles). However, based on the sediment dating results, these units appear to be significantly less erodible compared to the Pico Formation siltstones. The samples with the lowest erosion rates (~300-600 t km^{-2} yr^{-1}) were from watersheds composed of geologically older rock units, which are expected to be more erosion resistant as compared to younger sedimentary units located elsewhere in the USCR watershed (Dibblee 1997: Warm Springs Mountain quadrangle). Somewhat unexpected, the sample with the lowest erosion rate (~300 t km^{-2} yr^{-1}) was from Haskell Canyon, which is composed of Pelona Schist—a unit considered by other researchers to be relatively less resistant to erosion as compared to similarly aged rock units, such as gneiss (Elizabeth Canyon), anorthosite (Indian Canyon), and granite (e.g., Spotila et al., 2002). An explanation for this difference between the measured erosion rates for the Pelona Schist is that others, such as Spotila et al. (2002), utilized different analytical techniques (e.g., thermochronology) to arrive at their estimates, which record exhumation of the landscape over different, and usually longer, time scales.

The erosion rate of the entire USCR watershed represents an integrated average for the contributing area, with a measured value of about 1,900 t km^{-2} yr^{-1} being greater than the lower yielding terrains (e.g., Precambrian quartz diorite-gneiss complex) but less than the highest yielding terrains (e.g., Pico Formation). An ongoing study of watershed erosion rates for several southern California rivers recently found similar erosion rates per unit area for the entire SCR watershed based on cosmogenic dating performed near the mouth of the river (B. Romans, pers. comm., 2011).

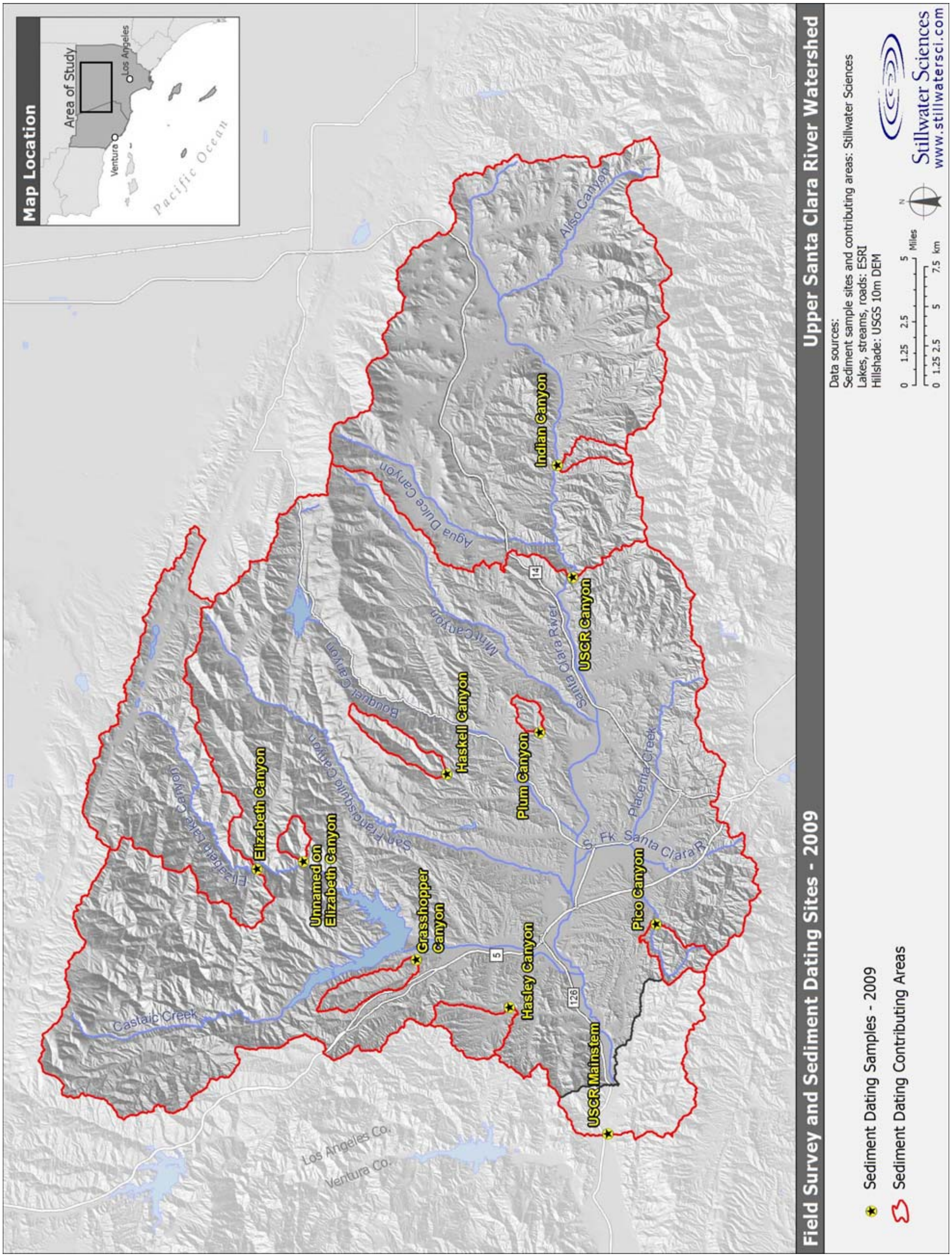

Figure 3-9. Locations and contributing watershed areas for cosmogenic nuclide sediment dating samples in the USCR watershed collected for this study.

Table 3-4. Erosion rates in the USCR watershed derived from sediment dating in select drainage basins.

Sampled watershed name (listed in upstream to downstream order)	Contributing area (km^2) [a]	Dominant rock type in contributing area [b]	Proportion of total USCR watershed area represented by the dominant rock type(s) [c]	Geology GLU category [d]	Bulk density class [e]	Annual average erosion rate ($g\ cm^{-2}\ yr^{-1}$)	Sediment yield per unit area ($t\ km^{-2}\ yr^{-1}$)	Equivalent denudation rate ($mm\ yr^{-1}$)	Time scale (yrs)
Indian Canyon	4.7	Mesozoic-Precambrian anorthosite (an)	4.8%	Competent Crystalline and Sandstones	Igneous/ Metamorphic	0.05 ±0.02	530 ±160	0.20 ±0.06	3,000
USCR in Soledad Canyon	405.7	Mix of older, coarse-grained rocks and alluvium	NA	Mix	Mix	0.05 ±0.02	530 ±200	0.19 ±0.07	3,000
Plum Canyon	3.1	Miocene Mint Canyon Formation sandstone and conglomerate (Tmc, Tmcg, Tmcv, Tmc1,2,3)	4.2%	Weak Metamorphics and Sandstones	Sedimentary	0.07 ±0.01	680 ±130	0.29 ±0.06	2,400
Haskell Canyon	8.8	Mesozoic Pelona schist (ps, psl, pso, psp, pi)	8.3%	Weak Metamorphics and Sandstones	Igneous/ Metamorphic	0.03 ±0.01	270 ±40	0.10 ±0.01	5,900
Pico Canyon	8.7	Pliocene Pico Formation siltstone and sandstone (Tp, Tpc, Tps)	2.4%	Siltstone, Weak Meta-morphics, and Sandstones	Sedimentary	0.60 ±0.29	5,970 ±2,910	2.60 ±1.27	300
Elizabeth Lake Canyon	119.2	Mesozoic-Precambrian quartz diorite-gneiss (qd, gn)	14.5%	Competent Crystalline and Sandstones	Igneous/ Metamorphic	0.05 ±0.02	510 ±190	0.19 ±0.07	3,100

Sampled watershed name (listed in upstream to downstream order)	Contributing area (km^2) [a]	Dominant rock type in contributing area [b]	Proportion of total USCR watershed area represented by the dominant rock type(s) [c]	Geology GLU category [d]	Bulk density class [e]	Annual average erosion rate (g cm^{-2} yr^{-1})	Sediment yield per unit area (t km^{-2} yr^{-1})	Equivalent denudation rate (mm yr^{-1})	Time scale (yrs)
Unnamed tributary to Elizabeth Lake Canyon	3.7	Paleocene San Francisquito Formation sandstone (Tsfs, Tsfc)	4.4%	Competent Crystalline and Sandstones	Sedimentary	0.06 ±0.02	610 ±180	0.26 ±0.08	2,600
Grasshopper Canyon	9.1	Miocene Castaic Formation siltstone (Tc)	2.3%	Siltstone	Sedimentary	0.10 ±0.04	1,000 ±440	0.43 ±0.19	1,600
Hasley Canyon	12.1	Pleistocene Saugus Formation sandstone and conglomerate (QTs QTsc, QTsg, Qsp, Qss, Qsu)	6.7%	Weak Metamorphics and Sandstones	Sedimentary	0.09 ±0.02	900 ±190	0.39 ±0.08	1,800
Entire USCR	1,718.1	Mix	NA	Mix	Mix	0.19 ±0.06	1,870 ±600	0.69 ±0.22	900

[a] Determined in GIS using USGS 10-m DEM.
[b] Source: Dibblee (various dates) and USGS (various dates). Mapping symbol given in parenthesis. See Appendix A for description of rock units.
[c] Dominant rock type is listed in the column to the left.
[d] See Section 3.4.4 for description of geology Geomorphic Landscape Unit (GLU) categories.
[e] Bulk density values: 2.7 t m^{-3} for Igneous/Metamorphic, 2.5 t m^{-3} for mixed Igneous/Metamorphic and Sedimentary, and 2.3 t m^{-3} for Sedimentary.
NA = not applicable because there is a mixture of rock types in the drainage area contributing to this sample location and, therefore, the proportion of total USCR watershed area represented by the dominant rock type cannot be calculated here; this sample represents an integration of rock types (and associated erosion rates) in the contributing drainage area.

3.3.3 Rates from debris basins and reservoir sedimentation yields

Regional sediment yield data are available from debris basins and some water storage reservoirs in Los Angeles County. These data sources provide a range of sediment yields for the region that can be corroborated by other regional metrics such as tectonic uplift and fault displacement.

For more than 50 years, LADPW has monitored debris basins throughout the county, including the Santa Clara River watershed, in order to protect inhabitants and property from high-energy debris flows. As developments within the county have expanded, the number of debris basins has expanded to over 100 (Lavé and Burbank 2004, LADPW-provided data 2010 [M. Araiza, pers. comm., 2010]). After each major winter storm the debris basins are inspected, and whenever accumulation exceeds 25%, the basins are excavated (Lavé and Burbank 2004). Using either a rapid geodetic survey or weighing by truck, volumes of sediment deposition are tracked, which can then be converted to annual and unit-area sediment yields. The county also maintains over 20 smaller debris retention structures, called debris retention inlets (DRIs), that similarly intercept debris flows; however, these structures do not have sediment cleanout or sediment measurement records (L. Thang, pers. comm., 2010) and therefore they were not considered further in our analysis.

Regional sediment yields were previously estimated by Lavé and Burbank (2004) using sediment removal records from approximately 115 debris basins in Los Angeles County. A majority of those basins are located outside of the USCR watershed in the southern foothills of the San Gabriel Mountains (i.e., the Los Angeles River watershed). Sediments deposited in the debris basins range in size from silts and clays up to boulders; however, because the debris basins are designed to intercept sediment-laden debris flows yet continue to convey water during storm events (in order to avoid having flows overtop the debris basin dams), they preferentially trap the coarser sediments (i.e., bed material load) (LADPW 2006). Sediment yields from the debris basins imply 200 to 14,700 t km^{-2} yr^{-1} of sediment production from the watersheds that feed them, with equivalent landscape denudation rates of 0.1 to 5.7 mm yr^{-1} (Lavé and Burbank 2004). As stated above, Lavé and Burbank note that anthropogenic fires have led to 60–400% increase in sediment production rates in the drainage areas contributing to the debris basins compared with the background, "natural" production rates in those drainage areas.

We have used the sedimentation records from eleven of the LADPW-maintained debris basins located within the USCR watershed (Table 3-5, Figure 3-10). Of these, two were considered by Lavé and Burbank in their study: Wildwood and William S. Hart debris basins, located near one another in the upper South Fork SCR watershed. All eleven debris basins have variable periods of operation over the past 42 years, where the average period of record is 16 years. In addition to the LADPW debris basins, sedimentation data from a series of three in-line debris basins situated along upper Castaic Creek at the Castaic Powerplant was used in this analysis (G. Wu, pers. comm., 2010). For the past 35 years, the Los Angeles Department of Water and Power (LADWP) has maintained these three debris basins for the purpose of preventing debris flows from upper Castaic Creek interrupting operations at the Castaic Powerplant, which is positioned along the upstream end of the Castaic Creek arm of Castaic Lake (i.e., Elderberry Forebay). Copies of sedimentation records at the LADPW and LADWP debris basins are included in Appendix D. An evaluation of the impacts of debris basins on watershed sediment yields and river morphology is presented in Section 4.2.1.5. Finally, sedimentation data from Bouquet and Castaic Lake reservoirs were also utilized in our analysis.

Sedimentation in Bouquet Reservoir was recorded for a relatively short time period just after dam closure in the 1930s (Appendix D). Minear and Kondolf (2009) compiled this data, adjusted the sediment mass value with measured values in nearby reservoirs, and estimated that the contributing area had an annual sediment yield of 450 t km^{-2} yr^{-1}. Unfortunately, sedimentation rates have not been recorded in Bouquet Reservoir since then (M. Sirakie, pers. comm., 2010). For Castaic Lake, Warrick (2002) estimated long-term suspended sediment yields intercepted by the reservoir by calculating the difference in average annual suspended sediment yield at the County line stream gauge (USGS 11108500) before and after closure of the dam. Warrick's estimate of suspended sediment yield (only) from the areas draining into Castaic Lake was approximately 1,000 t km^{-2} yr^{-1} for the time period of 1972-1996 (and the total load 10-20% higher; see Section 4.3.2).

Prior to construction of Castaic Lake Dam, a USGS study (Lustig 1965) estimated the total sediment yield in the area above the un-built dam to be approximately 1,500 t km^{-2} yr^{-1}, which is similar to Warrick's (2002) estimate for the same contributing area. The approach followed by the USGS involved compiling known sediment yields from neighboring watersheds in the San Gabriel Mountains (e.g., Pacoima and Big Tujunga reservoirs), comparing geomorphic parameters in those watersheds to Castaic Creek, plotting a best-fit regression through these data (sediment yield versus watershed area), and then interpreting a sediment yield value for upper Castaic Creek watershed by relating its watershed area to the regression equation (i.e., scaled by its watershed area).

Table 3-5. Debris basin and reservoir sedimentation data used to quantify rates of sediment delivery in the USCR watershed.

Name	Contributing area (km^2) [a]	Years evaluated (water years)	Largest flood event in the USCR during sedimentation evaluation period (year of event)	Number of wildfires in contributing area since 1911 (year of most recent fire)	Number of wildfires in contributing area during sedimentation evaluation period	Annual average sediment yield ($m^3\ yr^{-1}$)	Sediment yield per unit area ($t\ km^{-2}\ yr^{-1}$) [b]	Equivalent denudation rate ($mm\ yr^{-1}$)
Debris basins [c]								
Crocker	1.75	26 (1983–2008)	2005	4 (2004)	1	407	442	0.23
Marston-Paragon	0.49	20 (1989–2008)	2005	7 (1981)	0	75	287	0.15
Oakdale	3.58	5 (2005–2009)	2005	5 (2004)	0	12,293	6,520	3.43
Saddleback #3	0.39	18 (1991–2008)	2005	2 (1960)	0	192	926	0.49
Shadow	2.45	11 (1995–2005)	2005	7 (2001)	1	1,216	942	0.50
Victoria	0.70	7 (2003–2009)	2005	7 (2007)	1	3,812	10,325	5.43
Wedgewood	2.41	5 (2002–2005)	2005	12 (2002)	1	246	194	0.10
Whitney	0.40	5 (2001–2004)	2004	6 (1976)	0	236	1,126	0.59
Wildwood	1.68	41 (1968–2008)	1969	7 (1985)	3	2,311	2,614	1.38
William S. Hart	0.23	25 (1984–2008)	2005	4 (1973)	0	15	124	0.07
Yucca	0.39	9 (1997–2005)	2005	2 (1946)	0	604	2,922	1.54
Castaic Powerplant [d]	173	35 (1975–2009)	2005	40 (2009)	8	74,703 (52,846)	822 (581)	0.43 (0.31)
Reservoirs								
Bouquet Reservoir [e]	35.2	5 (1934–1939)	1938	30 (2007)	2	15,814	449	0.45
Castaic Lake [f]	402	25 (1972–1996)	1983	116 (2009)	38	470,000	1,200	1.2
Castaic Creek watershed above the proposed dam [g]	402	36 (1927–1962)	1938	116 (2009)	18	310,000	1,500	0.8

[a] Determined in GIS using USGS 10m DEM.
[b] Assumed bulk density of 1.9 t m^{-3} (after Lavé and Burbank 2004), except for Bouquet and Castaic Lake reservoirs (see footnotes [e] and [f] below).
[c] All debris basin sediment removal data provided by LADPW, except for removal records from Castaic Powerplant.
[d] Sediment removal data for the series of three debris basins along Castaic Creek at the Castaic Powerplant was provided by LADWP. The power plant is part of the West Branch of the California Aqueduct and is situated at the upstream end of the Elderberry Forebay of Castaic Lake reservoir. Sediment yield and denudation rate values presented in parenthesis exclude an estimate of ~1 million yds^3 (765,000 m^3) made by LADWP in the reservoir immediately below the debris basins.
[e] Source data: Minear and Kondolf (2009). The assumed bulk density used in the conversion from volume to mass is 1.0 t m^{-3}, based on an average of estimates of 0.96 t m^{-3} and 1.04 t m^{-3} made by Minear and Kondolf (2009) and Warrick (2002), respectively. The estimate from the former were based on all sedimentation data considered in the authors' analysis of California reservoirs, while the estimate from the latter was derived by the author from sedimentation data in the nearby Lake Piru reservoir between 1955–1975.
[f] Source data: Warrick (2002). Method used to determine natural suspended sediment yields from upper Castaic Creek watershed into the reservoir was based on quantifying a reduction factor in suspended sediment discharge at the County line stream gauge (USGS 11108500) for periods before (1956–1971) and after (1972–1996) dam closure. The total sediment yield estimate reported here assumes that the bed material load fraction accounts for 17% of the total load, following assumptions made by Williams (1979) for the USCR at the County line stream gauge. The assumed bulk density used in the conversion from mass back to volume is 1.0 t m^{-3} (see footnote e above for details).
[g] Source data: Lustig (1965). Method used to determine long-term sediment yields from upper Castaic Creek watershed into the proposed reservoir area was based on a comparison of geomorphic parameters for watersheds in the San Gabriel Mountains, for which there was long-term sediment yield data records, and for the Castaic Creek watershed.

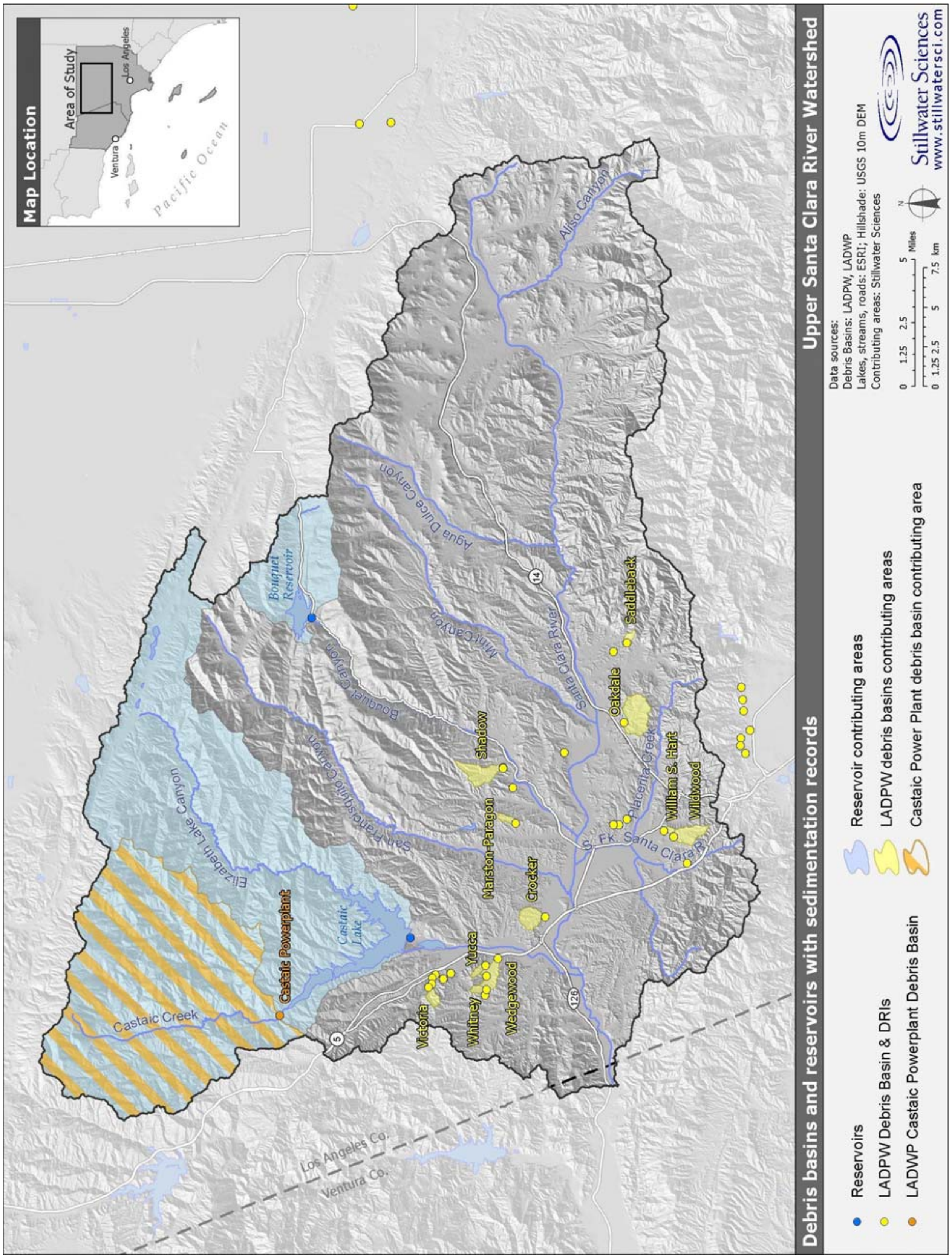

Figure 3-10. Locations of debris basins and reservoirs utilized in this study to estimate watershed-wide sediment yields.

Annual average total sediment yields, as estimated at the eleven LADPW-maintained debris basins, the Castaic Powerplant debris basins, and Bouquet and Castaic Lake reservoirs, range between 30 and 620,000 tonnes per year (t yr^{-1}). Figure 3-11 displays the data compensating for watershed size, producing a log-linear regression equivalent to the average per unit area sediment yield. This regression can be refined slightly by excluding the sedimentation records having less than 5 years of data. Converting the volume to mass using a bulk density of 1.9 t m^{-3} (Lavé and Burbank 2004), the slope of the best-fit line indicates an annual average sediment yield of approximately 2.8 million t yr^{-1} for the entire USCR watershed, equivalent to a sediment yield per unit area of **1,700 t km^{-2} yr^{-1}**. This value equates to a landscape denudation rate of about 0.9 mm yr^{-1}, which is within the range estimated by Lavé and Burbank (2004) for the San Gabriel Mountains. This denudation rate is also within the (admittedly broad) range of nearby, localized uplift rates reported above (0.1–9.0 mm yr^{-1}).

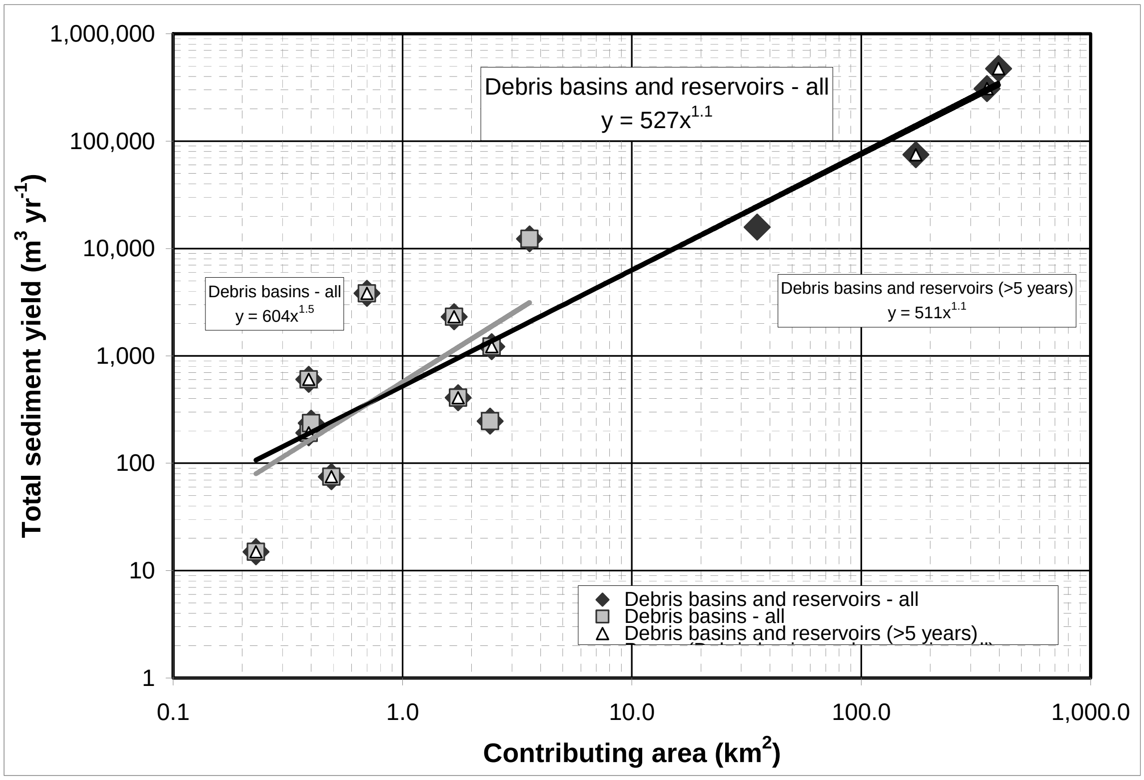

Figure 3-11. Relationship of estimated sediment yields from debris basins and reservoirs in the USCR watershed to their contributing watershed area. Original sediment yield values given volumetrically as reported by debris basin and reservoir managers and by other sedimentation researchers.

As can be seen in Table 3-5 and Figure 3-11, there is significant variability in the debris basin and reservoir derived sediment yields, especially in those basins of less than 10 km^2, which is likely due to environmental controls unique to the drainage areas above structure. From an examination of several potential factors, the primary ones appear to be drainage area size, sediment connectivity, dominant lithology, and hillslope gradient. To a lesser extent, other factors include vegetation cover and land use. Storm events and wildfires are major factors influencing sediment yields at the watershed scale, but likely do not affect the variations seen between the LADPW debris basins because all were operational during the 2005 storm events and have experienced no more than one fire since they began operation. The one exception is at Wildwood debris basin, which also has the longest period of record and was operational during the 1969 and 2005 storm events and during three wildfires. This debris basin correspondingly has the fourth greatest sediment yield per unit area when compared against all debris basins and reservoirs. The two debris basins having the highest sediment yields—Oakdale and Victoria—are the only two that receive sediment from geologically young siltstone rock units. In terms of sediment connectivity, the drainage areas feeding nearly all debris basins and reservoirs appear to have high sediment delivery ratios indicating that sediment is efficiently delivered to those structures. One exception is at Wedgewood debris basin where Whitney and Yucca debris basins are situated upstream in the same catchment, thereby causing sediment yields in Wedgewood to be lower than they would be if those other debris basins were not present. The Wedgewood debris basin yields are further reduced because a large portion of its contributing area hosts a dense residential development that acts to disrupt sediment connectivity (Wedgewood debris basin has the second lowest sediment yield per unit area compared to the other debris basins and reservoirs).

3.3.4 Rates from geomorphic landscape unit (GLU) analysis

Sediment-production rates were estimated throughout the USCR watershed for the purpose of identifying areas and tributary basins having relatively high, medium, or low sediment production potential. Our approach for the USCR watershed followed that previously developed for Santa Paula Creek (Stillwater Sciences 2007b), Sespe Creek (Stillwater Sciences 2010), and upper San Francisquito Creek (Stillwater Sciences 2009). We identified watershed factors judged critical to determining the sediment-production potential of the landscape, and we divided them into discrete categories to define “geomorphic landscape units” (GLUs) across the watershed. We assigned relative, qualitative rates of sediment production to each of these GLUs (“High”, “Medium”, and “Low”, commonly abbreviated H, M, and L throughout this report). Finally, we determined numeric sediment-production rates for each category of GLU on an annual unit-area basis, displaying their spatial distribution on maps and integrated their contributions into a single value of average annual sediment production across the watershed. These steps are described in greater detail in the following sections.

3.3.4.1 Relative rates of sediment production using the GLU approach

Although many factors can determine sediment-production rates from hillslopes, this and previous studies focused on three that were judged to impose the greatest range of variability over the USCR watershed: rock type, vegetation cover, and hillslope gradient. Data sources for each were compiled in a GIS environment over the entire watershed at a resolution determined by the coarsest dataset (30 m). Wildfire was not explicitly considered in this approach even though it has been found to strongly influence landscape erosion rates in small watersheds (see above). Because wildfires across the watershed are highly variable in space, time, and intensity, we considered the use of wildfire data in this analysis to add an unnecessary level of complexity that ultimately would not provide us with a more accurate estimate of watershed-wide sediment-production rates over a decadal time frame. Further, areas burned most frequently are represented in the vegetation cover data as those portions of the landscape hosting minimal to modest vegetation cover (e.g., grassland, scrub/shrub); forested areas generally have the lowest wildfire frequency (see Figures 3-3 and 3-12).

Rock types were based on the 1:24,000-scale geologic maps of Dibblee and the USGS (see Figure 1-4). The relative erodibility of the 100+ mapped rock types in the USCR watershed was evaluated through review of published information and on field observations made specifically for this project. Both Dibblee and the USGS provide useful descriptions of their mapped rock units (see Appendix A for description of rock units), which generally indicate that the geologically older igneous and meta-igneous rocks found in the mountainous areas are the most resistant to erosion, while the young sedimentary rocks found closer to the Santa Clarita and Acton basins are the least resistant. Spotila et al. (2002) investigated controls on erosion patterns in the San Gabriel Mountains and ranked the relative erodibility of several of the major igneous and meta-igneous rocks found there (no sedimentary rock units were considered), estimating that granite and the Lowe Granodiorite Complex (chiefly found in the Aliso Canyon subwatershed) were the most erosion-resistant and the sheared and fractured Pelona Schist (present across the middle Bouquet and San Francisquito subwatersheds) was the least resistant. Warrick and Mertes (2009) found that areas of the western Transverse Ranges, from which the USCR is a part of, with the highest sediment yields consistently have weakly consolidated bedrock (e.g., Quaternary-Pliocene marine formations, like the Pico Formation). We found a similar trend when comparing rock type (as grouped in this GLU analysis) against sediment yield at each debris basin and reservoir considered in this study (see Appendix A). These various assessments are in full agreement with our field observations and with erosion rates derived from our sediment dating analysis.

Mapped units were therefore grouped into categories of competent crystalline and sandstones (resistant yet fractured igneous, volcanic, and sandstone units), weak metamorphics and sandstones (highly fractured schists and poorly consolidated sandstone/conglomerate units), siltstones (weak siltstone/claystone and shale units), and “unconsolidated” (young, weakly lithified river sands/gravels, alluvial fans, paleo-landslides) (Figure 3-1). Qualitatively, the units listed here are done so in order of relative erodibility, with the competent crystalline and sandstone units exhibiting the greatest resistance to erosion and the siltstone and unconsolidated units exhibiting the least.

Land cover was based on the 2001 National Land Cover Database (Homer et al. 2004) at 30-m resolution (see Figure 1-6). By an automated classification system, five grouped categories were identified; they largely correspond to vegetation covers of forest, scrub/shrub, agriculture/grassland, developed land, and open water (Figure 3-12). For this analysis, areas having greater vegetation cover (e.g., forest) are assumed to have lower sediment-production rates, while those areas having lower cover (e.g., agriculture/grassland) have higher sediment-production rates for the following reasons: (1) plant roots physically hold soils in place; (2) vegetation canopy mutes the otherwise erosive effects of rain splash erosion by interception of precipitation; and (3) organic barriers (e.g., tree trunks, stems, downed branches, and litter) diffuse the erosive force of overland flow and trap sediments transporting down-gradient towards stream channels by acting as physical barriers. The scrub/shrub category, which accounts for the largest proportion of the total watershed area, is assumed to afford a moderate vegetation cover to the underlying land surface. Observations for this and prior studies broadly and consistently confirm this assumption.

In the USCR watershed, the “developed” category predominantly represents those moderately to extensively urbanized areas of Santa Clarita and its developed surroundings where impervious surfaces are prevalent. Therefore, portions of the landscape covered by the developed category are now considered to have low sediment-production rates because: (1) soil and rock surfaces are rarely exposed to erosional forces; and (2) connectivity between any exposed surfaces and the stream network are substantially limited due to landscape alteration and controlled flow routing and sediment entrapment (i.e., stormwater system and debris basins). The “developed, open space” category contained within the source data represents areas that are unpaved and are therefore exposed to erosional forces. This category was accordingly grouped with the agricultural/grassland land cover category for this analysis. Finally, the open water category primarily represented three water storage reservoirs—Bouquet, Castaic Lake, and Dry Canyon—where sediment production is considered here to be zero as these features function as depositional basins. A few other ponds are present in the watershed as well and captured in this category by the land-cover analysis (e.g., Sand and Oak Spring canyons).

Lastly, hillslope gradients were generated directly from the digital elevation model (DEM), which in turn was based on a USGS 10m DEM. Based on the distribution of slopes and on observed ranges of relative erosion and slope instability, the continuous range of hillslope gradients was categorized into three groups: 0–20%, 20–60%, and steeper than 60% (Figure 3-13). In general, the <20% slope terrains are located in valley bottoms and were noted during our field surveys to have a relatively low propensity for erosion (for similar geology and land cover); the 20–60% hillslopes have a medium erosion potential; and the >60% slopes are prone to a relatively high degree of erosion, inner-gorge landsliding, and debris-flow activity.

The relative proportions of the geology, land cover, and hillslope gradient GLU classes, in addition to other supporting information on the development of the GLUs for this study, are presented in Appendix A.

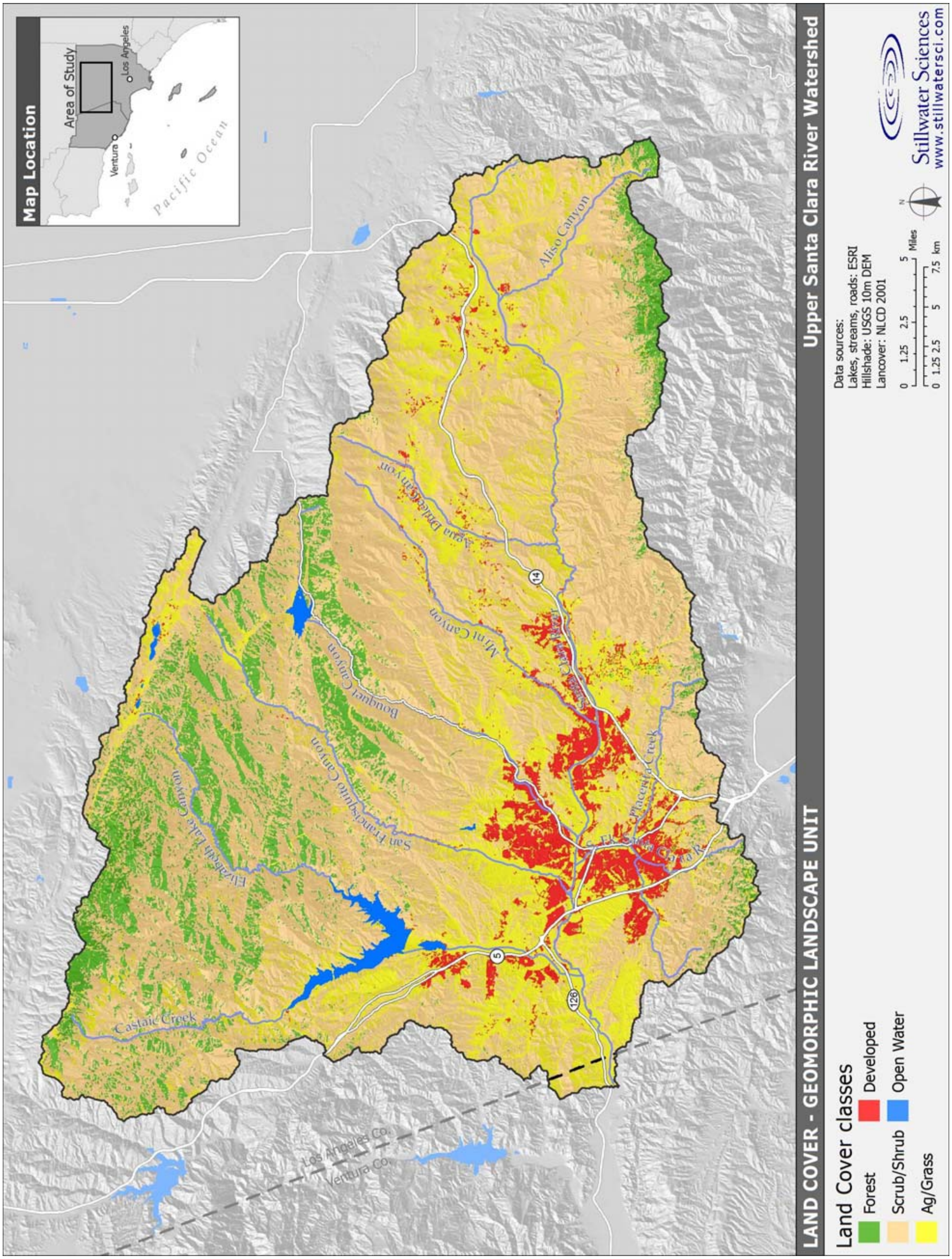

Figure 3-12. Generalized land cover categories used for the GLU analysis.

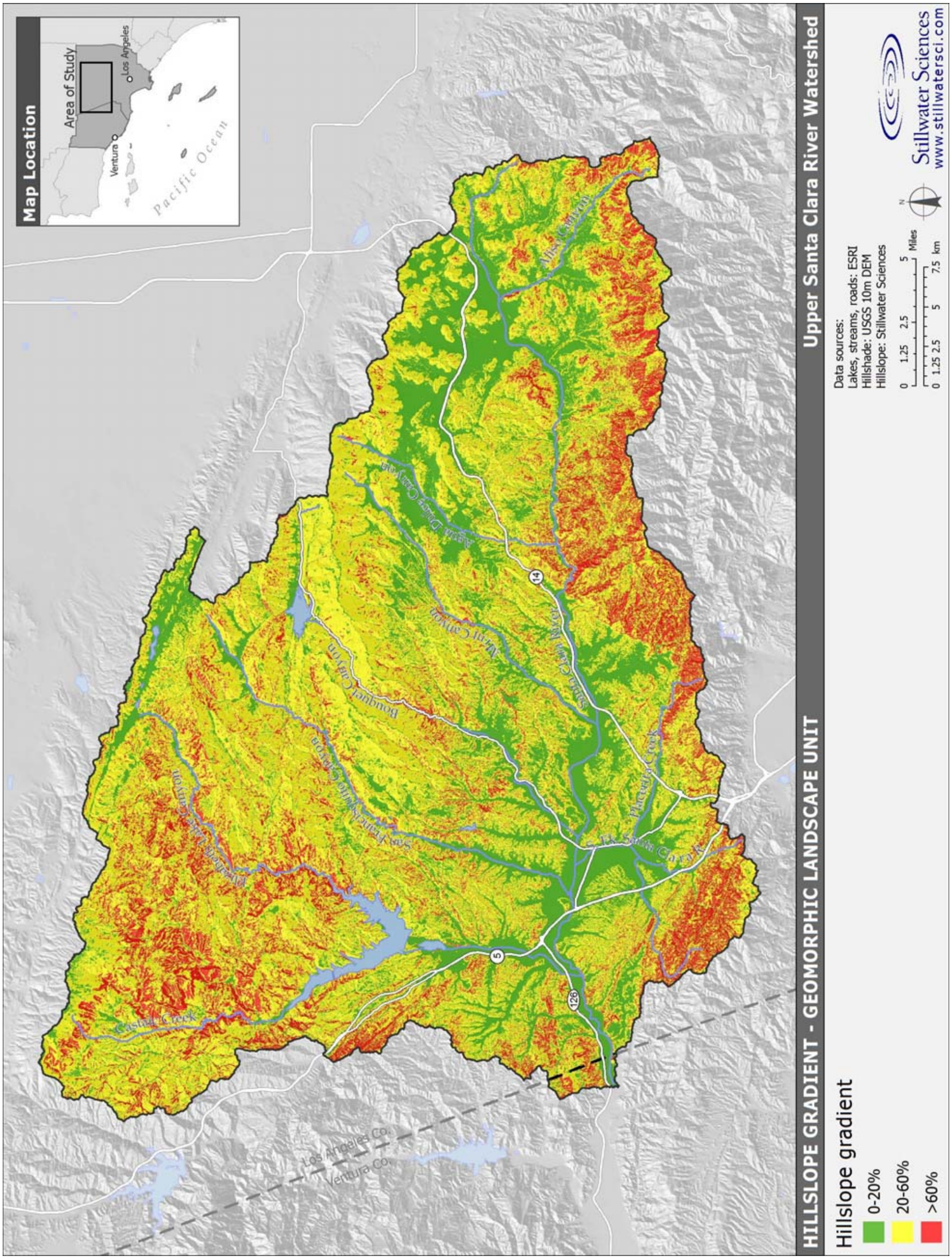

Figure 3-13. Generalized hillslope gradient categories used for the GLU analysis.

The classifications of geology (4 classes), land cover (5 classes), and slope (3 classes) can theoretically result in 60 possible unique combinations, or "geomorphic landscape units" (GLUs). While every possible combination did occur somewhere in the watershed, just over half of the entire watershed is represented by just four GLUs, namely: (1) Competent Crystalline and Sandstones, Scrub/Shrub, and 20-60%; (2) Weak Metamorphics and Sandstones, Scrub/Shrub, and 20-60%; (3) Unconsolidated, Ag/Grass, and 0-20%; and (4) Competent Crystalline and Sandstones, Scrub/Shrub, and >60% (Table 3-6). Only 20 of the possible combinations cover more than one percent of the total watershed area, and in total these 20 GLUs account for more than 92% of the watershed area (Table 3-6).

Table 3-6. Geomorphic landscape units (GLUs) over as a percent of total watershed area (representation = 92.6% of the watershed).

Geomorphic landscape units	% of watershed area
Competent Crystalline & Sandstones; Scrub/Shrub; 20–60%	21.6%
Weak Metamorphics & Sandstones; Scrub/Shrub; 20–60%	13.5%
Unconsolidated; Ag/Grass; 0–20%	8.7%
Competent Crystalline & Sandstones; Scrub/Shrub; >60%	6.9%
Competent Crystalline & Sandstones; Forest; 20–60%	5.1%
Unconsolidated; Scrub/Shrub; 0–20%	4.4%
Weak Metamorphics & Sandstones; Ag/Grass; 20–60%	4.0%
Competent Crystalline & Sandstones; Scrub/Shrub; 0–20%	3.7%
Unconsolidated; Developed; 0–20%	3.3%
Competent Crystalline & Sandstones; Ag/Grass; 20–60%	3.2%
Weak Metamorphics & Sandstones; Scrub/Shrub; 0–20%	2.5%
Unconsolidated; Scrub/Shrub; 20–60%	2.4%
Weak Metamorphics & Sandstones; Scrub/Shrub; >60%	2.4%
Siltstone; Scrub/Shrub; 20–60%	2.4%
Competent Crystalline & Sandstones; Forest; >60%	2.1%
Unconsolidated; Ag/Grass; 20–60%	1.4%
Weak Metamorphics & Sandstones; Forest; 20–60%	1.4%
Weak Metamorphics & Sandstones; Ag/Grass; 0–20%	1.4%
Siltstone; Ag/Grass; 20–60%	1.2%
Competent Crystalline & Sandstones; Ag/Grass; 0–20%	1.0%

Representative areas in each of the major GLUs were visited in the field and categorized into three relative sediment-production rates, based on observed indications of erosion and mass-wasting processes. Relative differences in sediment-production rates between many of the different GLUs appeared dramatic, lending confidence to this three-fold division of relative rates. The assignments of relative sediment-production rates were further refined from prior observations made in Santa Paula, upper San Francisquito, and Sespe creeks (Stillwater Sciences 2007b, 2009, 2010). Figure 3-14 illustrates some of these differences in relative sediment-production processes. The assignments of relative sediment production by type of GLU are listed in Table 3-7.

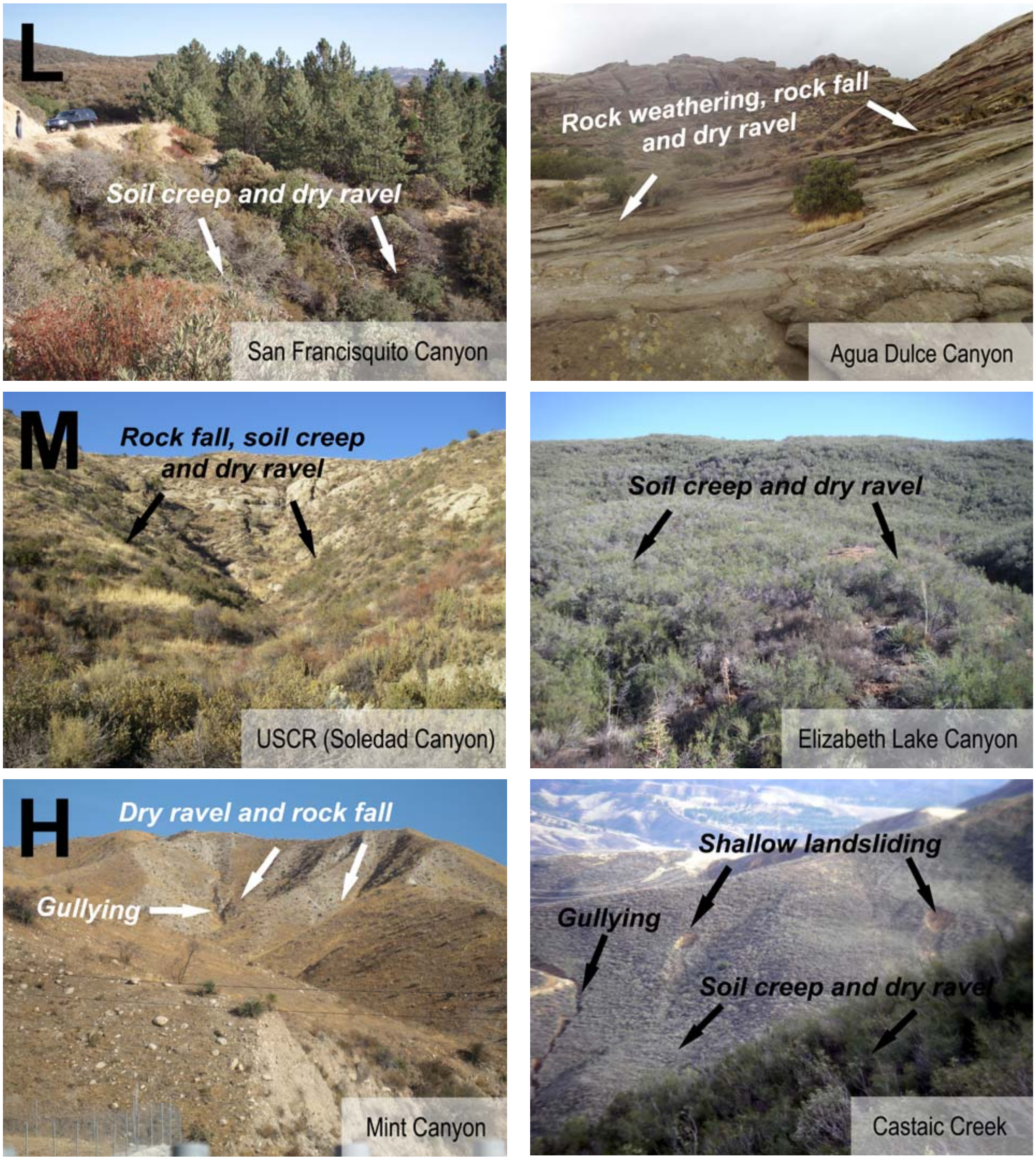

Figure 3-14. Examples of different geomorphic landscape units (GLUs) and their relative levels of sediment production. Top left, low production: *Competent Crystalline and Sandstones; Forest; 20-60%*; top right, low production: *Competent Crystalline and Sandstones; Ag/Grass; 0-20%*; middle left, medium production: *Competent Crystalline and Sandstones; Scrub/Shrub; >60%*; middle right, medium production: *Weak Metamorphics and Sandstones; Scrub/Shrub; 20-60%*; bottom left, high production: *Weak Metamorphics and Sandstones; Ag/Grass; >60%*; bottom right, high production: *Siltstone; Scrub/Shrub; >60%*.

Table 3-7. Relative total sediment-production rates by geomorphic landscape unit (GLU) (n=60).

Geomorphic landscape unit [a]	Relative total sediment production	Relative coarse sediment production [b]
Competent Crystalline and Sandstones; Developed; 0–20%	Low	Low
Competent Crystalline and Sandstones; Developed; 20–60%	Low	Low
Competent Crystalline and Sandstones; Developed; >60%	Low	Low
Weak Metamorphics and Sandstones; Developed; 0–20%	Low	Low
Weak Metamorphics and Sandstones; Developed; 20–60%	Low	Low
Weak Metamorphics and Sandstones; Developed; >60%	Low	Low
Siltstone; Developed; 0–20%	Low	Low
Siltstone; Developed; 20–60%	Low	Low
Siltstone; Developed; >60%	Low	Low
Unconsolidated; Developed; 0–20%	Low	Low
Unconsolidated; Developed; 20–60%	Low	Low
Unconsolidated; Developed; >60%	Low	Low
Competent Crystalline and Sandstones; Forest; 0–20%	Low	Low
Competent Crystalline and Sandstones; Forest; 20–60%	Low	**Med**
Competent Crystalline and Sandstones; Scrub/Shrub; 0–20%	Low	Low
Competent Crystalline and Sandstones; Ag/Grass; 0–20%	Low	Low
Weak Metamorphics and Sandstones; Forest; 0–20%	Low	Low
Siltstone; Forest; 0–20%	Low	Low
Unconsolidated; Forest; 0–20%	Low	Low
Competent Crystalline and Sandstones; Forest; >60%	Med	Med
Competent Crystalline and Sandstones; Scrub/Shrub; 20–60%	Med	Med
Competent Crystalline and Sandstones; Scrub/Shrub; >60%	Med	**High**
Competent Crystalline and Sandstones; Ag/Grass; 20—60%	Med	**High**
Weak Metamorphics and Sandstones; Forest; 20–60%	Med	Med
Weak Metamorphics and Sandstones; Forest; >60%	Med	Med
Weak Metamorphics and Sandstones; Scrub/Shrub; 0–20%	Med	Med
Weak Metamorphics and Sandstones; Scrub/Shrub; 20–60%	Med	Med
Weak Metamorphics and Sandstones; Ag/Grass; 0–20%	Med	**Low**
Siltstone; Forest; 20–60%	Med	**Low**
Siltstone; Forest; >60%	Med	**Low**
Siltstone; Scrub/Shrub; 0–20%	Med	**Low**
Siltstone; Ag/Grass; 0–20%	Med	**Low**
Unconsolidated; Forest; 20–60%	Med	Med
Unconsolidated; Forest; >60%	Med	Med
Unconsolidated; Scrub/Shrub; 0–20%	Med	Med
Unconsolidated; Scrub/Shrub; 20–60%	Med	Med
Unconsolidated; Ag/Grass; 0–20%	Med	Med
Competent Crystalline and Sandstones; Ag/Grass; >60%	High	High
Weak Metamorphics and Sandstones; Scrub/Shrub; >60%	High	High
Weak Metamorphics and Sandstones; Ag/Grass; 20–60%	High	High
Weak Metamorphics and Sandstones; Ag/Grass; >60%	High	High
Siltstone; Scrub/Shrub; 20–60%	High	**Low**
Siltstone; Scrub/Shrub; >60%	High	**Low**
Siltstone; Ag/Grass; 20–60%	High	**Low**

Geomorphic landscape unit [a]	Relative total sediment production	Relative coarse sediment production [b]
Siltstone; Ag/Grass; >60%	High	**Low**
Unconsolidated; Scrub/Shrub; >60%	High	**Med**
Unconsolidated; Ag/Grass; 20–60%	High	**Med**
Unconsolidated; Ag/Grass; >60%	High	**Med**

[a] This table excludes 12 GLUs generated for this analysis because they contain the "open water" land cover category. Landscapes with this attribute are considered to have zero sediment production potential as this category represents water storage reservoirs that function exclusively as depositional basins.
[b] See Section 3.4.4.3—Delivery of coarse sediment for a discussion of these data. Bold entries highlight those with values different from their associated *total* sediment production.

A map showing the distribution of the 22 most frequent GLU categories across the entire watershed is displayed in Figure 3-15; the GLU distribution by relative sediment production category from Table 3-7 is shown in Figure 3-16. The remaining 38 GLU categories are not shown in Figure 3-13 as they collectively represent less than 6% of the total USCR watershed area.

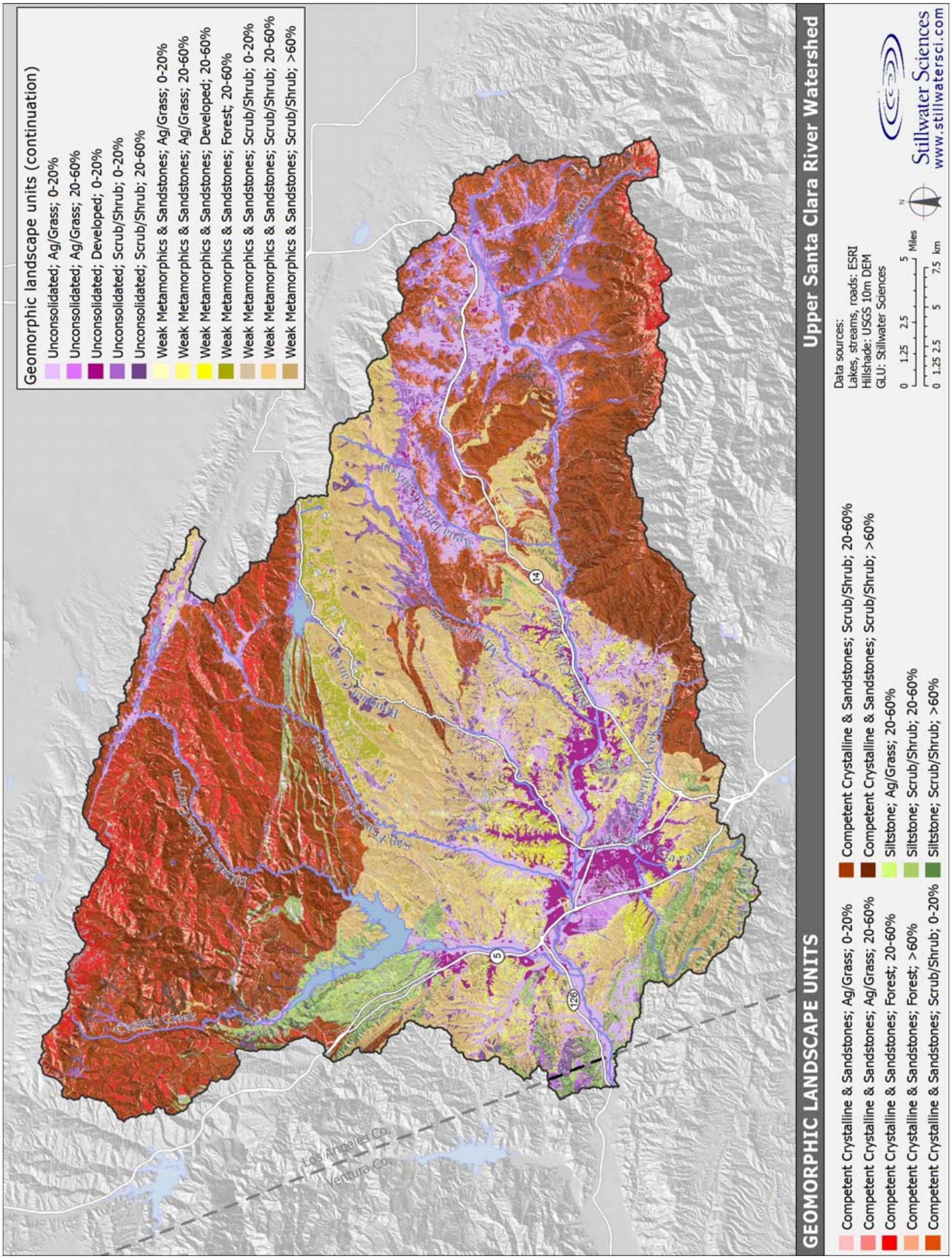

Figure 3-15. Geomorphic Landscape Units (GLUs) in the USCR watershed.

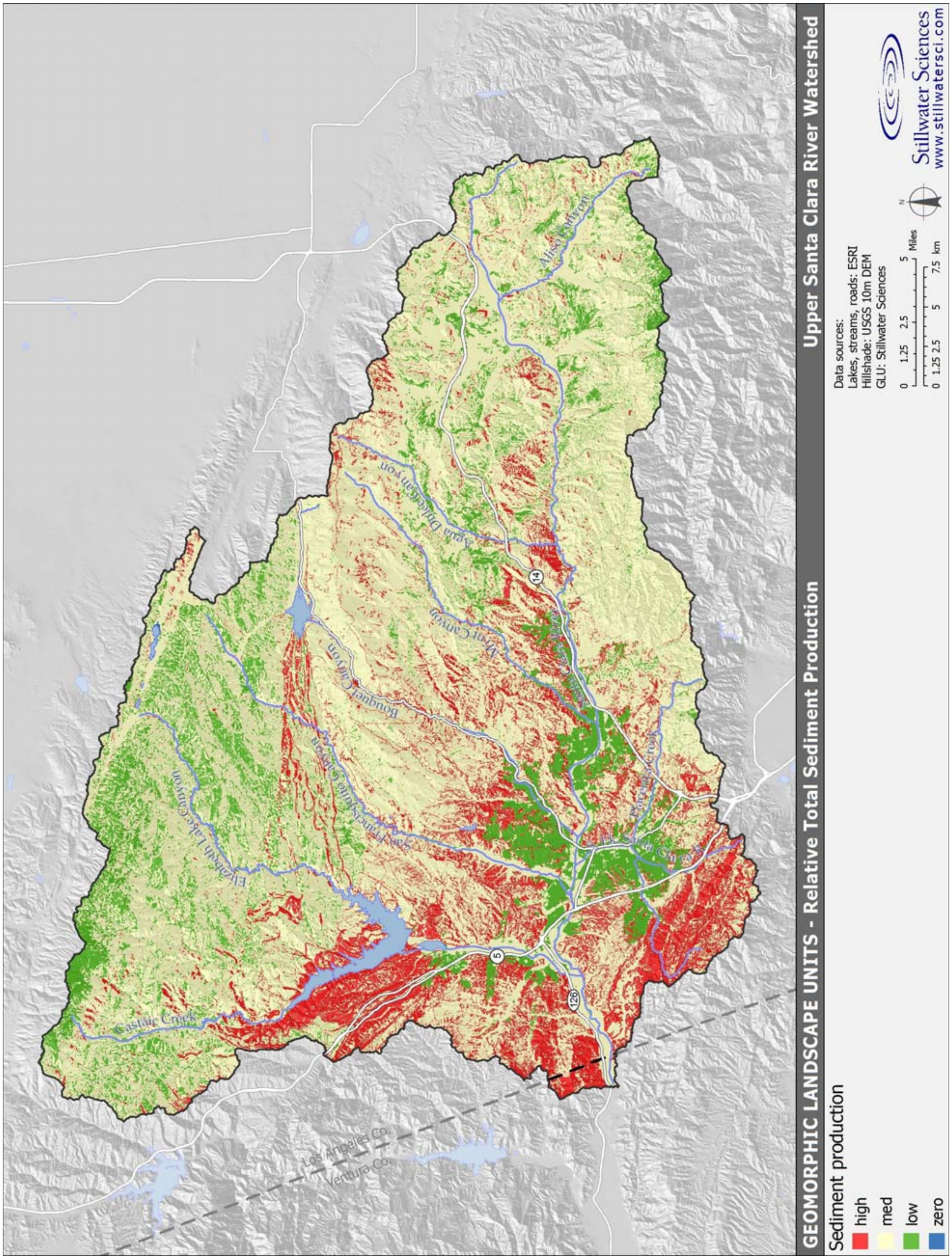

Figure 3-16. Predicted relative rates of total sediment production in the USCR watershed.

The map shown in Figure 3-16 represents a prediction of the relative production of sediment from every part of the watershed. The most striking attribute of this map is the variability in the distribution of low, medium, and high sediment-producing units across the watershed. Specifically, the majority of low-producing units are concentrated in two areas: the forested, high-elevation mountainsides in the northern half of the watershed and along the southern divide (i.e., upper Castaic, San Francisquito, and Aliso Canyon creeks), and the urban areas of the Santa Clarita basin. The vast majority of the high sediment-producing units are concentrated around the perimeter and partly within those developed areas where steep bare or grass-covered hillsides underlain by weak, young sedimentary rock occurs. These spatial patterns reflect the underlying combination of geology, land cover, and hillslope gradient that place about 70% of the watershed area into our assigned sediment-production category of “Medium” (see Table 3-8 in the following section). Portions of the watershed with “Zero” sediment production potential are shown where the GLUs contain the open water land cover category, such as within the boundaries of reservoirs and lakes (e.g., Bouquet Reservoir and Castaic Lake), which function exclusively as depositional basins.

This spatial prediction is lacking in two significant respects, however. The first is that the GLU analysis does not account for any routing or storage of sediment within the channel network. This makes it difficult to equate estimated sediment production with actual delivery to the stream channels. Particularly in the valley reaches of the watershed with substantial opportunities for sediment storage because of low hillslope gradients and the presence of floodplain areas (i.e., the Acton and Santa Clarita basins), most sediment produced on adjacent hillslopes with minimal tributary density would simply deposit at the base of the hillside and/or the floodplain. If assumed to be equivalent to our sediment production estimates, sediment delivery rates from the adjacent hillsides is likely overestimated in these areas. In the upland areas of the watershed, however, sediment production likely approximates sediment delivery to the tributary channels given the steep slopes and minimal storage potential occurring there. Given the distribution of steep slopes across the USCR watershed, we anticipate any overestimation of sediment delivery, as derived from our sediment production estimates, will be only modest in the upper watershed but potentially significant at sites downstream of the major depositional basins along the river (see next section).

The second inadequacy of this analysis is that it is based on the vegetation cover of the 2001 Landsat imagery, which obviously predates and so does not include any influence of recent wildfires (particularly the 2007 Buckweed and 2009 Station fires). For considering long-term rates and spatial patterns, however, this is not a significant shortcoming.

3.3.4.2 Quantified rates of total sediment production and delivery

Although a qualitative characterization of sediment-production zones is useful for understanding how the watershed behaves, numeric values for the rates of production and, ultimately, downstream sediment delivery are particularly valuable for applied studies such as this one. They can be used to assess the magnitude of downstream sediment loads and the potential consequences of vegetation changes (particularly by urbanization or wildfire), and they can also inform the locations where greatest management attention should be invested.

As summarized in Section 3.3.3, data from debris basins and water storage reservoirs in the USCR watershed provide a range of sediment yields that is corroborated by other regional metrics such as tectonic uplift and fault displacement. To quantify rates of total sediment delivery in the USCR watershed, we first defined GLUs across each of the watersheds contributing to the debris basins and reservoirs. They were categorized into areas of “high”, “medium”, “low”, and “zero” sediment production, using the criteria described above for the entire USCR watershed (Table 3-9). We then assigned specific numeric values to the relative categories of "high," "medium," and "low" sediment production by GLU, recognizing that these values will not be particularly well constrained. The "low" and "middle" values were selected to be close to the lowest rate and the median of the rates in Table 3-5: 120 and 930 t km^{-2} yr^{-1}, respectively. The "high" value was selected to be close to the second highest rate in the table (6,500 t km^{-2} yr^{-1}), rather than the highest rate (10,000 t km^{-2} yr^{-1}) because that highest value (Victoria debris basin) deviated substantially from the regression of all debris basin and reservoir sediment yield values versus their respective drainage areas (see Figure 3-11). Furthermore, the data source of the second highest value, Oakdale debris basin, had the greatest contributing area of any LADPW debris basin, which therefore should be more representative when extrapolating to the rest of the USCR watershed. The values chosen for the GLU categories are reported in Table 3-8.

Table 3-8. Sediment production results from the GLU analysis in the USCR watershed.

Relative sediment production	Area (km^2)	Area (% entire drainage area)	Sediment production per unit area (t km^{-2} yr^{-1})	Average annual sediment production (t yr^{-1})	Landscape denudation rate (mm yr^{-1})
Zero	13	1%	0	0	0.0
Low	263	16%	200	53,000	0.1
Medium	1,169	69%	1,000	1,170,000	0.5
High	234	14%	7,000	1,640,000	3.7
Watershed total	**1,679**	**100%**	**1,700**	**2,860,000**	**0.9**
Watershed below dams	**1,242**	**73%**	**1,900**	**2,330,000**	**1.0**

For comparative purposes, the values applied for Santa Paula Creek (Stillwater Sciences 2007b) were 22,000, 2,400, and 300 t km^{-2} yr^{-1} for the GLUs identified as "high," "medium," and "low," respectively, based on a set of debris-basin data from Ventura County and watershed-scale sediment-delivery rates calculated by Warrick (2002). Values used for Sespe Creek (Stillwater Sciences 2010) were based on the rates from the Santa Paula Creek study as well as a set of "reduced factors" with H = 20,000, M = 2,000, and L = 300 t km^{-2} yr^{-1}. Finally, the values used for upper San Francisquito Creek (Stillwater Sciences 2009) in the dry, eastern part of the USCR watershed were considerably lower than those used in the two previous studies, with H = 5,500, M = 1,350, and L = 150 t km^{-2} yr^{-1}. The present study uses values more similar to those used for the upper San Francisquito Creek watershed, especially for the "high" category, because we anticipate that lower rainfall in this eastern half of the Santa Clara River watershed results in relatively lower sediment yields as compared to those occurring in the relatively wetter Santa Paula and Sespe Creek watersheds to the west (see Figure 1-5). The "high" value used in the present study, based on data from the Oakdale debris basin, was judged to be more appropriate than the (lower value) upper San Francisquito Creek study, however, because of the presence of several highly erosive, young sedimentary formations (e.g., Pico, Castaic, Saugus, and Mint Canyon formations) that dominate the Santa Clarita basin and surrounding upland areas.

To improve the confidence of our sediment production estimates reported in Table 3-8, we compared the measured sediment yields for the debris basins and reservoirs of Table 3-5 within the USCR watershed with predicted rates using our GLUs within their contributing drainage areas

(Figure 3-17). The yields for many individual basins are moderately to very overpredicted by the GLU methodology, likely a consequence of hillslope or in-channel sediment storage and/or the wash-out of the finer sediment fractions before clean-out. Most of the best-matched results are seen in the largest watersheds, which suggests greatest confidence for watershed areas greater than tens of square kilometers (>10 km^2).

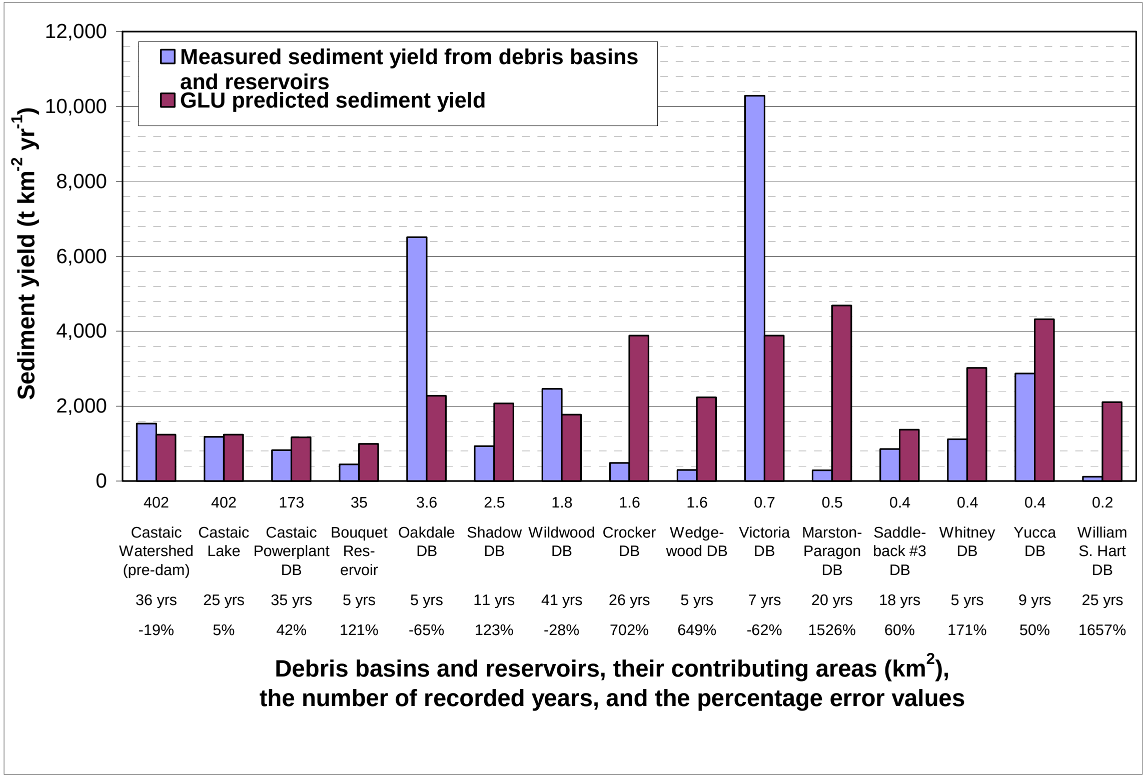

Figure 3-17. Measured and predicted debris basin and reservoir sediment yields. The measured sediment yield values are summarized in Table 3-5. Predicted values were generated using our GLU methodology.

By integrating these rates across our relative sediment production categories, this results in a predicted annual sediment-production rate of 2.9 million t yr^{-1} and a unit-area rate of **1,700 t km^{-2} yr^{-1}** over the entire USCR watershed. This is equivalent to a watershed-averaged landscape denudation rate of 0.9 mm yr^{-1}. When considering only those portions of the watershed below Bouquet Canyon and Castaic dams (area = 1,242 km^2), our predicted annual sediment-production rate reduces to 2.3 million t yr^{-1} but produces a higher unit-area rate of 1,900 t km^{-2} yr^{-1}.

Although by convention these rates are all expressed on a "per year" basis, both geomorphic theory and common sense acknowledge that actual sediment production is highly episodic, with many years of relatively little production punctuated by erratic pulses of very high production and delivery associated with large storms. These values are averaged over the period of debris basin and reservoir records, namely a few decades, and so they have significant uncertainty—truly extreme rainfall (or rain following fire) events are not included, nor are multi-decadal droughts. Year-to-year variability may be of the same order, or more, as the predicted "annual" values themselves.

More quantitative corroboration of the relation between predicted sediment-production rates, and achieved sediment yields, can be derived from direct monitoring of sediment transport rates at stream gauging stations. The USGS stream gauge for the mainstem river at the County line (USGS 111008500 and 11109000) was the site of sediment discharge measurements during the 1970s–1980s. When combined with the 47-year discharge record at the gauge (see Section 4.1), these data indicate a total average annual quantity of sediment in the river from the USCR watershed (below dams) of nearly 900,000 t yr^{-1}. This estimate differs from our GLU-based estimate of watershed sediment production of 2.3 million t yr^{-1} (below dams) by over a factor of 2, suggesting that a significant fraction (about half) of the hillslope-generated sediment is not reaching the County line. One likely explanation is that considerable sediment storage is likely occurring along the length of the river, particularly as it flows through the Acton and Santa Clarita basins. Our analysis on river bed level changes and sediment transport capacity supports this inference, and that long-term aggradation (i.e., sediment accumulation) has been occurring along the river channel through much of the Santa Clarita basin during recent decades (see Sections 4.3.2 and 4.3.4).

An alternative approach for assessing watershed sediment-production rates has been developed to establish criteria for designing debris basins. The LADPW's Sedimentation Manual (LADPW 2006) provides equations and empirical values for calculating the quantity of sediment produced by a saturated watershed significantly recovered after burn (i.e., more than 4 years post-fire) as a result of a 50-year, 24-hour rainfall event (referred as a Design Debris Event [DDE]). Their methodology subdivides Los Angeles County into Debris Potential Areas (DPA) and develops Debris Production (DP) curves for each of the DPA. These subdivisions are a function of isohyetal maps of 24-hour rainfall intensities of a 50-year event. The entire USCR watershed lies in the DPA-3, DPA-5, DPA-8, and DPA-9 for the Santa Clara Basin. Using the DP curves for these areas and the respective drainage areas in each area, the estimated DDE (50-year, 24-hour rainfall intensity) sediment delivery is approximately 30 million t (or 20,000 t km^{-2}). By way of comparison, these values are approximately a factor of 10 greater than the annual average sediment-production rates predicted with using our GLU approach. Recalling that the DDE is meant to characterize an extreme 50-year event, a 10-fold increase over the predicted annual average is on par with the observed 10- and 22-fold increases over the annual average in measured sediment flux during the 2005 and 1969 floods, respectively, at the County line stream gauge (USGS 11108500 and 11109000) (see Chapter 4 below for details).

A final approach for validating our GLU-derived sediment production rates is by comparing our estimates against our cosmogenic nuclide sediment dating results at the sampled drainage areas. Figure 3-18 shows these comparisons, which reveal generally good agreement, particularly with the entire watershed area (USCR Mainstem End sampled at the County line) and at Pico Canyon (sample of the highly erodible Pico Formation siltstones). For the other samples, our GLU-derived sediment-production rates over-predicted erosion rates by about a factor of two, except for Haskell and Grasshopper canyons which were over-predicted by about a factor of five. It is worth considering that these data span different time scale, where our GLU-derived values represent erosion rates over the past several decades and the sediment dating values go back centuries and, in some instances, millennia. Given that erosion rates over a longer time frame might be expected to be higher than those over shorter ones, due to inherent stochastic properties (i.e., bigger floods), this excellent agreement between the watershed-wide erosion rates from the GLU and the sediment dating approaches is unexpected. A possible explanation for this agreement is either: (1) the recent past has been very much stormier than the long-term expectation, possibly as a function of natural ENSO fluctuation or climate change effects; or (2) anthropogenic effects have significantly destabilized the landscape. The latter possible explanation must be at least part of the answer.

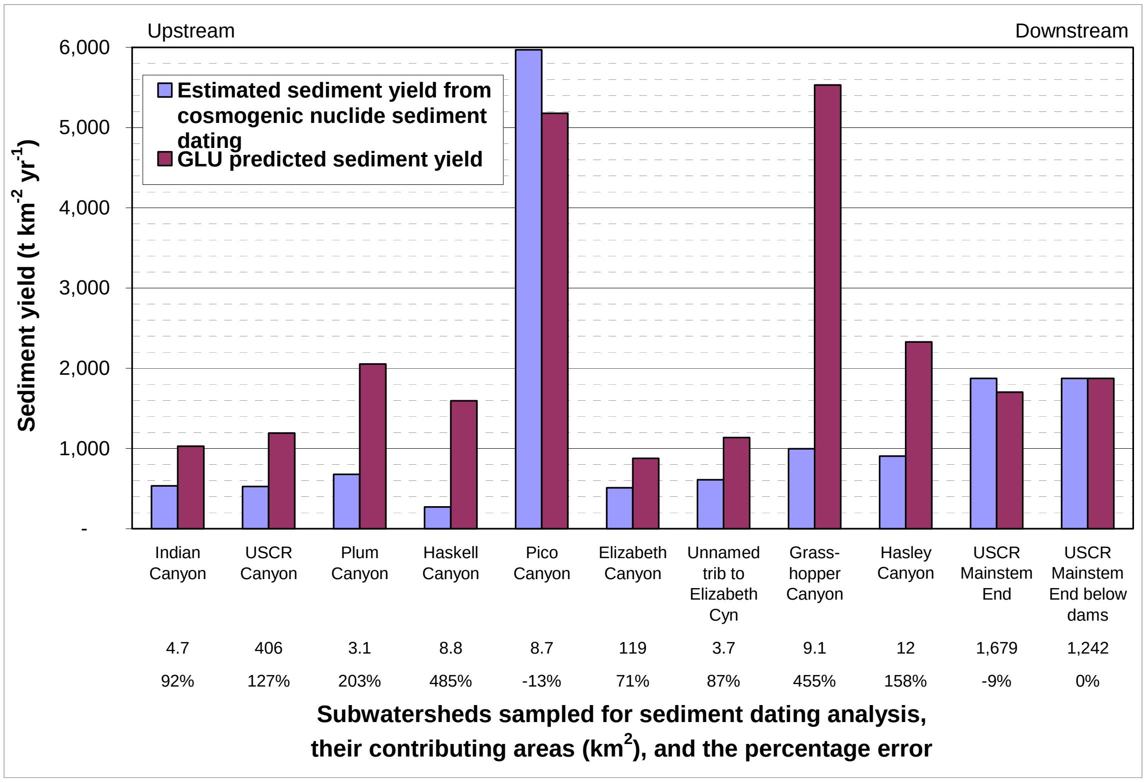

Figure 3-18. Measured sediment yields from cosmogenic nuclide sediment dating and predicted sediment yields generated from our GLU methodology. The measured sediment yield values are summarized in Table 3-4.

Although the range is quite broad, the County line stream gauge sediment yield, DPA sediment production values, and cosmogenic dating erosion rates do bracket our estimated total sediment-production rate for the USCR watershed using our GLU approach. They provide some independent confirmation that our estimates are well within the correct order of magnitude, and that the values may therefore prove not only reasonable but also useful in subsequent management applications.

3.3.4.3 Production of coarse sediment

Analogous to the procedure for total sediment, geomorphic landscape units across the USCR watershed were evaluated for their relative contribution of coarse sediment (i.e., gravel and cobble from sandstone and granitic rocks) into the channel. This component of the sediment load is highlighted because of the overriding influence of this resistant lithology on the bedload and morphology of the river. For this analysis, areas mapped as having sandstone/conglomerate- or igneous/metamorphic-dominated lithologies were included, together with modern and older fluvial deposits (which have a high proportion of cobbles and boulders). In terms of our GLU categories, the coarse-bearing units included all of the Competent Crystalline and Sandstones unit, Weak Metamorphics and Sandstones unit, and most of the Unconsolidated unit. This probably results in a modest under-representation of actual cobble- and boulder-contributing areas, because even the shaley units include interbeds of sandstone that were observed to constitute as much as about 10 percent of the deposit.

The assignments of GLUs into coarse sediment-production categories are listed above in Table 3-7. Their spatial distribution across the watershed is displayed in Figure 3-19. In contrast to our analysis of total sediment production discussed above, however, we have found no measured data to provide numeric values to quantify the relative categories of “High,” “Medium,” and “Low” coarse sediment production (or to their spatial integration across the watershed as a whole). We therefore have not quantified the absolute rate of coarse sediment production (or delivery) into the USCR on the spatial distribution of relative coarse-sediment production areas.

Inspection of Figure 3-19 emphasizes several features of the predicted sources of coarse sediment. First, sources of coarse sediment are widely distributed across the watershed, and so the channel likely has ready access to coarse sediment throughout its length. Second, about 18 percent of the total map area is predicted to be zones of “high” delivery. These zones are primarily steep and nominally grass- or shrub-covered slopes, based on the GIS-based land cover classifications. Field inspection revealed that many of these high-delivery areas have a very sparse vegetative cover that does not significantly impede the processes that deliver coarse blocks to the channel network (Figure 3-20).

Unlike the movement of fine sediment, which tends to correspond closely to the flow of water down the channel network, coarse bedload sediment moves only episodically and is subject to the vagaries of local flow competency, long-term floodplain storage, and hydraulic constrictions. Thus the “coarse sediment connectivity” (Hooke 2003) of a channel network can influence the downstream flux of bedload material as significantly as the initial hillslope supply itself.

The only potentially significant constriction along the mainstem channel of the USCR is Soledad Canyon (reaches M19 through M23; see Chapter 4) (Figure 3-20). Upstream of the canyon in the Acton basin, the river has a braided alluvial pattern, or wash, with abundant sediment stored on active point and mid-channel bars and in the near-channel floodplain. Once in the canyon reaches, however, the channel is highly confined and expresses little sediment storage. Downstream of the canyon in the Santa Clarita basin, sediment deposition is again voluminous, suggesting that the canyon is primarily a transport zone (see Chapter 4) but one that may not significantly impede the downstream delivery of material.

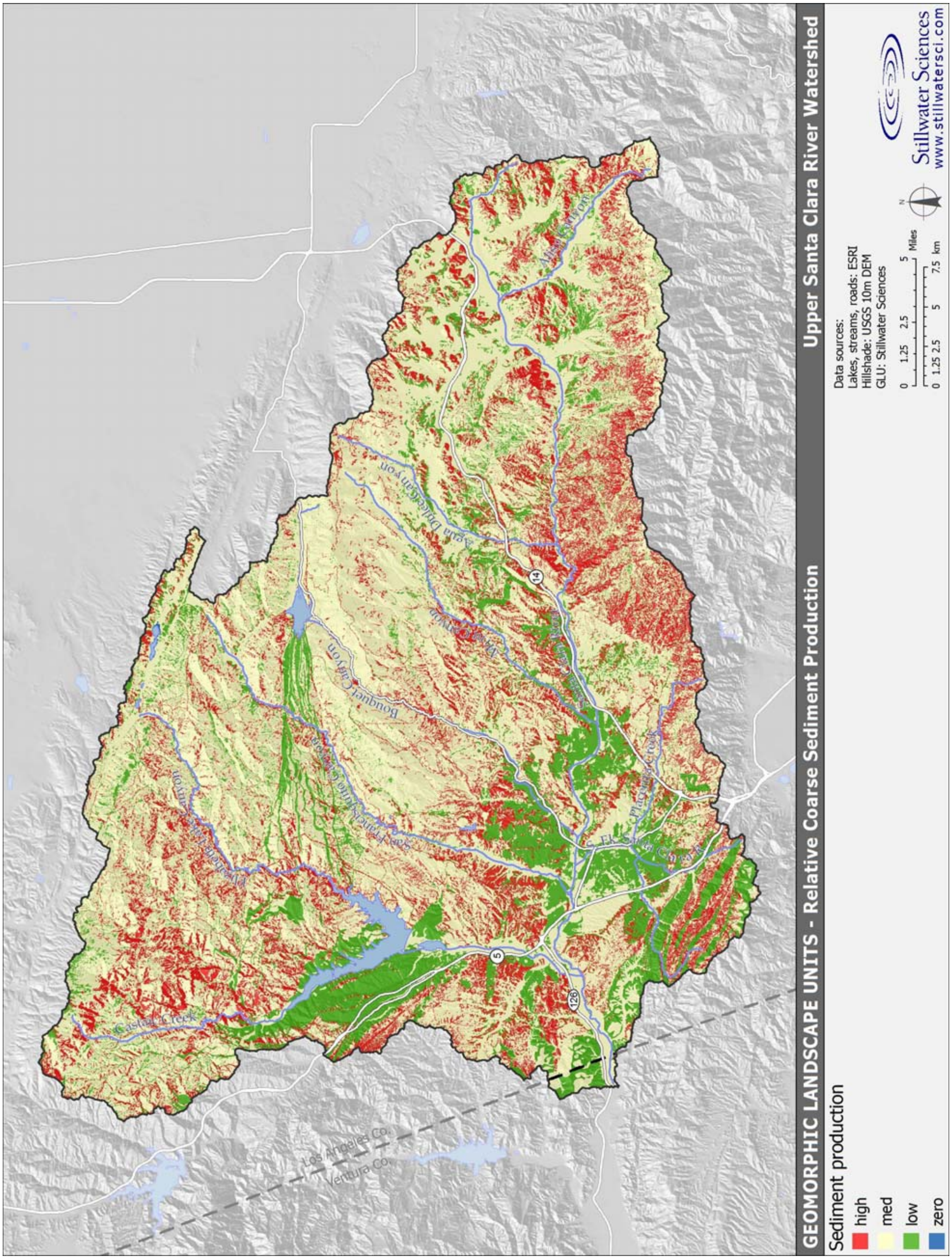

Figure 3-19. Predicted relative rates of coarse sediment production in the USCR watershed.

Figure 3-20. Relatively rapid delivery of anorthosite (crystalline) rock boulders into the USCR from steep, nominally shrub-covered hillslopes along Soledad Canyon. Note the presence of the Southern Pacific Railway on river right, which further constricts the canyon reaches of the USCR.

3.4 Sediment Delivery from Tributaries to the Upper Santa Clara River Valley

3.4.1 Episodic sediment delivery from tributaries

Over the short term, sediment delivery to the mainstem USCR from its tributaries is likely to be much more episodic than the rate of supply from hillslopes directly adjacent to the river. Storms of all sizes help move sediment down slopes and into channels by rain impact, overland flow, and mass wasting, leading to nearly continuous inputs to tributaries from slopes during the wet season. In the dry season, hillslope sediment production continues via dry raveling (Scott and Williams 1979). In contrast, sediment is delivered from tributaries to the mainstem more episodically, in flows associated with big storms and also in moderate storms that follow fires (Wells 1981; Florsheim et al. 1991).

Sediment transport along the mainstem USCR is even more episodic than delivery of sediment from tributaries. Extreme events associated with major storms are the primary movers of sediment in the watershed, as discussed in greater detail in Chapter 4 below.

3.4.2 Contributions from tributaries along the river corridor

Use of our GLU methodology, quantified using the watershed sediment-yield estimates from measured debris basin and reservoir sedimentation data provides a means to estimate sediment-production rates from drainage areas of the major streams in the USCR watershed. Table 3-9 summarizes our sediment-production estimates for each of these subwatersheds, listed in order of greatest to lowest sediment-production rate per unit area. Figure 3-21 graphically represents the relative differences in sediment production from the subwatersheds, including the remaining areas of the USCR watershed. For Bouquet Canyon and Castaic Creek, we split their watersheds into upper and lower portions, divided at their respective dams.

As represented in this figure, the subwatersheds predicted to exhibit the greatest sediment-production rates per unit area (>2,500 t km^{-2} yr^{-1}) are located in the western portion of the USCR watershed where landscapes are characterized by sparse vegetation cover, weak lithologies, and moderate to steep slopes (rainfall is also greater in this part of the watershed, but that factor is not explicitly incorporated into the GLU analysis). Specifically, these subwatersheds are lower Castaic Creek, Lion, Long, Portrero, San Martinez Grande, and San Martinez Chiquito canyons, and the South Fork SCR. All of these tributaries have direct connectivity with the mainstem river as they are positioned close to the river in the Santa Clarita basin. The presence of debris basins and debris retention inlets in portions of lower Castaic Creek (e.g., Hasley Canyon area) and the South Fork SCR do, however, effectively reduce the total sediment-production rates (particularly coarse-grained material) from these subwatersheds. These structures are absent in the other five high producing subwatersheds, suggesting that these areas have the highest sediment delivery in the watershed (see Figure 3-10).

In contrast, the subwatersheds predicted to exhibit the lowest sediment-production rates per unit area (<1,200 t km^{-2} yr^{-1}) are located in the eastern portions of the USCR watershed: Acton, Aliso, Bear, Kentucky Springs, Soledad (eastern-most end of USCR watershed), Trade Post, and upper Bouquet canyons. These landscapes are also characterized by less erodible bedrock types (Competent Crystalline and Sandstones category of our GLU analysis). Sediment derived from upper Bouquet Canyon is very effectively intercepted and stored indefinitely by Bouquet Reservoir and, therefore, never reaches the mainstem river channel. The other low-producing subwatersheds are connected almost directly to the mainstem in the Acton basin with minimal infrastructure influences.

Results and discussion of sediment transport capacities estimated for the major tributaries listed in Table 3-9 are presented below in Section 4.3.2. Discussion on the effects of infrastructure on sediment delivery processes is presented below in Section 4.2.

Table 3-9. Sediment production results from the GLU analysis in the major tributary streams of the USCR watershed, listed in order of greatest to least average annual sediment-production rate per unit area. [a]

Major stream name	Area (km^2) [b, c]	Average annual sediment production (t yr^{-1}) [b, c]	Sediment production per unit area (t km^{-2} yr^{-1}) [b, c]
Towsley Canyon	14.9	69,000	4,600
S. M. Grande Canyon	8.6	38,000	4,400
Lyon Canyon	3.6	15,000	4,200
Gavin Canyon	29.4	120,000	4,200
Potrero Canyon	11.6	47,000	4,100
Violin Canyon 2	9.6	37,000	3,900
S. M. Chiquito Canyon	12.4	49,000	3,900

Major stream name	Area (km^2) [b, c]	Average annual sediment production ($t\ yr^{-1}$) [b, c]	Sediment production per unit area ($t\ km^{-2}\ yr^{-1}$) [b, c]
Pico Canyon	17.6	67,000	3,800
Violin Canyon 1	15.1	57,000	3,800
So. Fork SCR	116.2	320,000	2,800
Long Canyon	4.0	10,000	2,600
Lion Canyon	2.2	5,600	2,600
Hasley Canyon	20.7	50,000	2,400
Vasquez Canyon	11.1	26,000	2,400
Haskell Canyon	28.4	60,000	2,100
Plum Canyon	8.2	17,000	2,100
Newhall Creek	21.3	44,000	2,100
Tick Canyon	14.8	30,000	2,000
Placerita Creek	23.1	44,000	1,900
Dry Canyon	19.7	35,000	1,800
Bouquet Canyon [c]	180.4 (145.2)	310,000 (280,000)	1,700 (1,900)
USCR (remainder) [d]	268.6	460,000	1,700
Castaic Creek [c]	524.6 (122.6)	860,000 (370,000)	1,600 (3,000)
Mint Canyon	75.8	120,000	1,600
Texas Canyon	28.2	46,000	1,600
San Francisquito Canyon	134.6	220,000	1,600
Young Canyon	7.3	10,000	1,400
Escondido Creek	24.6	32,000	1,300
Agua Dulce Canyon	76.1	98,000	1,300
Red Rover Mine	5.7	7,100	1,200
Sand Canyon	33.0	41,000	1,200
Hughes Canyon	8.0	9,400	1,200
Acton Canyon	54.4	64,000	1,200
Oak Springs Canyon	14.6	17,000	1,200
Kentucky Springs	23.5	27,000	1,100
Soledad Canyon	23.2	25,000	1,100
Iron Canyon	6.9	7,500	1,100
Bear Canyon	15.1	16,100	1,000
Aliso Canyon	63.2	64,000	1,000
Trade Post	6.7	6,600	980
Acton Canyon 2	6.5	6,300	980
Gleason Canyon	15.5	12,000	780

[a] Locations of the subwatersheds with their relative GLU-derived sediment production values are shown in Figure 3-21.
[b] Values given for the major streams with a direct connection with the USCR include the total area and sediment-production rate for that subwatershed (i.e., includes values from any tributary subwatersheds).
[c] Areas and sediment-production rates for regulated areas below dams are given in parenthesis.
[d] Portion of the USCR watershed excluding the major stream watersheds listed in this table.

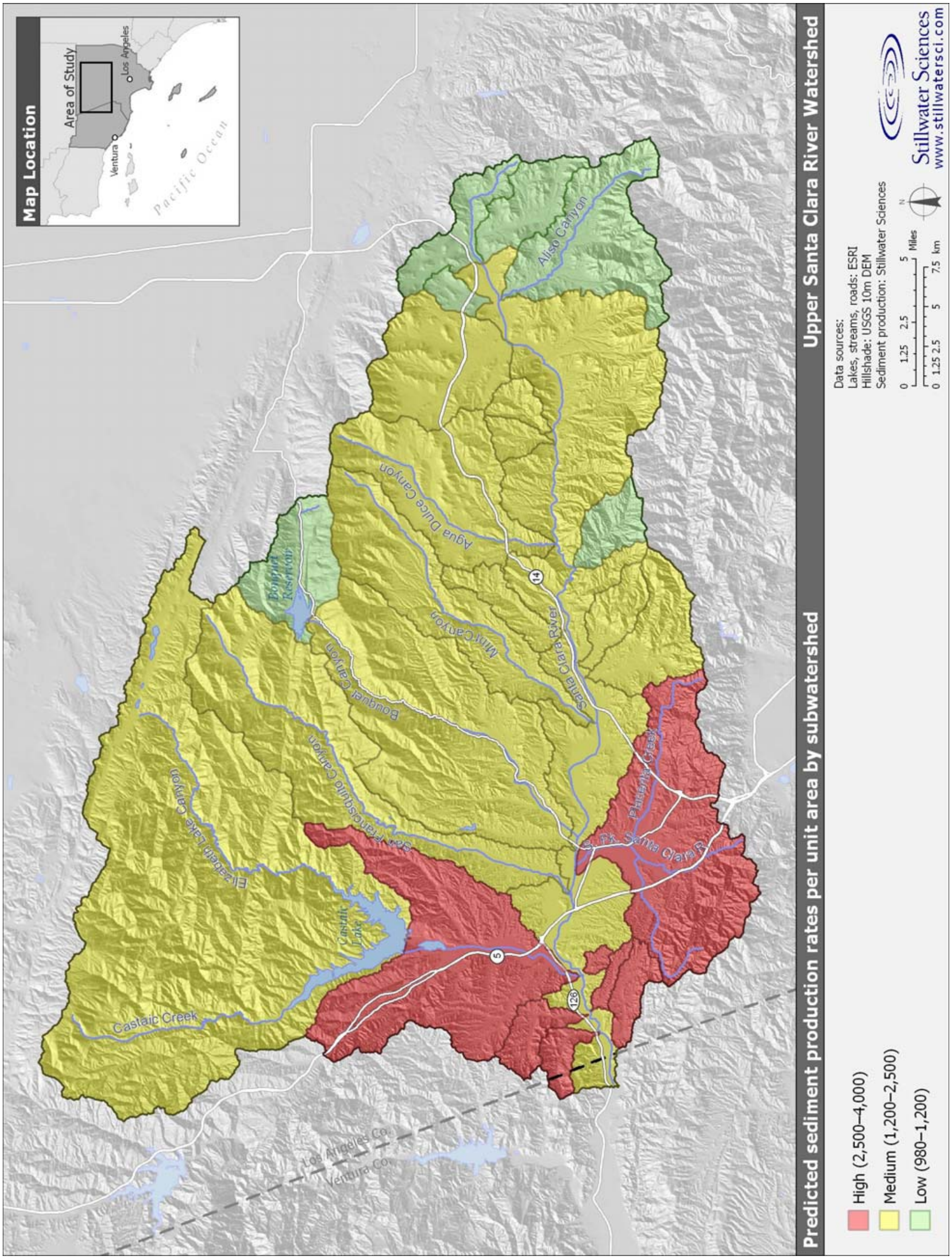

Figure 3-21. Predicted sediment-production rates per unit area by subwatershed in the USCR watershed.

4 TRIBUTARY AND MAINSTEM SEDIMENT TRANSPORT AND MAINSTEM MORPHOLOGICAL CHANGE

This chapter focuses on the factors affecting the morphology of the mainstem USCR and its major tributaries. First, we present a summary on the characteristics of sediment transport and the episodic events that convey the vast majority of sediment through the drainage network and river channel. Specific elements of water system and urban infrastructure and their potential effects on the river's morphology and sediment transport rates are discussed next. In the following section, we present detailed descriptions of the geomorphically-based river reaches and the major tributaries. In support of these descriptions are the results of computed sediment transport capacities and delivery rates in mainstem river and tributary reaches that, together, serve to evaluate channel stability in select locations of the Feasibility Study area. We also present the results of historical changes in the active channel widths and the bed levels of the mainstem river reaches over the past 80 years. The chapter concludes with a comprehensive summary of the reach-level dynamics and overall fluvial geomorphic processes along the USCR.

4.1 Frequency and Magnitude of Sediment Transport

Sediment transport processes in the USCR are dominated by extreme events associated with the river's highest flows (Table 4-1). These events transfer water and sediment from the hillslopes to the drainage network, and they are integral to changes in form of the mainstem USCR and its floodplain over time. The exchange of sediment between the river channel and floodplain during flood events (i.e., episodes of erosion and deposition) determines the hazards and assets of the river corridor. In an apparent contradiction, the hydrologic and geomorphic processes that create hazards (such as flooding, unwanted bed and bank erosion, and deposition) are the same processes that help sustain river ecosystems by creating assets (such as aquatic and riparian habitat diversity). Hence, understanding the fluvial geomorphic processes in the USCR watershed is a necessary precursor for understanding both the risks and the opportunities of the river corridor.

Table 4-1. Annual maximum peak discharges since WY 1928 on the USCR, gauged or estimated to be in excess of 283 $m^3 s^{-1}$ (10,000 cfs), covering all flows greater than about a 4-year recurrence.

Date	USCR at the County line (USGS 11108500 and 11109000) [a]		USCR near Saugus (USGS 11108000 and LADPW F92B-R and F92-R) [a]	
	Drainage area			
	1,679 km^2	**648 mi^2**	**1,064 km^2**	**411 mi^2**
	Period of record (Water Year [WY])			
	USGS 11108500: 1953–1996; USGS 11109000: 1928–1932, 1997–present		**1930–1977, 1979, 1983, 1985–1991, 1997–present**	
	Discharge [b]			
	$m^3 s^{-1}$	**cfs**	**$m^3 s^{-1}$**	**cfs**
3/12–13/1928	*14,000–23,000* [c]	*500,000–800,000* [C]		
3/2/1938	765 [d]	27,020 [d]	680	24,010
1/23/1943	n.d.	n.d.	425	15,010
2/22/1944	n.d.	n.d.	629	22,210
12/29/1965	906	32,000	328	11,580
1/25/1969	1,948	68,800	no record	no record
2/25/1969	no record	no record	900	31,780
2/11/1973	362	12,800	135	4,770
2/9/1978	646	22,800	n.d.	n.d.
2/16/1980	394	13,900	n.d.	n.d.
3/1/1983	866	30,600	423	14,930
2/15/1986	348	12,300	no record	no record
1/12/1992	348	12,300	n.d.	n.d.
2/18/1993	303	10,700	n.d.	n.d.
1/10/1995	484	17,100	n.d.	n.d.
2/3/1998	283	10,000	no record	no record
2/23/1998	no record	no record	538	19,000
1/9/2005	906	32,000	592	20,910
1/2/2006	354	12,500	20	710

[a] Instantaneous peak discharge. Sources: USGS National Water Information System Annual Peak Streamflow Data for the Santa Clara River at the County line (USGS 11108500 and 11109000) and near Saugus (USGS 11108000) and LADPW records near Saugus (aka: Old Road Bridge; LADPW F92B-R and F92-R).

[b] Absence of reported peak flow values during a period of gauge operation is indicated by "no record" for that event. Absence of values during a period of gauge non-operation indicated by "n.d.", meaning no data.

[c] Estimated peak flood flow following the St. Francis Dam failure near the County line (Simons, Li & Associates 1983, Begnudelli and Sanders 2007).

[d] Estimated value (no gauging information available) (see Stillwater Sciences 2007a).

4.1.1 Sediment discharge

Sediment discharge dynamics in the USCR were examined in two ways. First, the daily mean flow record for the USCR was combined with a sediment-rating curve to determine sediment yield both for individual flood events and on an annual basis. Secondly, the sediment-rating curve was combined with the distribution of daily mean flows (i.e., flow frequency) to determine the magnitude and frequency of sediment transporting flows within the watershed and investigate the "dominant discharge" in the USCR (i.e., the range of discharges that transports the most sediment over time).

Flow and sediment discharge data used in the analysis were from the downstream end of the USCR near the County line (USGS 11108500 and 11109000). The daily mean flow data were compiled for WY 1953–2009 (Figure 4-1) and flow frequency was determined by dividing the daily mean flow into log-based bins (i.e., bins were defined by increasing the exponent by 0.1) ranging from 10^{-2} (0.01) $m^3 s^{-1}$ to 10^3 (1,000) $m^3 s^{-1}$ and fitting a regression through the relationship (Figure 4-2). The sediment discharge rating curve was calculated as a combination of the suspended sediment load and bedload. The suspended sediment discharge data (and the associated flow data) for the County line gauges was compiled and a regression was fitted through the relationship. Bedload discharge at the gauge was calculated as 6% of the total suspended load and a regression was fitted through the data. This 6% value was used in previous analyses of sediment transport dynamics in the LSCR watershed (Stillwater Science 2007a; see Section 4.3.2). Combining the suspended load and bedload rating curves gives an overall total sediment rating curve for the USCR (Figure 4.3).

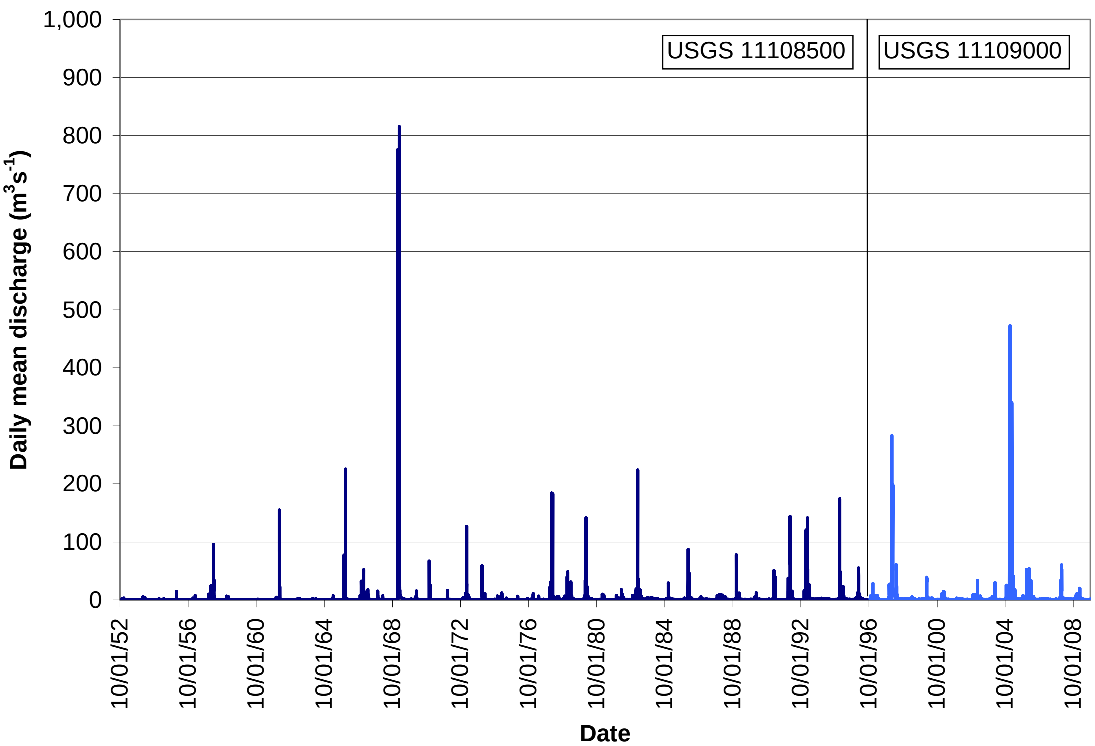

Figure 4-1. Daily mean discharge for the USCR at the County line (USGS 1118500 and 11109000) between WY 1953 and 2009.

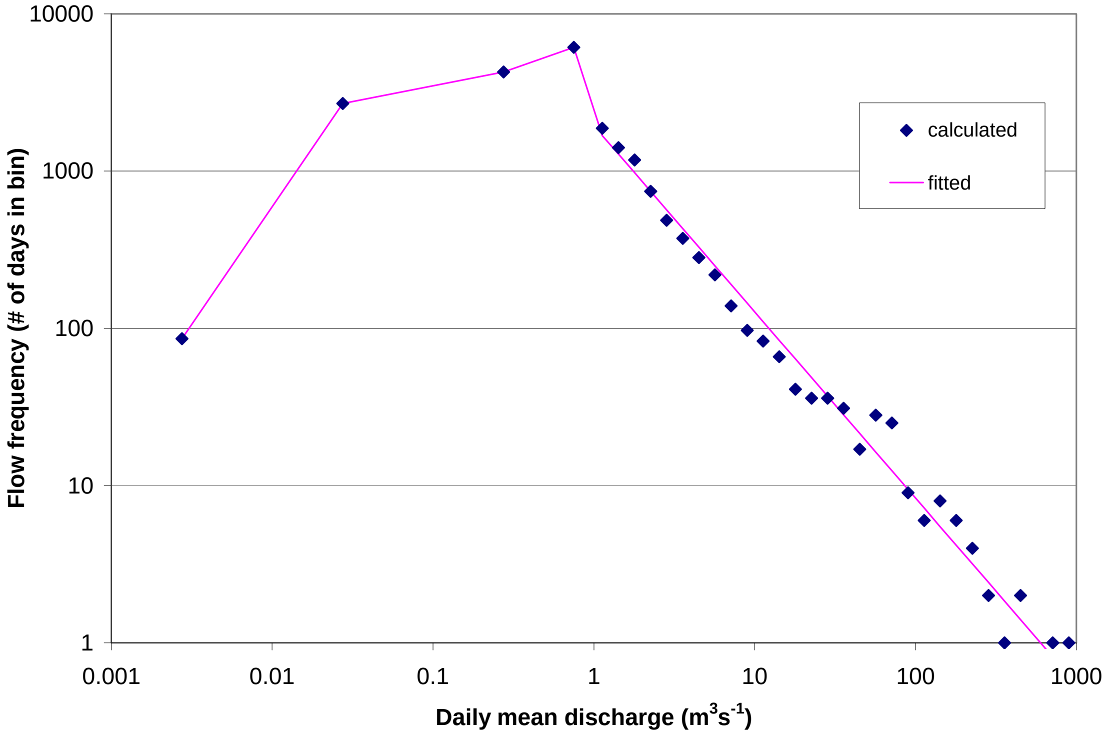

Figure 4-2. Daily mean flow frequency distribution for the USCR at the County line (USGS 1118500 and 11109000) between WY 1953 and 2009.

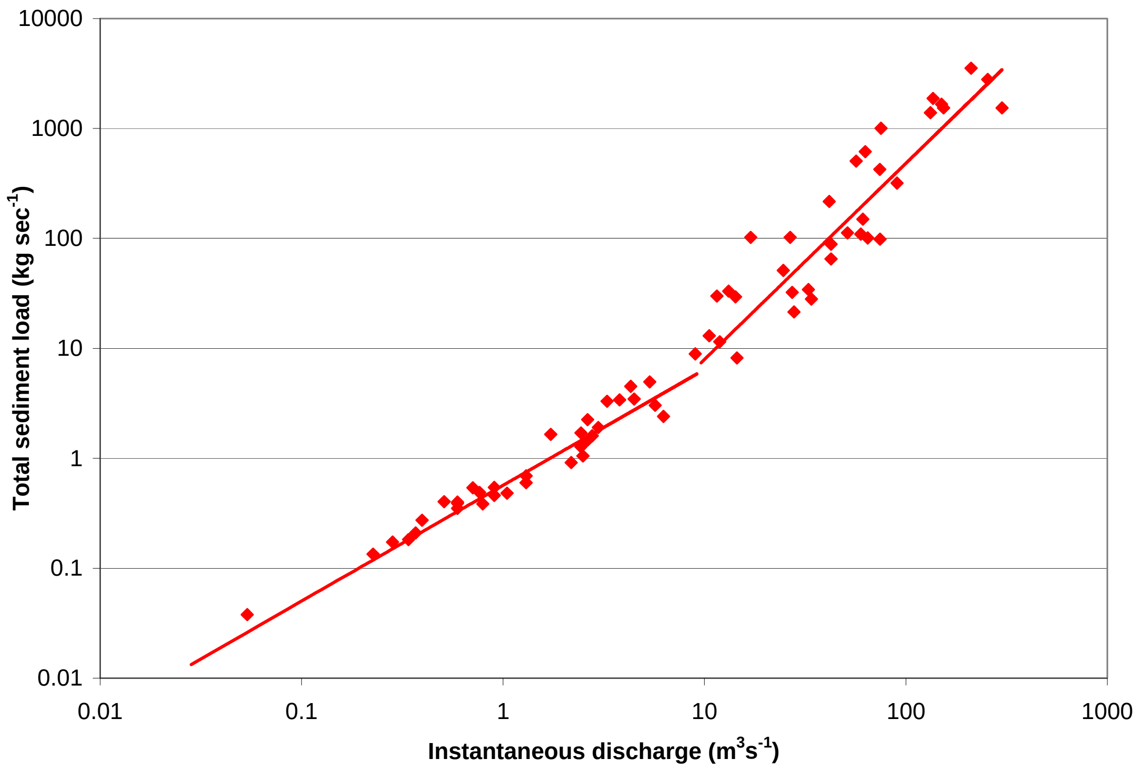

Figure 4-3. Total sediment load (suspended load + bedload) rating curve for the USCR at the County line gauges (USGS 11108500 and 11109000).

The average annual total sediment yield estimate for WY 1953 to 2009 for the USCR near the County line is approximately 900,000 t yr^{-1}, or a yield per unit area of 720 t km^{-2} yr^{-1}, from the effective contributing area (i.e., downstream of Bouquet and Castaic dams) of 1,242 km^2 (Figure 4-4). Annual sediment discharge over the past 57 years, however, is estimated to have varied by a factor of more than **50,000**—from a low of approximately 410 tonnes (WY 1961) to more than 22 million tonnes (WY 1969, which contains the flood of record). The two water years that contain the highest annual maximum instantaneous discharge (1969 and 2005) account for over half of the total sediment yield out of the USCR. In contrast, over one-half of all years have an annual total sediment yield less than 10% of the average annual total sediment yield.

The coarse fraction (>0.0625 mm) of the total average annual sediment yield is approximately 190,000 t yr^{-1}, or a per unit area contribution of 155 t km^{-2} yr^{-1} (from areas downstream of Bouquet and Castaic dams). This coarse sediment includes virtually all of the bed material load, together with any other sediment larger than 0.0625 mm but is nonetheless transported as suspended load.

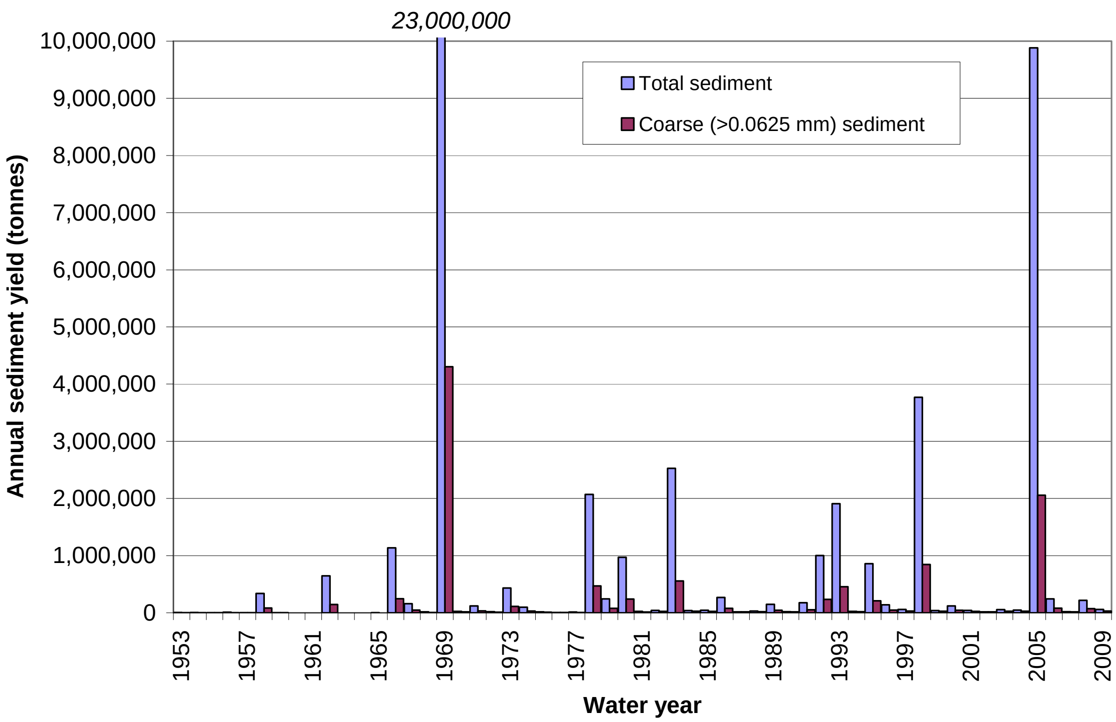

Figure 4-4. Calculated total sediment yield (suspended load + bedload) and coarse (>0.0625 mm) sediment yield for the USCR at the County line gauges (USGS 1118500 and 11109000).

4.1.2 Dominant discharge characteristics

The majority of sediment transport in the USCR mainstem occurs during very short periods of time. For instance, an estimated 50% of the roughly 51.2 million tonnes (56.4 million tons) of sediment that passed the County line stream gauge (USGS 11108500 and 11109000) between 1953 and 2009 was transported during high flows in just five days. Similarly, Warrick (2002) concluded that for the period 1928–2000, 25% of the total sediment discharge out of the entire Santa Clara River watershed occurred in just four days.

These results contrast sharply with the observations of alluvial rivers in humid environments, which have provided the historic basis for many of the classic generalizations of fluvial geomorphology, including the concept of "dominant discharge"—presumed to be the flow that, over the long term, performs the most work in terms of sediment transport (Wolman and Miller 1960, Emmett and Wolman 2001). In humid rivers, that flow most commonly occurs at an intermediate discharge, because a steadily increasing sediment transport rate with increasing flow coupled with the rapidly decreasing durations of large (and uncommon) flows produce a maximum total sediment load (calculated as the product of the sediment transport rate and flow frequency) at flows neither very small (because little sediment is moved) nor very large (because they occur so rarely and so briefly)—thus, "intermediate."

For the USCR, a very different picture emerges from the data, as shown in Figure 4-5, where flow frequency, sediment transport rate, and total coarse sediment load are plotted for data collected at the County line stream gauge over the period 1953–2009. The flow frequency (blue line) shows the typical pattern of discharges over several orders of magnitude, up to and exceeding 790 $m^3 s^{-1}$ (28,000 cfs). Yet total sediment load, calculated as the product of flow frequency and sediment transport rate, does not follow the trend suggested by the "classic" dominant-discharge model over the range of historic floods. Instead, the total load increases with discharge across the entire range of data, with its greatest value at the highest projected flow. Hence the "dominant discharge" for the USCR is the largest discharge on record. This pattern is consistent throughout the entire Santa Clara River watershed, including near the mouth of Sespe Creek and near the mouth of the mainstem Santa Clara River near Montalvo (see Stillwater Sciences 2007a and 2010). There is, surely, *some* large discharge that is so infrequent that the contribution to total sediment movement is smaller than a discharge of lesser magnitude but greater frequency—but unlike humid-region rivers, the range of discharges over which this occurs must have a recurrence much longer than that of a 100-year flood.

Correspondence of the dominant discharge with the largest flow on record has important implications for channel-forming processes. Dominant discharge is often described as the "channel-forming" flow, at the center of a range of flows that are most directly responsible for shaping and maintaining the channel in its characteristic "equilibrium" morphology (e.g., Wolman and Leopold 1957). The fact that the dominant, channel-forming flow is the largest flow on record implies that the USCR does not necessarily behave like a classic humid-region, alluvial river, but instead like arid channels as theorized by Wolman and Gerson (1978). For example, there is no reason to expect that the channel will overflow its banks every 1 to 3 years, or maintain a well-defined, regularly spaced riffle-pool sequence. In general, morphology will not exhibit equilibrium tendencies, with small, year-to-year fluctuations around a long-term "average" condition. Instead, the channel and its floodplain will experience dramatic changes due to episodically high flows that change the dynamics of the entire system, altering roughness and channel shape, and potentially leading to significant fluctuations in local channel bed elevation that persist for years, decades, or longer.

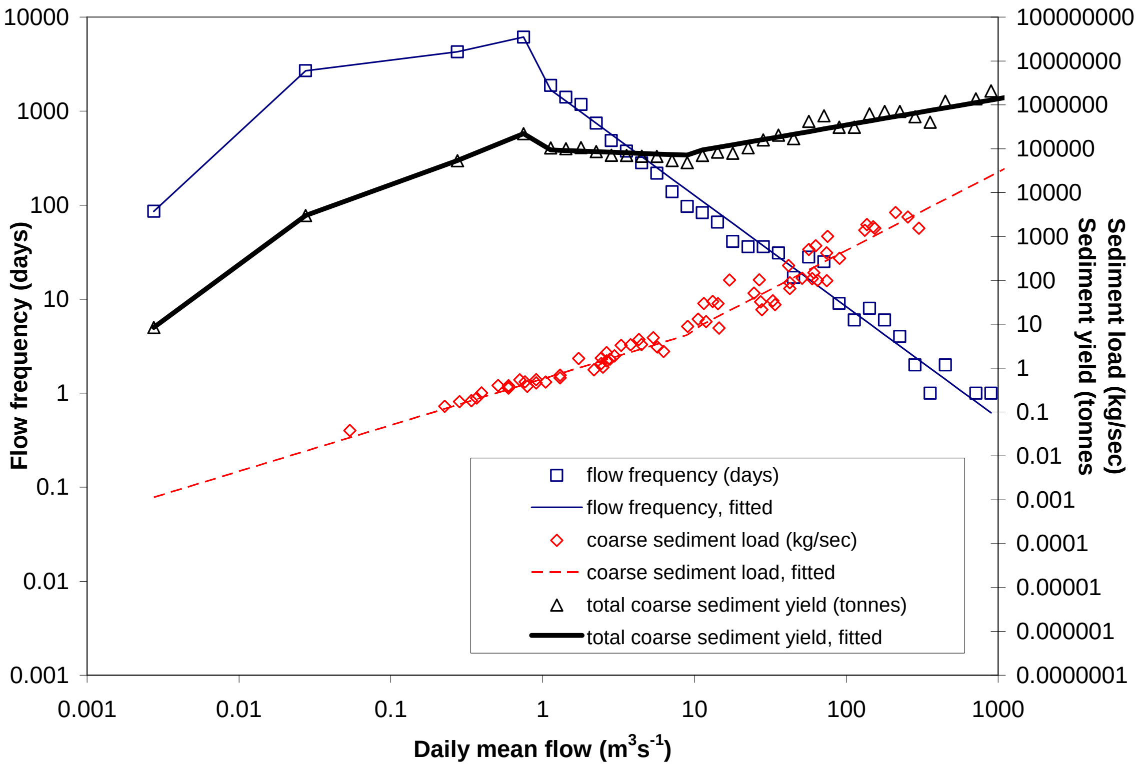

Figure 4-5. Flow frequency and coarse (>0.0625 mm) sediment load for long-term daily mean flow record for USCR at the County line stream gauge (USGS 1118500 and 11109000). Unlike classic alluvial rivers, the variation of sediment yield with flow does not exhibit a peak at "intermediate" discharges (as defined by the range of flows seen over the last century).

4.1.3 Effects of the El Niño-Southern Oscillation on flow magnitude and sediment delivery

The El Niño-Southern Oscillation (ENSO) is a climatic phenomenon that is characterized by warming and cooling cycles (oscillations) in the waters of the eastern equatorial Pacific Ocean. ENSO cycles have a 1–1.5 year duration and a 3–8 year recurrence interval, and they are related to changes in atmospheric circulation, rainfall, and upper ocean heat content (see Deser et al. 2004 and references contained therein). In southern California, ENSO years are characterized by relatively high rainfall intensities, with rivers and streams exhibiting higher annual peak flows than they do in non-ENSO years (Cayan et al. 1999, Andrews et al. 2004). This difference in flow magnitude is shown quantitatively in an analysis of the instantaneous peak flow record for the USCR (at the County line stream gauges) for ENSO and non-ENSO years between WY 1953 and 2009. For ENSO years there is an almost 50% probability of peak flow exceeding 280 $m^3 s^{-1}$ (10,000 cfs) (Figure 4-6: open symbols) whereas a non-ENSO year has only a 10% probability of peak flows exceeding that same value (Figure 4.6: closed symbols).

ENSO-induced climate fluctuations occur on a multi-decadal time scale that is consistent with the observed shift from a relatively dry climate (averaged over the period 1944–1968) to a relatively wet climate (averaged over the period 1969–1995) in North America's Pacific region (Inman and Jenkins 1999). The wet-period ENSO cycle, which existed to the end of the Inman and Jenkins study (1995) and has likely continued to the present, has been marked by strong ENSO years every 3–7 years, and mean sediment fluxes for Southern California rivers (from the Pajaro River south to the Tijuana River) that have been approximately 5 times greater than during the preceding dry period (1944–1968) (Inman and Jenkins 1999). For the entire Santa Clara River, the annual net sediment yield during the recent wet period was approximately 8 times greater than it was during the preceding dry period (Inman and Jenkins 1999). The characteristic episodic delivery of sediment from southern California watersheds in general, and the entire Santa Clara River watershed in particular, is strongly linked to ENSO-induced precipitation events with high day or multi-day rainfall totals. Within the USCR watershed, a good example of this phenomenon is a 10-day period during and directly after the January 2005 storm event accounting for approximately 10% of the total sediment delivered from 1953–2009 (i.e., 10% of the total sediment was delivered in 0.05% of the total time). In summary, sediment transport is highly concentrated in very brief periods of time.

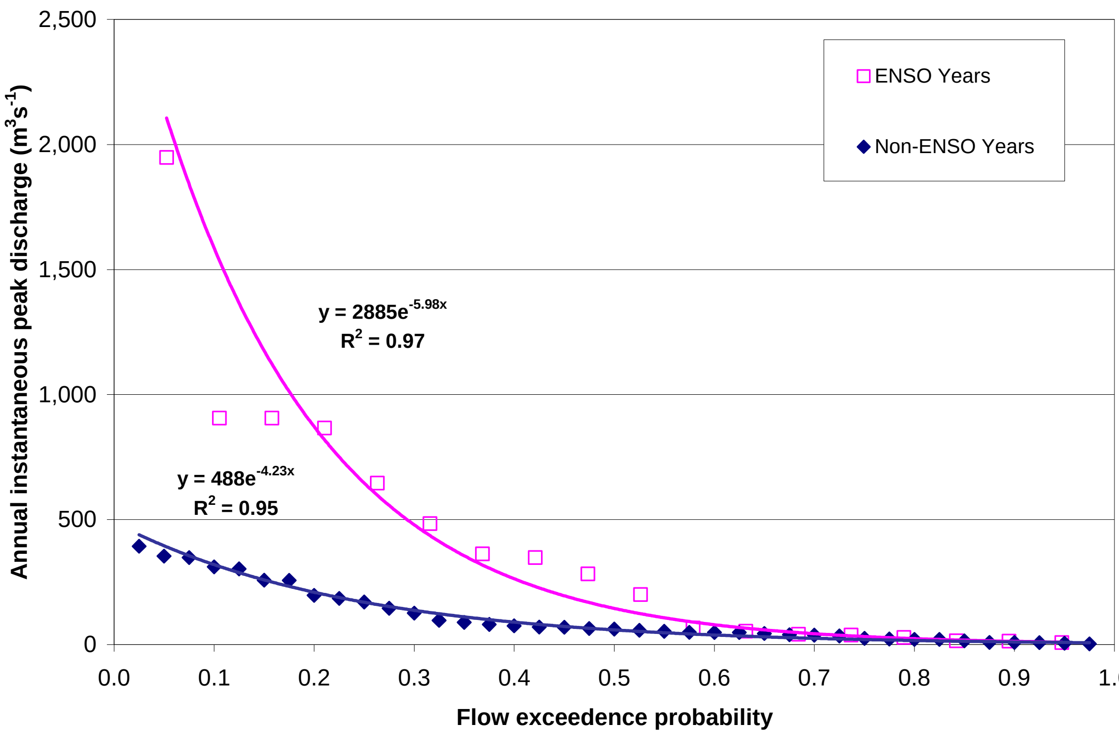

Figure 4-6. Flow exceedance for ENSO/non-ENSO years (from WY 1953-2009) for the USCR at the County line gauges (USGS 1118500 and 11109000).

4.2 Potential Impact of Infrastructure and Anthropogenic Channel Modifications

Channel-related infrastructure and modifications and land-use changes within the watershed since the arrival of European settlers (see Chapter 2) have affected fluvial geomorphology throughout the entire Santa Clara River, and they have contributed to several contemporary challenges for river management in both Los Angeles and Ventura counties. Infrastructure changes include dams constructed during the twentieth century, the failure of the St. Francis Dam in 1928, water diversions, instream aggregate mining, and the construction of roads, bridges, and levees. The most direct and substantive channel modifications are expressed by the armored and/or concrete-lined lower reaches of many of the tributaries into the USCR, with associated reductions in channel width and loss of sediment storage. Other direct impacts have included agricultural and, increasingly, urban occupation of the floodplain; levee construction to protect the increasing development of areas adjacent to the river; and the lowering of the channel bed that accompanied instream aggregate mining and cross-channel structures that block downstream sediment movement.

4.2.1 Dams and debris basins

Along tributaries to the USCR, dams on Castaic Creek and Bouquet Canyon regulate roughly 26% of the drainage area of the USCR watershed (Figures 1-2 and 3-10), impounding water for consumptive use and effectively reducing both downstream flow and downstream sediment delivery compared with what it would have been in the absence of the dams.

4.2.1.1 Bouquet Dam and Reservoir

Bouquet Dam impounds imported water in Bouquet Reservoir, in the moderately dry north-central portion of the watershed. Completed in 1934, the facility has a capacity of 42 million m^3 (34,000 ac-ft) and affects less than 3% of the USCR watershed area. Its effects on watershed hydrology are probably not great, due to its location and small regulated watershed area, although it does intercept the influx of water and sediment from the upstream contributing area. The discharge record near the mouth of Bouquet Canyon (e.g., Figure 4-7) reflects the combination of low and generally episodic rainfall, coupled with regulation of the upper quarter of the subwatershed. Most of the impounded water, however, arrives from the Los Angeles Aqueduct (State Water Project waters); the dam performs much the same functions of regulating releases and storing water in the case of an interruption upstream as did the ill-fated St. Francis Dam (see below).

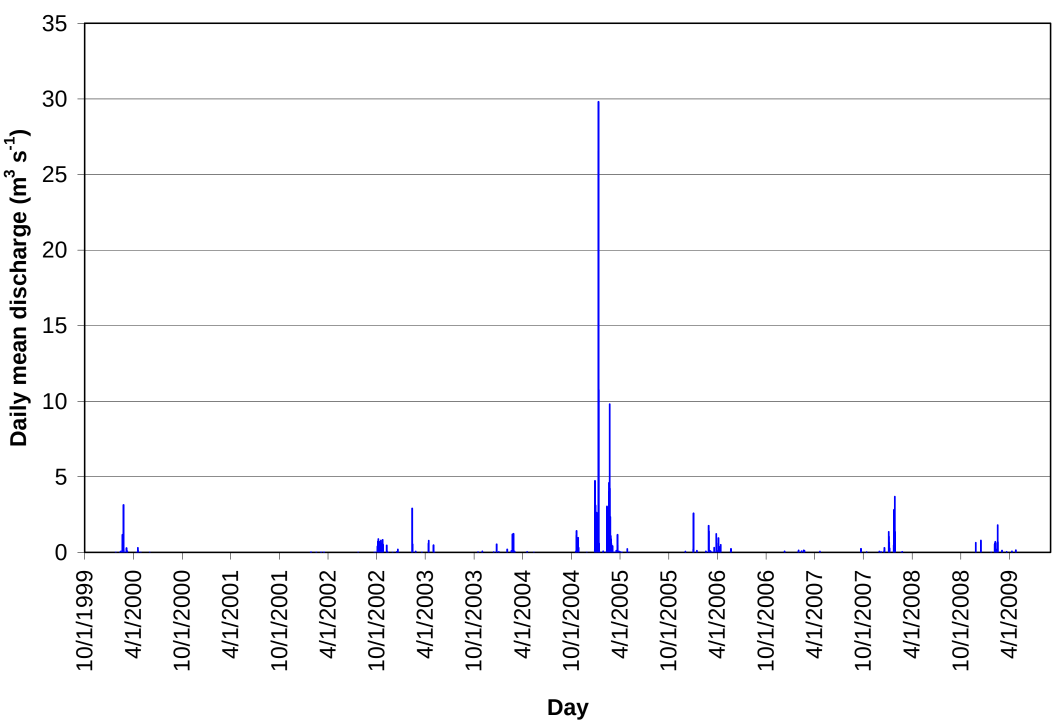

Figure 4-7. Example of the recent discharge record on Bouquet Canyon, showing the extremely episodic nature of flows low in this subwatershed (USGS 11107860, LADPW F377-R, LADPW 377B-R).

4.2.1.2 Castaic Dam and Lake

Castaic Dam, completed in 1972, is a State Water Project facility located on Castaic Creek, well upstream of its confluence with the USCR. The facility (capacity 401 million m^3 [325,000 ac-ft]) is designed to contain water imported from northern California. It also effectively blocks all but the largest flows from its contributing 397 km^2 (153 mi^2) watershed, as indicated by the record of the USGS stream gauge located immediately downstream of the impoundment (Figure 4-8).

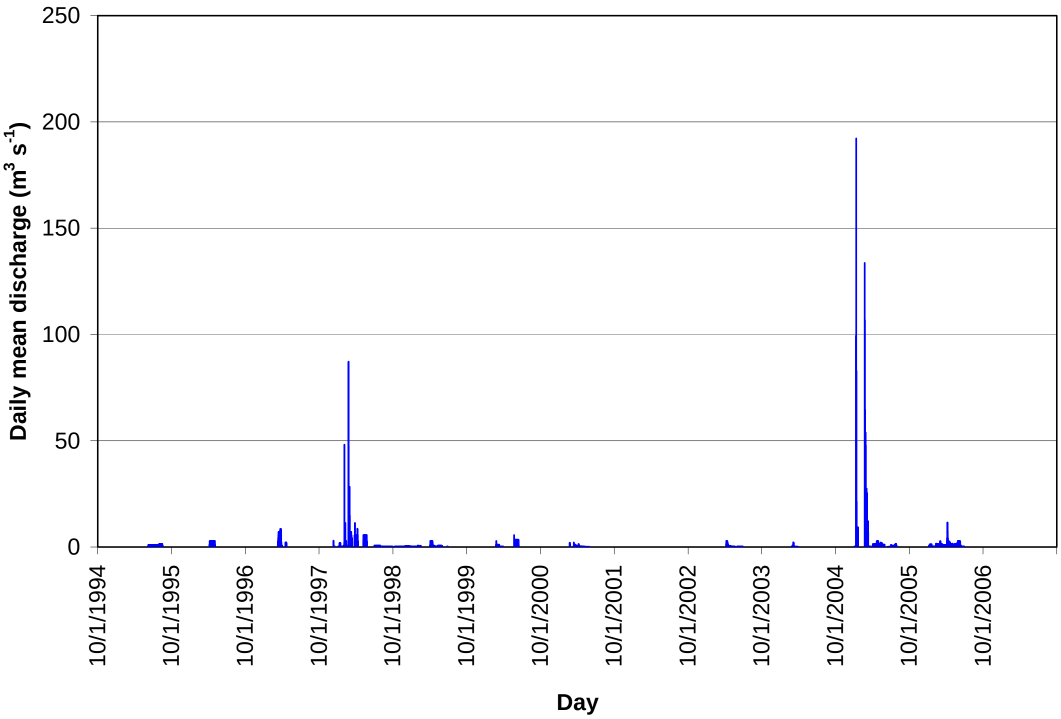

Figure 4-8. Stream gauge record for 12 years of discharge from Castaic Dam (USGS 11108134), displaying periods of nearly two years' duration with no flow at all (e.g., late May 2001 through early April 2003).

4.2.1.3 St. Francis Dam

In 1924, construction began on the St. Francis Dam, near Saugus in San Francisquito Canyon. Its reservoir was to serve as a backup water supply for local farmers in the event that supply from Owens Valley was interrupted. The dam was finished to a height of 57 m (187 ft) in 1926 and eventually filled with nearly 50 million m^3 (41,000 ac-ft) of water. Just before midnight on March 12, 1928, a large section of the dam suddenly collapsed, sending a wall of water down the valley towards the Pacific Ocean, 87 km (54 mi) away. The peak water level has been estimated at 24 m (78 ft), and peak flow between the dam failure and the County line on the Santa Clara River was probably between approximately 15,000 and 30,000 m^3s^{-1} (500,000 and 1,000,000 cfs) (Simons, Li & Associates 1983; Begnudelli and Sanders 2007). Large volumes of mud and debris were entrained in the flow as it rushed first down San Francisquito Canyon, and then down the Santa Clara River Valley, affecting the established communities along the way out to the ocean (Figure 4-9; see flood scour path on Figure 4-23 a–c and Figure 4-24 a–c below).

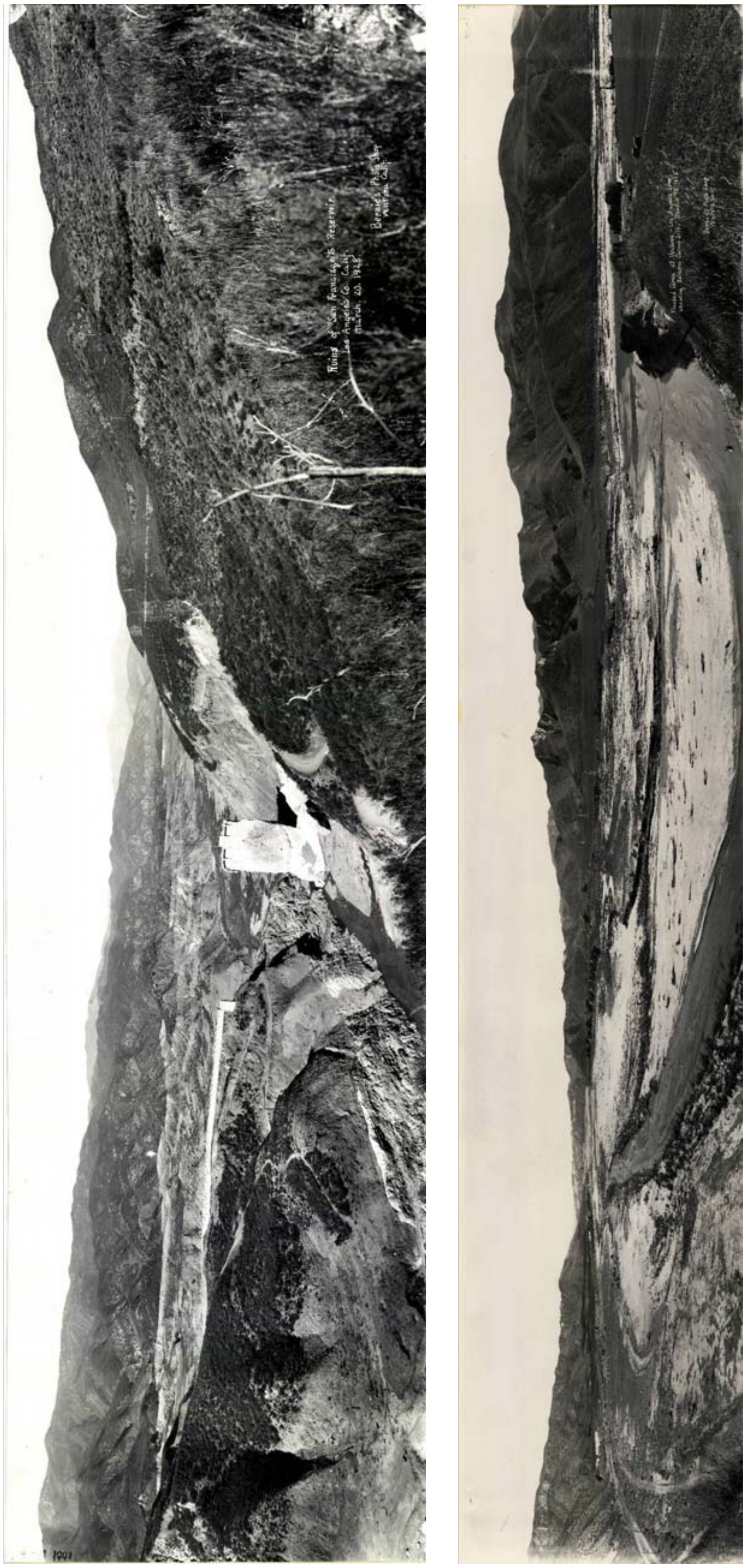

Figure 4-9. The remains of the St. Francis Dam after collapsing just before midnight on March 12, 1928, in the San Francisquito subwatershed (above). Below, a downstream view of the mainstem Santa Clara River near the County line, five days after the dam break flood. Photos courtesy of the VCWPD.

The reservoir contents emptied into the ocean less than six hours after the dam broke, but the effects of the flood were far more long-lasting. Nearly 500 people died in the disaster, and parts of Ventura lay under 20 m (70 ft) of mud; total property damage was approximately $5.5 million in 1928 dollars (University of Southern California 2004). The St. Francis Dam failure changed perceptions about dam safety and water projects in California and was the impetus for the creation of the California Division of Safety of Dams, which regulates non-federal dams in the state (CDSD 2005).

4.2.1.4 Effects of dams on the delivery of water and sediment to the USCR

The two major dams on tributaries of the USCR watershed (Bouquet Canyon and Castaic Creek) control the discharge from nearly 30% of the upper watershed and 10.4% of the total Santa Clara River watershed. Over 90% of this controlled area lies behind Castaic Dam, which was calculated by Warrick (2002) to contribute almost two-thirds of the suspended sediment of the USCR watershed (from data measured at USGS County line stream gauges 11108500 and 11109000) prior to dam construction. Assuming 100% sediment trapping efficiency (Williams 1979), this suggests that sediment delivery has been dramatically reduced in lower Castaic Creek and the lowermost 8 km (5 mi) of the USCR and beyond. The consequences of reduced sediment loads are generally most severe immediately downstream of dams, where channel incision is commonly observed due to more effective erosion of the channel bed by sediment-starved water (e.g., Williams and Wolman 1984). The effect diminishes with increasing distance downstream as sediment-laden water from tributaries is added to the flow (Petts 1984). Simons, Li & Associates (1987) compared pre- and post-dam profiles of Castaic Creek and found that an average of about 1 m (3.9 ft) of degradation (6 ft maximum) had occurred between 1964 and 1980, which they attribute to the blockage of sediment from the dam. Any continuing influence of this reduction in sediment delivery to the USCR would be progressively attenuated by the relative differences in watershed size and then by the right-bank inflows from Violin and Hasley canyons, shortly below the confluence of the mainstem with Castaic Creek. Our own field observations of lower Castaic Creek support these findings and further note that Violin Canyon does indeed appear to provide a significant source of sediment to the lower Castaic Creek (see Appendix F, Lower Region reach descriptions).

Simons, Li & Associates (1987) found no data to quantify any bed-elevation effects of Bouquet Dam. On San Francisquito Creek, any downstream effects of sediment trapping in St. Francis Dam, albeit very minimal because the reservoir existed for less than two years, would have been entirely obliterated by the subsequent dam-break flood together with the last eighty years of relatively uninterrupted sediment delivery down that channel.

Beyond transient sediment trapping in the short-lived reservoir pool, however, St. Francis Dam had persistent effects on river morphology as a result of the dam break, not only in San Francisquito Creek but throughout the entire Santa Clara River downstream of the tributary confluence. The peak flow of between 15,000 and 30,000 m^3s^{-1} (500,000 and 1,000,000 cfs), implied by anecdotal accounts, is 8–15 times greater than any subsequent peak flow that has occurred at the County line stream gauge. Based on a recent flood frequency analysis (URS 2005), the dam-break flow had a hydrological return period of 200–1,000 years in the lower river. Our analysis of active channel widths and bed level changes reveals that the lower reaches of the USCR overall have been progressively narrowing and aggrading since the disaster, suggesting that the flood's primary morphological impact was extensive broadening and incision of the channel and floodway (see Sections 4.3.3 and 4.3.4 below). These morphological changes since the dam failure event may have also been exacerbated in part by other factors, including reduction of flow caused by Castaic Dam and urban encroachment on the floodplain. However, in consideration of the sheer magnitude of the dam failure event, we conclude that the disaster was the most recent and significant "channel-forming" flow, and so many of the large-scale characteristics of the mainstem river channel and floodway, from the confluence and downstream past the County line, are likely relicts of the effects of the dam-break flood.

4.2.1.5 Effects of debris basins on watershed sediment yields and river morphology

A detailed background on debris basins and debris retention inlets operated by LADPW to protect urban infrastructure from debris flows in and around the Santa Clarita basin, in addition to the debris basins operated by LADWP at the Castaic Powerplant, was presented earlier in Section 3.3.3. Because the Castaic Powerplant debris basins are positioned upstream of Castaic Dam, these debris basins do not impact the USCR's contemporary sediment yield or morphology.

The LADPW debris basins and debris retention inlets collectively cut off only 1.4% of the total USCR watershed area. As a result, they reduce watershed sediment yields and impact tributary and river morphology to a much lesser extent than the large water-storage dams and reservoirs. Taken together, the debris basins intercept approximately 50,000 t of sediment annually, but they preferentially trap coarser sediments. This rate is approximately 5% of the average annual total sediment yield calculated at the County line stream gauge (900,000 t yr-1). It is approximately 2% of the average annual total sediment-production rate derived from our GLU approach (2.3 million t yr-1). The accuracy of this estimated rate is moderate at best given that many of the debris basins have relatively short sedimentation records. Thus, it is also not precisely known how much sediment is intercepted by the debris retention inlets as these smaller, but more numerous, structures do not require record keeping (L. Thang, pers. comm., 2010), but the amount intercepted on an average annual basis is probably on the same order of magnitude as that incepted by the debris basins based on similarities in size and landscape characteristics of their contributing drainages.

Downstream effects of these structures on the tributary channel morphology is generally minimal because most are situated above completely channelized (and even subsurface) reaches that lock the channel geometry in place. For this reason, it is difficult to directly assess the effects of the debris basins alone on the mainstem river channel morphology. Our field observations did not note any obvious channel instabilities in the river directly below the confluence of any tributaries with debris basins or debris retention inlets. Therefore, it appears that the most significant effect of these structures on the river is their trapping of sediments of bed-material size.

4.2.2 Instream aggregate mining

In the USCR, the effects of aggregate mining may be less broadly significant than those of dam construction (and failure), channelization, and urban development, but their effects are nonetheless apparent along the mainstem river. Large volumes of aggregate resources designated by the California Geological Survey (CGS) in the USCR watershed (in the Saugus-Newhall Production-Consumption Region [SNPCR] of Los Angeles County) have attracted long-standing interest in aggregate mining, extracted from both in- and off-channel sources (see Chapter 2). One large-scale, in-channel operation continues to extract aggregate resources from the bed and adjacent floodplain of the USCR, east of Santa Clarita near the mouth of Soledad Canyon.

Total aggregate production in the Soledad Canyon area between 1960 and 1980—a boom period for urban development in the greater Los Angeles area—was estimated by the CGS to range between about 200,000–1,000,000 t yr^{-1}, with the peak value being reached in the early 1970s (Joseph et al. 1987). This estimate does not discriminate between in-channel and off-channel aggregate production rates; however, information provided by the USACE suggests that the 30-year average annual extraction rate as reported from the only instream operation was approximately 270,000 tonnes (300,000 tons), with a maximum of about 450,000 tonnes (500,000 tons) per year (A. Allen, pers. comm., 2010). This average annual extraction rate accounts for approximately one-third of the average annual total sediment yield of the USCR watershed as calculated at the County line stream gauge (900,000 t yr^{-1}; see Section 4.1.1). Because the stream gauge record overlaps much of this aggregate mining period, this finding implies that the watershed's average annual sediment yield at the County line would be greater when including this difference (in the absence of the instream mining activities). Instream aggregate extraction has reportedly diminished somewhat in the years since Los Angeles County re-authorized the mining permit in 1994, but the exact extraction quantities are not known (A. Allen, pers. comm., 2010).

Determining the degree of recent channel degradation in the USCR resulting from aggregate mining is hampered by limited data and by channel-spanning grade controls, which not only anchors the bed elevation but also disrupts downstream sediment transport. The area of most prominent change is at Lang Station Road (Figure 4-10), immediately within the area of most active ongoing aggregate extraction and itself a significant impediment to downstream sediment movement; interruption of sediment movement is evident from the visible change in river morphology up- and downstream of this location.

The dynamic nature of this reach of the USCR was also highlighted by Simons, Li & Associates (1987), who reported up to 8 m (26 ft) of degradation between 1964 and 1977. They also noted that the bed recovered about one-half of this downcutting between 1977 and 1981 (the last reported measurement in their report). They ascribed the aggregated mining here as the most likely cause of the bed-elevation changes (p. 6.28). Our own analysis of bed level changes between the years 1928 and 2005 supports this finding for the reaches immediately upstream and downstream of the Lang Road Crossing; the reach average change in thalweg elevation for the two reaches is, respectively, -2 m (-7 ft) and -6 m (-20 ft) (see Section 4.3.4 and Figure 4-25 presented therein).

Figure 4-10. Lang Station Road and location of ongoing instream aggregate mining on the USCR near the mouth of Soledad Canyon. As visible in the NAIP 2006 aerial photograph (above), sediment is impounded on the upstream side of the 75 m (250 ft) long grade control structure. Active floodplain and instream aggregate mining is visible downstream. The bottom photo taken during our spring 2010 field surveys shows a profile view of the 5–6 m (15–20 ft) high crossing with the river’s flow being routed through large culverts (flow direction is toward the left).

4.2.3 Levees, bank protection, and channelization

Many of the lowermost reaches of the USCR tributaries have been confined into concrete channels to minimize the risk of adjacent flooding. Further, beginning at the watershed divide downstream to Agua Dulce Canyon, the valley of the USCR is host to Soledad Canyon Road and the railway line connecting to the Antelope Valley, and so bank armoring to protect this infrastructure is ubiquitous. Between Agua Dulce Canyon and Lang Station Road, the railroad confines the north side of the channel against the mountainside, locally narrowing the river to as little as about 10 m wide (see photo shown in Figure 3-17). The river is then paralleled for about 5.5 km (4 mi) by the Antelope Valley Freeway, which forms the north boundary of the river channel. For the next 14 km (9 mi) to the crossing of Interstate 5, the river flows in a tightly constrained corridor through the most heavily developed part of the entire watershed, where bank protection on one (and commonly both) sides of the river is typical (Figure 4-11). Review of river crossings by roads and other linear features (e.g., Los Angeles Aqueduct, railroad, oil pipelines) locatable in 2009 aerial photographs reveal approximately 37 features that presently cross the entire length of the USCR, with the majority of these being concrete road spans that confine the river channel at their respective locations (and the vast majority of these in the Santa Clarita basin). Besides the previously mentioned Lang Station Road crossing, another notable crossing that interrupts bedload transport in the river is Arastre Road near Acton where the concrete crossing impounds sediment on its upstream site.

Other tributaries to the USCR are even more severely constrained. Hasley Canyon has 2 of its lowermost 3 km confined in a concrete channel. Over one-quarter of the total length of Bouquet Canyon below the Bouquet Dam is in a concrete channel, which is joined by the similarly confined lowermost reaches of Dry Canyon and Haskell Canyon. In total, this right-bank channel system comprises over 14 km (9 mi) of concrete channel before entering the USCR. Other concrete channels are located at the lower ends of Tick Canyon, Oak Springs Canyon, Sand Canyon, and various tributaries of the South Fork USCR (Figure 4-11).

AMEC (2005) listed flood-protection features along the USCR based on their review of the 1996 Flood Protection Report (VCWPD and LADPW 2006):

> Acton basin: *"In the Acton area, the floodplain changes to a broad shallow plain varying in width from 1000 to 2000 feet. Private property owners have built some levees to protect recreational areas."*
>
> Lang gauging station to Interstate 5: *"The floodplain varies in width from 500 feet at the 1-5 Freeway to 2000 feet near Bouquet Canyon Road. West of Whites Canyon Road to the 14 Freeway, the 100-year floodplain is contained with levees on either one side or both sides of the river. East of the 14 Freeway, the flood plain widens to an average of 1000 to 1500 feet. At Lang Station, it narrows down to less than 500 feet. Between Oak Springs Canyon and Sand Canyon, there are some permitted levees on the south bank of the river"*
>
> Interstate 5 to County line: *"The Santa Clara River passes primarily through privately owned land. Property owners have built some levees to protect farming areas. Newhall Land and Farming Company is proposing a 'Natural River Concept', currently under review by the Los Angeles County, for the portion of the river within their property"*

Figure 4-11. Floodplain developments and flood control structures (non-federal levees shown in red [source: CDWR 2009]) in the Santa Clarita basin. Dense urban developments on the floodplain, adjacent to the river channel, and roads crossing the river are shown in the NAIP 2009 aerial photograph (upper) of the eastern end of Santa Clarita near the Mint Canyon confluence (right side). Hardened banks with rock revetment on the left bank and an earthen levee along the right bank of the downstream end of the South Fork SCR are visible in this photo (lower) taken during high flows on 12 December 2009.

Levees confine high discharges that would otherwise spill onto neighboring floodplains, reduce the effective flow width during floods, and are frequently intended to stabilize the river's planform. However, because they exceed the natural elevation of the floodplain, the contained flood flows run deeper and generate increased shear stresses on the channel bed compared to the conditions if the flow was able to spill over the banks. Increased shear stresses increase the chance of channel bed incision but, because flood sediments are also confined within the channel rather than being deposited onto the floodplain, large amounts of sediment may be deposited instream as the flood recedes. Hence, the net change in bed elevation along reaches that are bounded by levees depends on multiple competing factors and is difficult to predict.

Where levees are used in conjunction with bank protection to “train” the channel to a particular planform there is the risk that, if the imposed channel planform does not align with the natural planform tendency during flood events (or if the channel is simply too narrow), the flood thalweg will flow directly towards the levee in certain locations. This will lead to high near-bank flow velocities and the potential for levee erosion and an increased risk of bank erosion. An additional impact of protected levees is that flood flows can be reflected towards an opposing, unprotected bank that would not otherwise be prone to substantial erosion.

4.2.4 Urban growth

4.2.4.1 Existing urban growth

Population in the watershed has increased approximately 30-fold since the 1950s (Table 4-2), with much of the growth occurring along the mainstem corridor and particularly in the vicinity of the present-day city of Santa Clarita (established in 1987 with the joining of four unincorporated towns: Canyon Country, Newhall, Saugus, and Valencia). Increases in population and urbanization will undoubtedly continue into the foreseeable future and are likely to have an increasingly noticeable effect on geomorphic processes in the lower river corridor.

Table 4-2. Population in the USCR watershed.

Year	Santa Clarita Valley		Acton [b]	Estimated total USCR watershed population
	City of Santa Clarita [a] (est. 1987)	Total		
1770		~1,000 (native Americans) [c]		~1,000 (native Americans) [c]
1870				265 [d]
1940				5,638 [e]
1950		2,527 [e]		10,001 [e]
1960		4,705 [e]		18,362 [f]
1970		18,754 [e]		52,700 [f]
1980		73,160 [e]		93,600 [f]
1990	110,642 [g, h]		1,471 [g]	~150,000 [i]
2000	151,131 [j]	212,611 [j]	2,390 [g]	225,603 [j]
2010	177,641 [k]	275,000 [e]	9,175 [l]	~300,000 [i]

[a] Incorporated in 1987 with the union of several communities: Canyon Country, Newhall, Saugus, and Valencia.
[b] Acton Census Designated Place (CDP) includes the town of Acton and surrounding area.
[c] Worden 1998
[d] Earle 2003
[e] U.S. Census Bureau 2010a; Newhall Division included: Canyon Country (CDP), part of Los Angeles city, Newhall (CDP), Saugus-Bouquet Canyon (CDP), and Valencia (CDP). The majority of USCR watershed was referred to as Soledad Township in the 1940 and 1950 censuses.
[f] Stillwater Sciences (2007a; Table 5-1)
[g] U.S. Census Bureau 2010b
[h] City of Santa Clarita 2004
[I] Estimated here by Stillwater based on population growth trend from available data.
[j] Kennedy/Jenks 2008
[k] CDF 2010
[l] City of Acton 2010

There are two major geomorphic effects on the USCR related to urbanization. The first arises where construction occurs close to the river and requires levees or channelization for flood protection and enhanced flow conveyance. Where the levees constrain the width of the river, accelerated erosion can result. This local effect has been discussed under levees and bank protection above. The second impact may be of greater regional consequence, and it arises from the increasing area of impermeable surface that accompanies population growth and urban expansion. The most widely recognized of these impacts, the hydrological changes that are expressed by higher peak flows and a more rapidly experienced peak flood flow, have been analyzed for nearly half a century (e.g., Leopold 1968). A less commonly recognized change in watershed conditions that can accompany urbanization, however, is the reduction in sediment delivery to stream channels, which for erodible channels can be as destabilizing as an increase in discharge. This is because the condition of “stable stream channels” reflects a balance between the capacity of the flow to transport sediment and the availability of sediment for transport. Under the broad geomorphic concept of dynamic equilibrium, this balance is not necessarily achieved at every moment in time or at every point along the stream channel. Over a period of time, however, an observed condition of equilibrium is commonly presumed to express such a water–sediment balance. Conversely, the balance of these components is normally considered to be the defining precondition for stability in adjustable, alluvial streams. Thus a change in either component of the river’s load, namely water or sediment (and urbanization commonly results in changes to both), can lead to a state of channel dis-equilibrium. In most cases within the USCR watershed, this has been (or is anticipated to be) expressed by channel incision or degradation (see Section 4.3.4).

Although the companion report on the LSCR (Stillwater Sciences 2007a) was unable to recognize any unequivocal effects of watershed urbanization on the form or behavior of the lower river, the consequences of rapid development are likely to be first expressed in the upper watershed, where the fraction of the land surface affected by urbanization is proportionally greater. However, this is also where the impacts related to channelization, flow constrictions, aggregate mining, flow impoundment and diversions, and, potentially, the St. Francis Dam failure are also most strongly expressed. Given these confounding influences, the most likely portions of the USCR to first express urban-related impacts will be the tributaries, because many have been less affected by dams or mining, and even a single development can affect a proportionally greater area of the contributing area. A review of existing and likely future development patterns, relative to the present (and potential future) condition of the channel, is therefore instructive.

Currently, the greatest concentrations of urban development are located in the catchment areas of the South Fork and lower mainstem of the USCR. This encompasses the city center of Santa Clarita and the Interstate 5 corridor; the lower valleys of San Francisquito, Dry, Haskell, and Bouquet canyons; the lower slopes of Pico Canyon; and the middle reaches of the USCR from Saugus upstream through Soledad Canyon along the Highway 14 corridor, also covering the lower ends of Mint and Tick canyons. The overriding pattern is that most urban development to date has been concentrated in the main valley of the river, with only modest parts of the lower tributaries being affected by expanding development (primarily medium-density residential subdivisions). Scattered low-density development is present over a much larger area of the watershed, particularly in Hasley and Agua Dulce canyons and in a broad swath along Highway 14 to the watershed divide, a pattern displayed on the current land-cover map (see Figure 3-10) as scattered pockets of “Developed” land within mixed grassland and scrub/shrub vegetation (“Ag/Grass” and “Scrub/Shrub” in the referenced figure). Dramatic downstream channel changes would not normally be anticipated from such low-density land uses, and to date they have not been recognized as such.

4.2.4.2 Urban growth effects on sediment production

Future land use as predicted by the regional zoning map (CNRA 2010), however, paints a somewhat different picture of development impacts. If activity proceeds in accord with current zoning, further densification and infilling along the main river valley are anticipated along with significant expansions of development into the lower areas of Castaic Creek (below Castaic dam), San Francisquito Canyon, Placerita Creek, Newhall Creek, and Railroad Canyon. The lower reaches of these streams would normally, therefore, be the first anticipated to display the combined effects of increased discharge and decreased sediment loading as a result of future urbanization. However, of this list only San Francisquito Canyon and Castaic Creek have not already been confined into concrete channels over much of their lower reaches, and the latter is already displaying the effects of a depleted sediment load from the effects of the upstream dam. Thus the effects of future urbanization are likely to be transmitted downstream to the USCR, with presumably less direct expression in these already severely impacted lateral tributaries. Of the major USCR tributaries, therefore, San Francisquito Canyon is poised to respond most freely to any significant future changes in watershed land use.

In an effort to predict how the anticipated urban growth will affect watershed sediment production and delivery, and therefore river morphology, we revised our GIS representation of land cover across the watershed where new developments are indicated by the regional zoning map to occur. We additionally considered the changes in development that have taken place since European settlement. That is, three land cover time periods were considered here: “Pre-European Settlement”, “Present-day”, and “Future” (Figure 4-12). Changes in land cover, in turn, change the unit-area contribution of sediment to the channel network. For the pre-European conditions, this can be simulated by replacing all existing “Developed” land cover classes with modest vegetation cover (i.e., “Scrub/Shrub”) that will have an appropriate relative sediment production rating (Table 4-3). For the future conditions, each land-cover category in our GLU analysis that will have new “Developed,” according to the regional zoning map (CNRA 2010), will have their status changed to an appropriate relative sediment production rating (Table 4-3). The present-day land cover was based on the 2001 National Land Cover Database (Homer et al. 2004) that was utilized in our analysis of existing sediment-production rates above (see Section 3.3.4.1). In effect, the total area of GLUs having a low relative sediment production rating would increase with the increased urban footprint in the watershed, thereby resulting in a reduced sediment yield from the watershed as a whole. Results from our GLU analysis indicate that the average annual watershed sediment-production rate has been reduced by about 3% (90,000 t yr^{-1}) since European settlement. If we assume production closely equaled net export from the watershed (i.e., sediment yield), then the construction of dams and debris basins have further reduced sediment yields from the watershed since pre-settlement times, as discussed above. Under future conditions where we follow the full build-out under current zoning, the average annual watershed sediment-production rate would be reduced by about 12% (350,000 t yr^{-1}). These reductions in sediment production, and in turn sediment yield, represent relatively small but not insignificant amounts, especially when further reductions in the river’s sediment yield are cumulatively considered, such as from dams, debris basins, and instream aggregate mining.

This analysis, however, carries a cautionary note for any prediction of urban growth effect on sediment production. Published literature (e.g., Booth 1990, Warrick and Rubin 2007) and common sense indicates that there is a well-understood, if not easily predicted, difference in erosion potential during the construction and post-construction phases of urban developments (i.e., short-term versus long-term). The GLU analysis is effectively predicting long-term changes in sediment production where the extent of impervious surfaces and presence of sediment and flow routing infrastructure have been established for some time. The GLU analysis does not factor in the short-term increase in erosion that is commonly observed during construction, where ground disturbance would be expected to lead to fine-sediment pulses being delivered to the drainage network, particularly if large rainfall events occur during the construction period. Presently in the Santa Clarita area, there are several half-complete residential developments where bare surfaces have remained so for several years (e.g., the unfinished developments along lower reaches of Plum Canyon, San Francisquito Canyon, and Castaic Creek).

Table 4-3. Past, present, and future sediment production results from the GLU analysis in the USCR watershed.

Relative sediment production	Sediment production per unit area ($t\ km^{-2}\ yr^{-1}$)	Pre-European settlement land cover conditions [a]			Present-day land cover conditions [b]			Future land cover conditions [c]		
		Area (km^2)	Area (% drainage area)	Average annual sediment production ($t\ yr^{-1}$)	Area (km^2)	Area (% drainage area)	Average annual sediment production ($t\ yr^{-1}$)	Area (km^2)	Area (% drainage area)	Average annual sediment production ($t\ yr^{-1}$)
Zero	0	0	0%	0	13	1%	0	13	1%	0
Low	200	173	11%	36,000	263	16%	53,000	404	24%	81,000
Medium	1,000	1,265	75%	1,270,000	1,169	69%	1,170,000	1,066	63%	1,070,000
High	7,000	236	14%	1,650,000	234	14%	1,640,000	195	12%	1,360,000
Watershed total		**1,679**	**100%**	**2,950,000**	**1,679**	**100%**	**2,860,000**	**1,679**	**100%**	**2,510,000**

[a] Pre-European land-cover/-use based on using the present-day conditions, except all GLUs having the "Developed" category were replaced with "Shrub/Scrub" category.
[b] Values reproduced from Table 3-8.
[c] Future land use based on CNRA 2010.

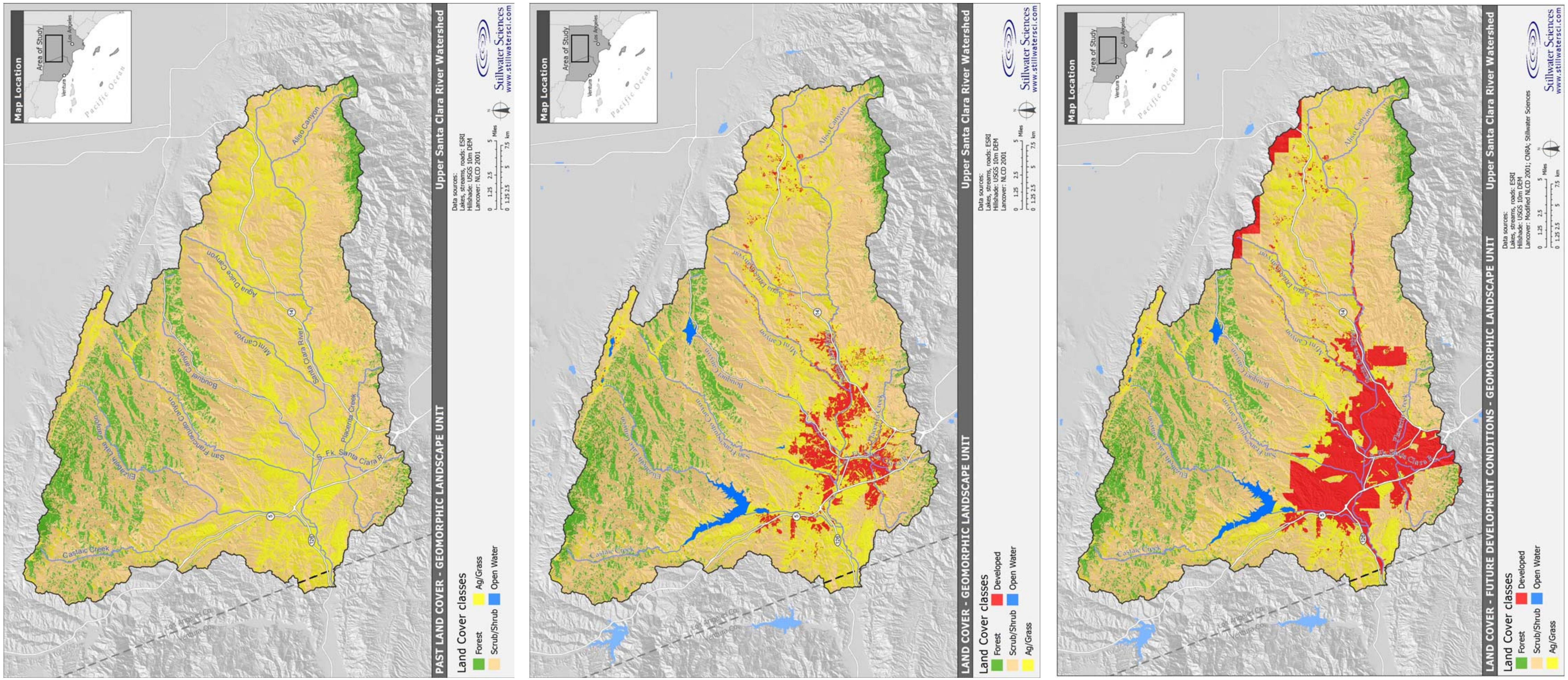

Figure 4-12. Generalized past (upper figure), present (middle figure), and future (lower figure) land-cover/-use categories used for the GLU analysis to predict changes in watershed sediment production.

4.3 Morphology and Channel Dynamics

4.3.1 Reach-level differences in channel form—overview

Understanding river morphologic and sediment character is a fundamental component in understanding the interplay between natural and anthropogenic impacts on the USCR. This understanding is key to identifying appropriate management actions into the future (e.g., Downs and Gregory 2004). Below, we describe the morphologic and sediment characteristics along the mainstem USCR and its 19 major tributaries, based on an analysis of preexisting data sources and field data collected for this study during spring 2010. The analysis focuses primarily on the mainstem USCR from the town of Acton downstream to the County line, and the tributary channels included in the Feasibility Study (both USACE and FEMA Feasibility Study reaches [see Table 1-1 and Figure 1-2]). Overall, the assessment is intended to describe current dominant processes and trends rather than to provide a comprehensive catalog of all channel conditions throughout the watershed which was not possible due to time and access constraints.

Preexisting data sources used in this analysis include bed sediment particle-size distribution data collected by Simons, Li & Associates (1990), Seward (2005), PWA (2006), and LADPW in 2005, which were compiled in the 2008 LADPW field investigation report for Los Angeles County (see listed citations therein) (Figure 4-13). The field investigation entailed visiting representative channel locations and assessing overall channel bed and bank conditions, sediment transport/deposition dynamics, controls on geomorphic processes, and bed sediment facies (i.e., areas of similar sediment sizes). At select locations, bed sediment texture was determined by analyzing bulk samples and by conducting surface pebble counts (Wolman [1954] pebble-count method). The channel erosion assessment included estimates of both bank and bed erosion, where the extent of recent bank erosion was determined by considering bank retreat relative to estimated tree age for exposed roots on the adjacent floodplain, and the amount of recent bed erosion (or channel incision) was estimated relative to the age of bank and in-channel vegetation. The laboratory results of our thirteen bulk sediment samples are presented in Appendix E.

The mainstem USCR flows approximately 60 km from the Aliso Canyon confluence downstream past the town of Acton and the city of Santa Clarita to the Los Angeles-Ventura County line (Figure 1-2). The upper portion of the river is located within the Acton basin, a large depositional basin that lies at the base of the San Gabriel Mountains and the Sierra Pelona range. The channel meanders west through the Acton basin with a relatively low degree of confinement and receives flow and sediment from several tributaries draining mountain catchments from the north, east, and south. At the downstream end of the basin, the enclosure of adjacent valley walls create a canyon reach, known as Soledad Canyon, causing the channel to become more confined, steep, and coarse-bedded. The few sizeable tributaries that deliver flow and sediment to the channel in the canyon reaches drain predominantly from the north. As the channel moves away from the valley walls and the degree of confinement decreases, the channel gradient drops considerably and the bed sediment becomes finer. In the lower portion of the mainstem channel, flow and sediment are delivered from several tributaries draining steep mountain catchments to the north and low-gradient catchments to the south. Local mainstem channel gradients range from 2.0% in the upstream bedrock-controlled reaches to 0.5% in the lower reaches towards the County line. Overall, the channel transports a mixed sediment load ranging from finer sediment (sand, silt, and clay) to boulder-sized sediment where local gradients are high.

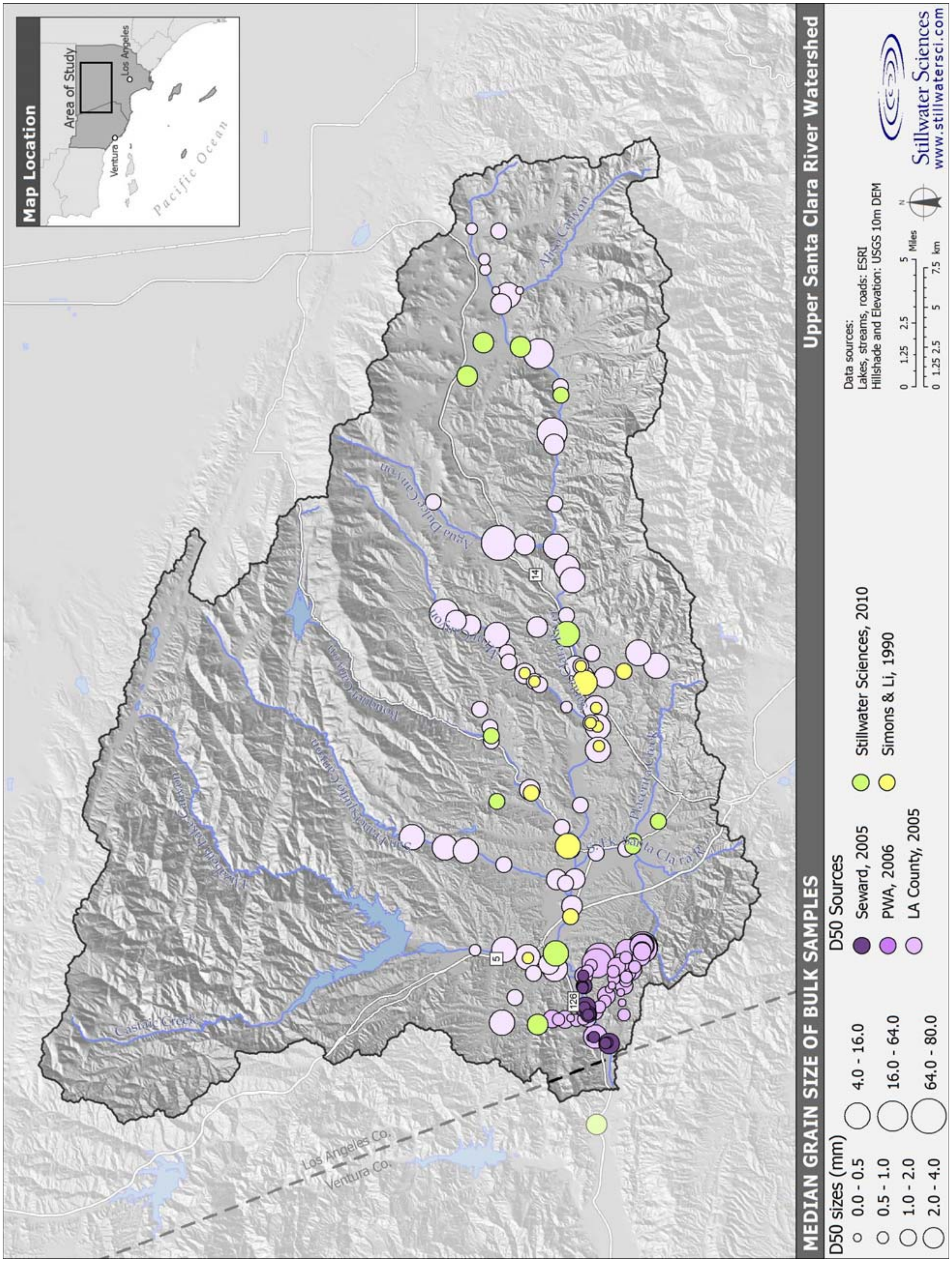

Figure 4-13. Median grain size (D_{50}) of bulk sediment samples collected throughout the USCR watershed.

In general, the morphology and sediment transport dynamics of the USCR mainstem and tributary channels are controlled by a combination of natural factors (e.g., geologic controls, precipitation dynamics) and anthropogenic influences (e.g., watershed development, in-channel infrastructure). The dominant bed sediment texture ranges from finer gravel in the upper reaches (D_{50} = 2-3 mm), to more variable sand and cobble in the steeper middle reaches (D_{50} = 1-200 mm), to sand and finer gravel in the lower reaches (D_{50} = <1-12 mm). Bed texture along the mainstem is strongly influenced by both tributary contribution and local hydraulic controls (both natural and man-made).

In order to characterize the channel geomorphic character and to develop an understanding of the controlling factors, the USCR mainstem and tributary channels within the Feasibility Study subwatersheds were separated into distinct reaches that are relatively homogenous with regard to their morphology and dominant geomorphic processes (Figure 4-14). In order to complement the companion report on the LSCR (Stillwater Sciences 2007a, which discriminated eleven reaches of the lower river), the mainstem USCR reaches established for this study continued their numeric designation in an upstream direction, beginning with Reach 11-B. Reach 11-B is the upstream extension of Reach 11 from the LSCR geomorphic assessment; its downstream boundary with the hereby Reach 11-A coincides with the County line. For this assessment, reach breaks were first indentified through spatial data (e.g., topographic data, aerial photographs) and were then finalized based on field observations. Reach delineation factored in several criteria, including the location of major tributary confluences, distinct changes in channel gradient, and degree of channel confinement. For the tributary channels, the degree of channel modification also used to delineate natural reaches (i.e., natural bed and banks) and engineered reaches (i.e., concrete bed and/or banks). In all, a total of 18 additional mainstem reaches were delineated and a total of 147 tributary reaches were delineated in the 18 Feasibility Study subwatersheds. The Upper Region (i.e., the watershed area draining to the Acton basin) contains 2 mainstem and 34 tributary channel reaches, the Middle Region (i.e., the watershed that drains to Soledad Canyon) contains 10 mainstem and 12 tributary channel reaches, and the Lower Region (i.e., the Santa Clarita basin upstream of the County line) contains 6 mainstem and 101 tributary channel reaches.

A summary of the key geomorphic features of the mainstem reaches and tributary reaches are presented in Tables 4-4 and 4-5 and Figures 4-15 through 4-18. A detailed description of geomorphic dynamics within the mainstem reaches and a description of the overall geomorphic dynamics of the contributing Feasibility Study subwatersheds are provided in Appendix F. A quantitative assessment of sediment transport and deposition dynamics within mainstem and several tributary reaches is provided below in Section 4.3.2.

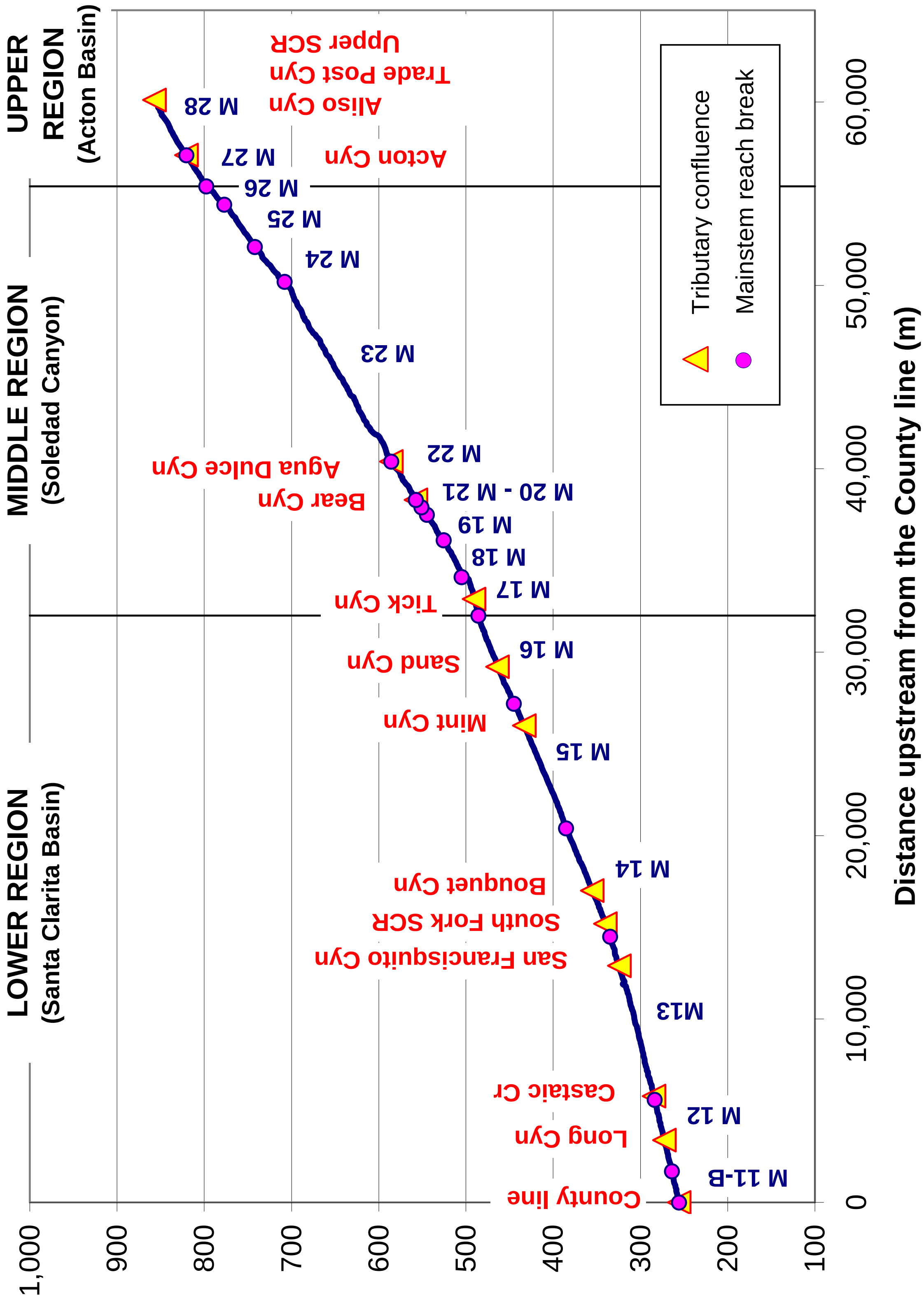

Figure 4-14. Longitudinal profile of the mainstem USCR derived from 2005 LiDAR.

Table 4-4. Summary of mainstem reach geomorphic characteristics in the USCR watershed.

Watershed region	Mainstem reach	Contributing Feasibility Study subwatersheds	Start location (km upstream from county line)	Centerline reach length (km)	Reach-average active width [a] (m)	Reach-average channel slope	D_{50} range [b] (mm)	Bed sediment facies [c]
Upper (Acton basin)	M28	Soledad Cyn Tradepost Cyn Aliso Cyn	57.1	3.1	304	0.0119	3	G_{vf}
	M27	Acton Cyn	55.4	1.7	57	0.0133	2	G_{vf}
Middle (Soledad Canyon)	M26		54.4	1.0	53	0.0204	4–32	G_f–G_c
	M25		52.1	2.3	51	0.0149	2	G_{vf}
	M24		50.2	1.9	14	0.0172	2	G_{vf}
	M23		40.4	9.8	39	0.0126	1	S
	M22	Agua Dulce Cyn	38.3	2.1	30	0.0133	9	G_m
	M21		37.9	0.4	34	0.0166	200	C_c
	M20		37.5	0.4	13	0.0165	15	G_m
	M19		36.1	1.4	29	0.0129	4	G_{vf}
	M18		34.1	2.0	128	0.0106	2	G_{vf}
	M17	Tick Cyn	32.0	2.1	109	0.0066	4	G_{vf}
Lower (Santa Clarita basin)	M16	Oak Springs Cyn Sand Cyn	27.2	4.8	202	0.0086	3–8	G_{vf}–G_f
	M15	Mint Cyn	20.4	6.8	150	0.0088	4–12	G_f–G_m
	M14	Bouquet Cyn So. Fk. SCR	14.5	5.9	178	0.0086	2–4	G_{vf}
	M13	San Francisquito Cyn Lion Cyn	5.6	8.9	145	0.0057	0.3–4	S–G_{vf}
	M12	Castaic Cr Long Cyn SM Chiquito Cyn	1.7	3.9	163	0.0051	0.7–2	S–G_{vf}
	M11-B [d]	SM Grande Cyn Potrero Cyn	0	1.7	195	0.0051	0.8–3	S–Gv_f

[a] Derived from GIS analysis of the portion of the channel that has a ‘high’ and ‘medium’ degree of flood-induced bed scour (see Section 4.3.3).
[b] A single value is reported if there was only one representative D_{50} value available. Otherwise, a D_{50} range is reported
[c] S = sand (<2 mm), G_{vf} = very fine gravel (2–4 mm), G_f = fine gravel (4–8 mm), G_m = medium gravel (8–16 mm), G_c = coarse gravel (16–32 mm), C_c = coarse cobble (128–256 mm).
[d] Reach M11-B is the upstream extension of Reach M11 from the LSCR geomorphic assessment (Stillwater Sciences 2007a).

Table 4-5. Summary of tributary channel geomorphic characteristics in the USCR watershed.

Watershed region	Mainstem reach	Feasibility Study subwatershed	Total subwatershed area [a] (km^2)	Tributary channel	Total tributary channel length within Feasibility Study area (km)	Number of tributary reaches	Tributary reach type [b]	Tributary teach length range (m)	Tributary reach slope range	D_{50} range [c] (mm)	Bed sediment facies [d]
Upper (Acton basin)	M28	Soledad	46.5	Soledad Cyn	4.80	1	N	4,800	0.030	0.8	S
				Kentucky Springs Cyn/ Soledad Cyn	5.95	4	N	430–3,330	0.015–0.031	0.2–1	S
		Tradepost	6.7	Tradepost Cr	3.32	6	N & E	370–830	0.016–0.051	2	G_{vf}
		Aliso	63.2	Aliso Cyn	5.33	2	N	1,630–3,700	0.013–0.021	0.3–100	S–C_f
	M27	Acton	54.4	Red Rover Mine Cyn	5.66	4	N	300–3,000	0.029–0.117	Unknown	Unknown
				Acton Cyn 2	5.94	4	N	1,010–1,940	0.035–0.107	2	G_{vf}
				Acton Cyn	9.26	6	N	760–2,190	0.015–0.105	1–2	S–G_{vf}
				Escondido Cr	10.34	7	N	520–4,620	0.015–0.084	2–3	G_{vf}
Middle (Soledad Canyon)	M22	Agua Dulce	76.1	Agua Dulce Cyn	12.30	10	N & E	370–3,580	0.012–0.042	1– 80	S–G_{vc}
	M17	Tick	14.8	Tick Cyn	3.25	2	N & E	1,330–1,920	0.019–0.021	3–16	G_{vf}–G_m
Lower (Santa Clarita basin)	M16	Oak Springs	14.6	Oak Springs Cyn	2.36	3	N	410–1,500	0.016–0.029	2–8	G_{vf}–G_f
		Sand	33.0	Iron Cyn	3.09	2	N	1,170–1,920	0.031–0.087	10	G_m
				Sand Cyn	6.63	4	N	610–2,650	0.017–0.035	2–11	G_{vf}–G_m
	M15	Mint	75.8	Mint Cyn	14.52	12	N & E	350–2,140	0.013–0.018	0.9–46	S–G_{vc}
	M14	Lower Bouquet (below dam)	145.2	Texas Cyn	1.22	1	N	1,220	0.024	24	G_c
				Plum Cyn	1.25	1	E	1,250	0.027	Unknown	Unknown
				Haskell Cyn	2.91	3	N & E	520–1,840	0.007–0.016	Unknown	Unknown
				Vasquez Cyn	4.16	3	N	820–2,010	0.017–0.025	2	G_{vf}
				Dry Cyn	5.81	2	N & E	600–5,210	0.014–0.019	2–11	G_{vf}–G_m
				Bouquet Cyn	12.17	10	N & E	290–2,710	0.007–0.019	1–22	S–G_c
		SF SCR	116.2	Lyon Cyn	0.63	2	N & E	190–440	0.022–0.023	Unknown	Unknown
				Newhall Cr	3.06	4	N & E	550–970	0.008–0.014	1–2	S–G_{vf}
				Placerita Cr	5.98	5	N	380–3,100	0.009–0.016	2–4	G_{vf}
				Pico Cyn	6.89	5	N & E	835–2,390	0.008–0.049	Unknown	Unknown
				So. Fk. SCR	8.84	8	N & E	348–3,060	0.004–0.027	1–18	S–G_c
	M13	San Francisquito	134.6	San Francisquito Cyn	13.33	4	N & E	1,360–5,740	0.007–0.014	2–18	G_{vf}–G_c
		Lion	2.2	Lion Cyn	1.89	2	N	730–1,160	0.040–0.042	0.5–5	S–G_f
	M12	Lowe Castaic (below dam)	122.6	Violin Cyn	4.62	5	N & E	220–1,480	0.013–0.023	4–11	G_{vf}–G_m
				Marple Cyn/Castaic Cr	8.06	4	N & E	280–4,460	0.006–0.015	0.6–12	S–G_m
				Hasley Cyn	5.28	3	N & E	1,150–2,120	0.017–0.025	1–8	S–G_f
		Long	4.0	Long Cyn	3.87	3	N	480–2,680	0.024–0.033	0.3–1	S
		SM Chiquito	12.4	SM Chiquito Cyn	5.29	4	N	440–2,060	0.023–0.027	0.4–2	S–G_{vf}
	M11-B	SM Grande	8.6	SM Grande Cyn	4.79	5	N	370–1,570	0.013–0.033	0.5–4	S–G_{vf}
		Potrero	11.6	Potrero Cyn	7.01	6	N	680–1,900	0.007–0.043	0.3–3	S–G_{vf}

[a] Value represents the total area of the tributary drainage area, which often extends beyond the range of the Feasibility Study area of interest.
[b] N = natural (i.e., natural bed and banks), E = engineered (i.e., concrete bed and/or banks).
[c] "Unknown" denotes tributary channels where there is no existing bed texture data and we were unable to visit during the field effort.
[d] S = sand (<2 mm), G_{vf} = very fine gravel (2–4 mm), G_f = fine gravel (4–8 mm), G_m = medium gravel (8–16 mm), G_c = coarse gravel (16–32 mm), G_{vc} = very coarse gravel (32–64 mm), C_f = fine cobble (64–128 mm).

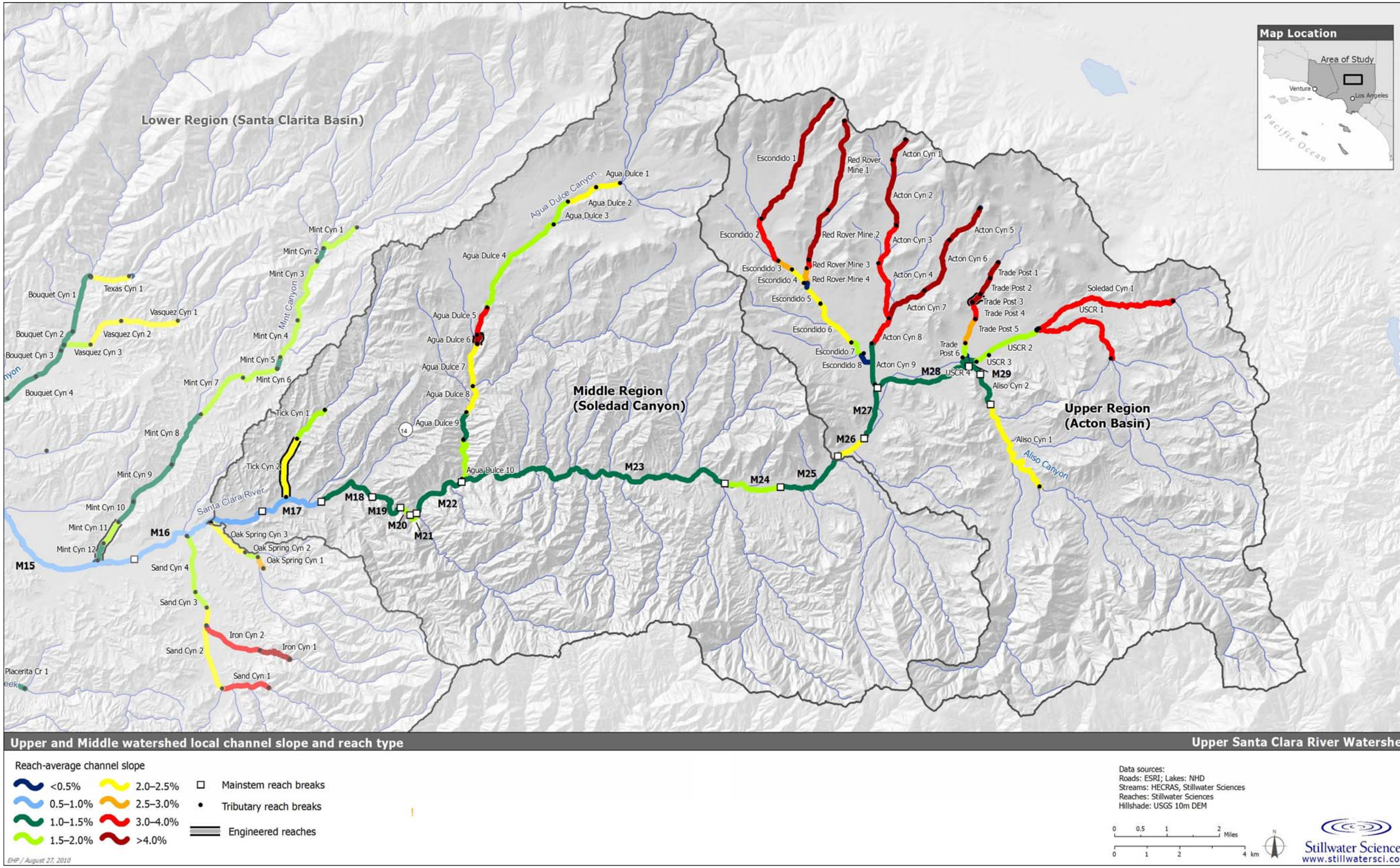

Figure 4-15. Mainstem and tributary reach slopes throughout the Upper and Middle regions of the USCR watershed.

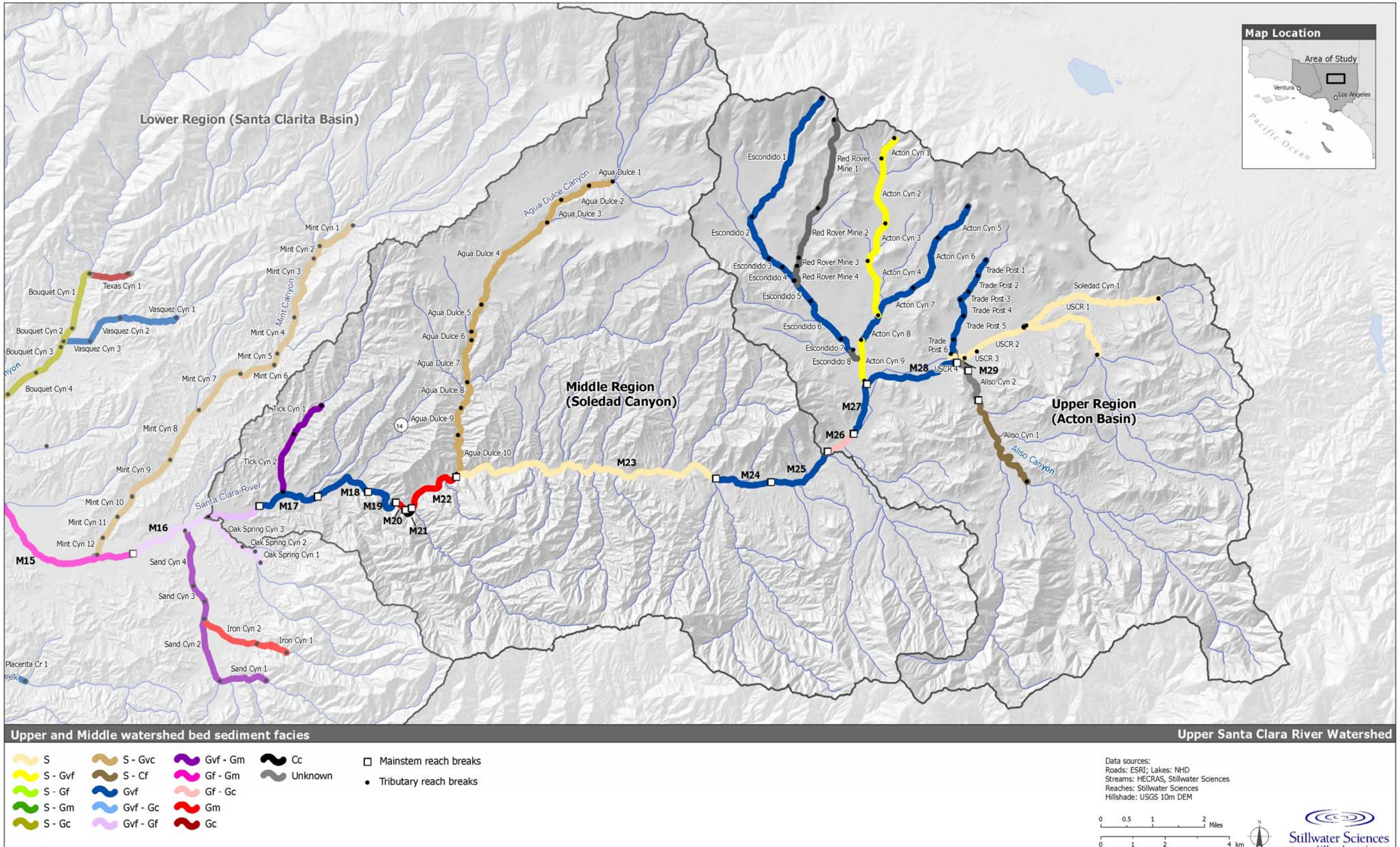

Figure 4-16. Mainstem and tributary reach bed facies throughout the Upper and Middle regions of the USCR watershed.

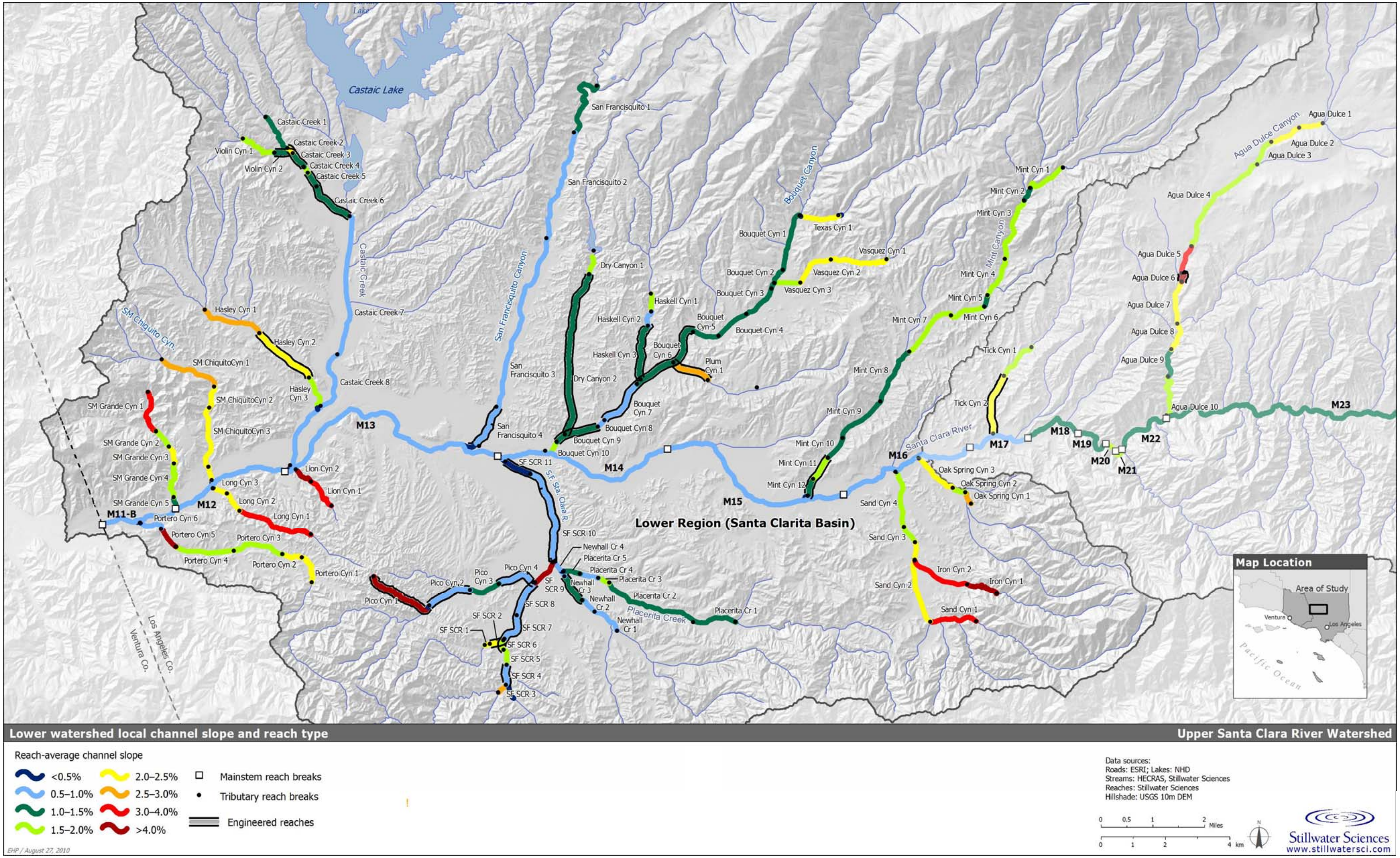

Figure 4-17. Mainstem and tributary reach slopes throughout the Lower Region of the USCR watershed.

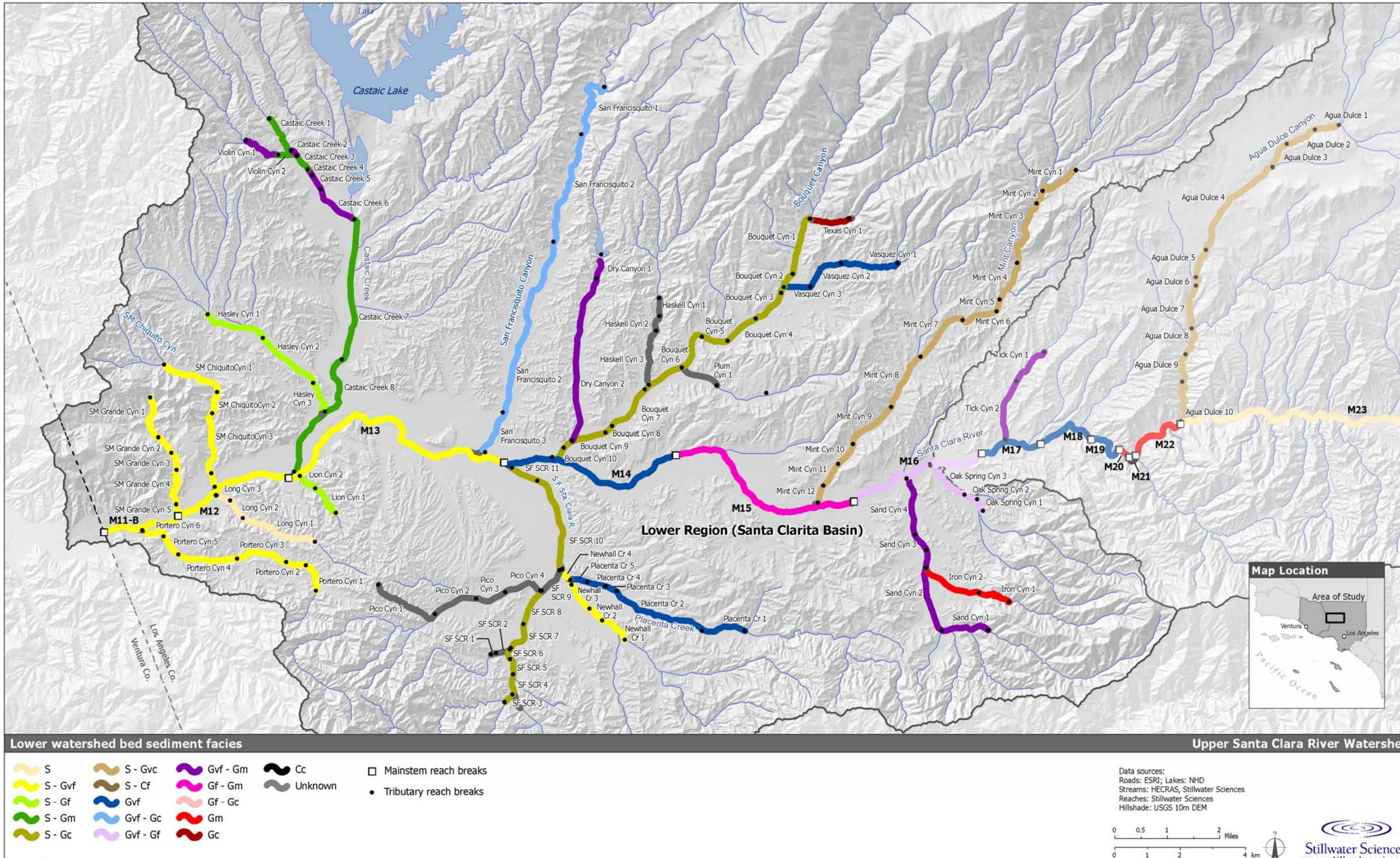

Figure 4-18. Mainstem and tributary reach bed facies throughout the Lower Region of the USCR watershed.

4.3.2 Sediment transport and channel conditions

Developing an understanding of sediment transport dynamics throughout a watershed is an effective approach to assess average channel conditions. Comparing sediment transport rates in the river with sediment inputs from upstream sources can help elucidate a channel's tendency, on average, to accumulate or evacuate delivered and stored sediment. This tendency translates into a general channel condition where: (1) channels that accumulate sediment are generally aggradational with an increasing bed elevation; and (2) channels that evacuate sediment are generally incising with a decreasing bed elevation. Over the long term, these conditions impact channel bank stability, overbank flooding frequency, and sediment transport downstream.

In an effort to define channel conditions throughout the Feasibility Study area (see Figure 1-2), an analysis of sediment transport rates at select tributary and mainstem USCR locations was conducted. The analysis involved developing estimates of average annual bedload transport rate from calculated bedload transport capacity (i.e., the amount of bedload the channel is capable of transporting). Bedload transport rates were then compared to estimates of bedload sediment yield from upstream to arrive at a preliminary assessment of channel condition (i.e., aggrading, stable, or incising). Finally, field observations were used as a check to confirm or modify the preliminary assessment.

Presented below are the methods used to determine average annual bedload sediment transport capacity and transport rate and the resulting assessment of channel conditions within tributary and mainstem locations within the Feasibility Study area. Later in the report, the results from this analysis are combined with bed level change data determined from topographic data to confirm average trends in sediment storage and channel conditions throughout the mainstem USCR over the past 50 years.

4.3.2.1 Bedload transport capacity

Bedload transport capacity curves were developed for several channel locations throughout the USCR watershed (Figure 4-19). The overall approach was to use channel physical characteristics combined with discharge data to determine the potential rate of bedload transport for the 2-year flow (Q_2) up to the 100-year flow (Q_{100}). The suite of sites selected to model sediment transport capacity were positioned at several locations, or nodes, in tributaries and along the mainstem USCR that captured key tributary sediment input sources to the mainstem and could be used to evaluate the mainstem's transport capacity relative to the tributary inputs. Criteria for selecting mainstem model sites also included being able to use model results to assess the effects of observed changes in reach-scale geomorphic characteristics (e.g., channel slope, valley confinement, and drainage area) that affect the continuum of fluvial sediment transport along the mainstem USCR.

Transport capacity modeling required the use of two equations whose application depended on relative bed texture. The Brownlie (1982) equation was used to determine sediment transport capacity for the finer-bedded reaches (D_{50} <4 mm) and the Parker and Klingman (1982) equation for the coarser-bedded reaches (D_{50} >4 mm). The Brownlie (1982) equation is one of the most reliable equations for rivers with relatively finer bed material particles (i.e., sand or slightly coarser), due in large part to the extensive amount of field data used to develop the equation. The Parker and Klingman (1982) equation is widely used to calculate transport capacity for coarser-grained sediment load based on surface bed particle size and has been shown to perform very well in many sediment transport investigations (e.g., Sutherland et al. 2002, Cui et al. 2008, Shvidchenko and Pender 2008).

A complete summary of the assumptions and equations employed in this analysis is presented in Appendix G. Also presented in this appendix are the bedload transport capacity curves generated from this analysis.

Once the general location of a key sediment transport site was identified, an iterative process was used to select the specific model locations based on the availability and quality of necessary input data. Transport capacity modeling requires four primary types of site-specific input data: a flow record, channel morphometric data (e.g., channel width, cross-sectional area), water surface slope (or energy gradient), and bed texture. Flow data throughout the watershed were provided by a recent hydrologic modeling effort (using the Hydrologic Simulation Program-Fortran [HSPF] model) based on stream gauge data (see Aqua Terra 2009). Channel morphometric and water surface slope data along the mainstem and tributaries were provided by a recent hydraulic modeling effort (using the USACE's Hydraulic Engineering Centers River Analysis System [HEC-RAS] model) conducted as part of the Feasibility Study. Local bed texture information came from previous recent studies in the USCR (Simons, Li & Associates 1990, Seward 2005, PWA 2006, as cited in LADPW 2008) and bed texture data collected as part of this study. Bed texture information came from bulk sediment samples or from surface Wolman pebble counts where bulk sediment data was not available.

The preliminary step in model site selection was to combine HEC-RAS cross-section locations, HSPF model nodes, and bed texture locations over recent aerial photography in a GIS to result in short channel reaches that were relatively straight and uniform with no adjacent flow or sediment inputs and that satisfied necessary data requirements. These sites were then evaluated within the HEC-RAS model to test whether the water surface slopes were relatively uniform over the model reach. Following site selection, bedload transport capacity rating curves were calculated for several site cross-sections and combined to obtain a representative reach-average curve for each site.

A single average annual bedload transport capacity value for each modeling site was then derived from the bedload transport capacity curves (see Appendix G for presentation of the output curves). This involved first extracting an average annual bedload transport capacity value from each reach-average curve using an appropriate water discharge value. Average annual bedload transport capacity is traditionally derived by combining an annual daily mean flow duration curve with a sediment rating curve. As the HSPF model outputs peak instantaneous flow values, we needed to derive a single representative discharge to use at all model locations in order to estimate average annual bedload transport capacity ($Q_{sed\ cap}$). This discharge was determined from the flow record for the County line stream gauge (USGS 11108500 and 11109000) and a bedload rating curve developed from sediment data collected at the gauge between 1968 and 2009 (see Section 4.1.1 for more detail). We found that the daily mean discharge value that outputs the average annual bedload yield is 14% of the 100-year instantaneous flow (Q_{100}). The Q_{100} at each model location was thus multiplied by 14% and the resulting daily mean discharge was entered into the bedload transport rating curve to obtain an estimate of the average annual bedload transport capacity value, acknowledging that this factor is not likely to be identical at every location in the channel network but lacking data to develop more site-specific results. Note that the average annual bedload transport capacity was derived by using $Q_{sed\ cap}$ as the daily mean flow for a single day.

A summary of transport capacity results for the tributary and mainstem sites is give in Tables 4-6 and 4-7.

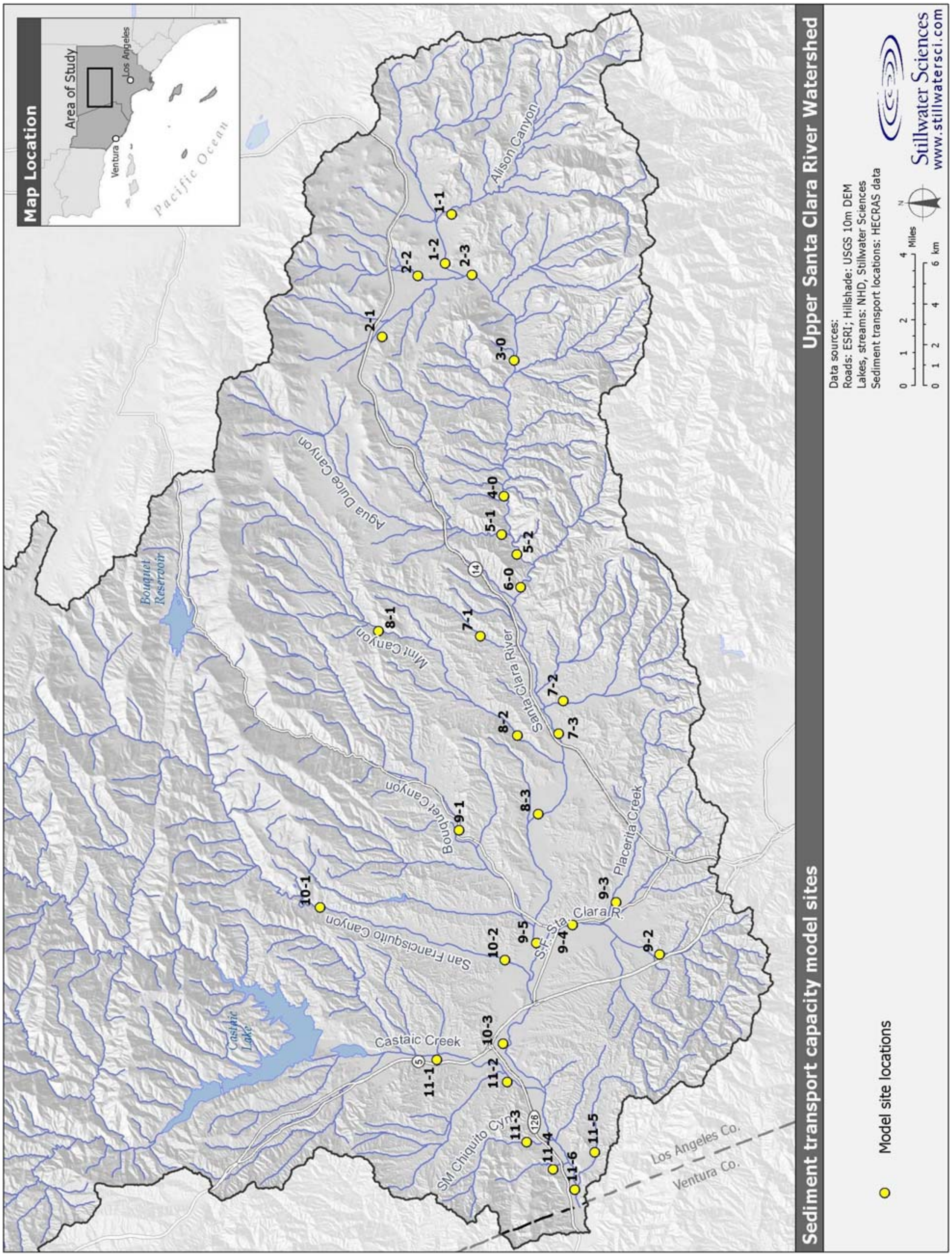

Figure 4-19. Locations of sediment transport capacity model sites throughout the USCR watershed.

Table 4-6. Summary of average annual bedload transport capacity values for tributary locations.

Watershed region	Tributary watershed	Tributary reach [a]	Sediment transport capacity model site	HSPF model node	Contributing area (km^2)	$Q_{sed\ cap}$ ($m^3\ s^{-1}$) [b]	Average annual bedload transport capacity ($t\ yr^{-1}$) [c]
Upper (Acton Basin)	Acton Canyon	Escondido Cr reach 3	2-1	CORPS_2327	16.6	5.6	22,000
		Acton Cyn reach 8	2-2	FEMA_TYPE1_555	54.4	6.6	3,600
Middle (Soledad Canyon)	Agua Dulce	Agua Dulce reach 10	5-1	CORPS_892	76.1	12	5,700
	Tick Canyon	Tick Cyn reach 1	7-1	CORPS_1833	10.4	5.7	1,700
	Sand Canyon	Sand Cyn reach 4	7-2	CORPS_1139	33.0	31	46,000
Lower (Santa Clarita Basin)	Mint Canyon	Mint Cyn reach 3	8-1	CORPS_490	47.5	17	32,000
		Mint Cyn reach 9	8-2	CORPS_388	75.8	17	96,000
	Bouquet Canyon	Bouquet Cyn reach 5	9-1	FEMA_Type1_442	75.9	37	50,000
	South Fork SCR	SF SCR reach 5	9-2	CORPS_1713	29.1	20	42,000
		Placerita Cr reach 4	9-3	CORPS_700	23.1	9.3	5,900
		SF SCR reach 10	9-4	FEMA_Type1_77	111	42	7,900
	San Francisquito Canyon	San Francisquito Cyn reach 1	10-1	CORPS_1256	112	57	44,000
		San Francisquito Cyn reach 3	10-2	FEMA_TYPE2_49	135	55	42,000
	Castaic Creek	Castaic Cr reach 7	11-1	CORPS_2122	79.8	56	17,000
		Castaic Cr reach 8	11-2	CORPS_2078	123	53	25,000
	SM Chiquito Canyon	SM Chiquito Cyn reach 3	11-3	CORPS_1492	12.4	1.8	2,000
	SM Grande Canyon	SM Grande Cyn reach 4	11-4	CORPS_1582	8.6	9.2	38,000
	Potrero Canyon	Portrero Cyn reach 6	11-5	CORPS_948	11.6	6.4	34,000

[a] Reaches decrease in number going downstream
[b] Defined as the daily mean discharge that has the capacity to transport the average annual bedload yield and was calculated as 14% of Q_{100}
[c] Calculated as a function of $Q_{sed\ cap}$.

Table 4-7. Summary of average annual bedload transport capacity values for mainstem locations.

Watershed region	Mainstem reach [a]	Sediment transport capacity model site	HSPF model node	Contributing area (km^2)	$Q_{sed\ cap}$ ($m^3\ s^{-1}$) [b]	Average annual bedload transport capacity ($t\ yr^{-1}$) [d]
Upper (Acton Basin)	M29	1-1	CORPS_1740	63	19	9,300
	M28	1-2	--	129	32 [c]	2,500
	M27	2-3	FEMA_Type1_726	185	48	33,000
Middle (Soledad Canyon)	M24	3-0	CORPS_1306	232	50	106,000
	M23	4-0	CORPS_1379	305	68	79,000
	M22	5-2	CORPS_1410	389	80	78,000
	M19	6-0	CORPS_1441	407	85	92,000
Lower (Santa Clarita Basin)	M16	7-3	FEMA_Type1_769	501	102	33,000
	M15	8-3	FEMA_Type1_800	594	117	39,000
	M14	9-5	FEMA_Type1_666	764	145	38,000
	M13	10-3	FEMA_Type1_621	1,040	210	64,000
	M11-B	11-6	FEMA_Type2_43	1,220	263	54,000 [e]

[a] Reaches decrease in number going downstream; not all reaches had a sediment transport capacity model site contained within.
[b] Defined as the daily mean discharge that has the capacity to transport the average annual bedload yield and was calculated to be 14% of Q_{100}.
[c] Determined from the relationship between modeled Q_{100} at the HSPF nodes and contributing watershed area.
[d] Calculated as a function of $Q_{sed\ cap}$.
[e] This value is equivalent to the average annual bedload transport rate calculated at the County line gauge (USGS 11108500 and 11109000) assuming bedload is 6% of the total sediment load.

4.3.2.2 Average annual bedload transport rate

Average annual bedload transport capacity values were converted to bedload transport rates based on general sediment transport characteristics. Modeling site reaches were categorized as either supply-limited or transport-limited with respect to bedload. Supply-limited reaches have a steep and/or oversized channel and a high potential to transport sediment, but their actual transport rate is limited primarily by the sediment supply from upstream. Transport-limited reaches are usually low-gradient alluvial channels and have a transport rate that is limited by local channel geometry (e.g., channel width and slope) rather than by upstream sediment supply. Modeling sites within supply-limited reaches were presumed therefore to have a bedload transport rate that was less than the calculated transport capacity, while sites in transport-limited reaches were considered to have a bedload transport rate equal to the transport capacity.

Channel reach types and corresponding average annual bedload transport rates for the tributary and mainstem modeling sites are shown in Tables 4-8 and 4-9. Most modeling sites were purposely located in transport-limited reaches, thereby allowing for direct determination of annual average bedload transport rate at all but three locations (sites 3-0, 9-1, and 10-1). These sites were located in a steep, oversized engineered reach (9-1) and steep, bedrock canyon reaches (9-1 and 10-1). Although the bedload transport rate could not be quantified at these supply-limited sites, the calculated transport capacity was viewed in the context of upstream and downstream bedload transport rates to assess the channel's capacity to transport bedload delivered from upstream and associated sediment aggradation/incision trends.

4.3.2.3 Bedload transport dynamics and channel condition

The final part of the analysis entailed determining reach-scale trends in sediment aggradation/incision and determining average long-term channel condition (i.e., trends of an aggrading, stable, or incising channel bed) within tributary and mainstem reaches. This was accomplished by first developing a preliminary assessment using bedload sediment transport rates at modeling sites combined with upstream sediment yield estimates. At the tributary sites (but not the mainstem river sites), the calculated bedload transport rate was compared to the GLU-derived sediment production rate in the contributing area from upstream. For the purposes of this analysis, the GLU-derived sediment production rates were treated as sediment yield, or supply, from upstream sources because hillslope sediment delivery ratios are assumed to be high in the tributary drainages. A site was considered potentially aggrading if the bedload transport rate was much less than the GLU-derived sediment yield and potentially incising if the bedload transport rate was greater than the GLU-derived yield. Sites in between these two extremes were considered potentially stable. For this analysis, supply-limited sites were considered inherently stable as they were located in either concrete (site 9-1) or bedrock (site 10-1) channels with high transport capacities (i.e., minimal sediment deposition and hard beds not easily incised).

Because there were many more model sites on the mainstem river, channel conditions were evaluated at mainstem modeling sites slightly differently than at the tributary sites. That is, the calculated bedload transport rate at a given site was compared to the combined bedload transport rate(s) from both mainstem and tributuary modeling site(s) directly upstream (representing the upstream supply to that given site) to get an indication of the site's tendency to accumulate or evacuate delivered bedload. Because it was not possible to account for all sediment being delivered to a modeling site from upstream using this method, the calculated bedload yield from upstream was considered a minimum estimate. Therefore, this comparison gave a definitive answer only when a site's bedload transport rate was substantially less than the bedload sediment yield from upstream (i.e., at least 10% less). Under this condition, the modeled channel site was considered potentially aggrading (i.e., the channel cannot transport the minimum estimate of bedload delivered from upstream). Where the bedload transport rate was greater than the bedload yield from upstream, the channel condition was not easily predicted because of the potential for unaccounted bedload sediment delivery between modeling sites. As with the tributary supply-limited sites, the channel at the one mainstem supply-limited site (site 3-0) was considered inherently stable.

Following the initial channel condition assessment using the comparison of modeled bedload transport rates and upstream sediment yields, field observations were used to make the final determination of channel condition at almost all modeling sites. It was not possible to visit Potrero Canyon during the field effort, so the final channel condition assessment there was based on the comparison of bedload sediment transport rate and upstream sediment yield combined with channel conditions shown in recent aerial photographs.

The channel conditions at the tributary and mainstem modeling sites are given in Tables 4-8 and 4-9, respectively, and shown in Figure 4-20. For the majority of tributary transport-limited sites, field observations of bed sediment aggradation/incision trends and bed elevations relative to an adjacent floodplain confirmed the initial channel condition assessments from the comparison of bedload sediment transport rate and GLU-derived upstream sediment yield. Field observations revealed that channels at the tributary modeling sites were generally aggradational where the ratio of bedload transport to upstream sediment yield was $\leq$ 0.05, incising where the ratio was $\geq$0.34, and stable at ratios in between. The only exception to this trend was at the mouth of Sand Canyon (site 7-2), where it is quite possible that the channel and bed sediment data used to calculate bedload sediment transport capacity pre-dates recent channel restoration efforts.

As expected, incising reaches were predominantly in the portions of tributary subwatersheds with the greatest degree of upstream development (e.g., sites 8-1 and 8-2 in Mint Canyon). Aggrading reaches were predominantly at the mouths of tributary subwatersheds with relatively high sediment yields (e.g., site 9-4 in the South Fork SCR).

At the transport-limited mainstem modeling sites, channel conditions ranged from predominantly stable in the Upper and Middle Region reaches and aggrading in the Lower Region reaches; no sites were found to be incisional. In most instances, field observations confirmed that the channel was generally aggrading in transport-limited reaches where the bedload transport rate was less than the calculated bedload yield from upstream. The only nominal exception was in the Soledad Canyon section of the mainstem (site 5-2), where the amount of bedload from upstream was slightly higher than the site’s bedload transport rate, but field observations suggested the channel was generally stable. All transport-limited mainstem modeling sites where the bedload transport rate was more than the calculated bedload yield from upstream were determined by field observations to be in stable channel reaches. The one supply-limited site (3-0) was presumed to be inherently stable and this condition was confirmed by field observatiojns. The average annual bedload sediment transport rate along the mainstem USCR is shown graphically in Figure 4-21.

The results of this analysis are synthesized with the results from our active channel width and bed level change analyses in Section 4.3.5 below.

Table 4-8. Summary of average annual bedload transport rates and channel conditions at tributary locations.

Watershed region	Tributary subwatershed	Sediment transport capacity model site	Average annual bedload transport capacity ($t\ yr^{-1}$)	Reach type [a]	Average annual bedload transport rate ($t\ yr^{-1}$) [b]	Average annual GLU-derived sediment yield ($t\ yr^{-1}$) [c]	Bedload transport rate/GLU-derived sediment yield [d]	Channel condition [f]
Upper (Acton Basin)	Acton Canyon	2-1	22,000	TL	22,000	23,000	0.96	Incising
		2-2	3,600	TL	3,600	64,000	0.06	Stable
Middle (Soledad Canyon)	Agua Dulce	5-1	5,700	TL	5,700	98,000	0.06	Stable
	Tick Canyon	7-1	1,700	TL	1,700	18,000	0.09	Stable
	Sand Canyon	7-2	46,000	TL	46,000	41,000	1.13 [e]	Stable
Lower (Santa Clarita Basin)	Mint Canyon	8-1	32,000	TL	32,000	64,000	0.50	Incising
		8-2	96,000	TL	96,000	124,000	0.78	Incising
	Bouquet Canyon	9-1	50,000	SL	< 50,000	142,000	0.35	Stable
	South Fork SCR	9-2	42,000	TL	42,000	123,000	0.34	Incising
		9-3	5,900	TL	5,900	44,000	0.13	Stable
		9-4	7,900	TL	7,900	316,000	0.03	Aggrading
	San Francisquito Canyon	10-1	44,000	SL	< 44,000	158,000	0.28	Stable
		10-2	42,000	TL	42,000	216,000	0.19	Stable
	Castaic Creek	11-1	17,000	TL	17,000	254,000	0.07	Stable
		11-2	25,000	TL	25,000	365,000	0.07	Stable
	SM Chiquito Canyon	11-3	2,000	TL	2,000	49,000	0.04	Aggrading
	SM Grande Canyon	11-4	38,000	TL	38,000	38,000	1.00	Incising
	Potrero Canyon	11-5	34,000	TL	34,000	47,000	0.72	Incising

[a] Supply-limited (SL) means the amount of sediment transported is controlled primarily by the sediment supply from upstream; transport-limited (TL) means the amount of sediment transported is controlled primarily by local morphologic factors (e.g., channel geometry and reach slope). The supply-limited sites include an engineered, concrete channel reach (site 9-1) and a bedrock canyon reach (site 10-1).
[b] Sites within supply-limited reaches have a transport rate < transport capacity; sites within transport-limited reaches have a transport rate = transport capacity.
[c] Average annual GLU-derived sediment yield calculated for watershed area upstream of model site
[d] Potentially aggrading ≤0.05, potentially stable >0.05 and <0.34, and potentially incising ≥0.34.
[e] The bedload transport capacity was likely calculated with pre-restoration channel dimensions, causing an unrealistically high bedload transport rate/GLU-derived sediment yield ratio.
[f] Channel condition derived from comparing bedload transport rate and GLU-derived sediment yield and checked with field observations.

Table 4-9. Summary of average annual bedload transport rates and channel conditions at mainstem locations.

Watershed region	Mainstem reach	Sediment transport capacity model site	Average annual bedload transport capacity ($t\ yr^{-1}$)	Reach type [a]	Average annual site bedload transport rate ($t\ yr^{-1}$) [b]	Average annual bedload yield to site ($t\ yr^{-1}$) [c]	Bedload transport rate ≤ upstream bedload yield	Channel condition [d]
Upper (Acton Basin)	M29	1-1	9,300	TL	9,300	--	--	Stable
	M28	1-2	2,500	TL	2,500	9,300	Yes	Aggrading
	M27	2-3	33,000	TL	33,000	6,000	No	Stable
Middle (Soledad Canyon)	M24	3-0	106,000	SL	< 106,000	33,000	No [e]	Stable
	M23	4-0	79,000	TL	79,000	< 106,000	No [e]	Stable
	M22	5-2	78,000	TL	78,000	84,000	Yes	Stable
	M19	6-0	92,000	TL	92,000	78,000	No	Stable
Lower (Santa Clarita Basin)	M16	7-3	33,000	TL	33,000	140,000	Yes	Aggrading
	M15	8-3	39,000	TL	39,000	129,000	Yes	Aggrading
	M14	9-5	38,000	TL	38,000	47,000	Yes	Aggrading
	M13	10-3	64,000	TL	64,000	80,000	Yes	Aggrading
	M11-B	11-6	54,000	TL	54,000	164,000	Yes	Aggrading

[a] Supply-limited (SL) means the amount of sediment transported is controlled primarily by the sediment supply from upstream; transport-limited (TL) means the amount of sediment transported is controlled primarily by local morphologic factors (e.g., channel geometry and reach slope). The supply-limited site (3-0) is within a bedrock canyon reach.
[b] Sites within supply-limited reaches have a transport rate < transport capacity; sites within transport-limited reaches have a transport rate = transport capacity.
[c] Upstream bedload yield derived from bedload transport rates at upstream tributary and mainstem transport-limited model sites and is considered a **minimum** bedload yield estimate.
[d] Channel condition derived from comparing bedload transport rate and upstream sediment yield and checked with field observations.
[e] It is assumed that the actual average annual bedload transport rate at the site is higher than the average annual bedload yield to the site.

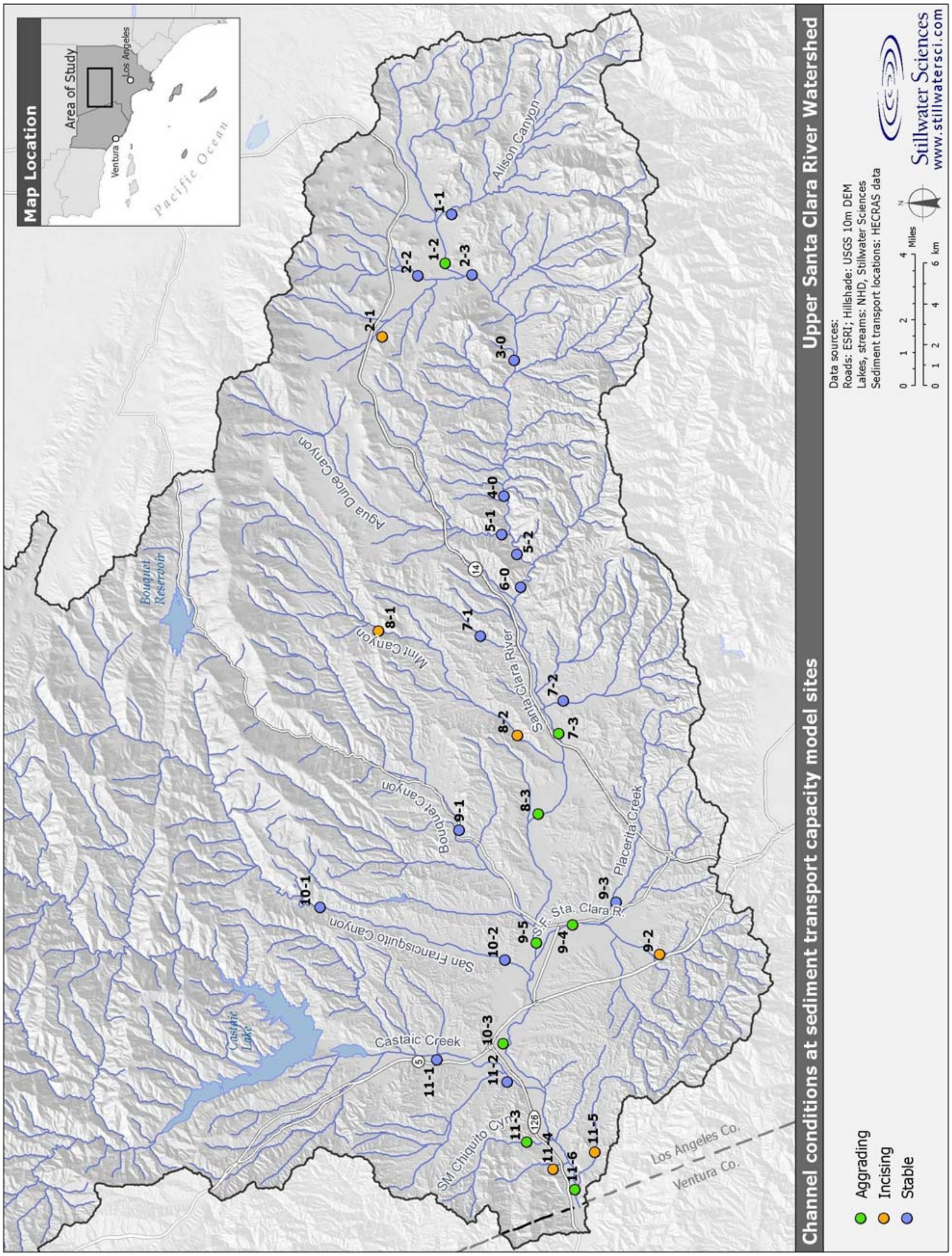

Figure 4-20. Channel conditions at sediment transport capacity model sites throughout the USCR watershed.

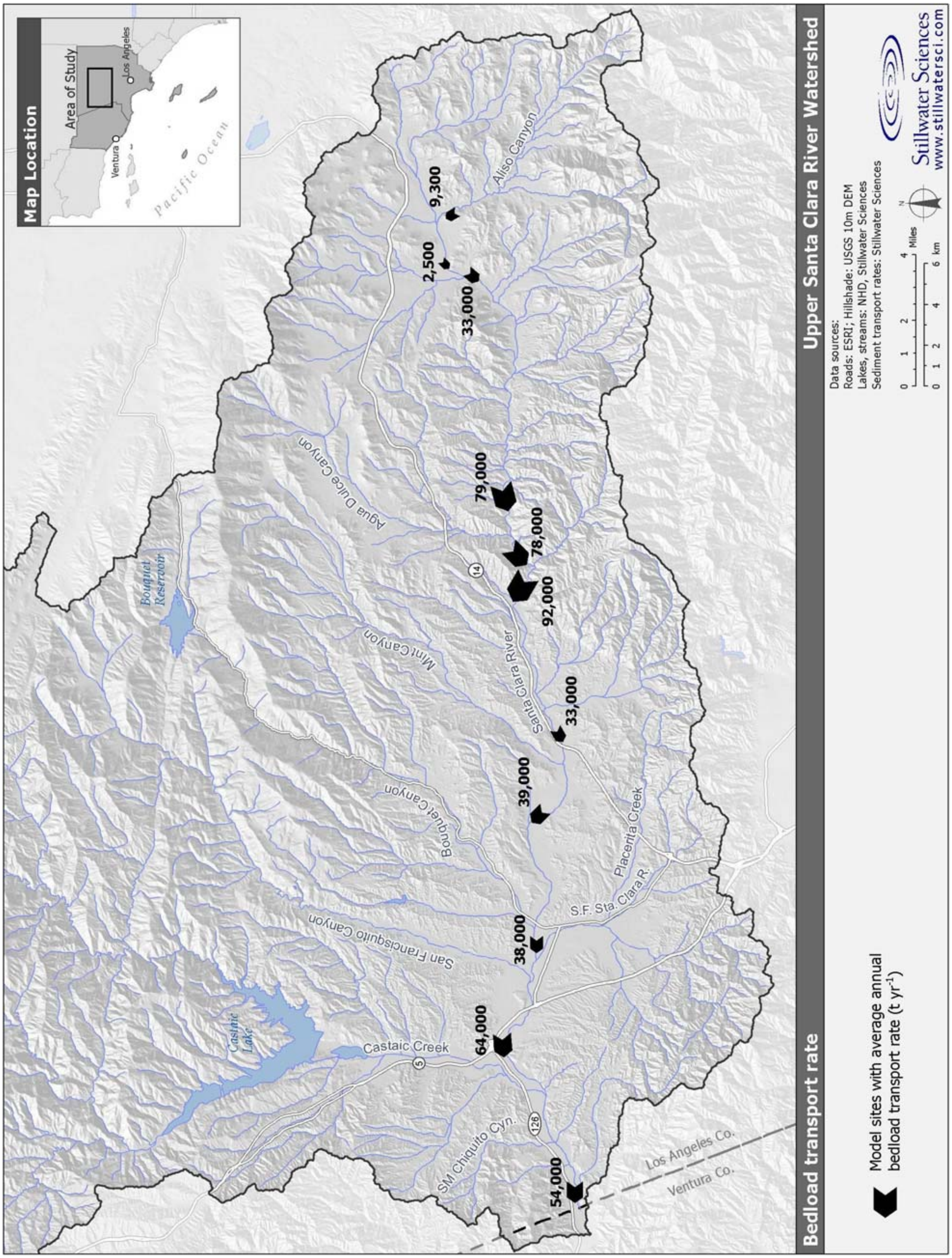

Figure 4-21. Average annual bedload sediment transport rate throughout the mainstem USCR.

4.3.3 Changes in active width: 1928–2005

As a predominantly braided but dryland river, the mainstem channel of the USCR within the Acton and Santa Clarita basins comprises a primary low-flow channel and various short-lived secondary channels. The low-flow channel boundary changes rapidly and completely during flood events according to the magnitude of the event and other factors, whereas the boundary of the larger mainstem channel changes less frequently but carries greater importance in determining the relationship between the river's geomorphology and human activities on the adjacent floodplain.

Unlike single-thread meandering channels that generally have a well-defined edge that separates the mainstem channel from its floodplain, the mainstem boundary of the USCR is less well-defined. Because of intermittent flow, changeable morphology and thalweg location, and rapid colonization of the channel bed by riparian vegetation between flood events, the separation between the floodplain and the mainstem is only evident following relatively large flood flows and is even then subject to interpretation according to the extent of apparent flow inundation and re-working of channel bed sediments achieved by the flood event. Prior empirical investigations of channel change have focused both on the position of the primary low-flow channel, to the extent it is discernable, and on the extent of the full width of flood flow (i.e., in the mainstem channel *and* upon the floodplain) evident from aerial photographs of the USCR (e.g., the maps and supporting text in Section VI of Simons, Li & Associates 1987). Because large flood events physically affect more than just the low-flow channel(s), our analysis considers the "geomorphically active channel" to be a more useful metric of quantifying the change in the river's morphology over time.

The geomorphically active channel, or "active channel width," is considered here as that part of the mainstem channel bed that carried a significant part of the flood and sediment discharge during the recent flood event. Ideally, the optimal and most accurate method to quantify channel change in response to a given flood event is to compare channel bed elevations represented in high-resolution elevation data collected just prior to and after the flood event (see example of how this method was employed in the lower Sespe Creek [Stillwater Sciences 2010]). For the USCR watershed, there are no available elevation data representing channel conditions immediately before *and* after any of the recorded large flood events. Therefore, delineation of the active channel width was accomplished here in a GIS using an analysis of large-scale aerial photographs from 1928, 1964, 1980–1981, 1994, and 2005, where visible channel bed scour is visible. This approach follows similar methods to studies in dryland rivers by Graf (1984, 2000), Tiegs and Pohl (2005), and Tiegs et al. (2005). The methods employed here specifically followed those initially developed for the companion LSCR study (Stillwater Sciences 2007a). A technical account of the methods is found in Appendix H. These aerial photographic sets were chosen because they were the most comprehensive available for use in this study and they closely, or nearly closely, followed a moderate to large flood event where evidence of channel change was apparent. Unfortunately, photographic coverage for years immediately following two of the watershed's largest flood events—1938 and 1969—were not available. Discrete polygons were digitized on the channel bed to define (1) clear-scoured channel bed without vegetation, and so clearly subjected to significant flow; (2) partially vegetated areas showing evidence of having been subjected to flow and erosion and/or deposition; and (3) densely vegetated areas on the channel bed without evidence for scour or deposition in the last flood. Hydrologically, the latter areas may have been inundated during the last flood event, but the effects related to geomorphic processes were minor. The extent of the active channel was designated to include all polygon types (1) and (2). The analysis was run for each set of aerial photographs over the entire USCR, or to the extent possible according to photographic coverage (see Appendix H).

Dividing the total area of active channel by the length of each channel reach provided a measure of the average active channel width for each date and a variety of associated statistics (Table 4-10). Figure 4-22 shows a general trend along the entire length of the USCR for the active channel width to have become narrower over time. Also clearly visible in the figure (and supported by the weighted average of the active channel widths in Table 4-10) is the differences in active channel width in the three regions of the watershed, with the widths in the Middle Region generally smaller than those in the Lower and Upper regions because the river passes through the highly confined Soledad Canyon. The normalized standard deviation of active channel widths presented in Table 4-10 indicates two distinct reach groups: those reaches that have been more changeable over time (reaches M11, M12, M13, M20, M24, and M26: normalized standard deviation >0.40) and those that have been less changeable (the remaining reaches: normalized standard deviation ≤0.36).

Identification of the river's active channel position over time provides a useful means to predict where the river may continue to be located and where the river's course may eventually be located. To identify the spatial extent of the river's active channel in the past, we created two sets of maps, overlaying the active channel areas delineated using each of the five sets of historical aerial photographs. Initially, the channel bed was plotted as a proportion of time since 1928 that the bed has occupied a given position (Figure 4-23 a–i) to indicate the relative likelihood of channel courses. Second, the width of the bed in successive floods was overlaid with the most recent on top (Figure 4-24 a–i) to indicate trends in active channel widths during floods. Also shown in Figures 4-24 a–i are the areas of low channel disturbance for all years considered (i.e., polygon class 3, as described above).

Reaches M11-B to M13 in the Lower Region have generally decreased in width since being heavily widened by the flood from the St. Francis Dam failure. The narrowing of these reaches is also likely due reduction in flow by Castaic Dam and development of the floodplain. The widths of the upper reaches in this region have fluctuated over time and in response to the individual floods. In many instances, the channel widths have been reduced due to channel encroachments by urban development, specifically in reaches M14 and M15 (Figures 4-24 c, d) where the city of Santa Clarita has grown considerably since the 1960s. In contrast, Reach M16, which is just east of the dense urban footprint of Santa Clarita, has progressively increased in width during this period.

The lower part of the Middle Region not within the highly confined Soledad Canyon (reaches M17 and M18) have exhibited progressive narrowing since the 1960s, particularly Reach M17 which has diminished to half the 1964 width (despite the 1969 and 1978 floods). This reach is situated immediately downstream of the Lang Station Road crossing where active instream aggregate mining has been occurring since the early 1960s. Therefore, it appears that the grade control structure (road crossing) and aggregate mining have served to create an incised, inset, and narrower channel in Reach M17 (see Section 4.3.4 below). The remaining reaches in confined sections of Soledad Canyon (i.e., reaches M20–M27) have had varied changes in their respective active channel widths, but similar to reaches M17 and M18 they have generally exhibited channel narrowing since the 1960s and/or early 1980s. The specific causes of this condition are difficult to identify as there have been few new developments in the river corridor in these reaches during this period. The 2005 flood event, which was larger than all preceding events since 1969 (see Table 4-1), should have effectively scoured a relatively wider channel area than that formed following either the 1978 or 1992–1993 floods. However, one of the most significant differences in the long-term morphologic changes occurring in Reach M17 and in those upstream is the pattern of aggradation, rather than incision, occurring in the canyon reaches (see Section 4.3.4 below).

Table 4-10. Width statistics for the USCR for the period of record 1928-2005 by reach.

Aerial photo date	Follows flow [a]			Active channel width (m) [b]																		
	Flood date	(m^3s^{-1})	(cfs)	Lower Region (Santa Clarita Basin)						Middle Region (Soledad Canyon)									Upper Region (Acton Canyon)			
				M11-B	M12	M13	M14	M15	M16	M17	M18	M19	M20	M21	M22	M23	M24	M25	M26	M27	M28	M29
2005	10 Jan 2005	906	32,000	195	163	145	178	150	202	109	128	29	13	34	30	39	14	51	53	57	304	54
1994	12 Jan 1992 18 Feb 1993	348 303	12,300 10,700	188	163	108	227	155	199	135	146	40	22	56	38	61	32	73	36	64	296	80
1980/81	9 Feb 1978 16 Feb 1980	646 394	22,800 13,900	194	282	98	263	171	183	149	152	49	22	70	41	75	58	80	68	60	322	213
1964	11 Feb 1962	258	9,100				261	184	189	208	163	32	21	53								
1928 [c]	13 Mar 1928	$\sim 2x10^4$	$\sim 7x10^5$	418	537	388	164	166	142	192	74	34	53	60	54	39	12	39	7	59	251	143
Weighted average (m)				313	389	260	209	168	170	174	118	37	35	58	46	50	25	54	29	60	278	139
Standard deviation (m)				113	166	140	45	10	25	31	39	6	16	9	9	15	18	18	25	2	30	49
Normalized standard deviation				0.36	0.43	0.54	0.22	0.06	0.15	0.18	0.33	0.17	0.48	0.15	0.19	0.30	0.73	0.34	0.89	0.03	0.11	0.35

[a] As measured at the County line stream gauges (USGS 11108500 and 11109000).
[b] Blank cells indicate that aerial photograph coverage in that reach was absent or incomplete.
[c] Peak discharge of St. Francis Dam failure flood predicted at the County line area by Begnudelli and Sanders (2007); applies only to reaches M11-B to M13 and the lower end of Reach M14. Last flood prior to 1928 above Reach M14 is unknown.

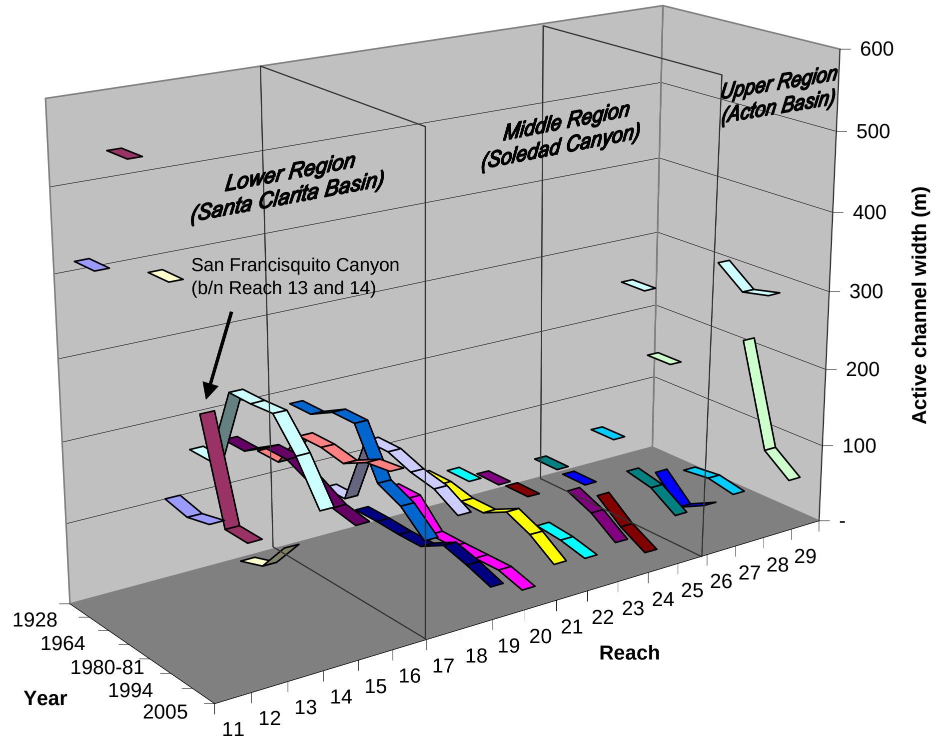

Figure 4-22. Channel width change by reach.

In the Upper Region, reaches M28 and M29 comprise the historically broad channel areas in the Acton basin. Reach M28 has generally maintained its active large width while Reach M29 has narrowed considerably over time. The primary cause for this reduction in channel width is the encroachment of a residential development directly in the active channel area at the confluence of Aliso Canyon and the USCR. This development, positioned in and around the intersection of Aliso Canyon and Carson Mesa roads, appears to have been constructed over a period of a few years in the late 1980s and early 1990s (i.e., between the aerial photographs taken in 1980/81 and 1994).

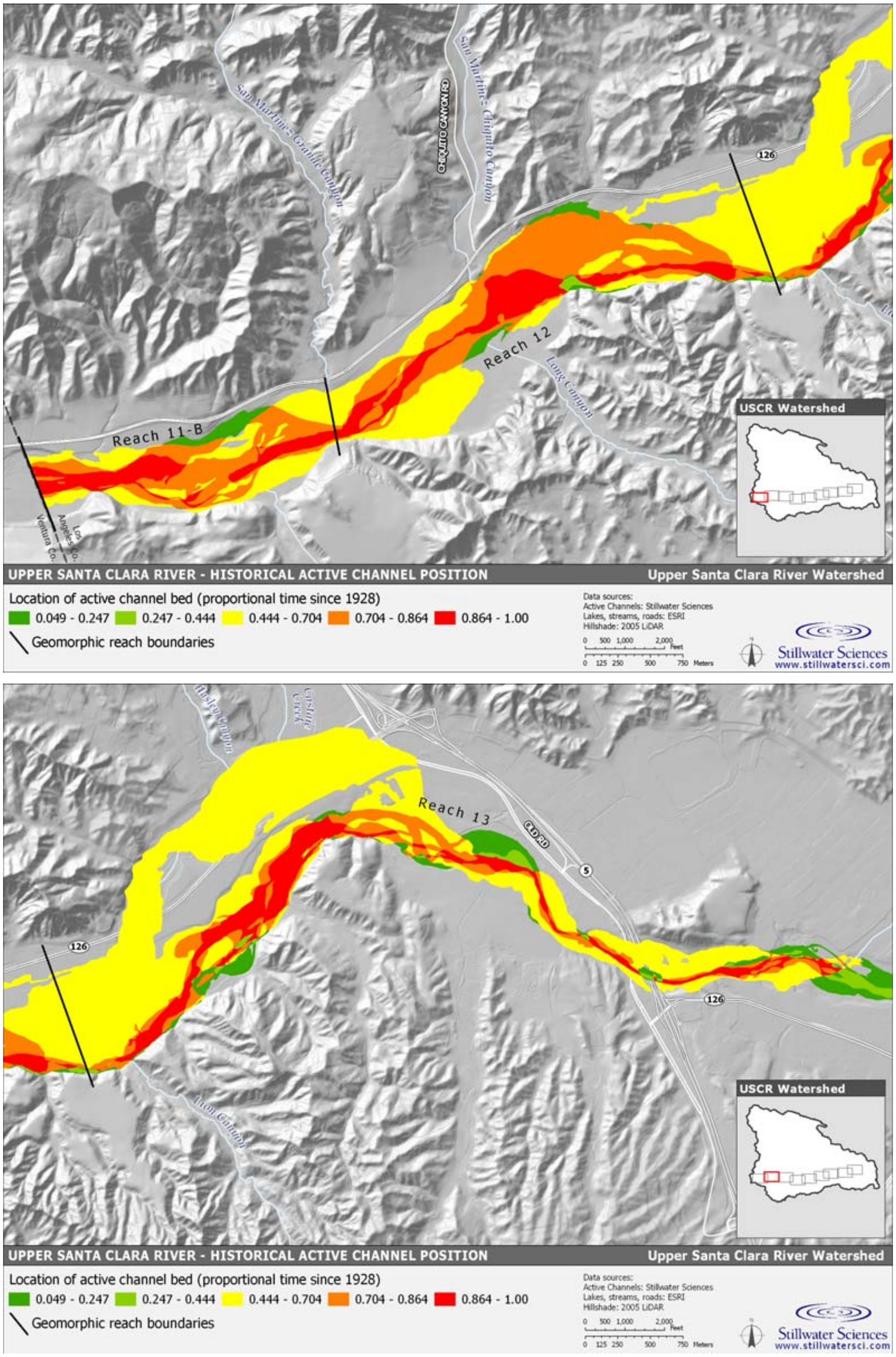

Figure 4-23 a, b. USCR historical channel position: proportion of time since 1928 that the active channel bed has occupied a given location.

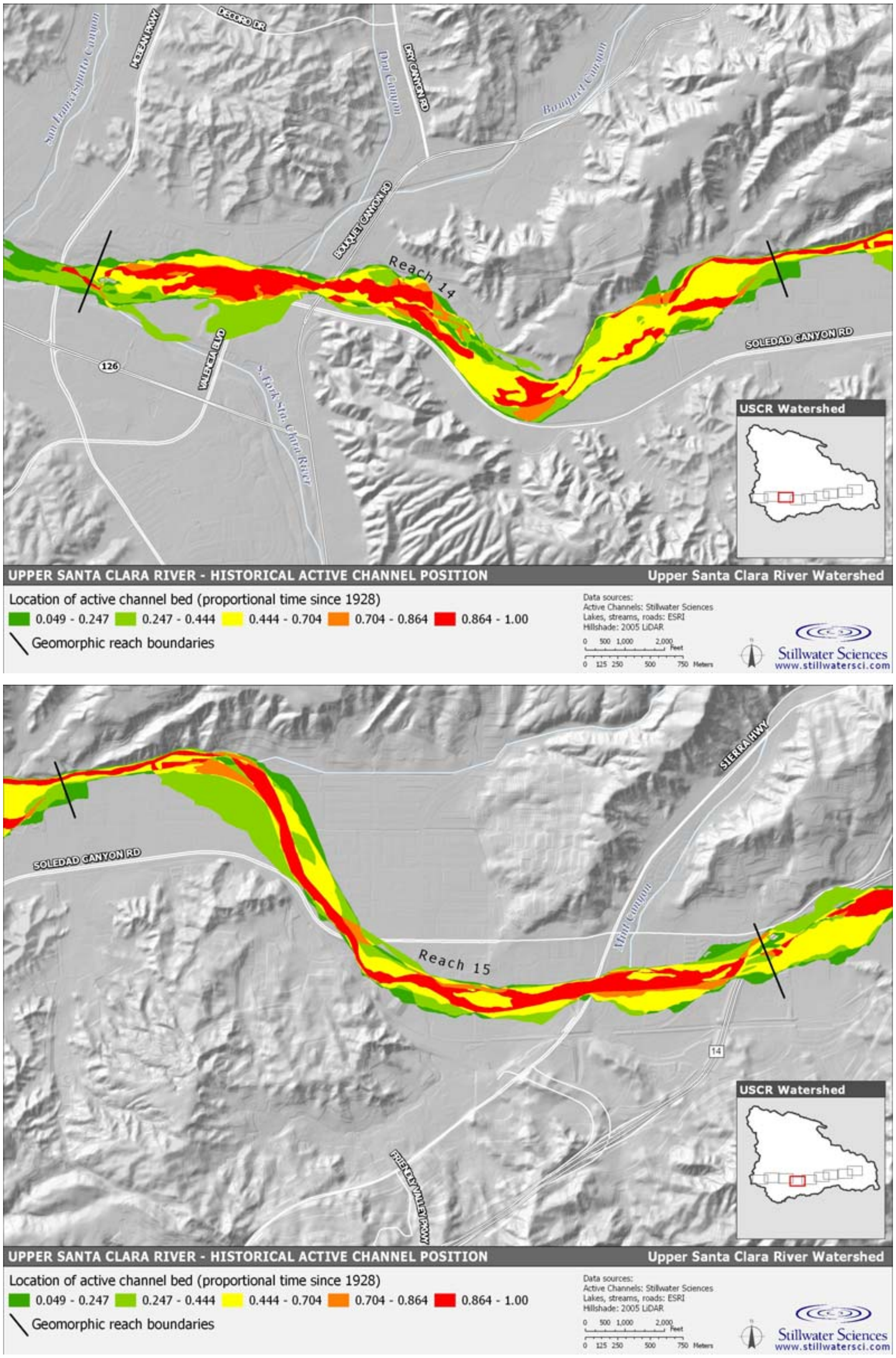

Figure 4-23 c, d. USCR historical channel position: proportion of time since 1928 that the active channel bed has occupied a given location.

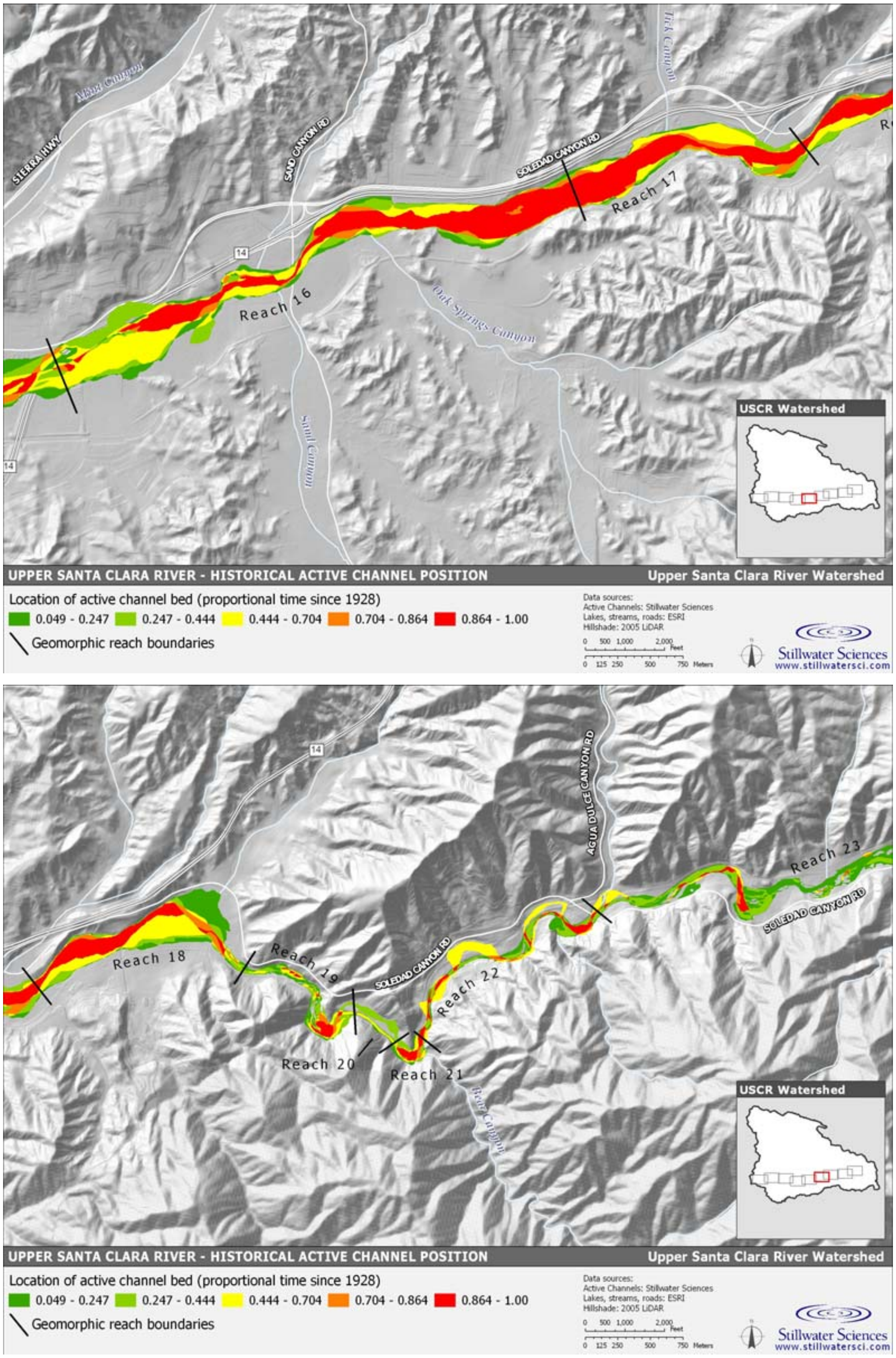

Figure 4-23 e, f. USCR historical channel position: proportion of time since 1928 that the active channel bed has occupied a given location.

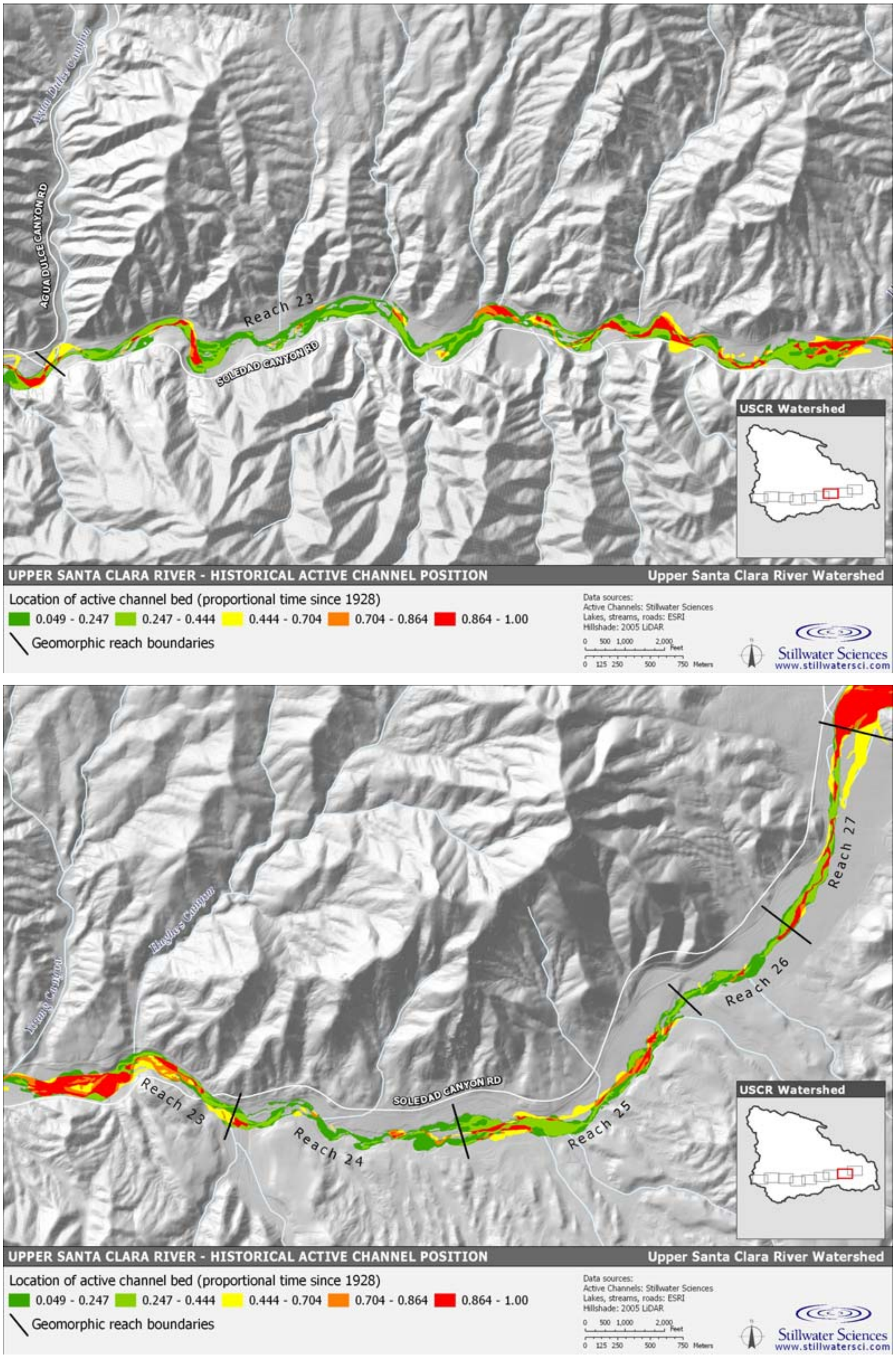

Figure 4-23 g, h. USCR historical channel position: proportion of time since 1928 that the active channel bed has occupied a given location.

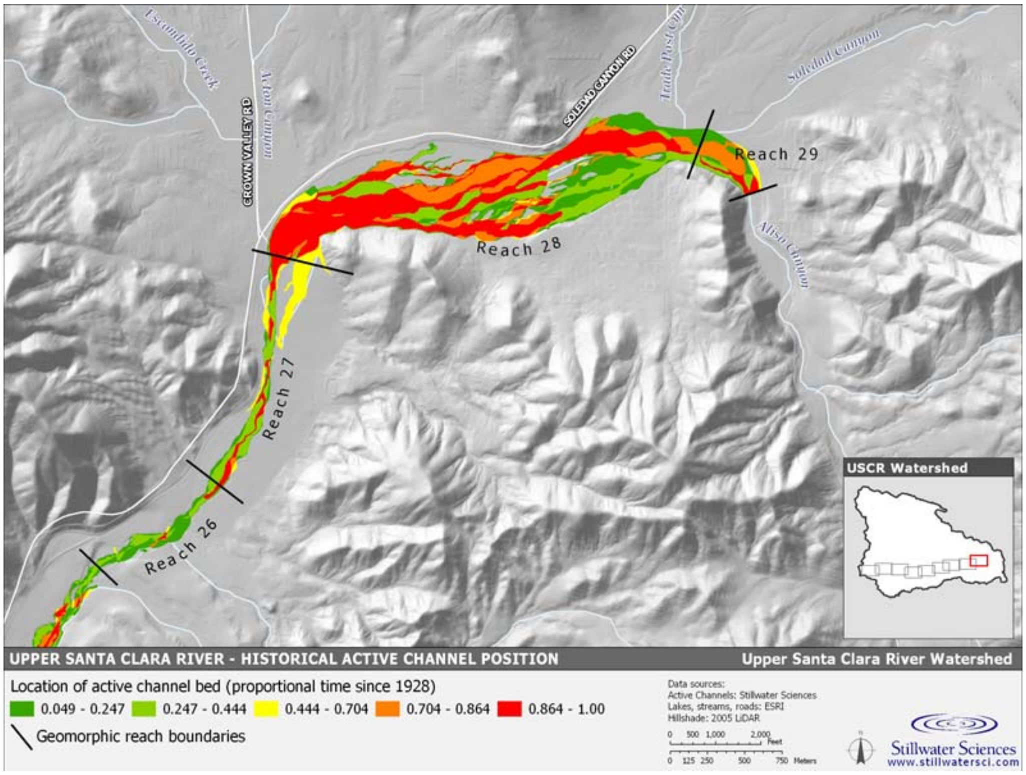

Figure 4-23 i. USCR historical channel position: proportion of time since 1928 that the active channel bed has occupied a given location.

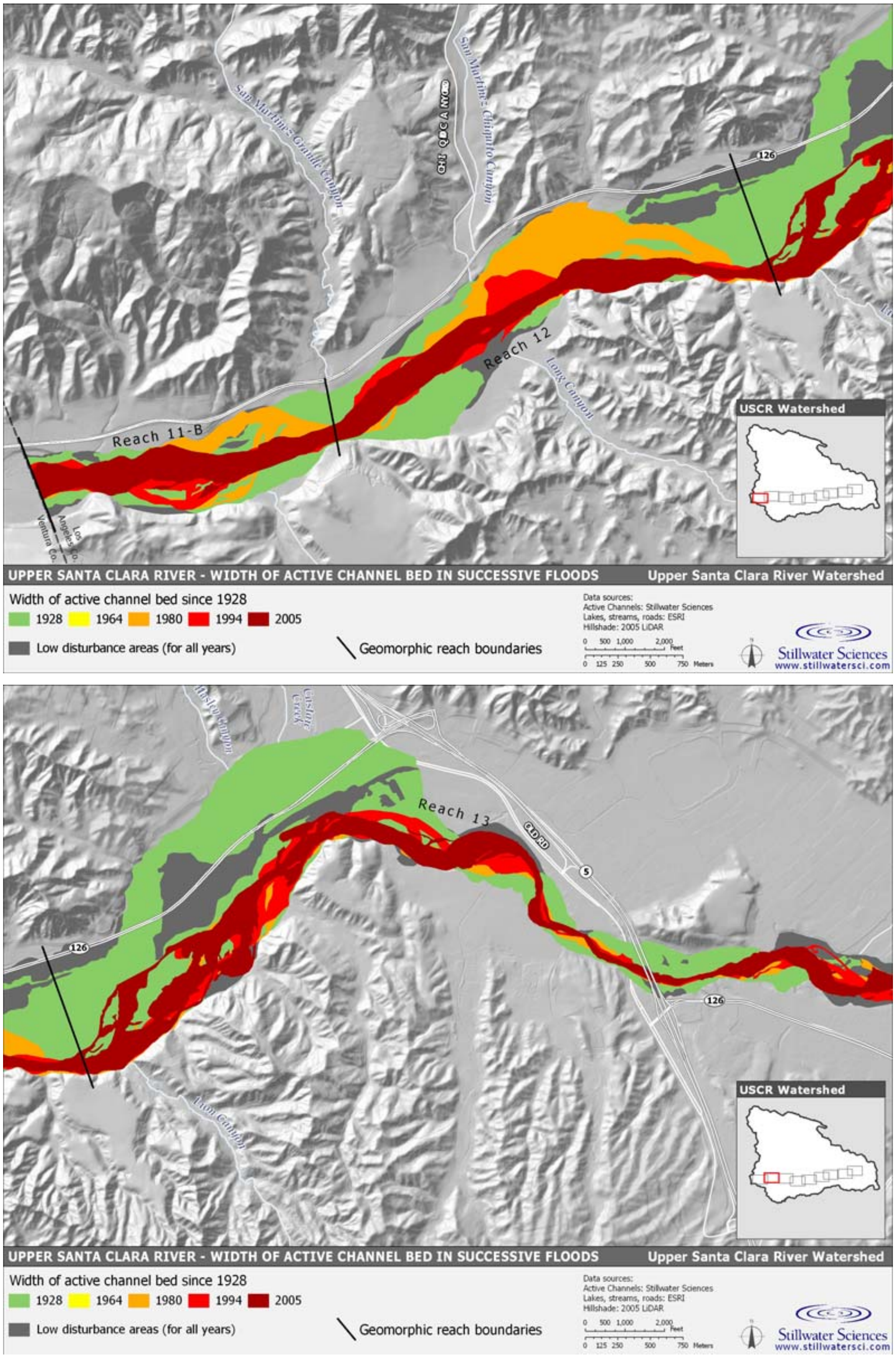

Figure 4-24 a, b. Active width of channel bed in successive floods since 1928 on the USCR. The more recent floods are on top.

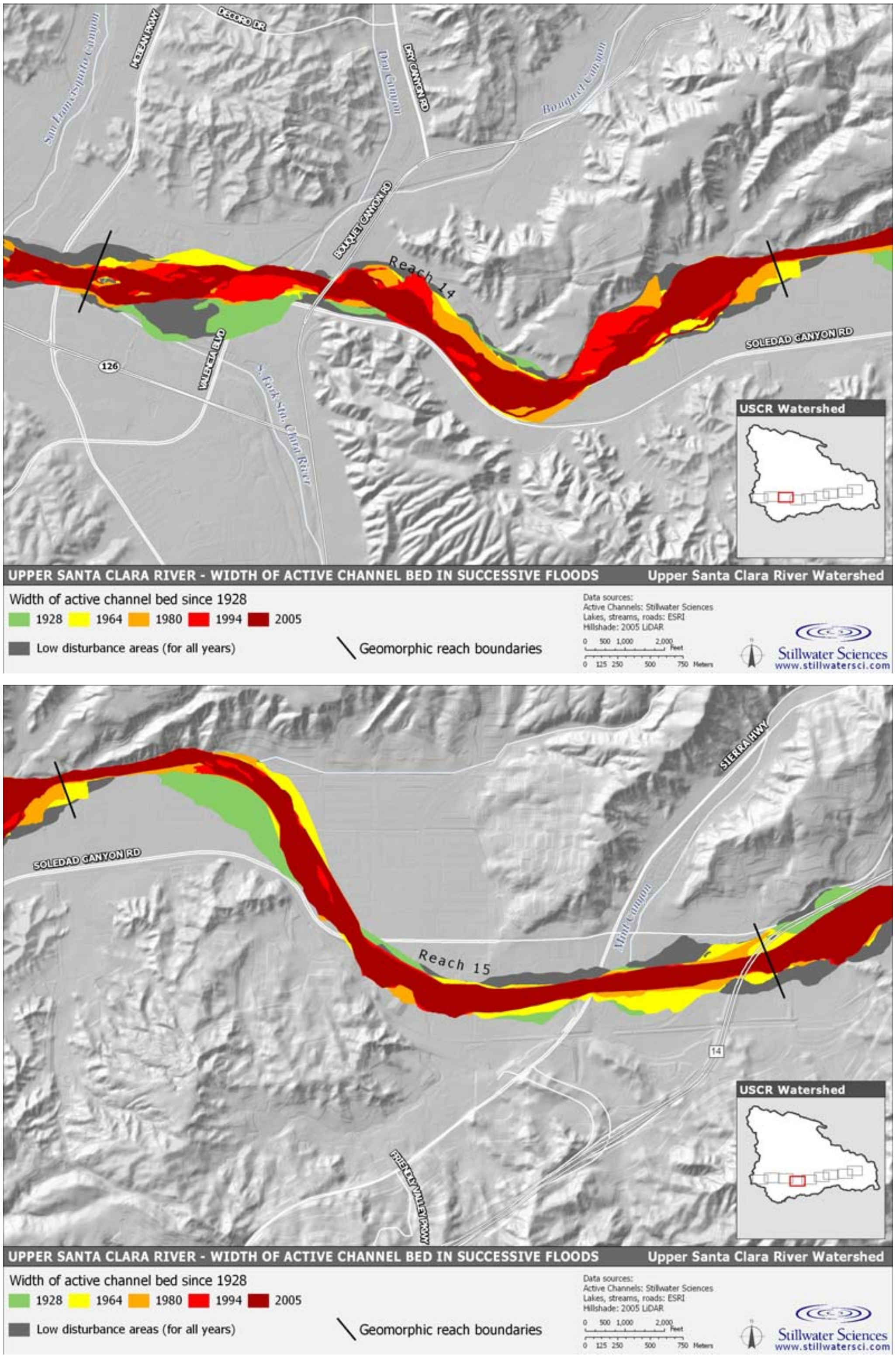

Figure 4-24 c, d. Active width of channel bed in successive floods since 1928 on the USCR. The more recent floods are on top.

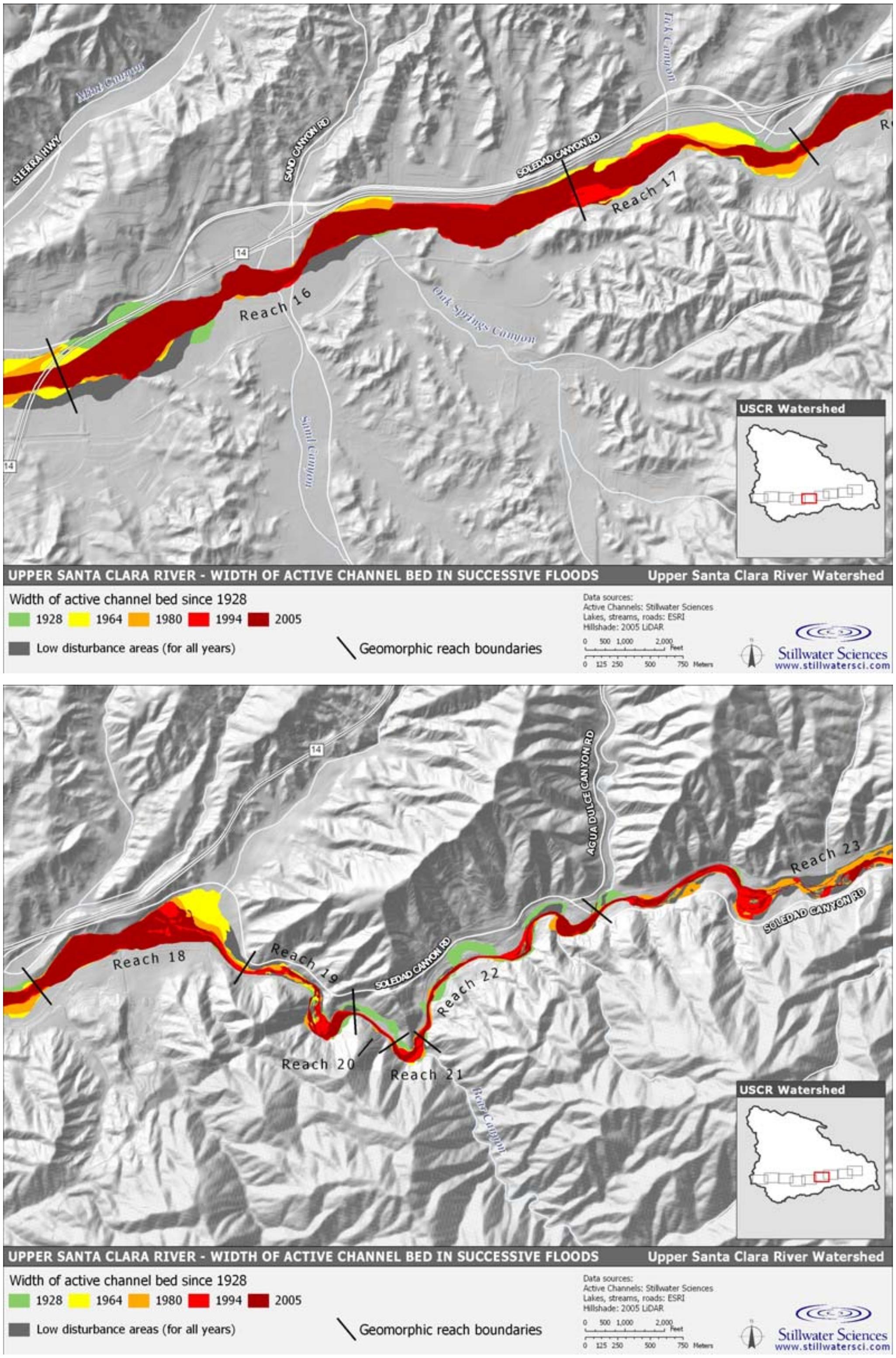

Figure 4-24 e, f. Active width of channel bed in successive floods since 1928 on the USCR. The more recent floods are on top.

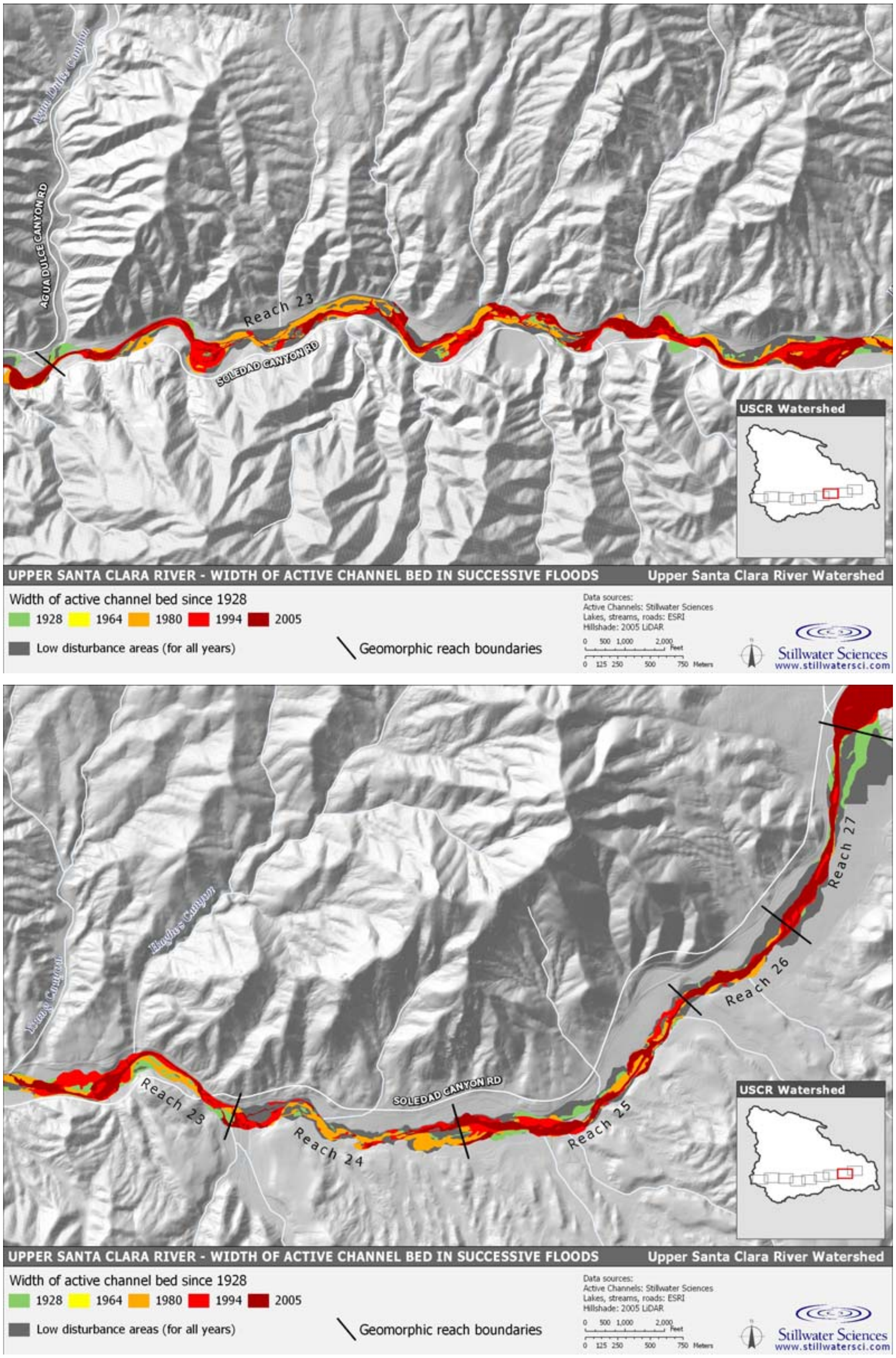

Figure 4-24 g, h. Active width of channel bed in successive floods since 1928 on the USCR. The more recent floods are on top.

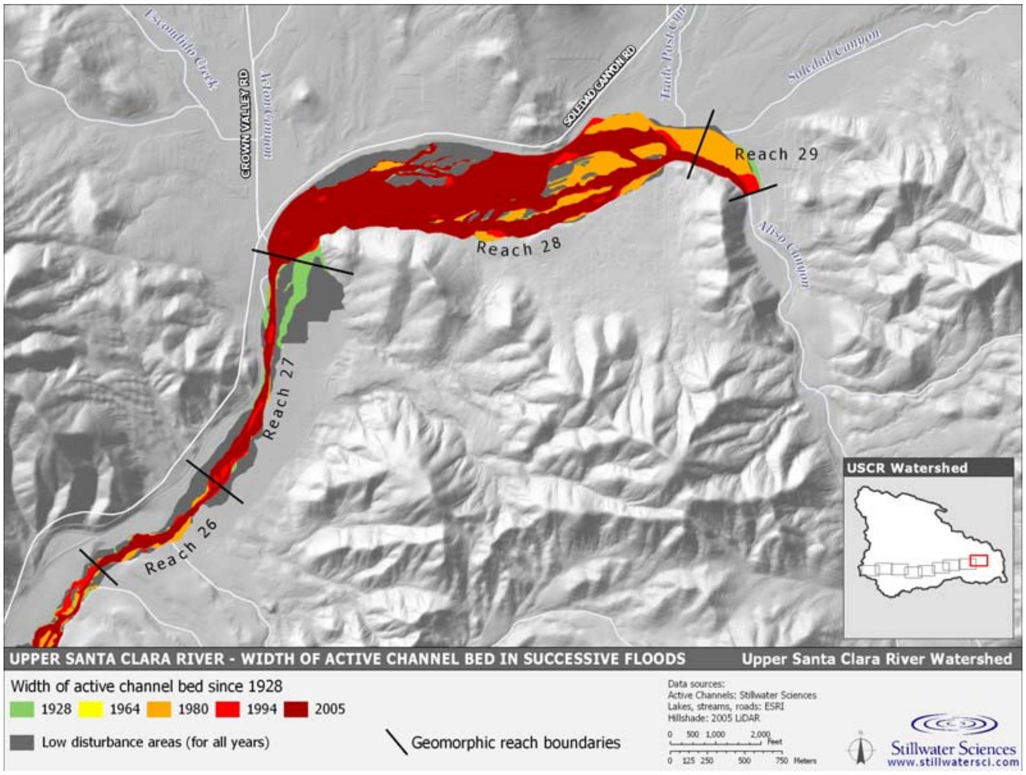

Figure 4-24 i. Active width of channel bed in successive floods since 1928 on the USCR. The more recent floods are on top.

4.3.4 Changes in channel bed level: 1928–2005

Changes in channel bed elevation over time reveal trends of incision and aggradation for discrete reaches within the mainstem USCR. Changes in the active channel width are also very likely to be linked to changes in bed elevation. Combining these data with known impacts to the river channel and surrounding watershed can help reveal causes for past incision/aggradation trends, and they can contribute to the understanding of future trends in incision/aggradation.

Simons, Li & Associates (1987) previously conducted a detailed geomorphic assessment of the fluctuations and long-term trends in the river's bed elevation using LADPW-provided topographic maps (2-ft contours generated photogrammetrically from 1964, 1977, and 1980/81 aerial photos). For the period between 1964 and 1981 and along the river between the County line and Bee Canyon at the downstream end of Soledad Canyon (our Reach M18), they found localized bed level changes, both rising and lowering, on the order of one to a few meters as averaged over each of their study reach lengths. Notable occurrences of aggradation were near the confluence with Castaic Creek, the Los Angeles Aqueduct crossing (halfway between Bouquet and Mint canyons), upstream of Highway 14, and Bee Canyon. Patterns of incision were found to be more common during this period, with much of it concentrated between Interstate 5 and Bouquet Canyon, between Mint Canyon and Highway 14, and between Sand Canyon and above Lang Station Road (see Table 6.1 of Simons, Li & Associates [1987]). This most upstream occurrence of incision exhibited the greatest amount of lowering (~15 m, which the authors attributed to being highly influenced by the instream aggregate mining activities near the Lang Station Road crossing.

In order to extend the study time period both backward and forward in time, we utilized historic and current elevation data to construct additional longitudinal profiles of the river's thalweg. A total of four different datasets—1928, 1964, 2001, and 2005—were initially considered in this analysis. The 1928 dataset was based on USGS 1:24,000-scale topographic quadrangle sheets with 5-ft contour intervals created by the USGS just after the St. Francis Dam failure. The 1964 dataset comprised 2-ft contour topographic sheets produced by LADPW (formerly Los Angeles County Flood Control District). This dataset was previously utilized by Simons, Li & Associates (1987) in their similar assessment of bed level changes along the USCR between 1964 and 1981. The 2001 dataset was a relatively high-resolution, digital elevation surface (5-m DEM; generated by IfSAR technology [or Interferometric Synthetic Aperture Radar]). The 2005 dataset, representing the most recent elevation data available for use in this analysis, was the very high resolution LiDAR (Light Detection and Ranging) collected across the entire USCR watershed within months after the 2005 flood event. The ortho-horizontal resolution of the 2005 LiDAR is 1 ft.

After extracting and comparing the four historic thalweg elevations within the area of common coverage (i.e., County line to Reach M21 within the downstream end of the canyon), the 1964 and 2001 source datasets were found to have used a projection and datum incompatible with the 1928 and 2005 datasets, which prevented their further use in this analysis. Therefore, only the 1928 and 2005 datasets, and their generated thalweg elevations, are considered here (Figure 4-25). We do, however, consider the results from the previous Simons, Li & Associates (1987) analysis to be accurate because their source data (1964 and 1981 aerial photographs) shared a common projection and datum.

The elevation profile depicted in Figure 4-25 is characterized by localized occurrences of thalweg rising and lowering, which is indicative of channel bed aggradation and incision, respectively. The change in bed elevations ranged between -8 m (-26 ft; incision) to +6 m (+20 ft; aggradation). The results here overlap well with the general trends previously reported by Simon, Li & Associates (1987): specifically, aggradation occurs between Castaic Creek and Interstate 5, between Bouquet and Mint canyons, and near the downstream end of the canyon; and incision occurs between Interstate 5 and Bouquet Canyon and near the Lang Station Road crossing. Aggradation is also identified downstream of Lion Canyon in reaches M11-B and M12, which agrees with our findings for the lower half of Reach M11 in Ventura County (Figure 5-18 in Stillwater Sciences [2007a] for the years 1949–2005). Because of the general agreement in bed level adjustments for the periods 1928–2005 and 1964–1981, it can be inferred here that the aggrading reaches and incising reaches have experienced those processes during the majority of the longer time period considered here. Of course, local deviations in these reach-scale changes have and will continue to occur.

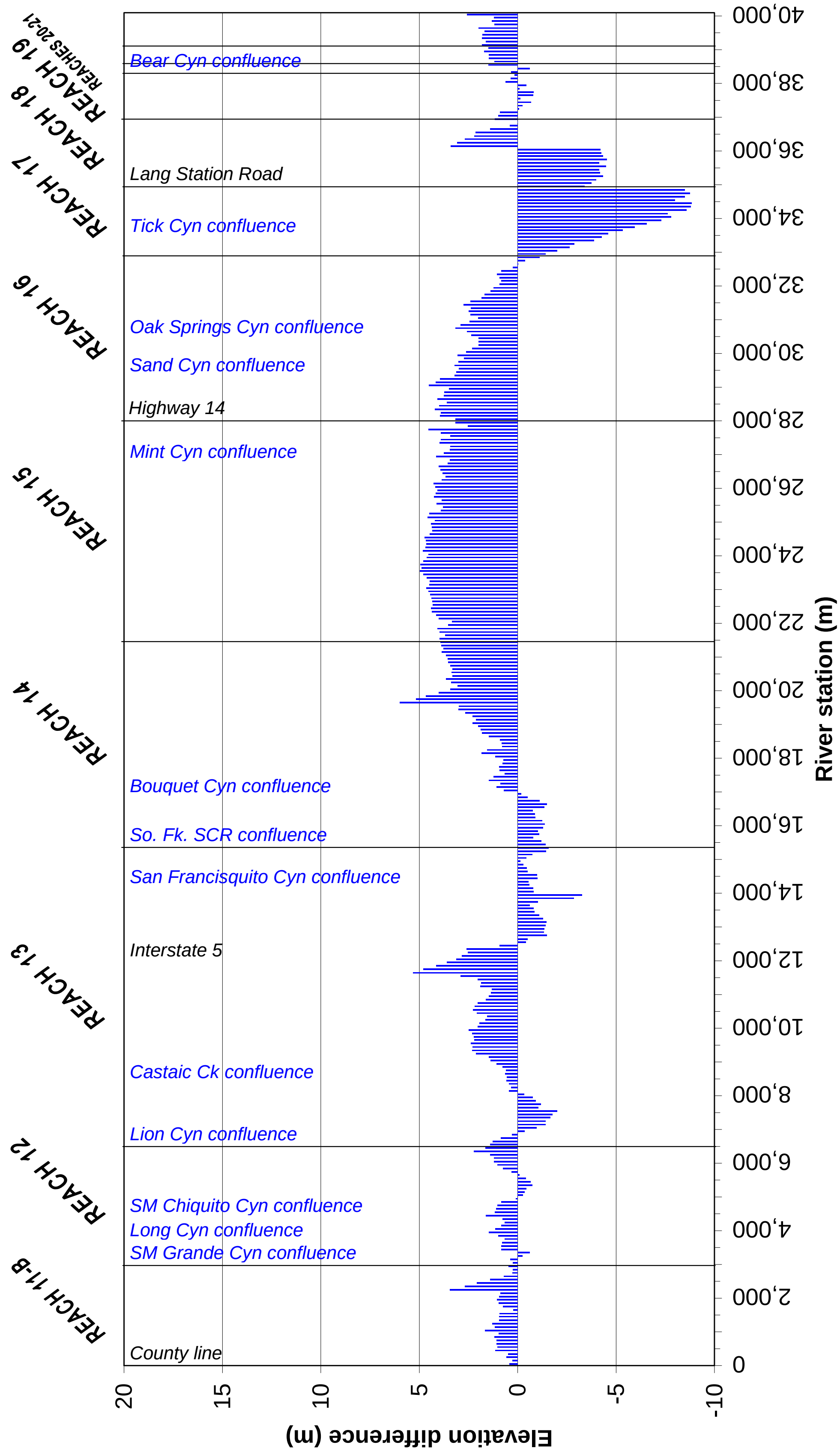

Figure 4-25. Net thalweg elevation change for the USCR from 1928 to 2005.

4.3.5 Summary of reach-level dynamics

In summary, we conducted several analyses to examine long-term trends in active channel width, bed elevation, and associated sediment transport and deposition dynamics. In total, the results from all analyses reveals dominant sediment transport trends and associated channel type, and changes to these conditions over time along the mainstem USCR (Table 4-11). These results are discussed most readily by reference to our division of the USCR into 18 reaches, based on observed differences in geomorphic characteristics. The reaches are grouped into three dominant regions that are characterized by the dominant morphological setting: the Lower Region includes the relatively expansive, low gradient, and developed Santa Clarita basin; the Middle Region includes the confined, coarse-grained Soledad Canyon; and the Upper Region includes the expansive and modestly developed Acton Basin. The river exhibits a braided-channel morphology in the Santa Clarita and Acton basins that adjusts in response to the largest floods on record. In the Middle Region, the river is considerably confined by the steep canyon walls (and is further impinged upon by Soledad Canyon Road and the railway line).

Overall, the river planform and bed elevation have adjusted episodically over the past century, as determined with examination of the reach-average active widths and thalweg elevations. Although the entire river has experienced changes in response to regional influences, such as episodic storm events (e.g., 1969 and 2005) and sediment pulses following large wildfires, the changes have been most pronounced in the Lower Region reaches. These changes have also been strongly influenced by four main anthropogenic factors: (1) the flood wave released during the St. Francis Dam failure in 1928; (2) flow and sediment input reductions with the closure of Castaic Dam in 1972; (3) instream aggregate mining at the downstream end of the Middle Region (Soledad Canyon) over the past several decades; and (4) distributed land-use changes in the watershed over the past century and more localized urban encroachment into the floodplain (and in some cases, within the active channel width) within the past few decades. These factors are referenced below where a link to a morphologic change can be reasonably inferred.

Moving upstream from the County line in the Lower Region, our analyses reveal an overall trend of narrowing and aggradation (bedload deposition) from Reach M11-B upstream through M15 over at least the past 42 years (i.e., the period of overlap between the various analyses). This aggradational trend is primarily reflects a broader river corridor as compared with the Middle Region reaches (and thus increase in sediment deposition potential) coupled with high sediment delivery from adjacent tributary subwatersheds. Tributary sediment yield is potentially very high throughout the entire Lower Region, with the five subwatersheds with the highest average annual sediment production rates draining into the mainstem between M11-B and M15. On average, the bedload sediment yield from these tributaries outpaces the channel's ability to transport bedload, resulting in continued sediment deposition and bed aggradation. This trend is not ubiquitous, however, with some areas of localized mainstem bed incision (e.g., at the confluences with Bouquet and San Francisquito canyon and Castaic Creek).

The general aggradational trend within the mainstem of the Lower Region has also likely contributed to decreased channel gradient and aggradational trends within the lower reaches of several tributary subwatersheds that carry relatively high sediment loads (e.g., San Martinez Chiquito Canyon and South Fork SCR). Reach M16, the uppermost reach in the Lower Region, similarly exhibits an aggradational trend, but its active width has been progressively increasing since 1928; the exact cause of this widening is not clear, particularly since Highway 14 represents a significant structural control on the river's ability to migrate in this reach.

The Lower Region reaches likely once transported sediment in the same fashion as the reaches upstream; however, localized changes in water and sediment supply and perhaps the occurrence of the St. Francis Dam failure appear to be the cause of the shift towards an aggradational, narrowing channel. Under undisturbed conditions, alluvial river channels tend to have little long-term net sediment accumulation or change in active channel width (i.e., the channel bed elevation and width are in quasi-equilibrium). It can be inferred from the results of our analyses that the long-term aggradational and narrowing trends exhibited in the Lower Region reaches may represent the river's response to the scouring floods released during the dam failure (i.e., recovery to an quasi-equilibrium bed elevation) and to the relatively high sediment inputs from historical land uses that occurred during the past century. The reduction in flows from Castaic Creek and, to a lesser degree, from Bouquet Canyon (due to dam operations) can also explain this general morphologic trend because the cumulative flow reductions limit the river's overall ability to efficiently transport sediment delivered to these lower mainstem reaches from other tributary sources. However, because each of these identified influences could explain the aggradational and narrowing trends in the river's morphology, untangling these influences from one another cannot be accomplished with any confidence.

In the Middle Region, the mainstem channel is confined through most of Soledad Canyon, resulting in a relatively steep channel gradient and subsequent high bedload transport rates compared to downstream and upstream reaches (Lower and Upper regions). Reaches M17 and M18 have been impacted over the past several decades by the instream aggregate mining activities occurring at the Lang Station Road crossing. In Reach M17, below the crossing, the USCR exhibits its greatest degree of incision, attributed to the aggregate mining activities in the river channel and to the crossing itself, which functions as a grade control structure that hinders the passage of coarse-grained sediments to this reach (Simons, Li & Associates 1987 and this study). Continuing upstream, the remaining reaches in this region have a relatively high channel gradient and confinement that result in high transport capacity and a channel bed elevation that remains relatively fixed as a result of underlying bedrock. Our analyses accordingly show a stable bed elevation, yet with a modest narrowing downstream trend in the active channel width. The cause of this narrowing is not well understood.

The Upper Region reaches in the relatively broad Acton basin have exhibited episodic adjustments when large, rare flood events occurred. The Arastre Road crossing that separates reaches M26 and M27 represents a relatively significant grade control structure that hinders coarse sediment passage from M27 to M26 and likely causes the observed incision below the crossing. Our sediment transport capacity analysis found that Reach M27 exhibits a stable bed elevation trend, which is not surprising considering that the road crossing at the reach's downstream end acts to maintain the bed elevation.

In Reach M28, the river is considerably broad with numerous braid channels that are prone to adjustment during large flood events. The bedload transport rate decreases along the mainstem channel between the Aliso and Trade Post canyons confluence and the Acton Canyon confluence (M28), causing this reach to trap a large portion of the delivered bedload, which is primarily delivered from the high yielding Aliso Canyon tributary.

Table 4-11. USCR reach morphodynamics: a summary of reach estimates derived elsewhere in this chapter.

Morphodynamic feature	M11-B	M12	M13	M14	M15	M16	M17	M18	M19	M20	M21	M22	M23	M24	M25	M26	M27	M28
	Lower Region (Santa Clarita Basin)						Middle Region (Soledad Canyon)									Upper Region (Acton Basin)		
Centerline reach length, 2005 (km)	1.7	3.9	8.9	5.9	6.8	4.8	2.1	2.0	1.4	0.4	0.4	2.1	9.8	1.9	2.3	1.0	1.7	3.1
Q_2 [a] ($m^3 s^{-1}$)	69	65	52	36	29	26	26	21	21	21	21	20	17	13	13	12	12	8
Q_{100} [a] ($m^3 s^{-1}$)	1,850	1,850	1,500	1,040	832	731	731	604	604	604	604	572	487	358	358	340	340	229
Reach-average slope, 2005 [b]	0.5%	0.5%	0.6%	0.9%	0.9%	0.9%	0.7%	1.1%	1.3%	1.6%	1.7%	1.3%	1.3%	1.7%	1.5%	2.0%	1.3%	1.2%
D_{50} range [c]	0.8-3	0.7-2	0.3-4	2-4	4-12	3-8	4	2	4	15	200	9	1	2	2	4-32	2	3
	S–Gv_f	S–G_{vf}	S–G_{vf}	G_{vf}	G_f–G_m	G_{vf}–G_f	G_{vf}	G_{vf}	G_{vf}	G_m	C_c	G_m	S	G_{vf}	G_{vf}	G_f–G_c	Gvf	Gvf
Reach-average active width, 2005 (m) [d]	195	163	145	178	150	202	109	128	29	13	34	30	39	14	51	53	57	304
Maximum reach-average active width change, historical (1928, 1964, 1980/81, or 1994) versus present day (2005)[d] (m)	-223 (1928-2005)	-374 (1928-2005)	-243 (1928-2005)	-85 (1980-2005)	-34 (1964-2005)	+60 (1928-2005)	-99 (1964-2005)	+54 (1928-2005)	-20 (1980-2005)	-40 (1928-2005)	-36 (1980-2005)	-24 (1928-2005)	-36 (1980-2005)	-44 (1980-2005)	-29 (1980-2005)	+46 (1928-2005)	-7 (1994-2005)	+53 (1928-2005)
Active width change trend [d]	Narrowing	Narrowing	Narrowing	Narrowing	Narrowing	Widening	Narrowing	Widening	Narrowing	Narrowing	Narrowing	Narrowing	Narrowing	Narrowing	Narrowing	Widening	Narrowing	Widening
Channel condition [e]	Aggrading [f]		Aggrading	Aggrading	Aggrading	Aggrading	--	--	Stable	--	--	Stable	Stable	Stable	--	--	Stable	Aggrading
Reach average bed elevation change, 1928-2005 [g] (m)	1.1	0.6	0.5	1.5	4.2	2.5	-5.9	-1.7	0.1	0.6	1.5	--	--	--	--	--	--	--
General trend in bed level elevation, 1928-2005 [g]	Aggrading	Aggrading	Aggrading	Aggrading	Aggrading	Aggrading	Incising	Incising	Stable	Aggrading	Aggrading	--	--	--	--	--	--	--

[a] From HSPF model output.
[b] From longitudinal profile generated in GIS with 2005 LiDAR data (see Figure 4-14).
[c] From compilation of bulk sediment size data; S = sand (<2 mm), G_{vf} = very fine gravel (2–4 mm), G_f = fine gravel (4–8 mm), G_m = medium gravel (8–16 mm), G_c = coarse gravel (16–32 mm), C_c = coarse cobble (128–256 mm). (see Table 4-4 and Figure 4-13, 4-16, 4-18).
[d] From active channel width analysis (1928, 1964, 1980/81, 1994, and 2005) (see Table 4-10 and Figures 4-22 through 4-24).
[e] From sediment transport capacity modeling analysis (see Table 4-8).
[f] The sediment transport capacity model results for the model site in M11-B represent conditions in M11-B through M12 (i.e., to the next upstream model site in M13).
[g] From bed level changes analysis (1928 topographic contours [5 ft for M11-M18, 25 ft for M19-M28] versus 2005 LiDAR data) (see Figure 4-25).
-- Results not generated. For the "Channel condition" row: no sediment transport capacity modeling sites were situated in this reach. For the "Reach average bed elevation change, 1928-2005" and the "General trend in bed level elevation, 1928-2005" rows: the bed level change analysis did not include this reach.

5 SYNTHESIS

This report has presented a geomorphic assessment of key natural and anthropogenically driven processes that have physically shaped and continue to influence the USCR and its watershed. The overlying forces controlling geomorphic processes and resulting conditions in the river and watershed are examined over past, present, and future time frames, and at watershed-wide through sub-reach spatial scales. This synthesis begins by summarizing the study's key findings and concludes with a list of remaining information gaps that have the potential to affect management decision-making in the USCR watershed.

5.1 Key Findings of the Watershed Geomorphic Assessment

The entire Santa Clara River functions in a relatively natural state along much of its entire length as compared to many other coastal rivers of southern California, particularly those in more urbanized basins such as the Los Angeles and Santa Ana rivers—where entire reaches have been channelized with concrete, the majority of their floodplains have been paved, and water and sediment originating from adjacent uplands have been intercepted. In contrast, the Santa Clara River, including the USCR, remains part of an active, dynamic system that supports a relatively rich ecosystem, subject to episodic, sediment mobilizing events that create and renew this ecosystem but which also represent hazards to existing human developments, particularly in the densely urbanized Santa Clarita basin. These hazards include episodic occurrences of high-intensity storms with associated flash floods and debris flows, earthquake-induced landslides, and wildfire-induced sediment pulses. The inherently unpredictable nature of hillslope erosion processes results in substantial year-to-year variability in tributary and river sediment loads. This behavior also makes the USCR unlike humid-region rivers, where moderate discharges of intermediate recurrence carries the majority of the sediment load—in contrast, the "dominant discharge" for the USCR is the largest discharge on record. As a consequence of the periodically intense delivery of water and sediment, the USCR exhibits a highly dynamic morphology subject to significant vertical and lateral adjustments, with localized migration into adjacent floodplain areas.

Future planning in the USCR watershed therefore requires informed consideration of these geomorphic processes, along with their associated area of influence and episodicity, in any planning effort in order to avoid: (1) placing projects at risk from nature and/or human-induced hazards; (2) further degrading the ecological functions and benefits of the system; and (3) creating unintended consequences that further destabilize local conditions. Continued expansion of the urban footprint in the Santa Clarita and Acton basins (particularly in steep upland areas or along active margins of the USCR) has great potential to place a greater proportion of the population and infrastructure closer to both the sources and the consequences of the watershed's major hazards. Continuing such urbanization while implementing measures to limit risks from these hazards will further degrade the watershed's ecologic quality, through alteration or loss of existing habitat and disruption of the geomorphic processes that (re)create new habitat. Such measures already implemented and likely to be expanded to protect the growing urban footprint include levee construction, bank stabilization, channelization, and flow and sediment routing structure (e.g., storm drains and debris basins). These hazard-prevention measures provide a measure of safety, but they also can cause explicable (though not precisely predictable) responses by the river during large flood events that can raise the risk to human safety and damage ecological functions.

5.2 Information Gaps Affecting Watershed Management Decision-making

The companion report on the LSCR (Stillwater Sciences 2007a) identified several key information gaps in the general understanding of geomorphic processes in the lower watershed. In keeping with that theme, we present here a similar list of information gaps in the understanding of the USCR watershed that we have identified over the course of this study. When acquired and analyzed, these data could further assist watershed managers with their assessment and planning endeavors.

- **Repeat channel survey data:** following the 2005 floods, an airborne LiDAR survey was flown in both Ventura and Los Angeles counties. It provides the highest resolution elevation dataset of the river bed to date. Previous bed elevation surveys, as discussed above in Section 4.3.4, included 1928 USGS topographic maps, 1964 LADPW contour sheets, and a 2001 IfSAR-produced DEM. Additional historical elevation datasets may also exist, such as 1977 and 1981 LADPW-produced contour sheets, as cited by Simons, Li & Associates (1987). However, these historic datasets lack the detail to accurately determine river bed elevation changes finer than their respective resolutions can reasonably afford when compared to each other or to the higher resolution LiDAR dataset. In order to more rigorously detect changes in the river's morphology in the future, additional elevation surveys that employ high-resolution data collection techniques, such as LiDAR, are needed. These surveys should be coupled with high-resolution aerial photography taken with the elevation surveys to provide another layer of critical information on watershed conditions.
- **Additional sediment transport measurements:** few bedload samples have been taken during high flows in the USCR, making sediment transport modeling problematic because coarse material transport is estimated from sediment transport equations that have uncertain applicability in the USCR. The sediment loads in the entire SCR are so high, and such an important component of planning for river management, that resources should be committed for regular sampling of both bedload and suspended load in major tributaries during high flow events.
- **Inventory of flood management structures:** there is currently no comprehensive spatial database that contains information on all existing levees (both federal and non-federal), bank protection (e.g., rock or concrete revetment), and channelized structures (concrete banks with or without concrete stream beds) throughout the USCR watershed, even within the more densely populated areas of Santa Clarita. The California Department of Water Resources is presently digitizing federal and non-federal levees from available maps as part of their flood management efforts (CDWR 2009) and LADPW possess numerous maps containing bridge, levee, debris basin, storm drain, and other flood management-related infrastructure locations. However, compilation of a single, easily referable spatial database containing the locations and attributes of all of these structures, particularly those that are located within a stream channel's active width, would greatly assist those attempting to assess (and model) the impacts of these existing structures and future structures on the hydrology, sediment transport capacity, and morphology of the river corridor and its tributaries.
- **Reservoir sedimentation measurements:** presently, there are no known measurements of sedimentation in Castaic Lake and sedimentation measurements in Bouquet Canyon Reservoir have not occurred since shortly after it was constructed in the early 1930s. These two reservoirs capture sediment being produced in nearly one-third of the total USCR watershed area. Measuring sedimentation rates in these two reservoirs via bathymetric

surveys, in addition to performing particle-size analysis of the accumulated sediments, would potentially provide much needed insight into watershed sediment production rates and processes. Because Castaic Lake is effectively split in two parts—Elderberry Forebay captures upper Castaic Creek and Castaic Lake proper captures Elizabeth Lake Canyon—production rates and the processes that control them could be further studied at a slightly finer scale when measuring sedimentation rates and patterns in those two parts.

- **Investigation of Northridge earthquake's effect on sediment supply:** the sediment legacy of the landslides triggered by the 1994 Northridge earthquake is not fully understood, but it could represent an important factor for management decisions related to development planning and flood and debris-flow management in those areas of the watershed. Subsequent storms have undoubtedly mobilized a portion of the earthquake-related landslide sediment downstream, but exactly how much of it remains in the watershed is unknown. Additional field reconnaissance might shed further light on this issue, and individual landslides should be visited and surveyed.
- **Investigation of the 1928 failure of the St. Francis Dam on geomorphic and sediment transport effects:** the impacts of the massive flood from the dam failure to the river and valley morphology within and downstream of San Francisquito Canyon are not wholly understood. Our analysis of historical changes in the river's active width and bed elevation indicate that narrowing and aggradation has generally occurred since this event. However, it is not known whether these adjustments have finally achieved a state of relative equilibrium (i.e., the river has recovered from the scouring flood), or whether the river is still adjusting in response to this catastrophic event. Future topographic surveys and aerial photography of both the Santa Clara River and lower San Francisquito Canyon would allow river managers a means to continue tracking the evolution of these channel corridors, which are becoming progressively more developed, that may still be adjusting to the dam failure event.
- **Monitoring of land-cover/use changes:** while land-cover data are available from as recently as 2001, continued updates to this spatial database is critical in assessing potential disturbances in the USCR watershed. Rapid urban development in the USCR watershed has already built out into areas that were not indicated as being "developed" in the 2001 land-cover database and so requires updating in the near future. Another major concern to watershed managers is how vegetation cover may change in response to climate change in the coming decades and centuries, as any changes to vegetation cover has the potential to influence sediment-production rates and wildfire susceptibility (which in turn influences sediment-production rates).

Pursuing these types of information to fill data gaps will allow for a better understanding of the dynamics of the USCR, and provide managers with useful tools to predict how the river will change and the likely outcomes of management, development, and restoration scenarios.

6 REFERENCES

Printed Sources

Ahnert, F. 1970. Functional relationships between denudation, relief, and uplift in large, mid-latitude drainage basins. American Journal of Science 268: 243–263.

AMEC (AMEC Earth and Environmental). 2005. Santa Clara River Enhancement and Management Plan (SCREMP). Public review document. Prepared for the Ventura County Watershed Protection District, Los Angeles County Department of Public Works, and the SCREMP Project Steering Committee.

Anderson, H. W., G. B. Coleman, and P. J. Zinke. 1959. Summer slides and winter scour, dry-wet erosion in southern California mountains. U.S. Department of Agriculture, Forest Service, Pacific Southwest Forest and Range Experiment Station, Berkeley, California.

Andrews, E. D., R. C. Antweiler, P. J. Neiman, and F. M. Ralph. 2004. Influence of ENSO on flood frequency along the California Coast. Journal of Climate 17:337–348.

Aqua Terra (Aqua Terra Consultants). 2009. Hydrologic Modeling of the Santa Clara River Watershed with the U.S. EPA Hydrologic Simulation Program - FORTRAN (HSPF). Revised Final Draft submitted to the Ventura County Watershed Protection District. July.

Ballais, J. L. and M. C. Bosc. 1994. The ignifracts of the Sainte-Victoire Mountain (Lower Provence, France). Pages 217–227 *in* M. Sala and J. L. Rubio, editors. Soil erosion and degradation as a consequence of forest fires. Geoforma Ediciones, Logroño, Spain.

Begnudelli, L. and B. F. Sanders. 2007. Simulation of the St. Francis Dam-break flood. Journal of Engineering Mechanics 133: 1200–1212.

Benda, L. and T. Dunne. 1997. Stochastic forcing of sediment supply to channel networks from landsliding and debris flow. Water Resources Research 33: 2849–2863.

Bendix, J. and C. M. Cowell. 2010. Impacts of wildfire on the composition and structure of riparian forests in southern California. Ecosystems 13: 99–107.

Blakley, E. R. and K. Barnette. 1985. Historical overview of Los Padres National Forest.

Blythe, A. E., D. W. Burbank, K. A. Farley, and E. J. Fielding. 2000. Structural and topographic evolution of the central Transverse Ranges, California, from apatite fissiontrack, (U/Th)/He and digital elevation model analyses. Basin Research 12: 97–114.

Booker, F. A. 1998. Landscape and Management response to wildfires in California. Master's thesis. University of California, Berkeley.

Booth, D. B. 1990. Stream-channel incision following drainage-basin urbanization. Water Resources Bulletin 26: 407–417.

Boughten, D. A., P. B. Adams, E. Anderson, C. Fusaro, E. Keller, E. Kelley, L. Lentsch, J. Nielsen, K. Perry, H. Regan, J. Smith, C. Swift, L. Thompson, and F. Watson. 2006. Steelhead of the south-central/southern California coast: population characterization for recovery planning. NOAA Technical Memorandum. Prepared by National Marine Fisheries Service.

Brownlie, W. 1982. Prediction of flow depth and sediment discharge in open channels.Doctoral thesis. California Institute of Technology, Pasadena, California.

Brozovic, N., F. A. Booker, and W. E. Dietrich. 1997. A seventy year record of erosion and sedimentation from the San Gabriel Mountains, southern California. American Geophysical Union, 1997 Fall Meeting 78.

Burbank, D. W., J. Leland, E. Fielding, R. S. Anderson, N. Brozovic, R. Reid-Mary, and C. Duncan. 1996. Bedrock incision, rock uplift and threshold hillslopes in the northwestern Himalayas. Nature 379: 505–510.

Cayan, D. E., K. T. Redmond, and L. G. Riddle. 1999. ENSO and hydrologic extremes in the Western United States. Journal of Climate 12:2881–2893.

CDF (California Department of Finance). 2010. January 2010 cities and counties ranked by size, numeric, and percent change. Prepared by CDF, Sacramento, California.

CDF FRAP (California Department of Forestry and Fire, Fire and Resource Assessment Program). 2010. Statewide fire history electronic database. Website. http://frap.cdf.ca.gov/data/frapgisdata/download.asp?rec=fire [Accessed 25 May 2010].

CDSD (California Division of Safety of Dams). 2005. Website: http://damsafety.water.ca.gov/about.htm

CDWR (California Department of Water Resources). 2009. 100-year floodplains based upon best available data (Los Angeles County). Website. http://www.water.ca.gov/floodmgmt/lrafmo/fmb/fes/best_available_maps/los_angeles/ [Accessed 30 November 2010].

Cerdà, A. and S. H. Doerr. 2005. Long-term soil erosion changes under simulated rainfall for different vegetation types following a wildfire in eastern Spain. Journal of Wildland Fire 14: 423–437.

Chang, H. H. 1990. Fluvial study of Santa Clara River for Curtis Sand and Gravel Mining. Prepared for Curtis Sand and Gravel, Canyon Country, CA through Manee Consulting, Yucaipa, California.

City of Acton. 2010. Acton, California. Website. http://www.cityofacton.org/[Accessed 26 Aug 2010].

City of Santa Clarita. 2004. City of Santa Clarita General Plan: housing element update.
CLWA (Castaic Lake Water Agency). 2003. Groundwater management plan, Santa Clara River Valley groundwater basin, east subbasin, Los Angeles, California. Prepared by Luhdorff & Scalmanini, Woodland, California for CLWA, Santa Clarita, California.

CNRA (California Natural Resources Agency). 2010. Statewide general plan map for California, GIS database. Prepared by the University of California at Davis.

Copeland, O. L. 1965. Land use and ecological factors in relation to sediment yields. Pages 72–84 *in* Proceedings of the federal interagency sedimentation conference, 1963. Miscellaneous Publication 970. U.S. Department of Agriculture, Washington, D.C.

Corbett, E. S. and R. M. Rice. 1966. Soil slippage increased by brush conversion. Research Note, PSW-128:1–8. U.S. Forest Service Pacific Southwest Forest and Range Experiment Station, Berkeley, California.

Cui, Y., J. K. Wooster, J. G. Venditti, S. R. Dusterhoff, W. E. Dietrich, and L.S. Sklar. 2008 Simulating sediment transport in a flume with forced pool-riffle morphology: examinations of two one-dimensional numerical models. Journal of Hydraulic Engineering 134: 892–904.

Davis, F., E. Keller, A. Parikh, and J. Florsheim. 1989. Recovery of the chaparral riparian zone after wildfire. General Technical Report PSW-110. USDA Forest Service, Pacific Southwest Research Station, Albany, California.

DeBano, L. F., D. G. Neary, and P. F. Ffolliott. 1998. Fire's effects on ecosystems. Wiley, New York.

De Koff, J. P., R. C. Graham, K. R. Hubbert, and P. M. Wohlgemuth. 2006. Prefire and postfire erosion of soil nutrients within a chaparral watershed. Soil Science 171: 915–928.

Densmore, A. L. and N. Hovius. 2000. Topographic fingerprints of bedrock landslides: Geology 28:371–374.

Deser, C., A. Capotondi, R. Saravanan, and A. Phillips. 2004. Tropical Pacific and Atlantic climate variability in CCSM3. Submitted to J. Climate CCSM# Special Issue.

Dibblee, T. W. 1996. Geologic map of the Acton quadrangle, Los Angeles County, California. Scale 1:24,000. Dibblee Geological Foundation, Santa Barbara, California.

Dibblee, T. W. 1996. Geologic map of the Agua Dulce quadrangle, Los Angeles County, California. Scale 1:24,000. Dibblee Geological Foundation, Santa Barbara, California.

Dibblee, T. W. 1997. Geologic map of the Green Valley quadrangle, Los Angeles County, California. Scale 1:24,000. Dibblee Geological Foundation, Santa Barbara, California.

Dibblee, T. W. 1997. Geologic map of the Sleepy Valley and Ritter Ridge quadrangles, Los Angeles County, California. Scale 1:24,000. Dibblee Geological Foundation, Santa Barbara, California.

Dibblee, T. W. 1997. Geologic map of the Warm Springs Mountain quadrangle, Los Angeles County, California. Scale 1:24,000. Dibblee Geological Foundation, Santa Barbara, California.

Dibblee, T. W. 1997. Geologic map of the Whitaker Peak quadrangle, Los Angeles County, California. Scale 1:24,000. Dibblee Geological Foundation, Santa Barbara, California.

Dibblee, T. W. 2001. Geologic map of the Pacifico Mountain and Palmdale (south half) quadrangles, Los Angeles County, California. Scale 1:24,000. Dibblee Geological Foundation, Santa Barbara, California.

Dibblee, T. W. 2002. Geologic map of the Burnt Peak quadrangle, Los Angeles County, California. Scale 1:24,000. Dibblee Geological Foundation, Santa Barbara, California.

Dibblee, T. W. 2002. Geologic map of the Lake Hughes and Del Sur quadrangles, Los Angeles County, California. Scale 1:24,000. Dibblee Geological Foundation, Santa Barbara, California.

Dibblee, T. W. 2002. Geologic map of the Liebre Mountain quadrangle, Los Angeles County, California. Scale 1:24,000. Dibblee Geological Foundation, Santa Barbara, California.

Dietrich, W. E., and T. Dunne. 1978. Sediment budget for a small catchment in mountainous terrain. Zeitschrift für Geomorphologie, Supplement, 29: 191–206.

Doerr, S. H., R. A. Shakesby, and R. P. D. Walsh. 2000. Soil water repellency, its characteristics, causes and hydro-geomorphological consequences. Earth-Science Reviews 51: 33–65.

Doerr, S. H., P. Douglas, R. Evans, C. P. Morley, N. Mullinger, R. Bryant, and R. A. Shakesby. 2005. Effects of heating and postheating equilibration times on soil water repellency. Australian Journal of Soil Research 43: 261–267.

Dorn, R. I. 2003. Boulder weathering and erosion associated with a wildfire, Sierra Ancha Mountains, Arizona. Geomorphology 55: 155–171.

Downs, P. W. and K. J. Gregory. 2004. River channel management: towards sustainable catchment hydrosystems. Arnold, London.

Dragovich, D. 1993. Fire-accelerated weathering in the Pilbara, Western Australia. Zeitschrift fur Geomorphologie 37: 295–307.

Duriscoe, D. M. and W. G. Wells, II. 1982. Effects of fire on certain physical properties of selected chaparral soils. Pages 594–595 *in* C. E. Conrad and W. C. Oechel, technical coordinators. Proceedings of the symposium on dynamics and management of Mediterranean-type ecosystems. General Technical Report PSW-58. USDA Forest Service, Pacific Southwest Forest and Range Experiment Station, Berkeley, California.

Duvall, A., E. Kirby, and D. Burbank. 2004. Tectonic and lithologic controls on bedrock channel profiles and processes in coastal California. Journal of Geophysical Research 109: F03002, doi:10.1029/2003JF000086.

Earle, D. 2003. Mining and ranching in Soledad Canyon and Antelope Valley. Online archives and repository of the Santa Clarita Valley Historical Society, Santa Clarita, California. http://www.scvhistory.com/scvhistory/earle-mining-0103.htm [Accessed 30 August 2010].

Emmett, W. W. and G. M. Wolman. 2001. Effective discharge and gravel-bed rivers. Earth Surface Processes and Landforms 26:1269–1380.

Florsheim, J. L., E. A. Keller, and D. W. Best. 1991. Fluvial sediment transport in response to moderated storm flows following chaparral wildfire, Ventura County, southern California. Geological Society of America 103: 504–511.

Freeman, V. M. 1968. People-land-water: Santa Clara Valley and Oxnard Plain, Ventura County, California. Lorrin L. Morrison, Los Angeles.

Gabet, E. J. 2000. Gopher bioturbation: field evidence for nonlinear hillslope diffusion. Earth Surface Processes and Landforms 25: 1419–1428.

Gabet, E. J. 2003. Sediment transport by dry ravel. Journal of Geophysical Research. doi:10.1029/2001JB001686.

Gabet, E. J. and T. Dunne. 2002. Landslides on coastal sage-scrub and grassland hillslopes in a severe El Niño winter: the effects of vegetation conversion on sediment delivery. Geological Society of America Bulletin 114: 983–990.

Gabet, E. J. and T. Dunne. 2003. A stochastic sediment delivery model for a steep Mediterranean landscape. Water Resources Research 39: 1237, doi:1210.1029/2003WR002341.

Goudie, A. S., R. J. Allison, and S. J. McLaren. 1992. The relations between modulus of elasticity and temperature in the context of the experimental simulation of rock weathering by fire. Earth Surface Processes and Landforms 17: 605–615.

Graf, W. L. 1984. Flood-related change in an arid region river. Earth Surface Processes and Landforms 8: 125–139.

Graf, W. L. 2000. Locational probability for a dammed, urbanizing stream: Salt River, Arizona, USA. Environmental Management 25: 321–335.

Granger, D. E., J. W. Kirchner, and R. Finkel. 1996. Spatially averaged long-term erosion rates from *in-situ* produced cosmogenic nuclides in alluvial sediment. Geology 104: 249-257.

Granger, D. E. and C. S. Riebe. 2007. Cosmogenic Nuclides in Weathering and Erosion. Pages 1-43 *in* H. D. Holland and K. K. Turekian, editors. Treatise on geochemistry. Volume 5 *in* J. I. Drever, editor. Surface and ground water, weathering, and soils. Elsevier, London.

Hamilton, J. 1999. Newhall County Water District: an historical perspective. Online archives and repository of the Santa Clarita Valley Historical Society, Santa Clarita, California. http://www.scvhistory.com/scvhistory/ncwd.html [Accessed 30 August 2010].

Harp, E. L. and R. W. Jibson. 1996. Landslides triggered by the 1994 Northridge, California earthquake. Bulletin of the Seismological Society of America 86: 319–332.

Heimsath, A. M. 1998. The soil production function. Doctoral dissertation/ University of California, Berkeley.

Homer, C., C. Huang, L. Yang, B. Wylie, and M. Coan. 2004. Development of a 2001 national landcover database for the United States. Photogrammetric Engineering and Remote Sensing 70: 829–840. http://www.mrlc.gov/.

Horton, R. E. 1945. Erosional development of streams and their drainage basins; hydrophysical approach to quantitative morphology. Bulletin of the Geological Society of America 56: 275–370.

Inman, D. L. and S. A. Jenkins. 1999. Climate change and the episodicity of sediment flux of small California rivers. Journal of Geology 107:251–270.

Iverson, R. M., M. E. Reid, and R. G. LaHusen. 1997. Debris-flow mobilization from landslides. Annual Reviews of Earth and Planetary Science 25: 85–138.

Joseph, S. E., R. V. Miller, S. S. Tan, and R. W. Goodman. 1987. Mineral land classification of the greater Los Angeles area: classification of sand and gravel resource areas, Saugus-Newhall Production-Consumption Region, and Palmdale Production-Consumption Region. California Division of Mines and Geology, Special Report 143, Part V.

Keeley, S. C., J. E. Keeley, S. M. Hutchinson, and A. W. Johnson. 1981. Postfire succession of the herbaceous flora in southern California chaparral. Ecology 62: 1608–1621.

Keeley, J. E. 1987. Role of fire in seed germination of woody taxa in California chaparral. Ecology 68: 434–443.

Keeley, J. E. and P. H. Zedler. 2009. Large, high-intensity fire events in southern California shrublands: debunking the fine-grain age patch model. Ecological applications 19: 69–94.

Kennedy/Jenks (Kennedy/Jenks Consultants). 2008. Upper Santa Clara River Integrated Regional Water Management Plan (IRWMP).

Kirchner, J. W., R. C. Finkel, C. S. Riebe, D. E. Granger, J. L. Clayton, and J. G. King. 2001. Mountain erosion over 10 yr, 10 k.y., and 10 m.y. time scales. Geology 29: 591–594.

Krammes, J. S. 1960. Erosion from mountain side slopes after fire in Southern California. Research Note No. 171. USDA Forest Service, PSW Forest and Range Experiment Station, Berkeley, California.

Krammes, J. S. 1965. Seasonal debris movement from steep mountain slopes in southern California. Pages 85–88 *in* Proceedings, Federal Inter-Agency Sedimentation Conference, U.S. Department of Agriculture Miscellaneous Publications 970. Jackson, Mississippi.

Krammes, J. S. and J. F. Osborne. 1969. Water repellent soils and wetting agents as factors influencing erosion. Pages 177–186 *in* L. F. DeBano and J. Letey, editors. Proceedings of the symposium on water-repellent soils. Riverside, California.

Krammes, J. S. and R. M. Rice. 1963. Effect of fire on the San Dimas Experimental Forest. Pages 31–34 *in* Proceedings of the 7th Annual Meeting .Arizona Watershed Symposium, Phoenix, Arizona.

LACFCD (Los Angeles County Flood Control District). 1959. Report on debris reduction studies for mountain watersheds of Los Angeles County. Los Angeles, California.

LADPW. 2008. Santa Clara River fluvial study: field investigation report. Volume 1: Los Angeles County. Prepared by LADPW, Water Resources Division.

LADPW. 2006. Sedimentation manual, 2nd Edition. Prepared by LADPW, Water Resources Division.

Lal, D. 1991. Cosmic-ray labeling of erosion surfaces: *in-situ* nuclide production rates and erosion models. Earth and Planetary Science Letters 104: 424–439.

Larsen, I. J. and L. H. MacDonald. 2007. Predicting postfire sediment yields at the hillslope scale: testing RUSLE and Disturbed WEPP. Water Resources Research 43: W11412, doi:10.1029/2006WR005560.

Lavé, J. and D. Burbank. 2004. Denudation processes and rates in the Transverse Ranges, southern California: erosional response of a transitional landscape to external and anthropogenic forcing. Journal of Geophysical Research 109: F01006, doi:01010.01029/02003JF000023.

Leopold, L. B. 1968. Hydrology for urban planning—a guidebook on the hydrologic effects of urban land use. U.S. Geological Survey Circular 554. Washington, D.C.

Loaiciga, H. A., D. Pedreros, and D. Roberts. 2001. Wildfire–streamflow interactions in a chaparral watershed. Advances in Environmental Research 5: 295–305.

Lustig, L. K. 1965. Sediment yield of the Castaic watershed, western Los Angeles County, California—A quantitative geomorphic approach. U.S. Geological Survey Professional Paper 422-F.

Manzer, D. 2006. Evolution of the local rancho. Online archives and repository of the Gazette, Santa Clarita, California. http://www.oldtownnewhall.com/gazette/gazette1202-manzer.htm [Accessed 30 August 2010].

Massie, G. 1989. Gold in the Placerita Canyon and the early days of Newhall. Gold Prospector magazine, September 1989. http://www.scvhistory.com/scvhistory/goldprospector989.htm [Accessed June 2010]

Mather, A. E., J. S. Griffiths, and M. Stokes. 2003. Anatomy of a 'fossil' landslide from the Pleistocene of SE Spain. Geomorphology 50: 135–149.

MacArthur, R. C. and B. R. Hall. 2008. Appendix E: Limited glossary of selected terms. Pages 1089-1101 *in* M. H. Garcia, editor. Sedimentation engineering: processes, measurements, modeling, and practice. ASCE Manual 110.

Meigs, A., D. Yuleb, A. Blythec, and D. Burbank. 2003. Implications of distributed crustal deformation for exhumation in a portion of a transpressional plate boundary, Western Transverse Ranges, Southern California. Quaternary International 101-102: 169–177.

Mensing, S. A., J. Michaelsen, and R. Byrne. 1999. A 560-year record of Santa Ana fires reconstructed from charcoal deposited in the Santa Barbara Basin, California. Quaternary Research 51: 295–305.

Metcalf, J. G. 1994. Morphology, chronology, and deformation of Pleistocene marine terraces, southwestern Santa Barbara County, California. Master’s thesis. University of California, Santa Barbara.

Miller, D. J. and J. Sias. 1998. Deciphering large landslides: linking hydrological, groundwater and slope stability models through GIS. Hydrological Processes 12: 923–941.

Minear, T. and G. M. Kondolf. 2009. Estimating reservoir sedimentation rates at large spatial and temporal scales: a case study of California. Water Resources Research, doi: 10.1029/2007WR006703.

Minnich R. A. 1983. Fire mosaics in Southern-California and Northern Baja California. Science 219, 4590: 1287–1294.

Moody, J. A. and J. D. Smith. 2005. Critical shear stress for erosion of cohesive soils subjected to temperatures typical of wildfires. Journal of Geophysical Research 110: F01004, doi:10.1029/2004JF000141.

Neary, D. G., C. C. Klopatek, L. F. DeBano, P. F. Ffolliott. 1999. Fire effects on belowground sustainability: a review and synthesis. Forest Ecology and Management 122: 51–71.

Neuendorf, K. K. E, J. P. Mehl, Jr., and J. A. Jackson, editors. 2005. Glossary of geology, fifth edition. American Geological Institute, Alexandria, Virginia.

NWS CPC (National Weather Service Climate Prediction Center). 2010. Cold and warm episodes by season. Website. http://www.cpc.ncep.noaa.gov/products/analysis_monitoring/ensostuff/ensoyears.shtml [Accessed 27 Dec 2010].

Orme, A. R. 1998. Late Quaternary tectonism along the Pacific coast of the Californias: a contrast in style. Pages 179–197 i*n* R. L. Stewart and C. Vita-Finzi, editors. Coastal tectonics, special publication 146. Geological Society, London.

Orme, A. R. and R. G. Bailey. 1971. Vegetation conversion and channel geometry in Monroe Canyon, Southern California. Yearbook - Association of Pacific Coast Geographers 33: 65–82.

Parker, G., P. C. Klingeman, and D. L. McLean. 1982. Bedload and size distribution in paved gravel bed streams. Journal of Hydraulics Division, ASCE. 108: 544-571.

Peterson, M. D. and S. G. Wesnousky. 1994. Fault slip rates and earthquake histories for active faults in southern California. Bulletin of Seismological Society of America 84: 1608–1649.

Peterson, M. D., W. A. Bryant, C. H. Cramer, T. Cao, M. Reichle, A. D. Frankel, J. J. Lienkaemper, M. A. McCrory, and D. P. Schwartz. 1996. Probabilistic seismic hazard assessment for the state of California. USGS Open-File Report 96-706.

Prosser, I. P. 1990. Fire, humans and denudation at Wangrah Creek, Southern Tablelands, N.S.W. Australian Geographical Studies 28: 77–95.

Prosser, I. P. and L. Williams. 1998. The effect of wildfire on runoff and erosion in native eucalyptus forest. Hydrological Processes 12: 251–265.

Pulling, H. A. 1944. A history of California's Range-Cattle Industry, 1770–1912. Doctoral dissertation. University of Southern California.

Reid, L. M. and T. Dunne. 1984. Sediment production from forest road surfaces. Water Resources Research 20: 1753–1761.

Reid, L. M., and T. Dunne. 1996. Rapid construction of sediment budgets for drainage basins. Catena-Verlag, Cremlingen, Germany.

Reneau, S. L., D. Katzman, G. A. Kuyumjian, A. Lavine, and D. V. Malmon. 2007. Sediment delivery after a wildfire. Geology 35: 151–154.

Rice, R. M. and G. T. Foggin. 1971. Effect of high intensity storms on soil slippage on mountainous watersheds in southern California. Water Resources Research 7: 1485–1496.

Rice, R. M., E. S. Corbett, and R. G. Bailey. 1969. Soil slips related to vegetation, topography, and soil in southern California. Water Resources Research 5: 647–659.

Ritter, D. F., R. C. Kochel, and J. R. Miller. 2002. Process geomorphology. Fourth edition. McGraw Hill, New York, New York.

Rockwell, T. 1988. Neotectonics of the San Cayetano fault, Transverse Ranges, California. Geological Society of America Bulletin 100: 500–513.

Rockwell, T. K., E. A. Keller, M. N. Clark, and D. L. Johnson. 1984. Chronology and rates of faulting of the Ventura terraces, California. Geological Society of America Bulletin 95: 1466–1474.

Roering, J. J., J. W. Kirchner, and W. E. Dietrich. 2005. Characterizing structural and lithologic controls on deep-seated landsliding: Implications for topographic relief and landscape evolution in the Oregon Coast Range. USA. Geological Society of America Bulletin 117: 654–668.

Roering, J. J., K.M. Schmidt, J. D. Stock, W. E. Dietrich, and D. R. Montgomery. 2003. Shallow landsliding, root reinforcement, and the spatial distribution of trees in the Oregon Coast Range. Canadian Geotechnical Journal 40: 237–253.

Rowe, P. B., C. M. Countryman, and H. C. Storey. 1954. Hydrological analysis used to determine effects of fire on peak discharge and erosion rates in southern California watersheds. U.S. Forest Service, Forest and Range Experiment Station, Berkeley, California.

Schmidt, K. M., J. D. Stock, M. N. Hanshaw, and G. W. Bawden. 2008. Constraining diffusivity and critical slope from post-fire sediment flux of the Day, Canyon, and Corral fires, California. Abstract. Eos Transactions of the American Geophysical Union, 89(53) Fall Meeting Supplement, Abstract H43F-1079.

Schwartzberg, B. and P. Moore. 1995. A history of the Santa Clara River, Santa Clara River enhancement and management plan.

Scott, K. and R. P. Williams. 1978. Erosion and sediment yields in the Transverse Ranges, Southern California. Geological Survey Professional Paper 1030.

Scott, D. F., D. B. Versfeld, and W. Lesch. 1998. Erosion and sediment yield in relation to afforestation and fire in the mountains of the Western Cape Province, South Africa. South African Geographical Journal 80: 52–59.

Seabloom, E. W., O. J. Reichman, and E. J. Gabet. 2000. The effect of hillslope angle on pocket gopher (*Thomomys bottae*) burrow geometry. Oecologia 125: 26–34.

Selby, M. J. 1993. Hillslope materials and processes. Oxford University Press, New York.

Shakesby, R. A. and S. H. Doerr. 2006. Wildfire as a hydrological and geomorphological agent. Earth-Science Reviews 74: 269–307.

Shen, Z. K., D. D. Jackson, and B. X. Ge. 1996. Crustal deformation across and beyond the Los Angeles basin from geodetic measurements. Journal of Geophysical Research 101: 27957–27980.

Shvidchenko, A. and G. Pender. 2008. Computer modelling of graded sediments in rivers. Water Management 161: 281–297.

Simons, Li & Associates. 1983. Hydraulic, erosion and sedimentation study of the Santa Clara River, Ventura County, California. Prepared for Ventura County Flood Control District, Ventura, California.

Simons, Li & Associates. 1987. Fluvial study of the Santa Clara River and its tributaries, Los Angeles County, California. Data collection, field reconnaissance, and qualitative geomorphic analysis of existing conditions. Prepared for Los Angeles County Department of Public Works, Los Angeles, California.

Simons, Li & Associates. 1990. Summary report: fluvial study of Santa Clara River and the tributaries. Prepared for Los Angeles County Department of Public Works, Los Angeles, California.

Sommerfield, C. K., and H. J. Lee. 2003. Magnitude and variability of Holocene sediment accumulation in Santa Monica Bay, California. Marine Environmental Research 56: 151–176.

Spotila, J. A., M. A. House, A. E. Blythe, N. A. Niemi, and G. C. Blank. 2002. Controls on the erosion and geomorphic evolution of the San Bernardino and San Gabriel mountains, southern California. Pages 205–230 *in* A. Barth, editor. Contributions to crustal evolution of the southwestern United States. Special Paper 365. The Geological Society of America, Boulder, Colorado.

Stillwater Sciences. 2007a. Santa Clara River Parkway floodplain restoration feasibility study: assessment of geomorphic processes for the Santa Clara River watershed, Ventura and Los Angeles counties, California. Prepared by Stillwater Sciences, Berkeley, California for the California State Coastal Conservancy, Oakland, California.

Stillwater Sciences. 2007b. Santa Paula Creek watershed planning project: geomorphology and channel stability assessment. Prepared by Stillwater Sciences, Berkeley, California for California Fish and Game, Santa Paula Creek Fish Ladder Joint Power Authority.

Stillwater Sciences. 2009. Hydrogeomorphic analysis of San Francisquito Creek at USFS Road 5N27 Crossing. Draft Report. Prepared by Stillwater Sciences, Berkeley, California for Power Engineers, Inc., and Los Angeles Department of Water and Power.

Stillwater Sciences. 2010. Sespe Creek hydrology, hydraulics, and sedimentation analysis: watershed assessment of hillslope and river geomorphic processes. Final Report. Prepared by Stillwater Sciences, Berkeley, California for Ventura County Watershed Protection District, Ventura, California.

Sutherland, D. G., M. Hansler-Ball, S. J. Hilton, and T. E. Lisle. 2002. Evolution of a landslide-induced sediment wave in the Navarro River, California. Geological Society of America Bulletin 114: 1036–1048.

Szabolcsi, K. 2000. Searching for Tataviam answers. Online archives and repository of the Santa Clarita Valley Historical Society, Santa Clarita, California. http://www.scvhistory.com/scvhistory/sg081898.htm [Accessed 30 August 2010].

Terry, J. P. and R. A. Shakesby. 1993. Soil water repellency effects on rainsplash: simulated rainfall and photographic evidence. Earth Surface Processes and Landforms 18: 519–525.

Tiedemann, A. R., C. E. Conrad, J. H. Dieterich, J. W. Hornbeck, W. F. Megahan, L. A. Viereck, and D. D. Wade. 1979. Effects of fire on water: a state-of-knowledge review. Proceedings of the national fire effects workshop. General Technical Report WO-10. USDA Forest Service.

Tiegs, S. D. and M. Pohl. 2005. Planform channel dynamics of the lower Colorado River: 1976-2000. Geomorphology 69: 14–27.

Tiegs, S. D., J. F. O'Leary, M. M. Pohl, and C. L. Munill. 2005. Flood disturbance and riparian diversity on the Colorado River Delta. Biodiversity and Conservation 14: 1175–1194.

Tiegs, S. D., and M. Pohl. 2005. Planform channel dynamics of the lower Colorado River: 1976–2000. Geomorphology 69: 14–27.

Trecker, M. A., L. D. Gurrola, and E. A. Keller. 1998. Oxygen-isotope correlation of marine terraces and uplift of the Mesa Hills, Santa Barbara, California, USA. Geological Society Special Publication 146: 57–69.

University of Southern California. 2004. William Mulholland and the collapse of the St. Francis Dam. http://www.usc.edu/isd/archives/la/scandals/st_francis_dam.html.

URS (URS Corporation). 2005. Santa Clara River Parkway floodplain restoration feasibility study—water resources investigations. Prepared for the California Coastal Conservancy, Oakland, California.

USACE and CDFG (U.S. Army Corps of Engineers and California Department of Fish and Game). 2009. Newhall Ranch resource management and development plan and the spineflower conservation plan draft EIS/EIR. http://www.dfg.ca.gov/regions/5/newhall/docs/.

U.S. Census Bureau. 2010a. Census of population and housing. Website. http://www.census.gov/prod/www/abs/decennial/index.html [Accessed 26 August 2010].

U.S. Census Bureau. 2010b. American fact finder. Website. http://factfinder.census.gov [Accessed 26 August 2010].

USFS (USDA Forest Service). 1954. Fire-flood sequences on the San Dimas Experimental Forest. USDA Forest Service, California Forest and Range Experiment Station 6.

USFS. 1997. Sespe Watershed analysis: Ojai Ranger District, Los Padres National Forest.

USFS. 2010. Angeles National Forest cultural history. http://www.fs.usda.gov/wps/portal/fsinternet/!ut/p/c4/04_SB8K8xLLM9MSSzPy8xBz9CP0os3gjAwhwtDDw9_AI8zPyhQoY6BdkOyoCAGixyPg!/?ss=110501&navtype=BROWSEBYSUBJECT&cid=STELPRDB5161139&navid=150140000000000&pnavid=150000000000000&position=Feature*&ttype=detail&pname=Angeles%20National%20Forest-%20History%20&%20Culture [Accessed 30 December 2010].

USGS (United States Geological Survey). 1997. Preliminary geologic map of the Mint Canyon 7.5' quadrangle, Southern California: a digital database. Compiled by R. F. Yerkes. Open-File Report 97-164. http://wrgis.wr.usgs.gov/open-file/of97-164/.

USGS. 1997. Preliminary geologic map of the Newhall 7.5' quadrangle, Southern California: a digital database. Compiled by R. F. Yerkes and R. H. Campbell. Open-File Report 95-800. http://pubs.usgs.gov/of/1995/of95-800/.

USGS. 1997. Preliminary geologic map of the Oat Mountain 7.5' quadrangle, Southern California: a digital database. Compiled by R. F. Yerkes and R. H. Campbell. Open-File Report 95-89. http://wrgis.wr.usgs.gov/open-file/of95-89/.

USGS. 1997. Preliminary geologic map of the San Fernando 7.5' quadrangle, Southern California: a digital database. Compiled by R. F. Yerkes. Open-File Report 97-163. http://pubs.usgs.gov/of/1997/of97-163/.

USGS. 1997. Preliminary geologic map of the Santa Susana 7.5' quadrangle, Southern California: a digital database. Compiled by R. F. Yerkes and R. H. Campbell. Open-File Report 97-258. http://wrgis.wr.usgs.gov/open-file/of97-258/.

USGS. 1997. Preliminary geologic map of the Sunland 7.5' quadrangle, Southern California: a digital database. Compiled by R. F. Yerkes. Open-File Report 97-270. http://pubs.usgs.gov/of/1997/of97-270/.

USGS. 1997. Preliminary geologic map of the Val Verde 7.5' quadrangle, Southern California: a digital database. Compiled by R. F. Yerkes and R. H. Campbell. Open-File Report 95-699. http://wrgis.wr.usgs.gov/open-file/of95-699/.

USGS. 2005. Preliminary geologic map of the Los Angeles 30' x 60' quadrangle, Southern California. Version 1.0. Compiled by R. F. Yerkes and R. H. Campbell. Scale 1:100,000. Open-File Report 2005-1019. http://pubs.usgs.gov/of/2005/1019.

VCWPD and LACDPW (Ventura Watershed Protection District Los Angeles County Department of Public Works). 1996. Flood protection report, June 1996. Prepared by the Ventura County Watershed Protection District (formerly Ventura County Flood Control District) and the Los Angeles County Department of Public Works, California.

Voight, B. 1978. Rockslides and Avalanches, Developments in geotechnical engineering. Elsevier, Amsterdam.

W&S Consultants (Whitley and Simon Consultants). 1995. Archival records search. Prepared for Newhall Ranch.

Warrick, J. A. 2002. Short-term (1997–2000) and long-term (1928–2000) observations of river water and sediment discharge to the Santa Barbara channel, California. Doctoral dissertation. University of California, Santa Barbara.

Warrick, J. A. and K. L. Farnsworth. 2009. Sources of sediment to the coastal waters of the Southern California Bight. Pages 39-52 *in* H. J. Lee and W. R. Normark, editors. Earth sciences in the urban ocean: the southern California continental borderland. Geological Society of America Special Paper 454, Boulder, Colorado.

Warrick, J. A. and L. A. K. Mertes. 2009. Sediment yield from the tectonically active semiarid western Transverse Ranges of California. Geological Society of America Bulletin 121: 1054–1070.

Warrick, J.A. and D. M. Rubin. 2007. Suspended-sediment rating-curve response to urbanization and wildfire, Santa Ana River, California. Journal of Geophysical Research 112, F02018, doi:10.1029/2006JF000662.

Warrick, J. A., J. Hatten, G. B. Pasternak, A. Gray, M. Goni, and R. Wheatcroft. In preparation. The effects of wildfire on the sediment yield of a coastal California watershed. Geological Society of America Bulletin.

Wells, W. G., II. 1981. Some effects of brushfires on erosion processes in coastal Southern California. Pages 305–342 i*n* T. Davies, and A. Pearce, editors. Erosion and sediment transport in Pacific Rim Steeplands. Proceedings of the Christchurch Symposium, 25-31 January 1981, Christchurch, New Zealand.

Wells, W.G ., II. 1985. The influence of fire on erosion rates in California chaparral. Pages 57–62 *in* J. J. DeVries, editor. Proceedings of the chaparral ecosystems research conference Water Resources Center, 62.

Wells, W. G., II. 1987. The effects of fire on the generation of debris flows in southern California. Geological Society of America, Reviews in Engineering Geology 7: 105–114.

Wells, W. G., II, P. M. Wohlgemuth, and A. G. Campbell. 1987. Postfire sediment movement by debris flows in the Santa Ynez Mountains, California. Pages 275–276 i*n* R. L. Beschta, editor. Erosion and sedimentation in the Pacific Rim. College of Forestry, Oregon State University,. Corvallis, Oregon.

Williams, R. P. 1979. Sediment discharge in the Santa Clara River basin, Ventura and Los Angeles counties, California. U.S. Geological Survey, Menlo Park, California.

Williams, G. P. and M. G. Wolman. 1984. Downstream effects of dams on alluvial rivers. Professional Paper 1286. U.S. Geological Survey, Washington D.C.

Wills, C. J., R. J. Weldon II, and W. A. Bryant. 2008. Appendix A: California fault parameters for the National Seismic Hazard Maps and working group on California earthquake probabilities 2007. USGS Open File Report 2007-1437A.

Wohlgemuth, P. M. 2003. Hillslope erosion following the Williams fire on the San Dimas experimental forest, southern California. Second international wildland fire ecology and fire management congress. American Meteorological Society.

Wohlgemuth, P., J. Beyers, C. Wakeman, and S. Conard. 1998. Effects of fire on grass seedling and soil erosion in southern California chaparral. 19th Forest Vegetation Management Conference.

Wolman, M. G. 1954. A method of sampling coarse river-bed material. Transactions of the American Geophysical Union 35: 951–956.

Wolman, M. G. and R. Gerson. 1978. Relative scales of time and effectiveness of climate in watershed geomorphology. Earth Surface Processes 3: 189–208.

Wolman, M.G. and L.B. Leopold. 1957. River flood plains: some observations on their formation. Professional Paper 271. U.S. Geological Survey, Washington D.C.

Wolman, M. G. and J. P. Miller. 1960. Magnitude and frequency of forces in geomorphic processes. Journal of Geology 68: 54–74.

Worden, L. 1998. Where once was water. Online archives and repository of the Santa Clarita Valley Historical Society, Santa Clarita, California. http://www.scvhistory.com/scvhistory/sg081898.htm [Accessed 30 August 2010].

Wright, H. and A. Bailey. 1982. Fire ecology: United States and southern Canada. Wiley, New York.

Yeats, R.S. 1981. Quaternary flake tectonics of the California Transverse Ranges. Geology 9: 16–20.

Personal Communications

Allen, A. 2010. Chief, USACE, North Coast Branch. E-mail correspondence with G. Leverich, Stillwater Sciences, providing historical aggregate mining information.

Araiza, M. 2010. Engineer, LADPW. E-mail correspondence with B. Amerson, Stillwater Sciences, providing debris basin data.

Orme, A. R. 2005. Professor, University of California, Los Angeles. Phone conversation with P. Downs, Stillwater Sciences, providing Northridge Earthquake landslide information.

Romans, B. 2011. Research geologist, Chevron Energy Technology Company. In person correspondence with G. Leverich, Stillwater Sciences, providing cosmogenic nuclide sediment dating results from the lower Santa Clara River.

Sirakie, M. 2010. Staff, LADWP, Water System. Phone conversation with G. Leverich, Stillwater Sciences, providing Bouquet Reservoir information.

Thang, L. 2010. Engineer, LADPW. E-mail correspondence with G. Leverich, Stillwater Sciences, providing debris basin information.

Wu, G. 2010. Staff, LADWP, Power System. E-mail correspondence with G. Leverich, Stillwater Sciences, providing sedimentation records for Castaic Powerplant debris basins.

Appendices

Appendix A

Geology and Geomorphic Landscape Units Supporting Materials

GEOLOGY AND GEOMORPHIC LANDSCAPE UNITS (GLUs) SUPPORTING MATERIALS

This appendix provides supplementary data that were used in the geomorphic landscape unit (GLU) analysis performed for this study to estimate relative sediment production rates across the Upper Santa Clara River (USCR) watershed. Specifically, data presented here were used in the development of the GLU analysis for this study. The results of the analysis, along with several tables and figures, are presented in the Chapter 3 of the main report.

Geologic Units

Underlying geology information used in the GLU analysis was based on information contained within geology maps published separately by Dibblee and the USGS (various dates) (see Figure 1-4 in the main report). Although mapping techniques used by Dibblee and the USGS to create their respective maps are generally similar, there are some differences in how each party labeled and/or described some common units found on both sets of maps. Therefore, we have elected not to integrate the Dibblee and the USGS units into one seamless map within common rock unit labels. All units are listed in the tables below: Table A-1 lists units mapped by Dibblee and Table A-2 lists units mapped by the USGS. Figure 3-1 in the main report shows the generalized geologic categories used in the GLU analysis. These categories represent relative erodibility (i.e., rock strength) of the unit and particle size of the unit's constituent materials (e.g., sand or silt). The relative proportions of the geology GLU categories in the watershed are presented below in Table A-3.

Table A-1. Geologic units mapped by Dibblee (various dates) within the USCR watershed.

Geologic unit		
Symbol	**Explanation**	**Age**
Qaf	Surficial sediments—artificial fill	Holocene
Qg	Surficial sediments	Holocene
Qa	Surficial sediments	Holocene
Qls	Landslide debris	Holocene and Pleistocene
Qoa	Older dissected surficial sediments	late Pleistocene
Qog	Older dissected alluvial sediments	late Pleistocene
Qos	Older dissected surficial sediments	late Pleistocene
QTs	Saugus Formation conglomerate	Pleistocene and Pliocene
Tps_db	Punchbowl Formation terrestrial fluviatile, lacustrine and alluvial fan deposits	Pliocene
Ttoc	Towsley Formation claystone, siltstone	early Pliocene
Ttog	Towsley Formation conglomerate	early Pliocene
Tas	Anaverde Formation terrestrial fluviatile and lacustrine	Pliocene
Tab	Anaverde Formation terrestrial fluviatile and lacustrine	Pliocene
Tac	Anaverde Formation terrestrial fluviatile and lacustrine	Pliocene
Tpv	Ridge Basin Group marine clastic, lacustrine and fluviatile—shale facies	late Miocene
Trr	Ridge Basin Group marine clastic, lacustrine and fluviatile—sandstone facies	late Miocene

Geologic unit		
Symbol	**Explanation**	**Age**
Tvib	Ridge Basin Group marine clastic, lacustrine and fluviatile—breccia facies	late Miocene
Trg	Ridge Basin Group clastic sedimentary sequence	late Miocene
Tc	Castaic Formation clay shale or claystone	late Miocene
Tcs	Castaic Formation sandstone	late Miocene
Tcgs	Castaic Formation sandstone-conglomerate	late Miocene
Tcg	Castaic Formation conglomerate	late Miocene
Tm	Monterey Formation shale	Miocene
Tmc	Mint Canyon Formation sandstone and conglomerate	middle Miocene
Tmcl	Mint Canyon Formation siltstone/claystone	late Miocene
Tmcv	Mint Canyon Formation sandstone	late Miocene
Tmcg	Mint Canyon Formation conglomerate/fanglomerate	middle Miocene
Tmr	Mint Canyon Formation red beds	middle Miocene
Tmsb	Mint Canyon Formation schist breccia	middle Miocene
Tpe	Mint Canyon Formation small exposure of shattered Pelona Schist below Tmsb	middle Miocene
Ttc	Tick Canyon Formation sandstone	early Miocene
Ttcg	Tick Canyon Formation conglomerate/fanglomerate	early Miocene
Tva	Vasquez Formation sedimentary rocks and subaerial volcanic deposits	Oligocene
tr	Vasquez Formation calcite travertine vein	Oligocene
ai	Vasquez Formation dike(?) or andesite	Oligocene
Tai	Andesitic intrusive rocks andesite	Oligocene
Tvt	Vasquez Formation tuff-breccia	Oligocene
Tvss	Vasquez Formation sandstone, conglomerate sandstone	Oligocene
Tvsb	Vasquez Formation sandstone	Oligocene
Tvca	Vasquez Formation conglomerate/fanglomerate/breccia	Oligocene
Tvcg	Vasquez Formation conglomerate/fanglomerate/breccia	Oligocene
Tvnb	Vasquez Formation breccia	Oligocene
Tvgb	Vasquez Formation breccia	Oligocene
Tvqb	Vasquez Formation landslide breccia	Oligocene
Tvcd	Vasquez Formation conglomerate/fanglomerate	Oligocene
Tvcs	Vasquez Formation conglomerate	Oligocene
Tvb	Vasquez Formation basalt-andesite	Oligocene
Tvbb	Vasquez Formation breccia	Oligocene
Tvssl	Vasquez Formation similar to Tvss	Oligocene
Tvab	Vasquez Formation andesitic breccia	Oligocene
Tvcgl	Vasquez Formation conglomerate/fanglomerate/breccia	Oligocene
Tvcal	Vasquez Formation conglomerate/fanglomerate/breccia	Oligocene
Tvrs	Vasquez Formation sandstone	Oligocene
Tvsh	Vasquez Formation clay shale and siltstone	Oligocene
Tvs	Vasquez Formation conglomerate and sandstone	Oligocene
rc	Vasquez Formation siltstone-claystone	Oligocene

Geologic unit		
Symbol	**Explanation**	**Age**
Tsfi	San Francisquito Formation sandstone and clay shale	Paleocene
Tsfs	San Francisquito Formation sandstone	Paleocene
Tsfc	San Francisquito Formation conglomerate	Paleocene
Tsfa	San Francisquito Formation clay shale and siltstone	Paleocene
KTsfa	San Francisquito Formation similar to Tsfa	Paleocene
gr	Granitic rocks—granite or quartz monzonite	Late Mesozoic
qm	Granitic rocks—granite to quartz monzonite	Late Cretaceous
grd	Granitic rocks—granodiorite	Late Mesozoic
qd	Granitic rocks—quartz diorite	Late Cretaceous
qds	Quartz Diorite-Gneiss Complex quartz diorite and gneiss	Late Mesozoic
lgd	Lowe Granodiorite—leucocratic	Early Triassic
lgdb	Lowe Granodiorite—gneissoid	Early Triassic
lgdp	Lowe Granodiorite—potassic feldspar	Early Triassic
lgdh	Lowe Granodiorite—hornblende	Early Triassic
lgdd	Lowe Granodiorite—dark, gneissoid	Early Triassic
di	Hornblende dioritic rocks—diorite	Mesozoic
hd	Hornblende dioritic rocks—hornblende diorite	Mesozoic
hdg	Hornblende diorite-gabbro	Early Triassic
my	Pelona Schist mylonite	Mesozoic
pi	Pelona Schist intrusion	Mesozoic
ps	Pelona Schist	Mesozoic
pso	Pelona Schist soapstone	Mesozoic
psl	Pelona Schist mica-albite-quartz schist	Mesozoic
psp	Pelona Schist schist of Portal Ridge	Mesozoic
talc	Pelona Schist talc occurrence	Mesozoic
actinolite	Pelona Schist actinolite occurrence	Mesozoic
an	Anorthosite-Gabbro Complex anothosite	Precambrian
sy	Anorthosite-Gabbro Complex syenite	Precambrian
syg	Anorthosite-Gabbro Complex syenite with gneiss	Precambrian
lgb	Anorthosite-Gabbro Complex leucogabbro	Precambrian
jgb	Anorthosite-Gabbro Complex jotunite-norite-gabbro-diorite	Precambrian
jgba	Anorthosite-Gabbro Complex jotunite-norite-gabbro-diorite with anorthosite	Precambrian
hgb	Anorthosite-Gabbro Complex hornblende gabbro	Precambrian
msg	Gneissic rocks—schist-gneiss	Precambrian
ggn	Gneissic rocks—granodiorite gneiss	Precambrian
dgn	Gneissic rocks dioritic—(amphibolitic) gneiss	Precambrian
agn	Gneissic rocks—augen gneiss	Precambrian
gn	Gneissic rocks—layered gneiss	Precambrian
gnb	Gneiss rocks—banded gneiss	Precambrian
ml	Gneissic rocks marble	Precambrian

Table A-2. Geologic units mapped by USGS (various dates) within the USCR watershed.

Geologic unit		
Symbol	**Explanation**	**Age**
Qaf	Artificial fill	Holocene
Qacf	Graded area	Holocene
Qal	Alluvium	Holocene
Qal1	Gravel, sand, silt and clay	Holocene and Pleistocene
Qal2	Gravel, sand, silt and clay—better sorted deposits along principal drainages	Holocene and Pleistocene
Ql	Lake deposits	Holocene
Qp	Pacoima Formation fanglomerate	Pleistocene
Qfp	Floodplain deposits	Holocene
Qf	Alluvial-fan deposits	Holocene
Qfo	Old alluvial-fan deposits	Pleistocene
Qc	Colluvium	Holocene and Pleistocene
Qls	Landslide deposits	Holocene and Pleistocene
Qsw	Slope wash deposits	Holocene and Pleistocene
Qt	Terrace deposits	Pleistocene
Qto	Old terrace deposits	Pleistocene
Qao	Old alluvium	Pleistocene
Qco	Old colluvium	Pleistocene
Qpa	Pacoima Formation fanglomerate	Pleistocene
QTs	Saugus Formation sandstone and pebble conglomerate	Pleistocene
Qsu	Saugus Formation non-marine sandstone and pebbly sandstone	Pleistocene
Qsp	Saugus Formation pebbly sandstone with schist	Pleistocene
Qss	Saugus Formation pebbly sandstone	Pleistocene
QTsg	Saugus Formation conglomerate at base of Saugus Formation	Pleistocene
QTsc	Saugus Formation conglomerate at base of Saugus Formation	Pleistocene
Tsr	Saugus Formation, Sunshine Ranch Member pebbly to cobbley sandstone	Pliocene
Tsru	Saugus Fm, Sunshine Ranch Member siltstone and mudstone	Pliocene
Tsrl	Saugus Fm, Sunshine Ranch Member sandstone, pebbly sandstone, and conglomerate	Pliocene
Tp	Pico Formation marine clayey siltstone and sandy siltstone	Pliocene
Tps_gs	Pico Formation siltstone	Pleistocene and Pliocene
Tpc	Pico Formation sandstone and conglomerate	Pleistocene and Pliocene
Tw	Towsley Formation sandstone, conglomerate, and mudstone	Pliocene
Twc	Modelo Formation sandstone	Miocene
Tws	Towsley Formation mudstone and siltstone	Pliocene
Tm	Modelo Formation mudstone, shale, or siltstone	Miocene
Tm2	Modelo Formation, member 2 sandstone	Miocene

Geologic unit		
Symbol	**Explanation**	**Age**
Tm3	Modelo Formation, member 3 shale	Miocene
Tm4	Modelo Formation, member 4 sandstone	Miocene
Tms	Modelo Formation sandstone	Miocene
Tcs	Castaic Formation marine shale	Miocene
Tmc	Mint Canyon Formation nonmarine sediments	Miocene
Tmcl	Mint Canyon Formation conglomerate sandstone	Miocene
Tmc1	Mint Canyon Formation, facies 1—lacustrine and lake-marginal fluvial deposits of arkosic sandstone and conglomeratic sandstone	Miocene
Tmc2	Mint Canyon Formation, facies 2 - lacustrine sandstone, silty sandstone, siltstone, claystone and thin beds and lenses of limestone	Miocene
Tmc3	Mint Canyon Formation, facies 3 - lacustrine deltaic sandstone	Miocene
Ttk	Tick Canyon Formation fluvial and lacustrine sandstone, siltstone and claystone, and conglomerates	Miocene
Tvz	Vasquez Formation sandstone, conglomerate, and interbedded andesite-basalt	Oligocene
Tvv	Vasquez Volcanics breccia masses and intrusive sheets of andesite and basalt	Oligocene
Td	Domengine Formation sandstone	Eocene
ps	Pelona Schist	Cretaceous
gr	Tonalite	Cretaceous
gd	Granodiorite	Mesozoic
gd/gn	Granodiorite gneiss	Mesozoic
dgn	Diorite gneiss	Mesozoic
gn	Gneiss complex	Paleozoic
pm	Placerita Formation metamorphosed sedimentary rocks	Paleozoic
an	Anorthosite	Proterozoic
gb	Gabbro	Proterozoic
gbm	Ilmenite-magnetite gabbro	Proterozoic
pCm	Mendenhall Gneiss	Proterozoic

Table A-3. Geology GLU categories within the USCR watershed.

Geology GLU category [a]	% of watershed area [b]
Competent crystalline and sandstones	45.0%
Weak metamorphics and sandstones	27.4%
Siltstones	6.1%
Unconsolidated	21.5%

[a] Geology GLU categories based on literature information and field observations.
[b] Proportion of geology GLU category within the total watershed area determined in GIS.

The relative sediment-production potential of the geology GLU categories was evaluated by examining the proportion of the categories contributing to debris basins and reservoirs with sedimentation records (Figure A-1). As represented in Figure A-2, the sediment-production rates as measured in debris basins and reservoirs were positively correlated best with the Siltstone category and, to a lesser extent, Unconsolidated and Weak Metamorphics & Sandstones categories. Production rates were negatively correlated with the Competent Crystalline & Sandstones category indicating that erosion rates were lower in landscapes having a relatively greater proportion of this geology GLU category.

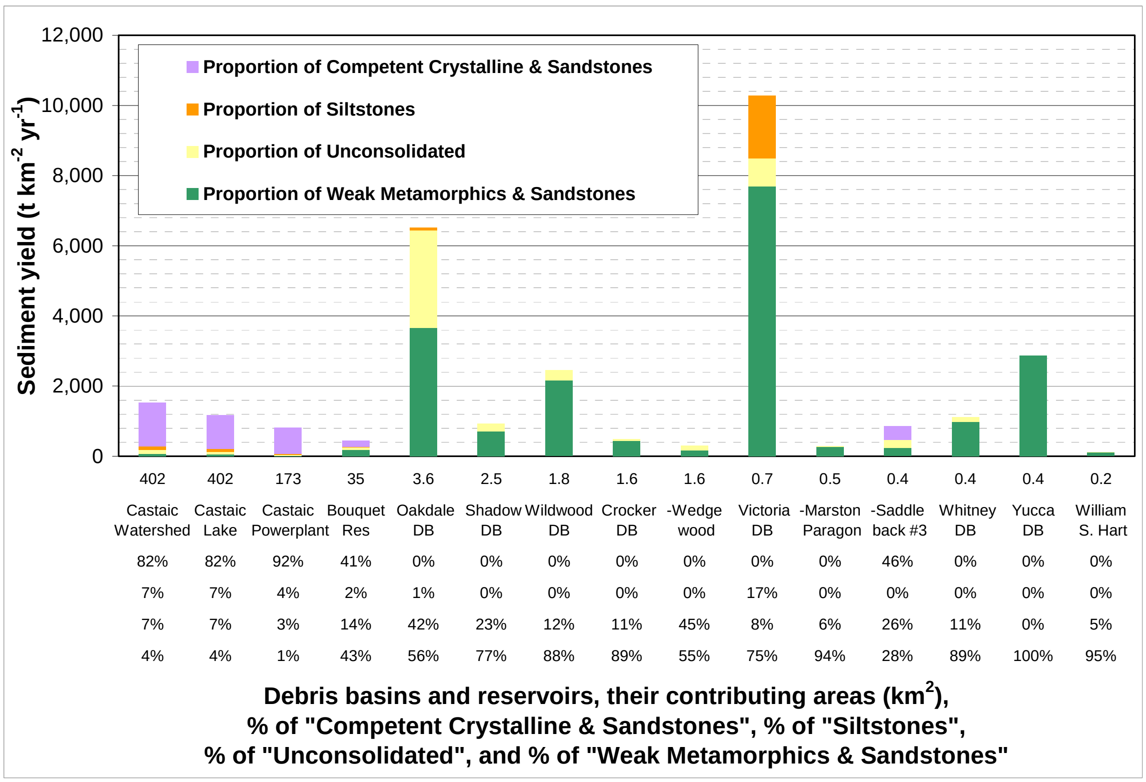

Figure A-1. Proportion of geology GLU categories contributing to debris basins and reservoirs in the USCR watershed.

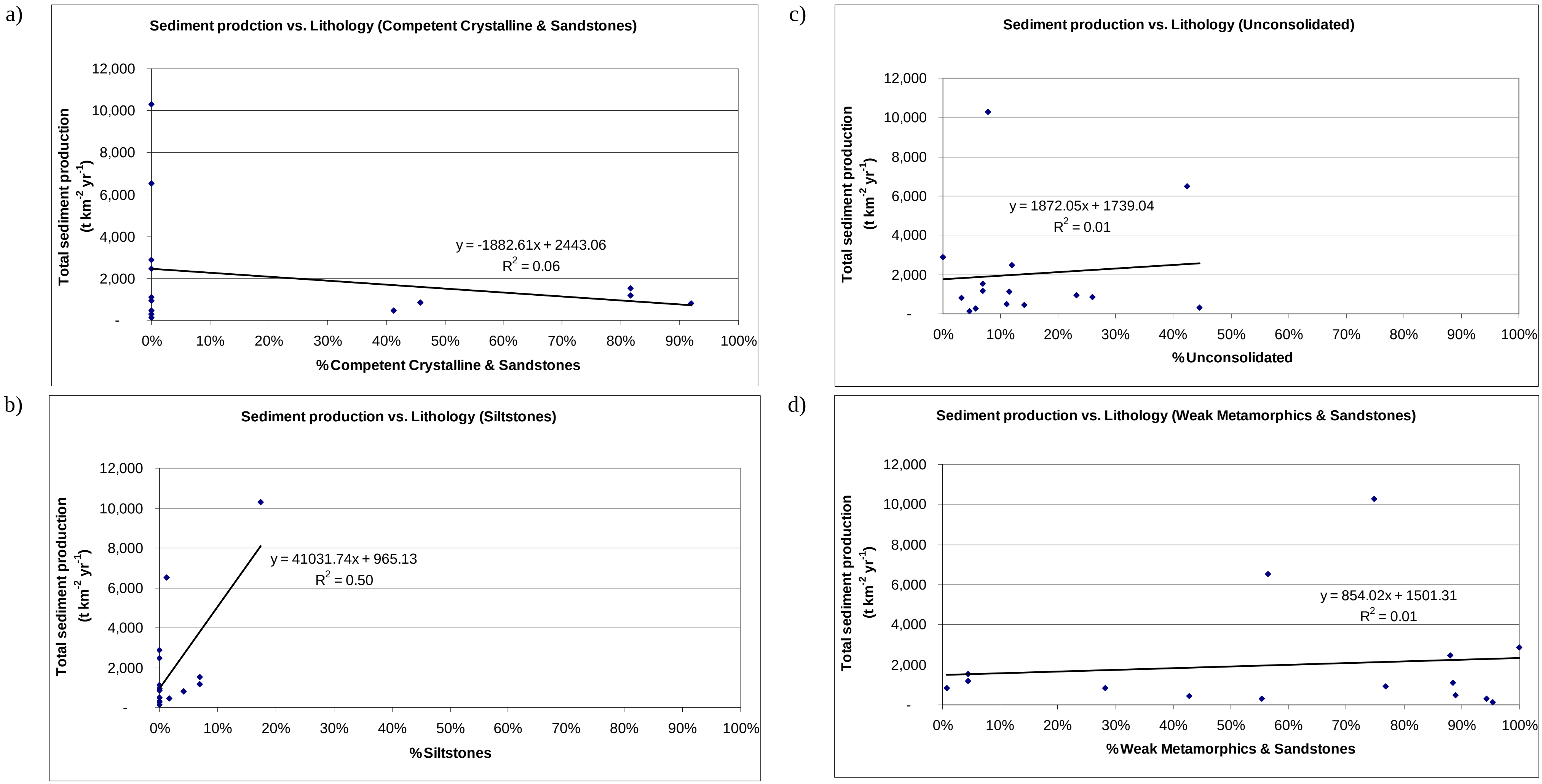

Figure A-2. Correlation of sediment production and lithology for the geology GLU categories.

Land cover units

Land cover was based on a data contained within the National Land Cover Database of 2001 (Homer et al. 2004) at 30-m resolution (see Figure 1-6 in the main report). A list of land cover types occurring within the watershed boundaries is presented below in Table A-4, along with relative proportions within the watershed and the assigned category used in the GLU analysis. Figure 3-12 in the main report shows the generalized land cover categories used in the GLU analysis. These categories represent a simplified division of land cover, or vegetation types as they relate to a relative degree of erosion resistance in different landscape units (e.g., forested hillslopes would be less erodible than those covered only with grasses). The relative proportions of the land cover GLU categories in the watershed are presented below in Table A-5.

Table A-4. Land cover classes within the USCR watershed.

Land cover classes [a]	% of watershed area [b]	GLU category [c]
Scrub/Shrub	61%	Scrub/Shrub
Grassland/Herbaceous	14%	Ag/Grass
Developed, Open Space	7%	Ag/Grass
Mixed Forest	7%	Forest
Evergreen Forest	3%	Forest
Developed, Low Intensity	3%	Developed
Developed, Medium Intensity	2%	Developed
Open water	1%	Open Water
Barren Land	1%	Ag/Grass
Pasture/Hay	1%	Ag/Grass
Woody Wetlands	0%	Scrub/Shrub
Cultivated Crops	0%	Ag/Grass
Emergent Herbaceous Wetland	0%	Ag/Grass
Developed, High Intensity	0%	Developed
Deciduous Forest	0%	Forest

[1] Source: National Land Cover Dataset of 2001 (Homer et al. 2004).
[2] Proportion of land cover category within the total watershed area determined in GIS.
[3] GLU category based on literature information and field observations.

Table A-5. Land cover GLU categories within the USCR watershed.

Land cover GLU category [a]	% of watershed area [b]
Agricultural/grassland	23.0%
Developed	5.1%
Forest	10.0%
Open water	0.8%
Scrub/shrub	61.1%

[a] Land cover GLU categories based on literature information and field observations.
[b] Proportion of land cover GLU category within the total watershed area determined in GIS.

The relative sediment-production potential of the land cover GLU categories was evaluated by examining the proportion of the categories contributing to debris basins and reservoirs with sedimentation records (Figure A-3). As represented in Figure A-4, the sediment-production rates as measured in debris basins and reservoirs were positively correlated only with Scrub/Shrub indicating that erosion rates were highest in landscapes having a relatively greater proportion of this land cover GLU category. Production rates were negatively correlated with the remaining categories.

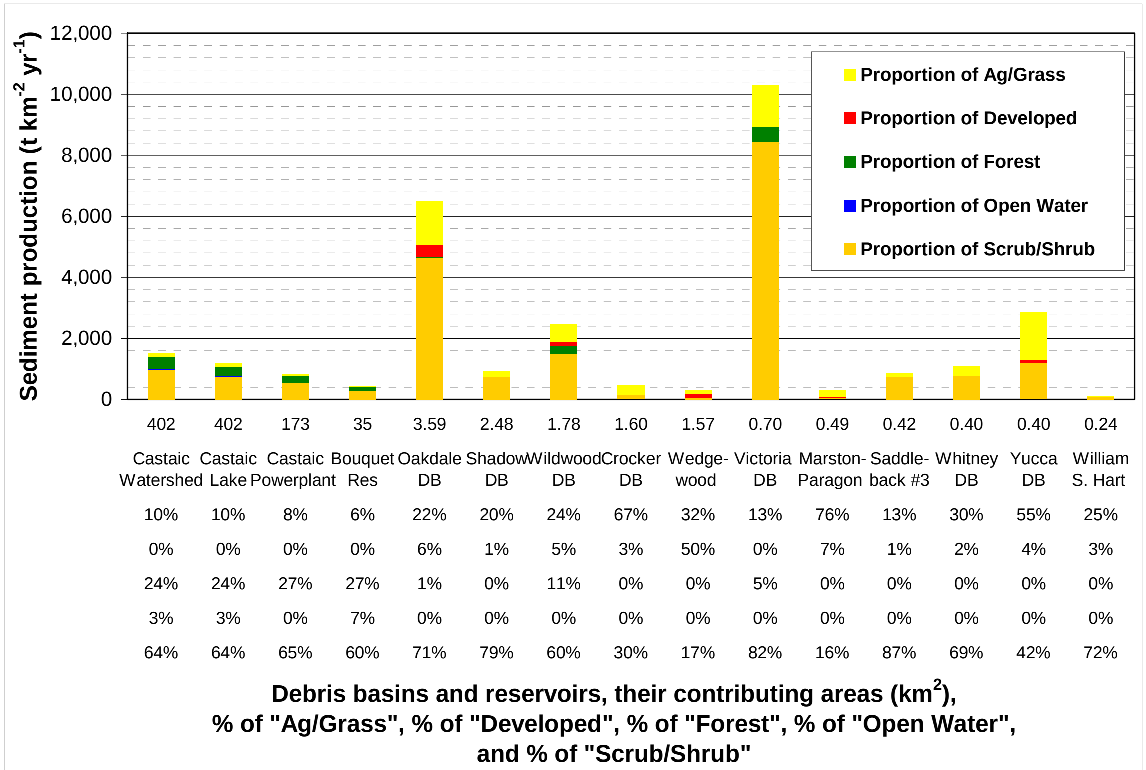

Figure A-3. Proportion of land cover GLU categories contributing to debris basins and reservoirs in the USCR watershed.

a)

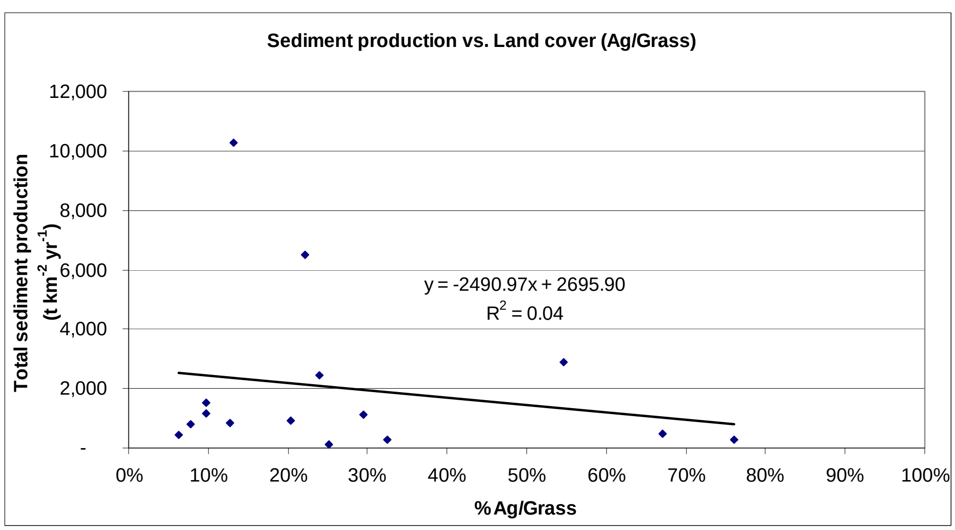

b)

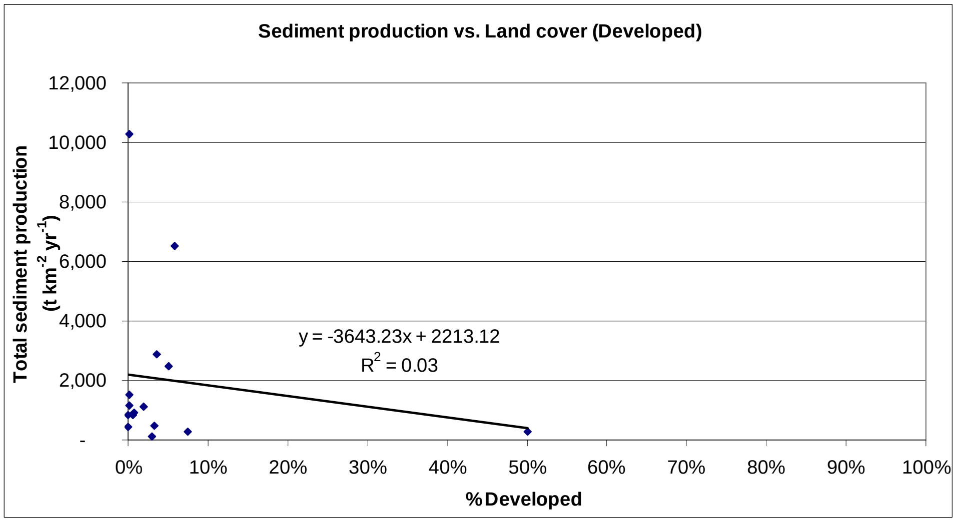
Sediment production vs. Land cover (Developed)
Total sediment production (t km-2 yr-1)
12,000
10,000
8,000
6,000
4,000
2,000
-
y = -3643.23x + 2213.12
R2 = 0.03
0% 10% 20% 30% 40% 50% 60% 70% 80% 90% 100%
% Developed

c)

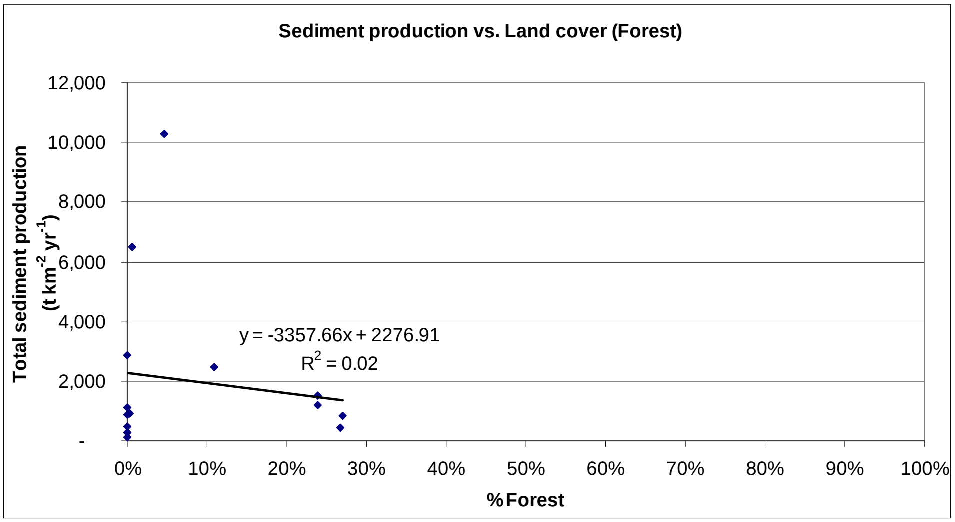
Sediment production vs. Land cover (Forest)
Total sediment production (t km-2 yr-1)
12,000
10,000
8,000
6,000
4,000
2,000
-
y = -3357.66x + 2276.91
R2 = 0.02
0% 10% 20% 30% 40% 50% 60% 70% 80% 90% 100%
% Forest

d)

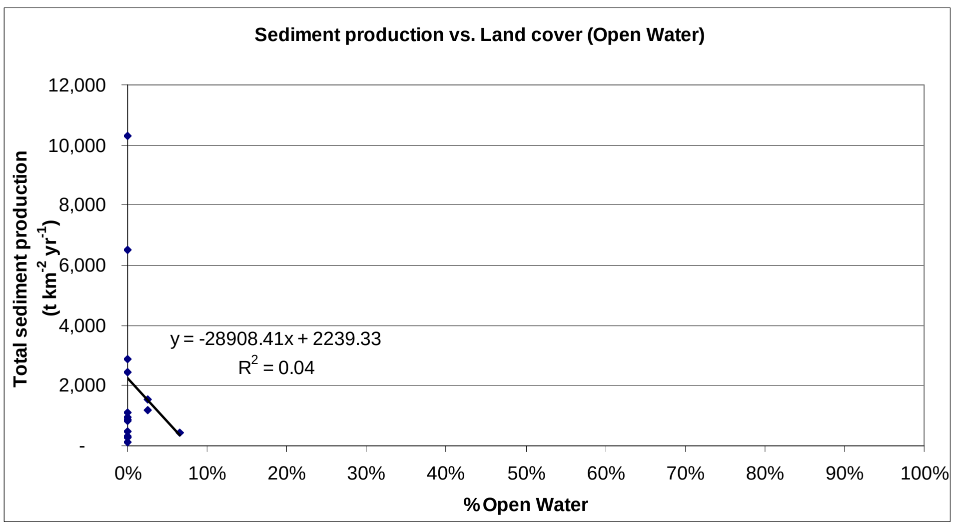
Sediment production vs. Land cover (Open Water)
Total sediment production (t km-2 yr-1)
12,000
10,000
8,000
6,000
4,000
2,000
-
y = -28908.41x + 2239.33
R2 = 0.04
0% 10% 20% 30% 40% 50% 60% 70% 80% 90% 100%
% Open Water

e)

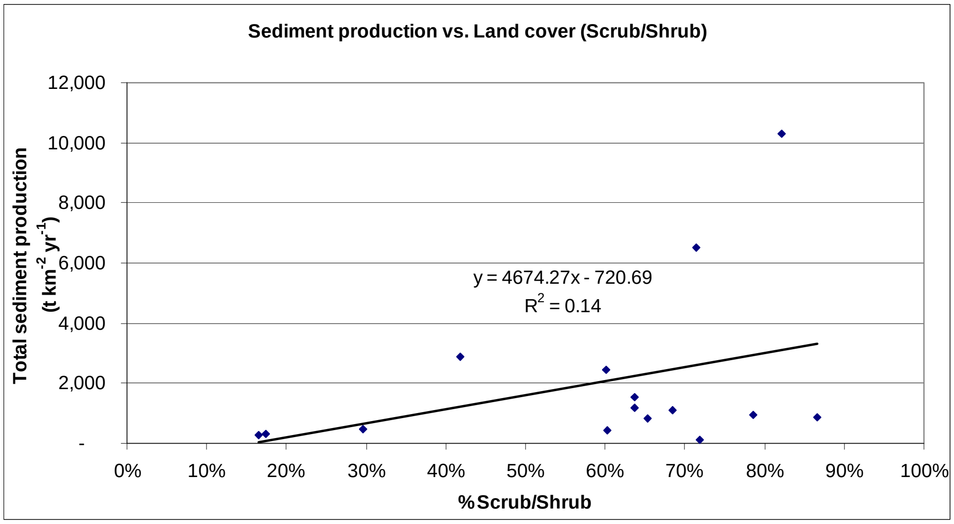

Figure A-4. Correlation between sediment-production rates and land cover/use for the five land cover GLU categories.

Hillslope gradient units

Hillslope gradients in the watershed were based on elevation data contained within a 10-m resolution digital elevation model (DEM) dataset provided by the USGS. Using this data in a GIS, a histogram of hillslope gradient values were plotted to visualize the distribution of slopes in the watershed (Figure A-5). For the purposes of the GLU analysis, it is necessary to group the slope values into as few classes as possible provided that each class represents unique ranges of relative erosion and slope instability in the watershed. Based on the distribution of slopes and on field observations, the continuous range of hillslope gradients was categorized into three groups: 0-20%, 20-60%, and steeper than 60% (Table A-6; see Figure 3-13 in the main report).

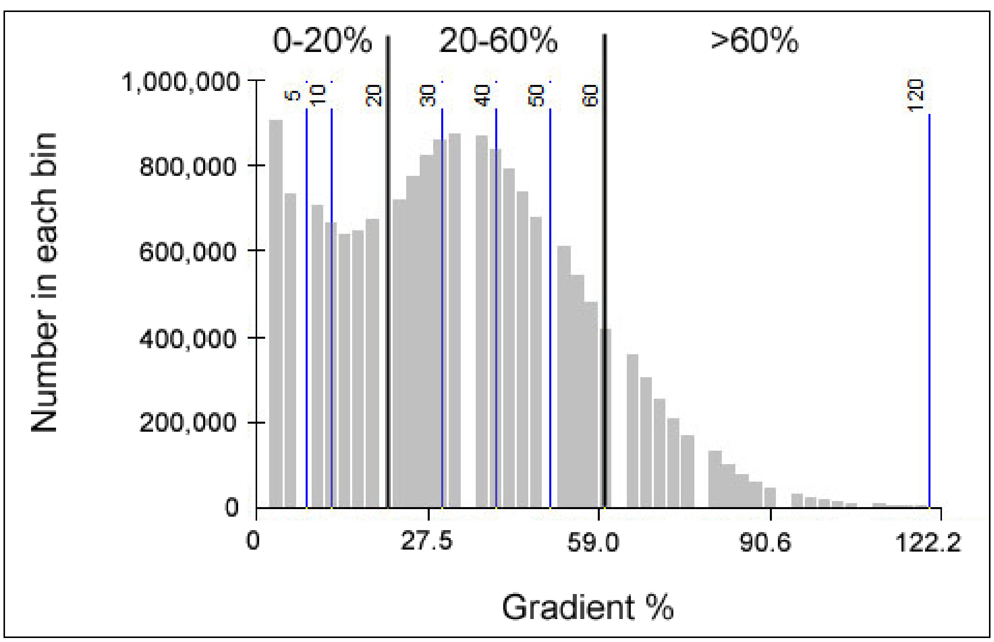

Figure A-5. Histogram of hillslope gradient values in the USCR watershed.

Table A-6. Hillslope gradient GLU categories within the USCR watershed.

Hillslope gradient GLU category [a]	% of watershed area [b]
0–20%	27.8%
20–60%	58.0%
>60%	14.2%

[a] Hillslope gradient GLU categories based on distribution histogram statistics and field observations.
[b] Proportion of hillslope gradient GLU category within the total watershed area determined in GIS.

The relative sediment-production potential of the hillslope gradient GLU categories was evaluated by examining the proportion of the categories contributing to debris basins and reservoirs with sedimentation records (Figure A-6). As represented in Figure A-7, the sediment-production rates as measured in debris basins and reservoirs were positively correlated only with >60% category indicating that erosion rates were highest in landscapes having the steepest hillslope gradients. Production rates were negatively (i.e., poorly) correlated with the remaining categories.

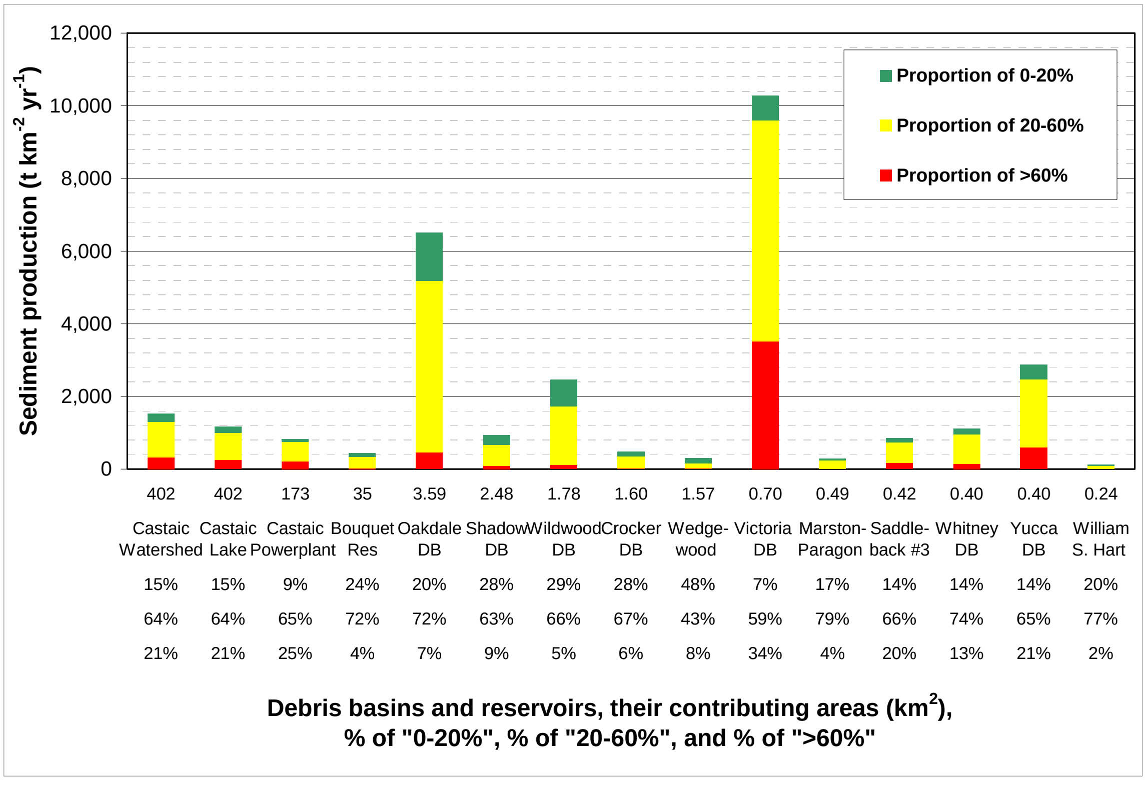

Figure A-6. Proportion of hillslope gradient GLU categories contributing to debris basins and reservoirs in the USCR watershed.

a)

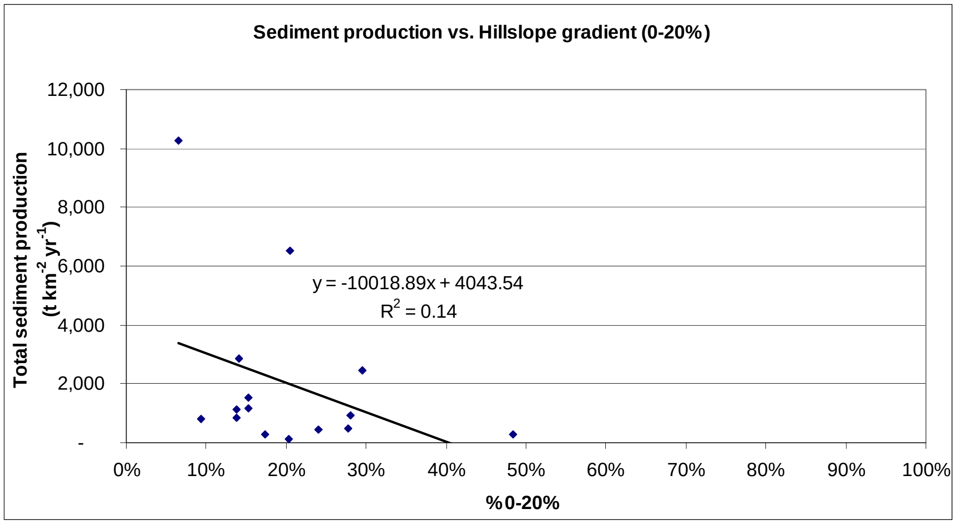

b)

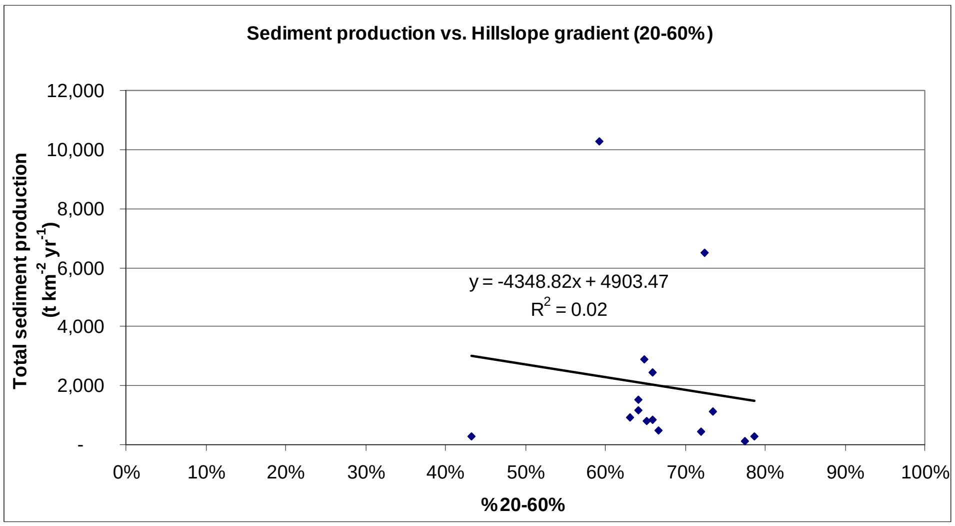

c)

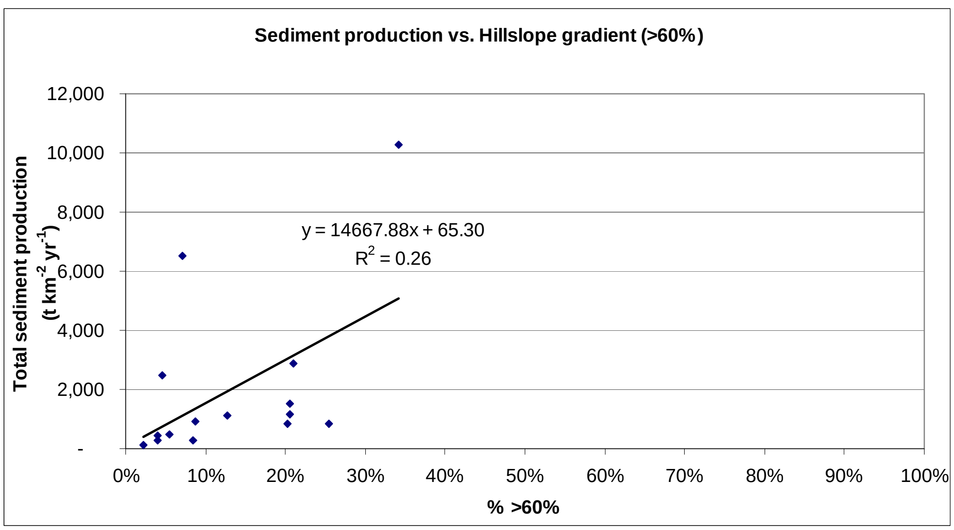

Figure A-7. Correlation between sediment-production rates and hillslope gradient for the three hillslope gradient GLU categories.

REFERENCES

Dibblee, T. W. 1996. Geologic map of the Acton quadrangle, Los Angeles County, California. Scale 1:24,000. Dibblee Geological Foundation, Santa Barbara, California.

Dibblee, T. W. 1996. Geologic map of the Agua Dulce quadrangle, Los Angeles County, California. Scale 1:24,000. Dibblee Geological Foundation, Santa Barbara, California.

Dibblee, T. W. 1997. Geologic map of the Green Valley quadrangle, Los Angeles County, California. Scale 1:24,000. Dibblee Geological Foundation, Santa Barbara, California.

Dibblee, T. W. 1997. Geologic map of the Sleepy Valley and Ritter Ridge quadrangles, Los Angeles County, California. Scale 1:24,000. Dibblee Geological Foundation, Santa Barbara, California.

Dibblee, T. W. 1997. Geologic map of the Warm Springs Mountain quadrangle, Los Angeles County, California. Scale 1:24,000. Dibblee Geological Foundation, Santa Barbara, California.

Dibblee, T. W. 1997. Geologic map of the Whitaker Peak quadrangle, Los Angeles County, California. Scale 1:24,000. Dibblee Geological Foundation, Santa Barbara, California.

Dibblee, T. W. 2001. Geologic map of the Pacifico Mountain and Palmdale (south half) quadrangles, Los Angeles County, California. Scale 1:24,000. Dibblee Geological Foundation, Santa Barbara, California.

Dibblee, T. W. 2002. Geologic map of the Burnt Peak quadrangle, Los Angeles County, California. Scale 1:24,000. Dibblee Geological Foundation, Santa Barbara, California.

Dibblee, T. W. 2002. Geologic map of the Lake Hughes and Del Sur quadrangles, Los Angeles County, California. Scale 1:24,000. Dibblee Geological Foundation, Santa Barbara, California.

Dibblee, T. W. 2002. Geologic map of the Liebre Mountain quadrangle, Los Angeles County, California. Scale 1:24,000. Dibblee Geological Foundation, Santa Barbara, California.

Homer, C., C. Huang, L. Yang, B. Wylie, and M. Coan. 2004. Development of a 2001 national landcover database for the United States. Photogrammetric Engineering and Remote Sensing 70: 829–840. http://www.mrlc.gov/.

USGS (United States Geological Survey). 1997. Preliminary geologic map of the Mint Canyon 7.5' quadrangle, Southern California: a digital database. Compiled by R. F. Yerkes. Open-File Report 97-164. http://wrgis.wr.usgs.gov/open-file/of97-164/.

USGS. 1997. Preliminary geologic map of the Newhall 7.5' quadrangle, Southern California: a digital database. Compiled by R. F. Yerkes and R. H. Campbell. Open-File Report 95-800. http://pubs.usgs.gov/of/1995/of95-800/.

USGS. 1997. Preliminary geologic map of the Oat Mountain 7.5' quadrangle, Southern California: a digital database. Compiled by R. F. Yerkes and R. H. Campbell. Open-File Report 95-89. http://wrgis.wr.usgs.gov/open-file/of95-89/.

USGS. 1997. Preliminary geologic map of the San Fernando 7.5' quadrangle, Southern California: a digital database. Compiled by R. F. Yerkes. Open-File Report 97-163. http://pubs.usgs.gov/of/1997/of97-163/.

USGS. 1997. Preliminary geologic map of the Santa Susana 7.5' quadrangle, Southern California: a digital database. Compiled by R. F. Yerkes and R. H. Campbell. Open-File Report 97-258. http://wrgis.wr.usgs.gov/open-file/of97-258/.

USGS. 1997. Preliminary geologic map of the Sunland 7.5' quadrangle, Southern California: a digital database. Compiled by R. F. Yerkes. Open-File Report 97-270. http://pubs.usgs.gov/of/1997/of97-270/.

USGS. 1997. Preliminary geologic map of the Val Verde 7.5' quadrangle, Southern California: a digital database. Compiled by R. F. Yerkes and R. H. Campbell. Open-File Report 95-699. http://wrgis.wr.usgs.gov/open-file/of95-699/.

USGS. 2005. Preliminary geologic map of the Los Angeles 30' x 60' quadrangle, Southern California. Version 1.0. Compiled by R. F. Yerkes and R. H. Campbell. Scale 1:100,000. Open-File Report 2005-1019. http://pubs.usgs.gov/of/2005/1019.

Appendix B

Watershed Impacts Chronology
Supporting Materials

WATERSHED IMPACTS CHRONOLOGY SUPPORTING MATERIALS

This appendix provides supplementary information that was used in the development of the Upper Santa Clara River (USCR) watershed impacts assessment presented in Chapter 2 and elsewhere throughout the main report. The watershed impacts chronology is summarized in detail in Table B-1.

The methods employed to determine the "wet" and "dry" periods in the USCR watershed, as depicted in Figure 2-1 in the main report, are also described here. Determining when wet and dry periods have occurred in the past provides valuable context of the watershed's historical hydrological conditions, which have had strong influences on the watershed and, particularly, the river's morphologic history and likely future trajectory. That is, the largest floods have typically occurred during wet years and, further, have typically been concentrated during wet periods (i.e., grouping of years). It is during these large floods when the vast majority of sediment transport (i.e., geomorphic activity) has occurred in the watershed and the river. For this analysis, two of the longest precipitation gauge records in the entire Santa Clara River (SCR) watershed were utilized:

- The Santa Paula station (#245A) operated by the Ventura County Watershed Protection District (VCWPD) was used to represent the lower Santa Clara River (LSCR) watershed. The station began measuring precipitation in water year 1873 and continues to present day. Data for this station can be accessed from VCWPD's website: http://www.vcwatershed.net/hydrodata/. Seasonal precipitation values prior to this period were estimated by Freeman (1968) for water years 1770–1872 based on information first published by Lynch (1931).
- San Franciscquito Canyon station (Powerhouse #1) operated by the Los Angeles Department Water and Power (LADWP) was used to represent the USCR watershed. Available data from this station are from water years 1918–2009.

The methodology used here to determine wet and dry periods at each station was initially developed by Lynch (1931), as described and refined by Freeman (1968). For our analysis, designation of wet and dry periods was determined by first calculating the departure of the total annual precipitation for each water year from the average annual precipitation over the entire period of record. The cumulative departure was then calculated for each water year and wet periods and dry periods were determined as a function of the trend in cumulative departure values. Wet periods were those periods of time when the cumulative departure values were consistently increasing with time (i.e., there was a positive trend in the plot of cumulative value versus water year) and dry periods were those periods of time when the cumulative departure values were consistently decreasing with time. Freeman (1968) described wet periods as "accumulation" periods and dry periods as "depletion" periods. The plots we generated from the Santa Paula and San Francisquito Canyon precipitation gauge data are presented in Figure B-1. Both plots show very similar patterns, with only two notable differences in their overall trends: the San Francisquito Canyon gauge location (i.e., USCR watershed) experienced dry periods during 1970–1977 and 1999–2004 while the Santa Paula gauge location (i.e., LSCR watershed) maintained wet characteristics during these time periods. This result speaks to the subtle hydrological differences between these two parts of the SCR watershed, where the USCR portion is more arid than the LSCR portion as it is positioned farther east from the coast. Our plot for Santa Paula is similar to the plot Freeman (1968) created for the water years he had available: 1770–1965 (Figure B-2).

Using a long-term record of wildfire data held by the state (CDF FRAP 2010), we applied a similar analysis as described above for the long-term precipitation records to determine periods since 1911 when a relatively high or low proportion of the USCR watershed has burned, termed here as "high burn" and "low burn" periods, respectively (Figure B-3).

Table B-1. Chronology of impacts to geomorphic processes in the USCR watershed.

Factor	Pre-1850	1851–1870	1871–1890	1891–1900	1901–1910	1910–1920	1921–1930	1931–1940	1941–1950	1951–1960	1961–1970	1971–1980	1981–1990	1991–2000	2001–2010 (present)	2010–2050 (future)
Climate																
El Nino Southern Oscillation (ENSO) Cycle (WY 1950-2010) [A]										**WY 1952** **WY 1958**	**WY 1964** **WY 1966** **WY 1969** **WY 1970**	**WY 1973** **WY 1977** **WY 1978**	**WY 1983** **WY 1987** **WY 1988**	**WY 1992** **WY 1995** **WY 1998**	**WY 2003** **WY 2005** **WY 2007** **WY 2010**	Expect contemporary ENSO Cycle recurrence interval of 3-8 years to continue
Floods >10,000 cfs & Dam Failure (WY 1928 – 2010) [B, C, D, E, F]	**1811** **1815** **1820-21** **1824-25** **1840**	**Jan 1862:** worst in 19th century, made an inland sea in Ventura Co.; eroded land; numerous landslides throughout watershed **1867:** Flood discharge unknown in USCR	**1884:** Flood discharge unknown in USCR, but flood waters reportedly "swept down Soledad Canyon and… spread out over the valley (rivaling) the Mississippi River."	**1895:** Flood discharge unknown in USCR	**1905:** Reportedly contained the "greatest rainstorm since 1884… there was a big washout near Castaic" **1906, 1907, 1909:** Flood discharges unknown in USCR;	**1911, 1914, 1916:** Flood discharges unknown, but reports of substantial damages in 1914 and all of the US southwest was impacted in 1916	**March 12–13, 1928:** St. Francis Dam failure (est. 500,000–1,000,000 cfs)	**Mar 2, 1938:** Saugus: 24,000 cfs Newhall Ranch Bridge destroyed; comparable to 1914, but < 1862 & 1884	**Mar 2, 1938:** Saugus: 24,000 cfs **Jan 23, 1943:** Saugus: 15,000 cfs **Feb 22, 1944:** Saugus: 22,200 cfs		**Dec 29, 1965:** Co-line: 32,000 cfs Saugus: 11,600 cfs **Jan 25, 1969:** largest recorded flood Co-line: 68,800 cfs **Feb 26, 1969:** caused more damage than Jan flood Saugus: 31,800 cfs	**Feb 11, 1973:** Co-line: 12,800 cfs **Feb 9, 1978:** Co-line: 22,800 cfs **Feb 16, 1980:** Co-line: 13,900 cfs	**Mar 1, 1983:** Co-line: 30,600 cfs Saugus: 14,925 cfs **Feb 15, 1986:** Co-line: 12,300 cfs	**Jan 12, 1992:** Co-line: 12,300 cfs **Feb 18, 1993:** Co-line: 10,700 cfs **Jan 10, 1995:** Co-line: 17,100 cfs **Feb 23, 1998:** Co-line: 10,000 cfs Saugus: 19,000 cfs	**Jan 9-11, 2005:** Co-line: 32,000 cfs Saugus: 20,900 cfs **Jan 2, 2006:** Co-line: 12,500 cfs	Expect contemporary 3–5 year recurrence interval of floods >10,000 cfs at the Co-line stream gauge to continue
Wildfires (10 largest fires in the watershed, 1878-2009) [G]						**1919 Ravenna Fire:** 88.6 km^2 (21,904 ac) Ravenna and into Soledad Canyon reach of USCR	**1922 Mint Canyon Fire:** 71.4 km^2 (17,637 ac) Upper Mint Canyon **1924 Unnamed Fire:** 77.7 km^2 (19,189 ac) Elizabeth Lake Canyon			**1960 Unnamed Fire:** 110 km^2 (27,177 ac) Soledad Canyon reach of USCR	**1968 Liebre Fire:** 130.3 km^2 (32,190 ac) Upper Castaic Creek **1970 Agua Dulce Fire:** 88 km^2 (21,756 ac) Lower Bouquet and Mint canyons			**1996 Marple Fire:** 66 km^2 (16,303 ac) Upper Castaic Creek	**2002 Copper Fire:** 77.2 km^2 (19,102 ac) San Francisquito Canyon **2007 Buckweed Fire:** 155.2 km^2 (38,347 ac) Bouquet Canyon **2009 Station Fire:** 92.8 km^2 (22,932 ac) Upper Aliso Canyon	Expect historical ~40-yr recurrence of "high burn" periods to continue
Channel Management																
Channelization & Bank Protection [F, H]							St. Francis Dam disaster prompts start of channelization on tributaries and bank protection on the river			**1950s – present:** Urban developments encroach on floodplain and prompt construction of hardened banks of river, some levees along the river channel, and highly channelized sections of the lower reaches of several tributaries, mostly within the Santa Clarita basin.						Expect increased need for flood and debris protection infrastructure as population and urban footprint increases

Factor	Pre-1850	1851–1870	1871–1890	1891–1900	1901–1910	1910–1920	1921–1930	1931–1940	1941–1950	1951–1960	1961–1970	1971–1980	1981–1990	1991–2000	2001–2010 (present)	2010–2050 (future)
Regulation [F, H]						**1912:** Dry Canyon Reservoir: 12 km^2 (4.5 mi^2); taken out of operation in 1966 due to seepage problems	**1926-1928:** San Francisquito Reservoir: 98 km^2 (38 mi^2); dam collapsed Mar 12-13, 1928	**1934:** Bouquet Reservoir: 35 km^2 (13.6 mi^2)				**1972:** Castaic Lake: 398 km^2 (154 mi^2)				No new reservoirs planned
Instream Aggregate Mining [B, F, I]					Start of small-scale aggregate mining in river					**1950s:** Instream aggregate mining begins in Soledad Canyon	**1960s – 1990s:** 30-year average annual instream extraction rate: ~300,000 tonnes per year, with a maximum of ~500,000 tonnes per year					Instream aggregate mining operations (SMP #86357) in Soledad Canyon expected to continue, but unknown when operations may cease and/or when new operations elsewhere along the USCR may initiate
												1970s: Total in- and off-channel production peak at ~1M tonnes per year		**Post-1995–present:** Average annual instream extraction rate: <300,000 tonnes per year; One remaining instream operation		
Management Policy [J]						**1912:** Los Angeles County Flood Control District formed				**1950s:** LA County begins taxing property based on housing and commercial potential, initiating large-scale urban development			**1985:** LADPW forms as consolidation of the Flood Control District, County Engineer, and Road Department		**Sept 29, 2004:** USACE, LADPW, and VCWPD initiated the Santa Clara River Feasibility Study	Watershed management agencies and actions would continue
Irrigation Infrastructure & Groundwater Extraction [H, K]			**By 1870s:** water demands high enough to need pumped water supplies in watershed			**1913:** First public water utility in the SCV established: Newhall Water System (now NCWD); 125 connections			**1947–1960s:** SCV groundwater pumping for agriculture: 27,000 – 42,000 AFY	**1960:** SCV groundwater pumping for municipal: 5,000 AFY	**1960s:** SCV groundwater pumping for municipal use: 10,000 AFY **1960s–1980s:** SCV groundwater pumping for agriculture: ~12,500 AFY	**1980:** State Water Project via Castaic Lake Water Agency begins to augment SCV groundwater supply **1980: SCV** groundwater pumping for municipal uses: 22,000 AFY	**1981–1990:** State Water Project delivers ~15,000 AFY **1980s–1990s:** SCV groundwater pumping for agriculture: 9,000 AFY	**1990s:** Groundwater production in SCV: 43,500 AFY; Acton basin: ~1,500 AFY **1991–2000:** State Water Project delivers ~19,000 AFY **1990s–2000s:** SCV groundwater pumping for agriculture: 13,500 AFY	**2000s:** Recycled water use begins **2000s:** Groundwater production in SCV and Acton basin: ~30,000 – 35,000 AFY **2001–2005:** State Water Project delivers ~44,000 AFY	Groundwater extraction rates expected to be similar to contemporary levels; Up to 95,200 AFY of State Water Project supply is available to CLWA Projected total water demand: **2010:** ~106,000 AFY **2020:** ~110,000 AFY **2030:** ~130,000 AFY

Factor	Pre-1850	1851–1870	1871–1890	1891–1900	1901–1910	1910–1920	1921–1930	1931–1940	1941–1950	1951–1960	1961–1970	1971–1980	1981–1990	1991–2000	2001–2010 (present)	2010–2050 (future)
Land Use Changes																
Agriculture [B, F, L, M]	**Early 1800s:** Ranching and farming begins with est. of Spanish Mission and Rancho Removal of riparian and scrub/shrub vegetation cover to grazing and farm land	**1863-1864:** drought decimates cattle industry, replaced initially by sheep, followed by recovery of cattle industry	**1880s:** 15,000 acres of wheat in SCV—largest exported of wheat in state Continued conversion of native vegetation areas to agricultural lands	**1892:** Angeles National Forest est.—federal control over land use in semi-protected area						**1960s–1990s:** agriculture in SCV diminishes as urban developments expand					**2000s–present:** Crop cultivation and ranching practices remain active in rural portions of watershed (e.g., Acton Basin)	Currently zoned agriculture (crops, ranching, etc.) lands remain in LA County's General Plan zoning maps
Urbanization [B, F, H, M, N]	**1770:** Portola Expedition encounters ~1,000 Native Americans living in the SCV **1797:** Mission San Fernando est. **1804:** Estancia de San Fernando Xavier est. **1839:** Rancho San Francisco est. **1850:** California gains US statehood	**1870:** SCV population: 265	**1878:** towns of Newhall and Saugus est. **1887:** town of Acton est.				**Mid-1920s:** town of Val Verde est.	**1940:** Watershed population 5,638	**1950:** Watershed population 10,001	**1960:** Watershed population 18,362	**1965:** town of Valencia est. **1970:** Watershed population 52,700	**1980:** Watershed population 93,600	**1987:** City of Santa Clarita incorporated with merging of the towns Canyon Country, Newhall, Saugus, and Valencia **1990:** Watershed population ~150,000	**2000:** Watershed population 225,603	**2010:** Watershed population ~300,000	Watershed population expected to increase: **2010:** ~300,000 **2020:** ~370,000 **2030:** ~430,000

Factor	Pre-1850	1851–1870	1871–1890	1891–1900	1901–1910	1910–1920	1921–1930	1931–1940	1941–1950	1951–1960	1961–1970	1971–1980	1981–1990	1991–2000	2001–2010 (present)	2010–2050 (future)
Linear Features Construction (road, rail, and aqueduct) [B, F, M]			**1870s:** So. Pacific Railroad constructed line from Newhall through Soledad Canyon **1880s:** Railway line constructed west to Ventura			**1910s–1920s:** Extensive development of paved roads; two primary roads in USCR watershed were through Soledad and San Francisquito canyons	**1921:** Mint Canyon Highway (aka: Sierra Highway) constructed				**1960s:** Interstate 5 and State Highway 14 constructed, bisecting drainages and re-routing water and sediment					Numerous city and county roads are planned and/or expected to be constructed according to the LA County General Plan

Abbreviations:
ac = acres   cfs = cubic feet per second km^2 = square kilometers   SCV = Santa Clarita Valley   USCR = Upper Santa Clara River   WY = water year
AFY = acre-feet per year   est. = established   LADPW = Los Angeles County Department of Public Works   USACE = U.S. Army Corps of Engineers   VCWPD = Ventura County Watershed Protection District

Sources:
[A] National Weather Service, http://www.cpc.ncep.noaa.gov/products/analysis_monitoring/ensostuff/ensoyears.shtml, accessed 30 August 2010.
[B] Historical accounts from the Santa Clarita Valley Historical Society webpage: http://www.scvhistory.com, accessed 30 August 2010.
[C] Discharge records from the County line gauge (USGS 11108500, 11109000), Santa Clara River near Saugus (USGS 11107922), and Santa Clara River at Old Road Bridge (LADPW F-92).
[D] Magnitude of St. Francis Dam flood: Begnudelli and Sanders (2007).
[E] Historical flood events: Freeman (1968), Schwartzberg and Moore (1995), Engstrom (1995), Paulson et al. (1991).
[F] General historical information: AMEC (2005).
[G] Wildfire name, date, and total area: CDF FRAP (2010); areal extent within the USCR watershed determined in GIS for this study.
[H] General historical information on water resources: Kennedy/Jenks Consultants (2008).
[I] In- and off-channel extraction rates estimated: Joseph et al. (1987); In-channel extraction rates by USACE (A. Allen, pers. comm., 2010);
[J] County tax policy: Worden (1995).
[K] Groundwater use history and pumping data: Hamilton (1999); NCWD (2010); CLWA (2003); Slade (2002, as cited in CDWR 2006); Slade (1990, as cited in CDWR 2004).
[L] Historical agriculture practices information: Manzer (2006)
[M] Future agriculture land zoning information: LACDRP (2009)
[N] Historical, current, and forecasted population data: Worden (1998), Earle (2003), U.S. Census Bureau (2010a, b), Stillwater Sciences (2007), City of Santa Clarita (2004), Kennedy/Jenks Consultants (2008), LACDRP (2009), CDF (2010), City of Acton (2010).

a)

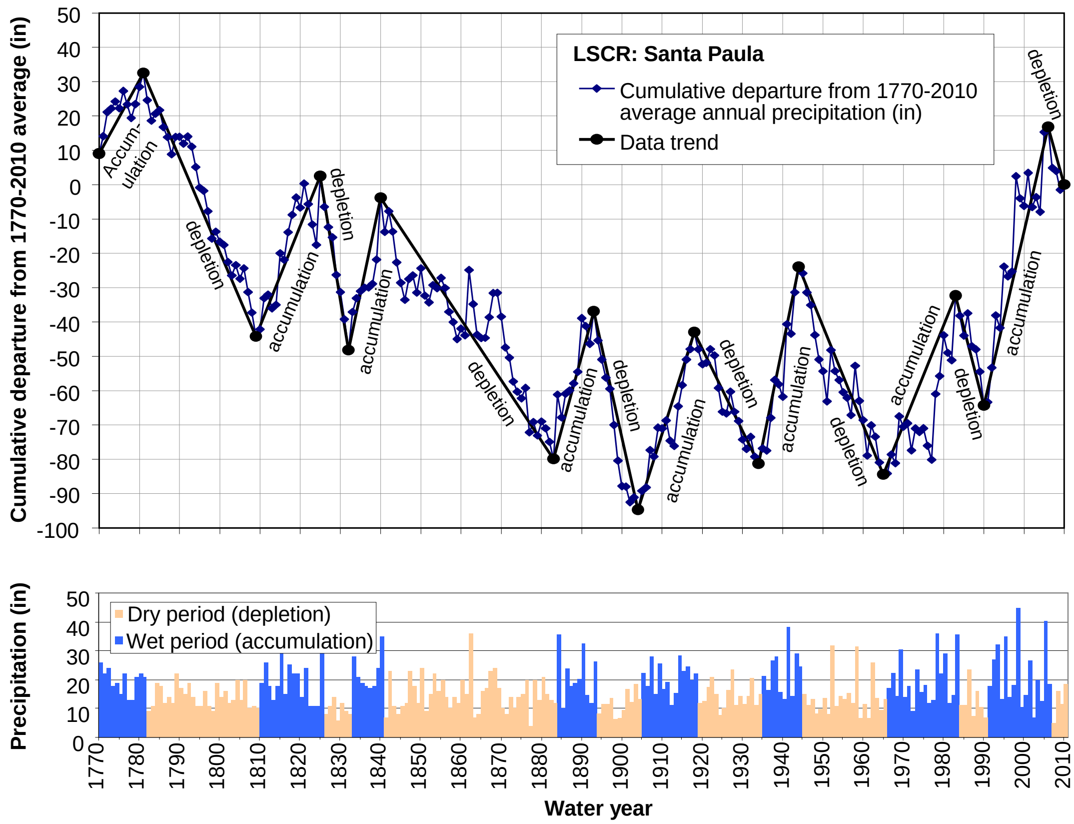

b)

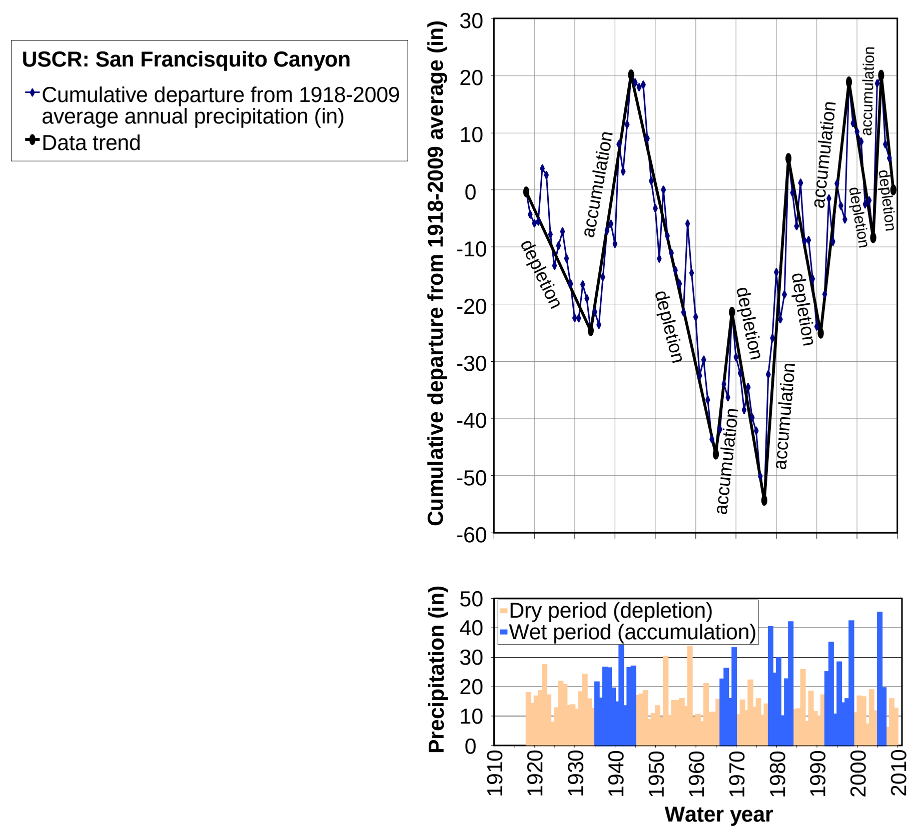

Figure B-1. Wet and dry periods at Santa Paula (a) and San Francisquito Canyon (b).

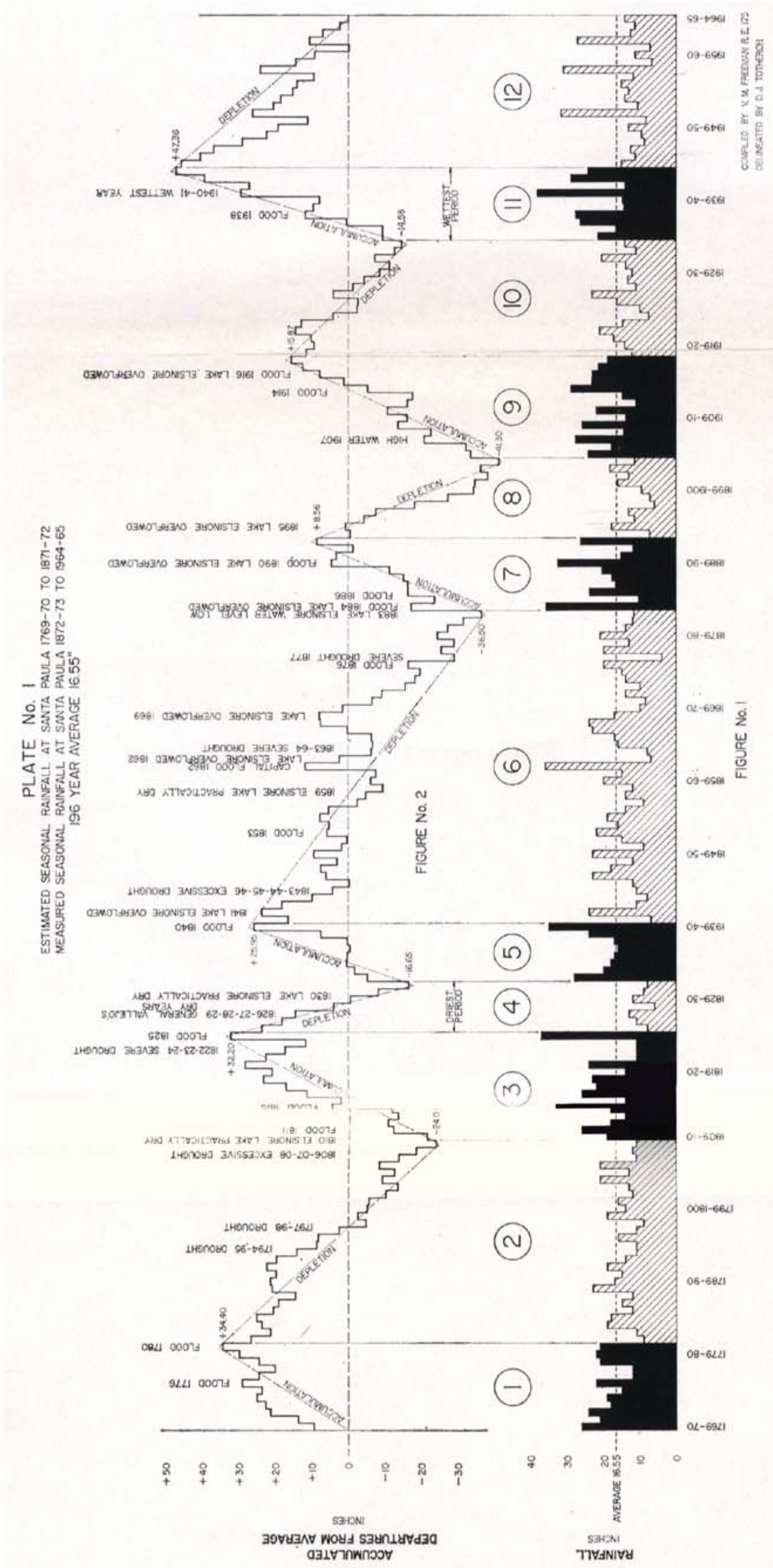

Figure B-2. Estimated and measured annual precipitation at Santa Paula 1770–1872 and 1873–1965, respectively, with delineations of periods of accumulation (wet) and depletion (dry) (from Freeman 1968, courtesy of Lorrin L. Morrison printer and publisher).

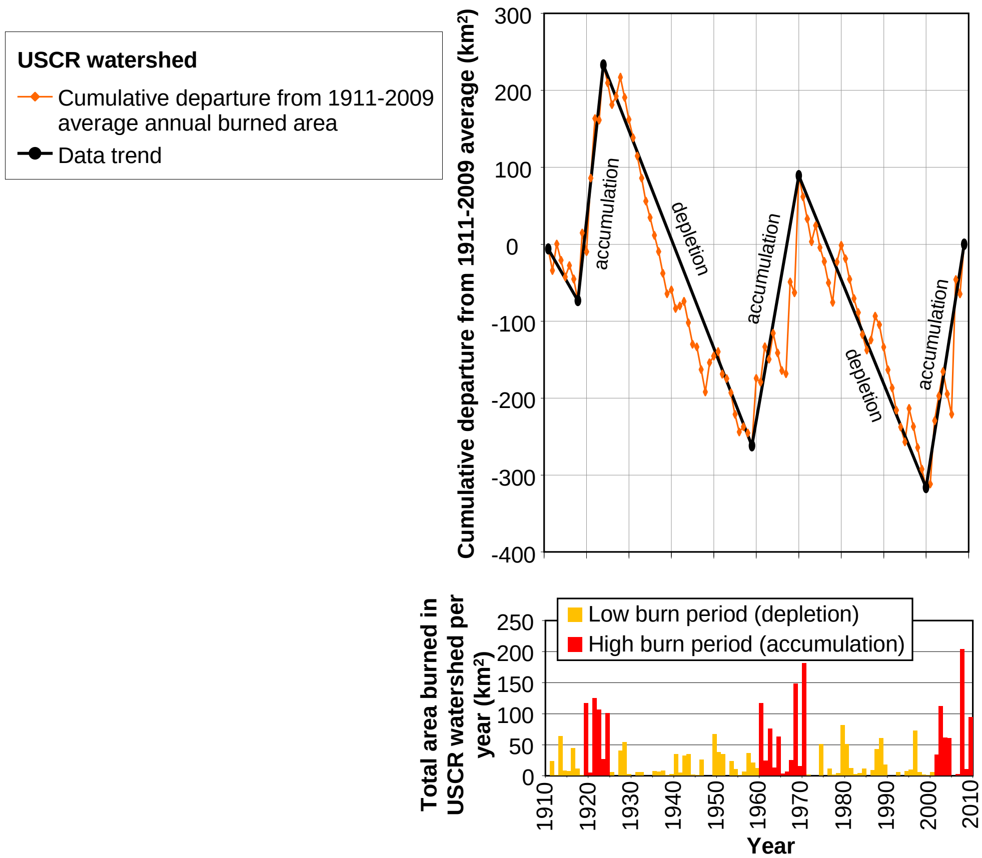

Figure B-3. High and low burn periods in the USCR watershed.

REFERENCES

AMEC (AMEC Earth & Environmental). 2005. Santa Clara River Enhancement and Management Plan (SCREMP). Prepared by AMEC, Santa Barbara, California for VCWPD, Ventura, California, LADPW, Alhambra, California, and SCREMP Project Steering Committee.

Begnudelli, L., and B. F. Sanders. 2007. Simulation of the St. Francis Dam-break flood. Journal of Engineering Mechanics 133: 1200–1212.

CDF (California Department of Finance). 2010. January 2010 cities and counties ranked by size, numeric, and percent change. Sacramento, California.

CDF FRAP (California Department of Forestry and Fire, Fire and Resource Assessment Program). 2010. Statewide fire history electronic database. Website. http://frap.cdf.ca.gov/data/frapgisdata/download.asp?rec=fire [Accessed 25 May 2010].

CDWR (California Department of Water Resources). 2004. California's groundwater, Bulletin 188: Acton Valley groundwater basin. http://www.dpla2.water.ca.gov/publications/groundwater/bulletin118/basins/pdfs_desc/4-5.pdf [Accessed 30 August 2010].

CDWR. 2006. California's groundwater, Bulletin 188: Santa Clara River Valley groundwater basin, Santa Clara River Valley east subbasin. http://www.water.ca.gov/pubs/groundwater/bulletin_118/basindescriptions/4-4.07.pdf [Accessed 30 August 2010].

City of Action. 2010. Action, California. Website. http://www.cityofacton.org/ [Accessed 26 Aug 2010].

City of Santa Clarita. 2004. City of Santa Clarita General Plan: housing element update.

CLWA (Castaic Lake Water Agency). 2003. Groundwater management plan, Santa Clara River Valley groundwater basin, east subbasin, Los Angeles, California. Prepared by Luhdorff & Scalmanini, Woodland, California for CLWA, Santa Clarita, California.

Earle, D. 2003. Mining and ranching in Soledad Canyon and Antelope Valley. Online archives and repository of the Santa Clarita Valley Historical Society, Santa Clarita, California. http://www.scvhistory.com/scvhistory/earle-mining-0103.htm [Accessed 30 August 2010].

Engstrom, W. N. 1995. The California storm of January 1862. Quaternary Research 46: 141–148.

Freeman, V. M. 1968. People-land-water: Santa Clara Valley and Oxnard Plain, Ventura County, California. Lorrin L. Morrison, Los Angeles.

Hamilton, J. 1999. Newhall County Water District: an historical perspective. Online archives and repository of the Santa Clarita Valley Historical Society, Santa Clarita, California. http://www.scvhistory.com/scvhistory/ncwd.html [Accessed 30 August 2010].

Joseph, S. E., R. V. Miller, S. S. Tan, and R. W. Goodman. 1987. Mineral land classification of the greater Los Angeles area: classification of sand and gravel resource areas, Saugus-Newhall

Production-Consumption Region, and Palmdale Production-Consumption Region. California Division of Mines and Geology, Special Report 143, Part V.

Kennedy/Jenks Consultants. 2008. Upper Santa Clara River integrated regional water management plan. Prepared by Kennedy/Jenks Consultants, Los Angeles, California.

LACDRP (Los Angeles County Department of Regional Planning). 2009. Draft Santa Clarita Valley area plan: one valley one vision. http://planning.lacounty.gov/ovov.

Lynch, H. B. 1931. Rainfall and stream run-off in southern California since 1769. Prepared for the Metropolitan Water District of Southern California, Los Angeles, CA.

Manzer, D. 2006. Evolution of the local rancho. Online archives and repository of the Gazette, Santa Clarita, California. http://www.oldtownnewhall.com/gazette/gazette1202-manzer.htm [Accessed 30 August 2010].

NCWD (Newhall County Water District). 2010. Online history. http://www.ncwd.org/history.htm [Accessed 30 August 2010].

Paulson, R. W., E. B. Chase, R. S. Roberts, and D. W. Moody. 1991. National water summary 1988–1989.

Schwartzberg, B. and P. Moore. 1995. A history of the Santa Clara River, Santa Clara River enhancement and management plan.

Slade, R. C. 1990. Assessment of hydrogeologic conditions within alluvial and stream terrace deposits, Acton area, Los Angeles County. Prepared for County of Los Angeles, Department of Public Works, and ASL Consulting Engineers.

Slade, R. C. and Associates. 2002. Hydrogeologic conditions in the alluvial and Saugus Formation aquifer systems. Volume I. Prepared for Santa Clarita Valley Water Purveyors.

U.S. Census Bureau. 2010a. Census of population and housing. Website. http://www.census.gov/prod/www/abs/decennial/index.html [Accessed 26 Aug 2010].

U.S. Census Bureau. 2010b. American fact finder. Website. http://factfinder.census.gov [Accessed 26 Aug 2010].

Worden, L. 1995. Prime Valencia real estate, $2 an acre. Online archives and repository of the Santa Clarita Valley Historical Society, Santa Clarita, California. http://www.scvhistory.com/scvhistory/signal/worden/lw060795.htm [Accessed 30 August 2010].

Worden, L. 1998. Where once was water. Online archives and repository of the Santa Clarita Valley Historical Society, Santa Clarita, California. http://www.scvhistory.com/scvhistory/sg081898.htm [Accessed 30 August 2010].

Appendix C

Cosmogenic Nuclide Sediment Dating
Laboratory Results

COSMOGENIC NUCLIDE SEDIMENT DATING LABORATORY RESULTS

A sediment dating analysis was performed as part of this study in order to provide accurate landscape erosion rates in select drainage areas of the USCR watershed. This appendix provides copies of the cosmogenic nuclide sediment dating results as issued by Dr. Cliff Riebe of the University of Wyoming (http://geology.uwyo.edu/?q=Dr.%20Cliff%20Riebe). Stillwater Sciences staff initially collected twelve sediment samples from various locations throughout the USCR watershed (see Figure 3-9 in the main report). Dr. Riebe processed the samples in his laboratory in order to extract quartz minerals (silica and oxygen) that contain concentrations of the cosmogenic nuclide-produced isotopes. During his preparation period, Dr. Riebe determined that two samples were unable to be further analyzed due to insufficient quartz content: "Unnamed Tributary Near Indian Canyon" (located on river's left side in Soledad Canyon, a few kilometers upstream from the Agua Dulce Canyon confluence) and "Aliso Canyon" (located on Aliso Canyon creek near the confluence with Beartrap Canyon). All ten of the remaining samples were fully prepared and subsequently analyzed for cosmogenic nuclide concentrations with an accelerator mass spectrometer (AMS) at the University of Purdue's PRIME laboratory (http://www.physics.purdue.edu/primelab/). One of these samples, Hasley Canyon, initially yielded insufficient concentrations to produce a viable sediment dating result, indicating that a re-preparation and subsequent re-analysis of this sample was warranted, which was accomplished some time later.

The available results from the PRIME laboratory were provided electronically to Dr. Riebe, who subsequently post-processed the raw results using a peer-reviewed online calculator to account for local watershed conditions (CRONUS: http://hess.ess.washington.edu/). The local conditions of interest are topography, hypsometry (ratio of relief to drainage area), and shielding factors (i.e., latitude and orientation to magnetic north).

The results as provided to us from Dr. Riebe are presented below in Figures C-1 through C-3. Figure C-1 presents the results from seven samples, including the original non-detectable results from the Hasley Canyon sample. Figure C-2 reports the detectable results from this sample's re-analysis. Figure C-3 reports the results from three samples, which required several rounds of processing due to the low concentrations of quartz in the parent materials. The details of the sediment dating analysis as utilized in this study are presented in Section 3.3.2 of the main report.

CRONUS-Earth ^{10}Be - ^{26}Al erosion rate calculator -- results

Version information --

Component	Version
Wrapper script:	2.2
Main calculator:	2.1
Objective function:	2.0
Constants:	2.2.1
Muons:	1.1

Comments:

Production rate calibration information: Using default calibration data set

^{10}Be results:

Results not dependent on spallogenic production rate model:				*Erosion rates -- constant production rate model:* Scaling scheme for spallation: Lal(1991) / Stone(2000)			
Sample name	Shielding factor	Production rate (muons) (atoms/g/yr)	Internal uncertainty (m/Myr)	Erosion rate (g/cm2/yr)	Erosion rate (m/Myr)	External uncertainty (m/Myr)	Production rate (spallation) (atoms/g/yr)
USCR_PICO	--	--	--	--	--	--	
USCR_PLUMCYN	--	--	--	--	--	--	
USCR_UNNAMEDELIZA	--	--	--	--	--	--	
USCR_ELIZABETH	--	--	--	--	--	--	
USCR_HASLEY	0.9900	0.219	85.31	0.09826	363.94	88.27	6.23
USCR_MAINSTEMEND	--	--	--	--	--	--	
USCR_GRASSHOPPER	--	--	--	--	--	--	

Erosion rates -- time-varying production models:

Scaling scheme for spallation:	Desilets and others (2003,2006)	Dunai (2001)	Lifton and others (2005)	Time-dependent Lal (1991)/Stone (2000)

Figure C-1a. Page 1 of the cosmogenic nuclide sediment dating results for the Pico Canyon, Plum Canyon, Unnamed Tributary to Elizabeth Lake Canyon, Elizabeth Lake Canyon, Hasley Canyon (non-detectable result), USCR at the County line, and Grasshopper Canyon samples.

Erosion rate results http://hess.ess.washington.edu/cgi-bin/matweb

Sample name	Erosion rate (g/cm2/yr)	Erosion rate (m/Myr)	External uncertainty (m/Myr)	Erosion rate (g/cm2/yr)	Erosion rate (m/Myr)	External uncertainty (m/Myr)	Erosion rate (g/cm2/yr)	Erosion rate (m/Myr)	External uncertainty (m/Myr)	Erosion rate (g/cm2/yr)	Erosion rate (m/Myr)	External uncertainty (m/Myr)
USCR_PICO	--	--	--	--	--	--	--	--	--	--	--	--
USCR_PLUMCYN	--	--	--	--	--	--	--	--	--	--	--	--
USCR_UNNAMEDELIZA	--	--	--	--	--	--	--	--	--	--	--	--
USCR_ELIZABETH	--	--	--	--	--	--	--	--	--	--	--	--
USCR_HASLEY	0.08787	325.45	80.47	0.08941	331.15	81.89	0.08850	327.78	79.99	0.09580	354.83	85.91
USCR_MAINSTEMEND	--	--	--	--	--	--	--	--	--	--	--	--
USCR_GRASSHOPPER	--	--	--	--	--	--	--	--	--	--	--	--

^{26}*Al results:*

	Results not dependent on spallogenic production rate model:			*Erosion rates -- constant production rate model:*			
				Scaling scheme for spallation: Lal(1991) / Stone(2000)			
Sample name	Shielding factor	Production rate (muons) (atoms/g/yr)	Internal uncertainty (m/Myr)	Erosion rate (g/cm2/yr)	Erosion rate (m/Myr)	External uncertainty (m/Myr)	Production rate (spallation) (atoms/g/yr)
USCR_PICO	0.9900	1.941	1308.10	0.61598	2281.40	1315.46	48.18
USCR_PLUMCYN	0.9900	1.854	58.95	0.07304	270.53	61.25	43.44
USCR_UNNAMEDELIZA	0.9900	2.080	81.00	0.06523	241.58	82.46	56.68
USCR_ELIZABETH	0.9900	2.202	72.99	0.05447	201.75	74.18	64.60
USCR_HASLEY	--	--	--	--	--	--	
USCR_MAINSTEMEND	0.9900	2.202	232.04	0.20011	741.14	236.85	64.42
USCR_GRASSHOPPER	0.9900	1.855	203.86	0.10787	399.51	205.32	43.55

Erosion rates -- time-varying production models:

Scaling scheme for spallation:	Desilets and others (2003,2006)			Dunai (2001)			Lifton and others (2005)			Time-dependent Lal (1991)/Stone (2000)		
Sample name	Erosion rate (g/cm2/yr)	Erosion rate (m/Myr)	External uncertainty (m/Myr)	Erosion rate (g/cm2/yr)	Erosion rate (m/Myr)	External uncertainty (m/Myr)	Erosion rate (g/cm2/yr)	Erosion rate (m/Myr)	External uncertainty (m/Myr)	Erosion rate (g/cm2/yr)	Erosion rate (m/Myr)	External uncertainty (m/Myr)
USCR_PICO	0.58443	2164.55	1252.46	0.58858	2179.91	1261.30	0.58903	2181.60	1259.44	0.62001	2296.35	1323.73
USCR_PLUMCYN	0.06591	244.12	56.50	0.06696	247.99	57.39	0.06642	245.99	56.15	0.07155	265.00	59.91
USCR_UNNAMEDELIZA	0.05936	219.84	76.01	0.06010	222.59	76.94	0.05992	221.92	76.14	0.06395	236.85	80.80
USCR_ELIZABETH	0.05001	185.21	68.94	0.05054	187.19	69.66	0.05055	187.23	69.18	0.05362	198.59	72.98

2 of 3 2/18/2011 01:57

Figure C-1b. Page 2 of the cosmogenic nuclide sediment dating results for the Pico Canyon, Plum Canyon, Unnamed Tributary to Elizabeth Lake Canyon, Elizabeth Lake Canyon, Hasley Canyon (non-detectable result), USCR at the County line, and Grasshopper Canyon samples.

USCR_HASLEY	--	--	--	--	--	--	--	--	--	--	--	--
USCR_MAINSTEMEND	0.18365	680.19	220.35	0.18564	687.57	222.70	0.18517	685.81	220.22	0.19549	724.03	231.16
USCR_GRASSHOPPER	0.09705	359.45	185.75	0.09864	365.32	188.74	0.09771	361.89	186.50	0.10520	389.65	200.25

(No Al-26 / Be-10 plot)

^{26}Al/^{10}Be ratios (relative to 07KNSTD!):

Sample	^{26}Al/^{10}Be ratio
USCR_PICO	--
USCR_PLUMCYN	--
USCR_UNNAMEDELIZA	--
USCR_ELIZABETH	--
USCR_HASLEY	--
USCR_MAINSTEMEND	--
USCR_GRASSHOPPER	--

Solver diagnostics:

Sample name:	Nuclide	fzero output status	Objective function value (atoms)	Solution time (s)	P_mu(z) calculation time (s)
USCR_PICO	Be-10	--	--	--	--
	Al-26	1 1 1 1 1	-2.01e-09 -5.69e-07 -3.3e-07 -2.77e-07 -5.02e-10	0.01 0.13 0.02 0.02 0.02	0.69
USCR_PLUMCYN	Be-10	--	--	--	--
	Al-26	1 1 1 1 1	-0.00676 0.00191 0.000206 0.000753 -1.79e-07	0.01 0.02 0.02 0.02 0.02	0.64
USCR_UNNAMEDELIZA	Be-10	--	--	--	--
	Al-26	1 1 1 1 1	2e-05 4.32e-06 0.000622 0.00502 0.00113	0.01 0.02 0.02 0.02 0.02	0.69
USCR_ELIZABETH	Be-10	--	--	--	--
	Al-26	1 1 1 1 1	0.00802 0.00087 0.000228 0.000221 0.0341	0.01 0.02 0.02 0.02 0.02	0.69
USCR_HASLEY	Be-10	1 1 1 1 1	-1.37e-07 -6.02e-09 -0.000101 -2.86e-09 0.000454	0.01 0.02 0.02 0.02 0.02	0.64
	Al-26	--	--	--	--
USCR_MAINSTEMEND	Be-10	--	--	--	--
	Al-26	1 1 1 1 1	0.000144 5.34e-06 -0.00179 3.83e-07 0.00272	0.01 0.02 0.02 0.02 0.02	0.69
USCR_GRASSHOPPER	Be-10	--	--	--	--
	Al-26	1 1 1 1 1	-0.00764 0.000689 4.04e-05 0.000262 -8.01e-08	0.01 0.02 0.02 0.02 0.03	0.64

Figure C-1c. Page 3 of the cosmogenic nuclide sediment dating results for the Pico Canyon, Plum Canyon, Unnamed Tributary to Elizabeth Lake Canyon, Elizabeth Lake Canyon, Hasley Canyon (non-detectable result), USCR at the County line, and Grasshopper Canyon samples.

CRONUS-Earth ^{10}Be - ^{26}Al erosion rate calculator -- results

Version information --	Component	Version
	Wrapper script:	2.2
	Main calculator:	2.1
	Objective function:	2.0
	Constants:	2.2.1
	Muons:	1.1

Comments:

Production rate calibration information: Using default calibration data set

^{10}Be results:

Results not dependent on spallogenic production rate model: / *Erosion rates -- constant production rate model:*

Scaling scheme for spallation: Lal(1991) / Stone(2000)

Sample name	Shielding factor	Production rate (muons) (atoms/g/yr)	Internal uncertainty (m/Myr)	Erosion rate (g/cm2/yr)	Erosion rate (m/Myr)	External uncertainty (m/Myr)	Production rate (spallation) (atoms/g/yr)
HASLEY	0.9900	0.219	85.31	0.09826	363.94	88.27	6.23

Erosion rates -- time-varying production models:

Scaling scheme for spallation:	Desilets and others (2003,2006)			Dunai (2001)			Lifton and others (2005)			Time-dependent Lal (1991)/Stone (2000)		
Sample name	Erosion rate (g/cm2/yr)	Erosion rate (m/Myr)	External uncertainty (m/Myr)	Erosion rate (g/cm2/yr)	Erosion rate (m/Myr)	External uncertainty (m/Myr)	Erosion rate (g/cm2/yr)	Erosion rate (m/Myr)	External uncertainty (m/Myr)	Erosion rate (g/cm2/yr)	Erosion rate (m/Myr)	External uncertainty (m/Myr)
HASLEY	0.08787	325.45	80.47	0.08941	331.15	81.89	0.08850	327.78	79.99	0.09580	354.83	85.91

Figure C-2a. Page 1 of the cosmogenic nuclide sediment dating results for the Hasley Canyon sample.

^{26}*Al results:*

Results not dependent on spallogenic production rate model:				*Erosion rates -- constant production rate model:* Scaling scheme for spallation: Lal(1991) / Stone(2000)			
Sample name	Shielding factor	Production rate (muons) (atoms/g/yr)	Internal uncertainty (m/Myr)	Erosion rate (g/cm2/yr)	Erosion rate (m/Myr)	External uncertainty (m/Myr)	Production rate (spallation) (atoms/g/yr)
HASLEY	--	--	--	--	--	--	

Erosion rates -- time-varying production models:

Scaling scheme for spallation:	Desilets and others (2003,2006)			Dunai (2001)			Lifton and others (2005)			Time-dependent Lal (1991)/Stone (2000)		
Sample name	Erosion rate (g/cm2/yr)	Erosion rate (m/Myr)	External uncertainty (m/Myr)	Erosion rate (g/cm2/yr)	Erosion rate (m/Myr)	External uncertainty (m/Myr)	Erosion rate (g/cm2/yr)	Erosion rate (m/Myr)	External uncertainty (m/Myr)	Erosion rate (g/cm2/yr)	Erosion rate (m/Myr)	External uncertainty (m/Myr)
HASLEY	--	--	--	--	--	--	--	--	--	--	--	--

(No Al-26 / Be-10 plot)

^{26}Al/^{10}Be ratios (relative to 07KNSTD!):

Sample	^{26}Al/^{10}Be ratio
HASLEY	--

Solver diagnostics:

Sample name:	Nuclide	fzero output status	Objective function value (atoms)	Solution time (s)	P_mu(z) calculation time (s)
HASLEY	Be-10	1 1 1 1 1	-1.37e-07 -6.02e-09 -0.000101 -2.86e-09 0.000454	0.01 0.13 0.03 0.03 0.02	0.67
	Al-26	--	--	--	--

Figure C-2b. Page 2 of the cosmogenic nuclide sediment dating results for the Hasley Canyon sample.

CRONUS-Earth ^{10}Be - ^{26}Al erosion rate calculator -- results

Version information --	Component	Version
	Wrapper script:	2.2
	Main calculator:	2.1
	Objective function:	2.0
	Constants:	2.2.1
	Muons:	1.1

Comments:

Production rate calibration information: Using default calibration data set

^{10}Be results:

Results not dependent on spallogenic production rate model: | *Erosion rates -- constant production rate model:*

Scaling scheme for spallation: Lal(1991) / Stone(2000)

Sample name	Shielding factor	Production rate (muons) (atoms/g/yr)	Internal uncertainty (m/Myr)	Erosion rate (g/cm2/yr)	Erosion rate (m/Myr)	External uncertainty (m/Myr)	Production rate (spallation) (atoms/g/yr)
USCR_HASKELL_11122009	0.9900	0.236	13.10	0.02869	106.28	14.83	7.44
USCR_USCRCYN_09122009	0.9900	0.277	76.57	0.05592	207.12	77.86	10.74
USCR_INDIAN_09122009	0.9900	0.259	60.67	0.05709	211.45	62.27	9.15

Erosion rates -- time-varying production models:

Scaling scheme for spallation:	Desilets and others (2003,2006)			Dunai (2001)			Lifton and others (2005)			Time-dependent Lal (1991)/Stone (2000)		
Sample name	Erosion rate (g/cm2/yr)	Erosion rate (m/Myr)	External uncertainty (m/Myr)	Erosion rate (g/cm2/yr)	Erosion rate (m/Myr)	External uncertainty (m/Myr)	Erosion rate (g/cm2/yr)	Erosion rate (m/Myr)	External uncertainty (m/Myr)	Erosion rate (g/cm2/yr)	Erosion rate (m/Myr)	External uncertainty (m/Myr)
USCR_HASKELL_11122009	0.02651	98.19	14.69	0.02694	99.77	14.93	0.02687	99.53	14.23	0.02869	106.24	14.74
USCR_USCRCYN_09122009	0.05139	190.35	72.43	0.05187	192.09	73.08	0.05199	192.54	72.69	0.05499	203.67	76.49
USCR_INDIAN_09122009	0.05210	192.97	57.85	0.05272	195.24	58.52	0.05266	195.05	57.79	0.05612	207.84	61.12

^{26}Al results:

Results not dependent on spallogenic production rate model: | *Erosion rates -- constant production rate model:*

Scaling scheme for spallation: Lal(1991) / Stone(2000)

Sample name	Shielding factor	Production rate (muons) (atoms/g/yr)	Internal uncertainty (m/Myr)	Erosion rate (g/cm2/yr)	Erosion rate (m/Myr)	External uncertainty (m/Myr)	Production rate (spallation) (atoms/g/yr)
USCR_HASKELL_11122009	--	--	--	--	--	--	
USCR_USCRCYN_09122009	--	--	--	--	--	--	
USCR_INDIAN_09122009	--	--	--	--	--	--	

Erosion rates -- time-varying production models:

Figure C-3a. Page 1 of the cosmogenic nuclide sediment dating results for the Haskell Canyon, USCR in Soledad Canyon, and Indian Canyon samples.

Scaling scheme for spallation:	Desilets and others (2003,2006)			Dunai (2001)			Lifton and others (2005)			Time-dependent Lal (1991)/Stone (2000)		
Sample name	Erosion rate (g/cm2/yr)	Erosion rate (m/Myr)	External uncertainty (m/Myr)	Erosion rate (g/cm2/yr)	Erosion rate (m/Myr)	External uncertainty (m/Myr)	Erosion rate (g/cm2/yr)	Erosion rate (m/Myr)	External uncertainty (m/Myr)	Erosion rate (g/cm2/yr)	Erosion rate (m/Myr)	External uncertainty (m/Myr)
USCR_HASKELL_11122009	--	--	--	--	--	--	--	--	--	--	--	--
USCR_USCRCYN_09122009	--	--	--	--	--	--	--	--	--	--	--	--
USCR_INDIAN_09122009	--	--	--	--	--	--	--	--	--	--	--	--

(No Al-26 / Be-10 plot)

$^{26}Al/^{10}Be$ ratios (relative to 07KNSTD!):

Sample	$^{26}Al/^{10}Be$ ratio
USCR_HASKELL_11122009	--
USCR_USCRCYN_09122009	--
USCR_INDIAN_09122009	--

Solver diagnostics:

Sample name:	Nuclide	fzero output status	Objective function value (atoms)	Solution time (s)	P_mu(z) calculation time (s)
USCR_HASKELL_11122009	Be-10	1 1 1 1 1	0.00113 4.59e-05 -0.016 -0.00244 0.00137	0.01 0.12 0.02 0.02 0.03	0.71
	Al-26	--	--	--	--
USCR_USCRCYN_09122009	Be-10	1 1 1 1 1	2.06e-06 5.64e-06 9.81e-07 -0.0036 5.77e-05	0.01 0.02 0.02 0.02 0.02	0.72
	Al-26	--	--	--	--
USCR_INDIAN_09122009	Be-10	1 1 1 1 1	-0.0025 7.16e-05 0.000997 0.00109 9.1e-05	0.01 0.02 0.02 0.02 0.02	0.70
	Al-26	--	--	--	--

Figure C-3b. Page 2 of the cosmogenic nuclide sediment dating results for the Haskell Canyon, USCR in Soledad Canyon, and Indian Canyon samples.

REFERENCES

Desilets, D., and M. Zreda. 2003. Spatial and temporal distribution of secondary cosmic-ray nucleon intensities and applications to in situ cosmogenic dating. Earth and Planetary Science Letters 206: 21–42.

Desilets, D., M. Zreda, and T. Prabu. 2006. Extended scaling factors for in situ cosmogenic nuclides: new measurements at low latitude. Earth and Planetary Science Letters 246: 265–276.

Dunai, T. J. 2001. Influence of secular variation of the geomagnetic field on production rates of in situ produced cosmogenic nuclides. Earth and Planetary Science Letters 193: 197–212.

Lifton, N. A., J. W. Bieber, J. M. Clem, M. L. Duldig, P. Evenson, J. E. Humble, and R. Pyle. 2005. Addressing solar modulation and long-term uncertainties in scaling secondary cosmic rays for in situ cosmogenic nuclide applications. Earth and Planetary Science Letters 239: 140–161.

Lal, D. 1991. Cosmic ray labeling of erosion surfaces: in situ nuclide production rates and erosion models. Earth Planetary Science Letters 104: 424–439.

Stone, J. O. 2000. Air pressure and cosmogenic isotope production. Journal of Geophysical Research 105: 23753–23759.

Appendix D

Debris Basin and Reservoir Sedimentation Records

DEBRIS BASIN AND RESERVOIR SEDIMENTATION RECORDS

This appendix provides the source data of sedimentation rates recorded in Los Angeles County Department of Public Works (LADPW) operated debris basins in the USCR watershed, Los Angeles County Department of Water and Power (LADWP) operated debris basins at Castaic Powerplant, and LADWP operated Bouquet Canyon Reservoir. All data were provided to us by early 2010 and represent the most current information available. Data from the LADPW debris basins were provided by Mr. Martin Araiza, engineer with LADPW (Table D-1). Data from the LADWP Castaic Powerplant debris basins were provided by Ms. Gloria Wu, technical staff member with LADWP (Table D-2). Finally, data from Bouquet Canyon Reservoir was provided by WICP ACWI (2010) (Figure D-1).

These sedimentation data were used in our analysis of sediment yields in the USCR watershed (see Section 3.3.3 of the main report), with the exception of debris basins “Knoll” and “Line ‘A’” which were not used because their periods of record were for only one year. The sedimentation data from Bouquet Canyon Reservoir was subsequently refined by Minear and Kondolf (2009) in order to better account for reservoir trapping efficiencies and more appropriate sediment density conversions.

The locations of the debris basins and reservoir structures are shown in Figure 3-10 of the main report. Additional information on the LADPW debris basins is provided in LADPW (2006).

Table D-1. Sedimentation records of the LADPW-operated debris basins located in the USCR watershed.

Debris basin name	Season	Water year	Cubic yards removed	Cubic meters removed
CROCKER	1982–83	1983	0.0	0.0
CROCKER	1983–84	1984	0.0	0.0
CROCKER	1984–85	1985	0.0	0.0
CROCKER	1985–86	1986	0.0	0.0
CROCKER	1986–87	1987	0.0	0.0
CROCKER	1987–88	1988	0.0	0.0
CROCKER	1988–89	1989	0.0	0.0
CROCKER	1989–90	1990	0.0	0.0
CROCKER	1990–91	1991	0.0	0.0
CROCKER	1991–92	1992	5865.0	4486.7
CROCKER	1992–93	1993	2707.0	2070.9
CROCKER	1993–94	1994	0.0	0.0
CROCKER	1994–95	1995	4864.0	3721.0
CROCKER	1995–96	1996	0.0	0.0
CROCKER	1996–97	1997	0.0	0.0
CROCKER	1997–98	1998	300.0	229.5
CROCKER	1998–99	1999	0.0	0.0
CROCKER	1999–00	2000	0.0	0.0
CROCKER	2000–01	2001	90.0	68.9
CROCKER	2001–02	2002	0.0	0.0
CROCKER	2002–03	2003	0.0	0.0
CROCKER	2003–04	2004	0.0	0.0
CROCKER	2004–05	2005	0.0	0.0
CROCKER	2005–06	2006	0.0	0.0

Debris basin name	Season	Water year	Cubic yards removed	Cubic meters removed
CROCKER	2006–07	2007	0.0	0.0
CROCKER	2007–08	2008	0.0	0.0
KNOLL	2004–05	2005	10250.0	7841.3
LINE "A"	2004–05	2005	683.0	522.5
MARSTON/PARAGON	1988–89	1989	0.0	0.0
MARSTON/PARAGON	1989–90	1990	879.0	672.4
MARSTON/PARAGON	1990–91	1991	0.0	0.0
MARSTON/PARAGON	1991–92	1992	0.0	0.0
MARSTON/PARAGON	1992–93	1993	0.0	0.0
MARSTON/PARAGON	1993–94	1994	130.0	99.5
MARSTON/PARAGON	1994–95	1995	140.0	107.1
MARSTON/PARAGON	1995–96	1996	0.0	0.0
MARSTON/PARAGON	1996–97	1997	0.0	0.0
MARSTON/PARAGON	1997–98	1998	0.0	0.0
MARSTON/PARAGON	1998–99	1999	0.0	0.0
MARSTON/PARAGON	1999–00	2000	0.0	0.0
MARSTON/PARAGON	2000–01	2001	0.0	0.0
MARSTON/PARAGON	2001–02	2002	800.0	612.0
MARSTON/PARAGON	2002–03	2003	0.0	0.0
MARSTON/PARAGON	2003–04	2004	0.0	0.0
MARSTON/PARAGON	2004–05	2005	0.0	0.0
MARSTON/PARAGON	2005–06	2006	0.0	0.0
MARSTON/PARAGON	2006–07	2007	0.0	0.0
MARSTON/PARAGON	2007–08	2008	0.0	0.0
OAKDALE	2004–05	2005	72744.0	55649.2
OAKDALE	2005–06	2006	0.0	0.0
OAKDALE	2006–07	2007	0.0	0.0
OAKDALE	2007–08	2008	0.0	0.0
OAKDALE	2008–09	2009	7600.0	5814.0
SADDLEBACK	1990–91	1991	0.0	0.0
SADDLEBACK	1991–92	1992	0.0	0.0
SADDLEBACK	1992–93	1993	20.0	15.3
SADDLEBACK	1993–94	1994	0.0	0.0
SADDLEBACK	1994–95	1995	2440.0	1866.6
SADDLEBACK	1995–96	1996	1060.0	810.9
SADDLEBACK	1996–97	1997	0.0	0.0
SADDLEBACK	1997–98	1998	0.0	0.0
SADDLEBACK	1998–99	1999	0.0	0.0
SADDLEBACK	1999–00	2000	0.0	0.0
SADDLEBACK	2000–01	2001	990.0	757.4
SADDLEBACK	2001–02	2002	0.0	0.0
SADDLEBACK	2002–03	2003	0.0	0.0
SADDLEBACK	2003–04	2004	0.0	0.0
SADDLEBACK	2004–05	2005	0.0	0.0
SADDLEBACK	2005–06	2006	0.0	0.0
SADDLEBACK	2006–07	2007	0.0	0.0
SADDLEBACK	2007–08	2008	0.0	0.0
SHADOW	1994–95	1995	0.0	0.0
SHADOW	1995–96	1996	0.0	0.0
SHADOW	1996–97	1997	0.0	0.0

Debris basin name	Season	Water year	Cubic yards removed	Cubic meters removed
SHADOW	1997–98	1998	0.0	0.0
SHADOW	1998–99	1999	0.0	0.0
SHADOW	1999–00	2000	0.0	0.0
SHADOW	2000–01	2001	0.0	0.0
SHADOW	2001–02	2002	0.0	0.0
SHADOW	2002–03	2003	5370.0	4108.1
SHADOW	2003–04	2004	0.0	0.0
SHADOW	2004–05	2005	12120.0	9271.8
VICTORIA	2002–03	2003	0.0	0.0
VICTORIA	2003–04	2004	0.0	0.0
VICTORIA	2004–05	2005	32208.0	24639.1
VICTORIA	2005–06	2006	0.0	0.0
VICTORIA	2006–07	2007	0.0	0.0
VICTORIA	2007–08	2008	0.0	0.0
VICTORIA	2008–09	2009	2670.0	2042.6
WEDGEWOOD	2001–02	2002	0.0	0.0
WEDGEWOOD	2002–03	2003	0.0	0.0
WEDGEWOOD	2003–04	2004	0.0	0.0
WEDGEWOOD	2004–05	2005	0.0	0.0
WEDGEWOOD	2004–06	2006	1611.0	1232.4
WHITNEY	2000–01	2001	0.0	0.0
WHITNEY	2001–02	2002	0.0	0.0
WHITNEY	2002–03	2003	0.0	0.0
WHITNEY	2003–04	2004	0.0	0.0
WHITNEY	2004–05	2005	1540.0	1178.1
WILDWOOD	1967–68	1968	2092.0	1600.4
WILDWOOD	1968–69	1969	15986.0	12229.3
WILDWOOD	1969–70	1970	1199.0	917.2
WILDWOOD	1970–71	1971	4830.0	3695.0
WILDWOOD	1971–72	1972	201.0	153.8
WILDWOOD	1972–73	1973	4013.0	3069.9
WILDWOOD	1973–74	1974	1422.0	1087.8
WILDWOOD	1974–75	1975	286.0	218.8
WILDWOOD	1975–76	1976	0.0	0.0
WILDWOOD	1976–77	1977	1020.0	780.3
WILDWOOD	1977–78	1978	16699.0	12774.7
WILDWOOD	1978–79	1979	4433.0	3391.2
WILDWOOD	1979–80	1980	13558.0	10371.9
WILDWOOD	1980–81	1981	933.0	713.7
WILDWOOD	1981–82	1982	549.0	420.0
WILDWOOD	1982–83	1983	5527.0	4228.2
WILDWOOD	1983–84	1984	0.0	0.0
WILDWOOD	1984–85	1985	0.0	0.0
WILDWOOD	1985–86	1986	0.0	0.0
WILDWOOD	1986–87	1987	0.0	0.0
WILDWOOD	1987–88	1988	911.0	696.9
WILDWOOD	1988–89	1989	0.0	0.0
WILDWOOD	1989–90	1990	0.0	0.0
WILDWOOD	1990–91	1991	0.0	0.0
WILDWOOD	1991–92	1992	13185.0	10086.5

Debris basin name	Season	Water year	Cubic yards removed	Cubic meters removed
WILDWOOD	1992–93	1993	4706.0	3600.1
WILDWOOD	1993–94	1994	0.0	0.0
WILDWOOD	1994–95	1995	5560.0	4253.4
WILDWOOD	1995–96	1996	0.0	0.0
WILDWOOD	1996–97	1997	0.0	0.0
WILDWOOD	1997–98	1998	13500.0	10327.5
WILDWOOD	1998–99	1999	0.0	0.0
WILDWOOD	1999–00	2000	0.0	0.0
WILDWOOD	2000–01	2001	1260.0	963.9
WILDWOOD	2001–02	2002	0.0	0.0
WILDWOOD	2002–03	2003	0.0	0.0
WILDWOOD	2003–04	2004	0.0	0.0
WILDWOOD	2004–05	2005	0.0	0.0
WILDWOOD	2005–06	2006	11983.0	9167.0
WILDWOOD	2006–07	2007	0.0	0.0
WILDWOOD	2007–08	2008	0.0	0.0
WILLAM S HART	1983–84	1984	0.0	0.0
WILLAM S HART	1984–85	1985	0.0	0.0
WILLAM S HART	1985–86	1986	321.0	245.6
WILLAM S HART	1986–87	1987	0.0	0.0
WILLAM S HART	1987–88	1988	0.0	0.0
WILLAM S HART	1988–89	1989	0.0	0.0
WILLAM S HART	1989–90	1990	0.0	0.0
WILLAM S HART	1990–91	1991	0.0	0.0
WILLAM S HART	1991–92	1992	0.0	0.0
WILLAM S HART	1992–93	1993	0.0	0.0
WILLAM S HART	1993–94	1994	0.0	0.0
WILLAM S HART	1994–95	1995	97.0	74.2
WILLAM S HART	1995–96	1996	0.0	0.0
WILLAM S HART	1996–97	1997	0.0	0.0
WILLAM S HART	1997–98	1998	0.0	0.0
WILLAM S HART	1998–99	1999	0.0	0.0
WILLAM S HART	1999–00	2000	0.0	0.0
WILLAM S HART	2000–01	2001	72.0	55.1
WILLAM S HART	2001–02	2002	0.0	0.0
WILLAM S HART	2002–03	2003	0.0	0.0
WILLAM S HART	2003–04	2004	0.0	0.0
WILLAM S HART	2004–05	2005	0.0	0.0
WILLAM S HART	2005–06	2006	0.0	0.0
WILLAM S HART	2006–07	2007	0.0	0.0
WILLAM S HART	2007–08	2008	0.0	0.0
YUCCA	1996–97	1997	0.0	0.0
YUCCA	1997–98	1998	0.0	0.0
YUCCA	1998–99	1999	0.0	0.0
YUCCA	1999–00	2000	2447.0	1872.0
YUCCA	2000–01	2001	0.0	0.0
YUCCA	2001–02	2002	0.0	0.0
YUCCA	2002–03	2003	0.0	0.0
YUCCA	2003–04	2004	0.0	0.0

Debris basin name	Season	Water year	Cubic yards removed	Cubic meters removed
YUCCA	2004–05	2005	4661.0	3565.7

Source: LADPW (M. Araiza, pers. comm., 2010), data presented as received with an addition of the extraction volume also reported in cubic meters per year

Table D-2. Sedimentation records of the LADWP-operated debris basins located at the Castaic Powerplant.

Rainfall Year	Rainfall (inch)	FY	#	Basin 1	Basin 2	Basin 3	Below CD3	Tailrace	Reservoir	Unspecified Location	TOTAL (CY)	Comments
74-75		75-76									0	
75-76		76-77									0	
76-77		77-78									0	
77-78	25.00	78-79	1								0	
78-79	25.96	79-80	1								0	
79-80	23.27	80-81	1						326,926		326,926	
80-81	0.00	81-82	1								0	No Rainfall info
81-82	10.78	82-83	1								0	
82-83	28.28	83-84	1		95,000						95,000	
83-84	11.30	84-85	1								0	
84-85	8.92	85-86	1				20,049	232,878			252,927	
85-86	22.91	86-87	1								0	
86-87	8.23	87-88	1								0	
87-88	15.33	88-89	1							83,000	83,000	
88-89	6.31	89-90	1								0	
89-90	8.26	90-91	1								0	
90-91	15.45	91-92	1								0	
91-92	33.13	92-93	1							40,000	40,000	
92-93	45.61	93-94	1								0	
93-94	14.67	94-95	1	54,100	54,260	53,900				25,000	187,260	
94-95	45.45	95-96	1				x	x		166,450	166,450	
95-96	15.01	96-97	1	74,175	53,250	113,775					241,200	
96-97	19.84	97-98	1	44,410	12,600	0					57,010	
97-98	43.55	98-99	1	65,162	56,469	96,819					218,450	
98-99	10.98	99-00	1								0	
99-00	15.49	00-01	1								0	Rev. on 7/26/2010
00-01	22.09	01-02	1								0	
01-02	6.79	02-03	1								0	
02-03	16.06	03-04	1								0	
03-04	11.60	04-05	1								0	
04-05	55.15	05-06	1	56,500	120,325	119,225					296,050	
05-06	16.84	06-07	1					208,350		Tailbay	208,350	There is ~1M CY of sedimentation near the edge of reservoir at the conflence of Bypass Channel & Tailrace Channel
06-07	6.24		1								0	
07-08	17.75		1								0	
08-09	14.18	09-10	1	134,450	70,345	40,370					245,165	
09-10	22.43		1								0	No work plan this year

Source: LADWP (G. Wu, pers. comm., 2010), table image from original .pdf

U.S. DEPARTMENT OF AGRICULTURE
RESERVOIR SEDIMENTATION DATA SUMMARY

Bouquet Canyon Reservoir 1/ (NAME OF RESERVOIR)

SOIL CONSERVATION SERVICE
70-7 (DATA SHEET NO.)

DAM

1. OWNER City of Los Angeles	2. RIVER Bouquet Creek	3. STATE California
4. SEC. 29 TWP. 6 N RANGE 14 W	5. NEAREST TOWN San Fernando	6. COUNTY Los Angeles
7. STREAM BED ELEV. 2,818	8. TOP OF DAM ELEV. 3,008	9. SPILLWAY CREST ELEV. 2,993

RESERVOIR

10. STORAGE ALLOCATION	11. ELEVATION TOP OF POOL	12. SURFACE AREA ACRES	13. STORAGE ACRE-FEET	14. ACCUMULATED ACRE-FEET	15. DATE STORAGE BEGAN
a. FLOOD CONTROL					March 1934
b. POWER					
c. WATER SUPPLY	2,993	628	36,500	36,500	16. DATE NORMAL OPER. BEGAN
d. IRRIGATION					
e. CONSERVATION					
f. INACTIVE					

17. LENGTH OF RESERVOIR 2.6 MILES | AV. WIDTH OF RESERVOIR 0.47 MILES

WATERSHED

18. TOTAL DRAINAGE AREA 12.6 SQ. MI.	22. MEAN ANNUAL PRECIPITATION 15 INCHES
19. NET SEDIMENT CONTRIBUTING AREA 11.6 SQ. MI.	23. MEAN ANNUAL RUNOFF INCHES
20. LENGTH MILES | AV. WIDTH MILES	24. MEAN ANNUAL RUNOFF AC.-FT.
21. MAX. ELEV. 4,975 | MIN. ELEV. 2,818	25. CLIMATIC CLASSIFICATION Semi-arid

SURVEY DATA

26. DATE OF SURVEY	27. PERIOD YEARS	28. ACCL. YEARS	29. TYPE OF SURVEY	30. NO. OF RANGES OR CONTOUR INT.	31. SURFACE AREA ACRES	32. CAPACITY ACRE-FEET	33. C/W RATIO AC.-FT. PER SQ. MI.
March 1934	-	-	-	-	628	36,500	2,897
June 1939	5 2/	5	Range Recon.	8	628	36,436	2,892

26. DATE OF SURVEY	34. PERIOD ANNUAL PRECIPITATION	35. PERIOD WATER INFLOW ACRE-FEET: a. MEAN ANNUAL	b. MAX. ANNUAL	c. PERIOD TOTAL	36. WATER INFL. TO DATE AC-FT.: a. MEAN ANNUAL	b. TOTAL TO DATE

26. DATE OF SURVEY	37. PERIOD SEDIMENT DEPOSITS ACRE-FEET: a. PERIOD TOTAL	b. AV. ANNUAL	c. PER SQ. MI.-YEAR	38. TOTAL SED. DEPOSITS TO DATE ACRE-FEET: a. TOTAL TO DATE	b. AV. ANNUAL	c. PER SQ. MI.-YEAR
June 1939	64	12.8	1.10	64	12.8	1.10

26. DATE OF SURVEY	39. AV. DRY WGT. LBS. PER CU. FT.	40. SED. DEP. TONS PER SQ. MI.-YR.: a. PERIOD	b. TOTAL TO DATE	41. STORAGE LOSS PCT.: a. AV. ANNUAL	b. TOT. TO DATE	42. SED. INFLOW PPM: a. PERIOD	b. TOT. TO DATE
June 1939	40*	958	958	0.04	0.18		

1/ Regulating and storage reservoir on Owens Valley aqueduct.
2/ Based on runoff seasons
* Assumed

Figure D-1. Sedimentation record of Bouquet Canyon Reservoir. (Source: Water Information Coordination Program, Advisory Committee on Water Information, http://ida.water.usgs.gov/ressed/datasheets/70-7.pdf)

REFERENCES

Araiza, M. 2010. Engineer, LADPW. E-mail correspondence with B. Amerson, Stillwater Sciences, providing debris basin data.

LADPW. 2006. Sedimentation manual, 2^{nd} Edition. Prepared by LADPW, Water Resources Division.

Minear, T. and G. M. Kondolf. 2009. Estimating reservoir sedimentation rates at large spatial and temporal scales: a case study of California. Water Resources Research, doi: 10.1029/2007WR006703.

WICP ACWI (Water Information Coordination Program, Advisory Committee on Water Information, Subcommittee on Sedimentation). 2010. Reservoir Sedimentation (RESSED) Database. Website. http://ida.water.usgs.gov/ressed/index.cfm [Accessed 11 Nov 2009].

Wu, G. 2010. Staff, LADWP, Power System. E-mail correspondence with G. Leverich, Stillwater Sciences, providing sedimentation records for Castaic Powerplant debris basins.

Appendix E

Bulk Sediment Size Analysis Results

BULK SEDIMENT SIZE ANALYSIS RESULTS

This appendix provides copies of the results and laboratory reports for the bulk sediment samples collected throughout the USCR watershed for this study. The locations of the samples are shown in Figure 4-13 of the main report. These data were used to assess the sediment character in the Feasibility Study reaches (see Section 4.3.1 and 4.3.2 in the main report and Appendix F). Figure E-1 is a plot of all sample data. Laboratory reports for each sample are presented below.

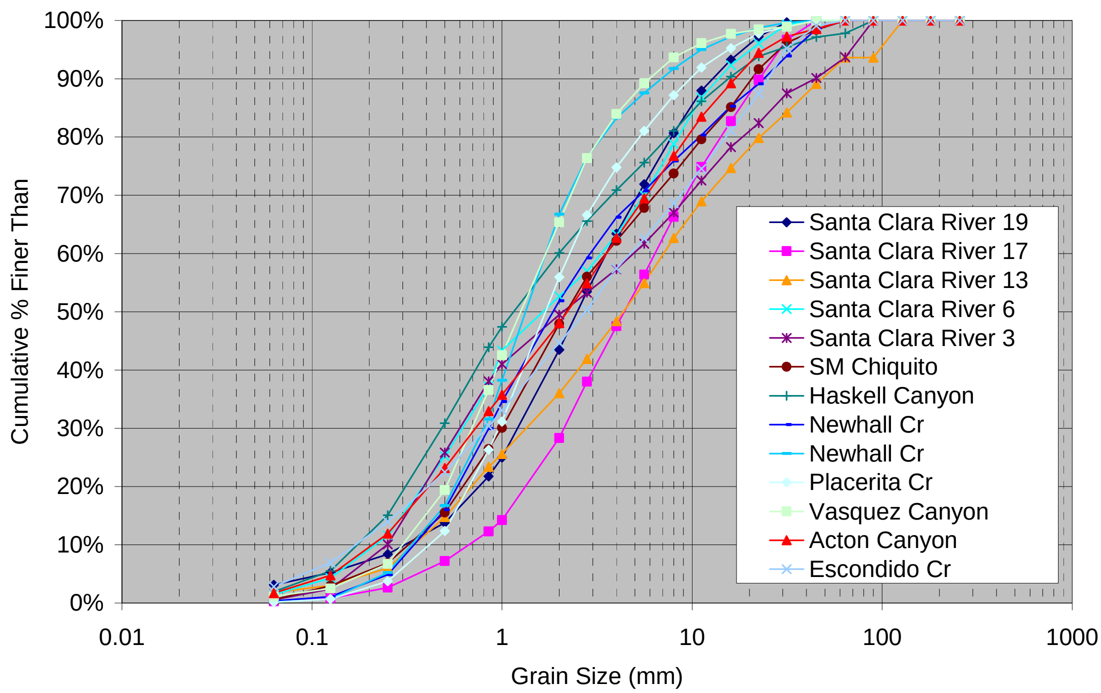

Figure E-1. Summary plot of all thirteen bulk sediment sample size distributions.

GMA GRAHAM MATTHEWS & ASSOCIATES

5435 Erickson Wy. Suite 1
Arcata, CA 95521
(707) 825-6681 voice

Hydrology -- Geomorphology -- Stream Restoration

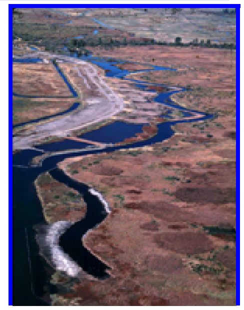

April 2010 Bulk Sample Processing
Laboratory Analysis Report

Graham Matthews & Associates coarse sediment laboratory was contracted to perform particle size analyses of bulk sediment samples collected by Stillwater Sciences. In April 2010, GMA laboratory received 13 samples, consisting of 22 buckets for particle size analysis.

Analysis of the samples was completed following GMA's standard operating procedures, as outlined in GMA's Coarse Sediment Laboratory Quality Assurance Program Manual, which can be made available upon request.

Completed data forms were transferred to John Wooster, via e-mail, on April 28, 2010. Please feel free to contact me with any questions regarding the processed samples.

Brooke Connell
Coarse Sediment Lab Manager

Copy of the laboratory report cover letter.

BULK SAMPLE: PARTICLE SIZE ANALYSIS

River:	Santa Clara River	Sample #	Stop 2; WP-067
Location (origi	MS Reach 19-20	Date Collected:	3/11/2010
Crew:	Dusterhoff, Reyman	Method of Collection:	Bulk
Reach	19	Surface/Sub-surface	
Sampler		Bag # of #	1, 2 of 2

Date Processed: 4/8/2010
Processed by: E. Olson
UNITS G

------------------ WEIGHT -----------

Sieve	Finer than	Final Net	%	Cum%<
256		0.0	0.0%	100.0%
180	256	0.0	0.0%	100.0%
128	180	0.0	0.0%	100.0%
90	128	0.0	0.0%	100.0%
64	90	0.0	0.0%	100.0%
45	64	0.0	0.0%	100.0%
31.5	45	62.2	0.3%	100.0%
22.4	31.5	459.0	2.4%	99.7%
16	22.4	759.5	4.0%	97.3%
11.2	16	1012.0	5.3%	93.3%
8	11.2	1398.5	7.3%	88.0%
5.6	8	1676.5	8.8%	80.7%
4	5.6	1620.0	8.5%	71.9%
2.8	4	1895.5	9.9%	63.4%
2	2.8	1913.7	10.0%	53.5%
1	2	3535.8	18.5%	43.5%
0.85	1	613.6	3.2%	25.0%
0.5	0.85	1524.9	8.0%	21.8%
0.25	0.5	1026.7	5.4%	13.8%
0.125	0.25	607.5	3.2%	8.4%
0.063	0.125	401.0	2.1%	5.2%
Pan	0.063	595.4	3.1%	3.1%
TOTAL:				

SIZE PARAMETERS

D5	0.1 mm
D16	0.6 mm
D25	1.0 mm
D35	1.5 mm
D50	2.5 mm
D65	4.3 mm
D75	6.4 mm
D84	9.3 mm
D90	12.8 mm
dg	2.5 mm
FREDLE	1.0 mm
T&B STEELHEAD SURVIVAL	-68.3 mm
T&B CHINOOK SURVIVAL	-136.1 mm
% LESS THAN 2 mm	43.5%
% LESS THAN 0.85 mm	21.8%

ADDITIONAL NOTES:

Dmax= 33.0 mm
Dmax mass= 62 g

Sample Dry Wt 19120 - Total Processed Wt 19102 = Net Loss: 18.4
% of Sample: 0.10%

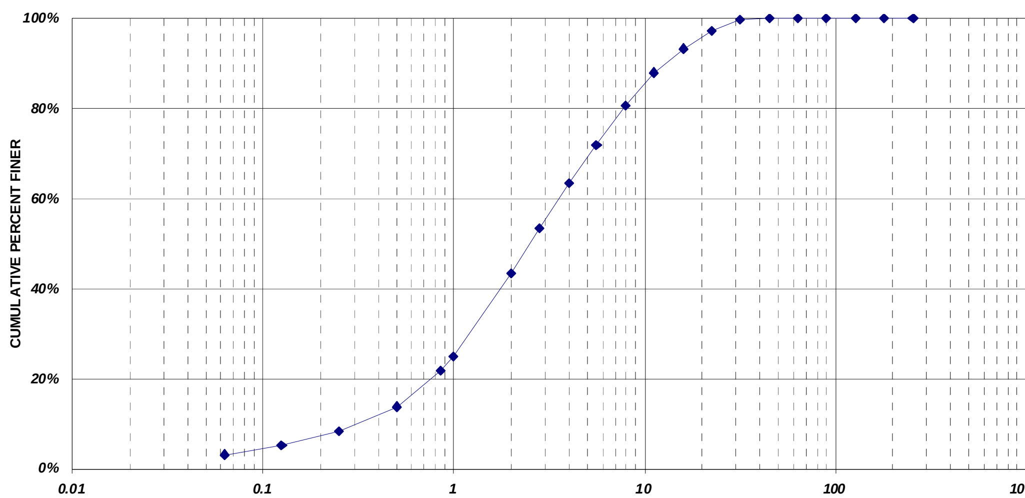

Figure E-2. Sediment size results from the USCR 19 sample.

GMA
Hydrology | Geomorphology | Stream Restoration

BULK SAMPLE: PARTICLE SIZE ANALYSIS

River:	Santa Clara River	Sample #	STOP-30
Location (origi	USCR Mainstem 17-18 (middle bar)	Date Collected:	3/13/2010
Crew:	Dusterhoff, Reyman	Method of Collection:	Bulk
Reach	17	Surface/Sub-surface	
Sampler		Bag # of #	1, 2 of 2

Date Processed: 4/12/2010
Processed by: E. Olson
UNITS G

------------------- WEIGHT ------------

Sieve	Finer than	Final Net		%	Cum%<
256		0.0		0.0%	100.0%
180	256	0.0		0.0%	100.0%
128	180	0.0		0.0%	100.0%
90	128	0.0		0.0%	100.0%
64	90	0.0		0.0%	100.0%
45	64	0.0		0.0%	100.0%
31.5	45	729.0		3.3%	100.0%
22.4	31.5	1522.0		6.9%	96.7%
16	22.4	1580.0		7.1%	89.8%
11.2	16	1740.5		7.9%	82.7%
8	11.2	1897.5		8.6%	74.9%
5.6	8	2190.0		9.9%	66.3%
4	5.6	1967.0		8.9%	56.4%
2.8	4	2109.2		9.5%	47.5%
2	2.8	2141.6		9.7%	38.0%
1	2	3123.4		14.1%	28.3%
0.85	1	434.2		2.0%	14.2%
0.5	0.85	1124.3		5.1%	12.3%
0.25	0.5	1010.9		4.6%	7.2%
0.125	0.25	405.0		1.8%	2.6%
0.063	0.125	123.1		0.6%	0.8%
Pan	0.063	58.3		0.3%	0.3%
TOTAL:					

SIZE PARAMETERS

D5	0.4 mm
D16	1.1 mm
D25	1.7 mm
D35	2.5 mm
D50	4.4 mm
D65	7.6 mm
D75	11.3 mm
D84	17.0 mm
D90	22.6 mm
dg	4.2 mm
FREDLE	1.6 mm
T&B STEELHEAD SURVIVAL	29.0 mm
T&B CHINOOK SURVIVAL	-7.3 mm
% LESS THAN 2 mm	28.3%
% LESS THAN 0.85 mm	12.3%

ADDITIONAL NOTES:

Dmax= 46.0 mm
Dmax mass= 133 g

Sample Dry Wt 22160 - Total Processed Wt 22156 = Net Loss: 4.0
% of Sample: 0.02%

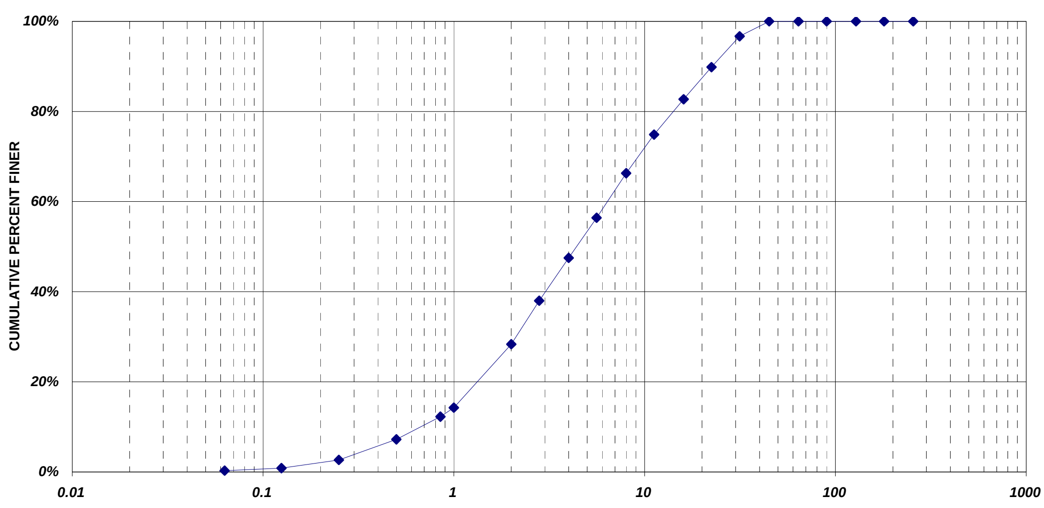

Figure E-3. Sediment size results from the USCR 17 sample.

Hydrology | Geomorphology | Stream Restoration

BULK SAMPLE: PARTICLE SIZE ANALYSIS

River:	Santa Clara River	Sample #	STOP- 75
Location (origi	Mainstem SCR	Date Collected:	3/16/2010
Crew:	Wooster, Reyman, Dusterhoff	Method of Collection:	Bulk
Reach	13	Surface/Sub-surface	
Sampler		Bag # of #	1, 2 of 2

Date Processed: 4/15/2010
Processed by: E. Olson

UNITS G

------------------- WEIGHT ------------

Sieve	Finer than	Final Net		%	Cum%<
256		0.0		0.0%	100.0%
180	256	0.0		0.0%	100.0%
128	180	0.0		0.0%	100.0%
90	128	1579.5		6.4%	100.0%
64	90	0.0		0.0%	93.6%
45	64	1121.0		4.5%	93.6%
31.5	45	1225.0		4.9%	89.1%
22.4	31.5	1076.0		4.3%	84.2%
16	22.4	1283.5		5.2%	79.9%
11.2	16	1421.0		5.7%	74.7%
8	11.2	1566.0		6.3%	69.0%
5.6	8	1916.0		7.7%	62.7%
4	5.6	1629.0		6.6%	54.9%
2.8	4	1610.6		6.5%	48.4%
2	2.8	1456.6		5.9%	41.9%
1	2	2593.5		10.4%	36.0%
0.85	1	550.7		2.2%	25.6%
0.5	0.85	2137.5		8.6%	23.4%
0.25	0.5	2173.1		8.8%	14.8%
0.125	0.25	740.1		3.0%	6.0%
0.063	0.125	302.0		1.2%	3.0%
Pan	0.063	450.0		1.8%	1.8%
TOTAL:					

SIZE PARAMETERS

D5	0.2 mm
D16	0.5 mm
D25	1.0 mm
D35	1.9 mm
D50	4.3 mm
D65	9.1 mm
D75	16.3 mm
D84	31.5 mm
D90	48.2 mm
dg	4.3 mm
FREDLE	1.0 mm
T&B STEELHEAD SURVIVAL	-53.4 mm
T&B CHINOOK SURVIVAL	-79.2 mm
% LESS THAN 2 mm	36.0%
% LESS THAN 0.85 mm	23.4%

ADDITIONAL NOTES:

Dmax= 111.0 mm
Dmax mass= 1580 g

Sample Dry Wt 24840 - Total Processed Wt 24831 = Net Loss: 8.9
% of Sample: 0.04%

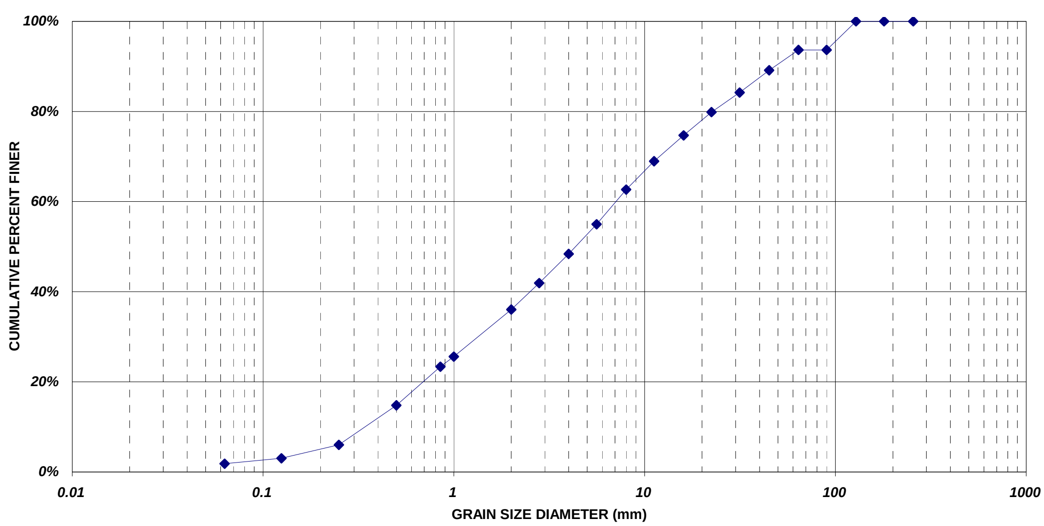

Figure E-4. Sediment size results from the USCR 13 sample.

GMA Hydrology | Geomorphology | Stream Restoration

BULK SAMPLE: PARTICLE SIZE ANALYSIS

River:	Santa Clara River	Sample #	STOP - 85
Location (origi	MSCR	Date Collected:	3/16/2010
Crew:	Wooster, Reyman	Method of Collection:	Bulk
Reach	6	Surface/Sub-surface	
Sampler		Bag # of #	1 of 1

Date Processed: 4/28/2010
Processed by: E. Olson
UNITS G

------------------- WEIGHT ------------

Sieve	Finer than	Final Net	%	Cum%<
256		0.0	0.0%	100.0%
180	256	0.0	0.0%	100.0%
128	180	0.0	0.0%	100.0%
90	128	0.0	0.0%	100.0%
64	90	0.0	0.0%	100.0%
45	64	0.0	0.0%	100.0%
31.5	45	126.5	0.7%	100.0%
22.4	31.5	578.5	3.2%	99.3%
16	22.4	663.0	3.7%	96.1%
11.2	16	996.0	5.6%	92.3%
8	11.2	1423.5	8.0%	86.8%
5.6	8	1571.0	8.8%	78.8%
4	5.6	1202.0	6.7%	70.0%
2.8	4	1124.9	6.3%	63.3%
2	2.8	776.4	4.3%	57.0%
1	2	1656.8	9.3%	52.6%
0.85	1	1112.7	6.2%	43.4%
0.5	0.85	2133.6	11.9%	37.2%
0.25	0.5	2433.2	13.6%	25.2%
0.125	0.25	1302.2	7.3%	11.6%
0.063	0.125	507.4	2.8%	4.3%
Pan	0.063	262.9	1.5%	1.5%
TOTAL:				

SIZE PARAMETERS

D5	0.1 mm
D16	0.3 mm
D25	0.5 mm
D35	0.8 mm
D50	1.6 mm
D65	4.4 mm
D75	6.9 mm
D84	10.0 mm
D90	13.8 mm
dg	1.8 mm
FREDLE	0.5 mm
T&B STEELHEAD SURVIVAL	-214.1 mm
T&B CHINOOK SURVIVAL	-288.8 mm
% LESS THAN 2 mm	52.6%
% LESS THAN 0.85 mm	37.2%

ADDITIONAL NOTES:

Dmax= 43.0 mm
Dmax mass= 77 g

Sample Dry Wt 17880 - Total Processed Wt 17871 = Net Loss: 9.5
% of Sample: 0.05%

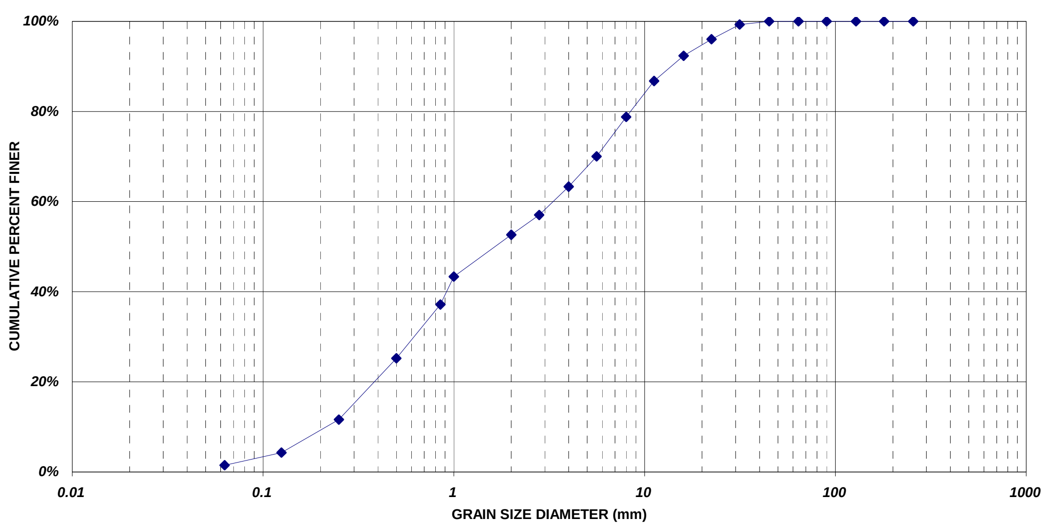

Figure E-5. Sediment size results from the USCR 6 sample.

Hydrology | Geomorphology | Stream Restoration

BULK SAMPLE: PARTICLE SIZE ANALYSIS

River:	Santa Clara River	Sample #	STOP - 96
Location (origi	SCR M3 - M4	Date Collected:	3/17/2010
Crew:	Wooster, Reyman	Method of Collection:	Bulk
Reach	3	Surface/Sub-surface	
Sampler		Bag # of #	1 of 1

Date Processed: 4/28/2010
Processed by: E. Olson

UNITS G

------------------- WEIGHT ------------

Sieve	Finer than	Final Net	%	Cum%<
256		0.0	0.0%	100.0%
180	256	0.0	0.0%	100.0%
128	180	0.0	0.0%	100.0%
90	128	0.0	0.0%	100.0%
64	90	1254.0	6.3%	100.0%
45	64	709.0	3.6%	93.7%
31.5	45	521.0	2.6%	90.1%
22.4	31.5	1016.5	5.1%	87.5%
16	22.4	816.5	4.1%	82.4%
11.2	16	1147.0	5.8%	78.3%
8	11.2	1092.5	5.5%	72.5%
5.6	8	1066.5	5.4%	67.0%
4	5.6	868.0	4.4%	61.7%
2.8	4	806.2	4.1%	57.3%
2	2.8	748.1	3.8%	53.3%
1	2	1691.0	8.5%	49.5%
0.85	1	584.2	2.9%	41.0%
0.5	0.85	2432.3	12.2%	38.1%
0.25	0.5	3132.6	15.7%	25.8%
0.125	0.25	1523.6	7.7%	10.1%
0.063	0.125	368.9	1.9%	2.4%
Pan	0.063	112.7	0.6%	0.6%
TOTAL:				

SIZE PARAMETERS

D5	0.2 mm
D16	0.3 mm
D25	0.5 mm
D35	0.7 mm
D50	2.1 mm
D65	7.0 mm
D75	13.0 mm
D84	25.0 mm
D90	44.2 mm
dg	2.7 mm
FREDLE	0.5 mm
T&B STEELHEAD SURVIVAL	-179.3 mm
T&B CHINOOK SURVIVAL	-213.5 mm
% LESS THAN 2 mm	49.5%
% LESS THAN 0.85 mm	38.1%

ADDITIONAL NOTES:

Dmax= 86.0 mm
Dmax mass= 620 g

Sample Dry Wt 19910 - Total Processed Wt 19891 = Net Loss: 19.2
% of Sample: 0.10%

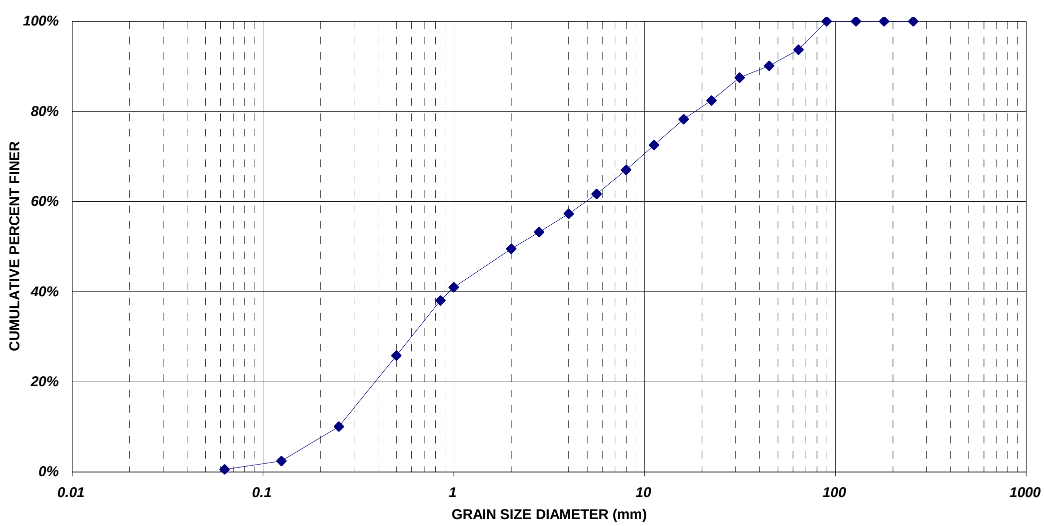

Figure E-6. Sediment size results from the USCR 3 sample.

Hydrology | Geomorphology | Stream Restoration

BULK SAMPLE: PARTICLE SIZE ANALYSIS

River:	SM Chiquito	Sample #	STOP- 9
Location (origi	Chiquito Canyon	Date Collected:	3/12/2010
Crew:	Dusterhoff, Reyman	Method of Collection:	Bulk
Reach	1	Surface/Sub-surface	
Sampler		Bag # of #	1, 2 of 2

Date Processed: 4/13/2010
Processed by: E. Olson

UNITS G

------------------ WEIGHT ------------

Sieve	Finer than	Final Net	%	Cum%<
256		0.0	0.0%	100.0%
180	256	0.0	0.0%	100.0%
128	180	0.0	0.0%	100.0%
90	128	0.0	0.0%	100.0%
64	90	0.0	0.0%	100.0%
45	64	310.0	1.6%	100.0%
31.5	45	432.0	2.2%	98.4%
22.4	31.5	886.5	4.5%	96.2%
16	22.4	1273.0	6.5%	91.7%
11.2	16	1083.0	5.5%	85.1%
8	11.2	1146.0	5.9%	79.6%
5.6	8	1153.5	5.9%	73.7%
4	5.6	1106.0	5.7%	67.8%
2.8	4	1203.4	6.2%	62.2%
2	2.8	1576.4	8.1%	56.0%
1	2	3490.7	17.9%	47.9%
0.85	1	710.8	3.6%	30.1%
0.5	0.85	2125.4	10.9%	26.4%
0.25	0.5	1696.1	8.7%	15.5%
0.125	0.25	753.0	3.9%	6.8%
0.063	0.125	468.0	2.4%	3.0%
Pan	0.063	116.1	0.6%	0.6%
TOTAL:				

SIZE PARAMETERS

D5	0.2 mm
D16	0.5 mm
D25	0.8 mm
D35	1.2 mm
D50	2.2 mm
D65	4.7 mm
D75	8.6 mm
D84	14.9 mm
D90	20.6 mm
dg	2.5 mm
FREDLE	0.8 mm
T&B STEELHEAD SURVIVAL	-99.1 mm
T&B CHINOOK SURVIVAL	-150.7 mm
% LESS THAN 2 mm	47.9%
% LESS THAN 0.85 mm	26.4%

ADDITIONAL NOTES:

Dmax= 59.0 mm
Dmax mass= 170 g

Sample Dry Wt 19530 - Total Processed Wt 19530 = Net Loss: 0.0
% of Sample: 0.00%

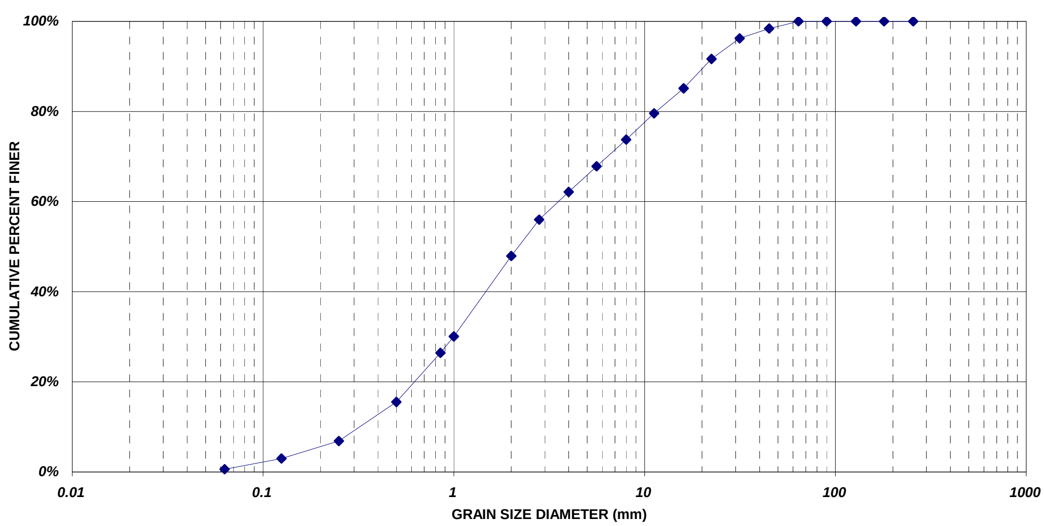

Figure E-7. Sediment size results from the San Martinez Chiquito Canyon 1 sample.

Hydrology | Geomorphology | Stream Restoration

BULK SAMPLE: PARTICLE SIZE ANALYSIS

River:	**Haskell Canyon**	**Sample #**	**STOP- 45**
Location (origi	**Haskell Canyon 0 - 1**	**Date Collected:**	**3/14/2010**
Crew:	**Dusterhoff, Reyman**	**Method of Collection:**	**Bulk**
Reach	**1**	**Surface/Sub-surface**	
Sampler		**Bag # of #**	**1, 2 of 2**

Date Processed: **4/13/2010**
Processed by: **E. Olson**

UNITS **G**

------------------- WEIGHT ------------

Sieve	Finer than	Final Net	%	Cum%<
256		0.0	**0.0%**	**100.0%**
180	256	0.0	**0.0%**	**100.0%**
128	180	0.0	**0.0%**	**100.0%**
90	128	0.0	**0.0%**	**100.0%**
64	90	443.5	**2.2%**	**100.0%**
45	64	141.0	**0.7%**	**97.8%**
31.5	45	334.5	**1.6%**	**97.1%**
22.4	31.5	339.5	**1.7%**	**95.5%**
16	22.4	713.0	**3.5%**	**93.9%**
11.2	16	866.5	**4.2%**	**90.4%**
8	11.2	1044.5	**5.1%**	**86.1%**
5.6	8	1112.5	**5.4%**	**81.0%**
4	5.6	965.5	**4.7%**	**75.6%**
2.8	4	1088.3	**5.3%**	**70.9%**
2	2.8	1121.6	**5.5%**	**65.6%**
1	2	2593.1	**12.7%**	**60.1%**
0.85	1	716.3	**3.5%**	**47.4%**
0.5	0.85	2676.3	**13.1%**	**43.9%**
0.25	0.5	3237.2	**15.8%**	**30.9%**
0.125	0.25	1954.5	**9.5%**	**15.1%**
0.063	0.125	727.4	**3.6%**	**5.5%**
Pan	0.063	399.8	**2.0%**	**2.0%**
TOTAL:				

SIZE PARAMETERS

D5	**0.1 mm**
D16	**0.3 mm**
D25	**0.4 mm**
D35	**0.6 mm**
D50	**1.2 mm**
D65	**2.7 mm**
D75	**5.4 mm**
D84	**9.7 mm**
D90	**15.5 mm**
dg	**1.6 mm**
FREDLE	**0.4 mm**
T&B STEELHEAD SURVIVAL	**-282.4 mm**
T&B CHINOOK SURVIVAL	**-364.5 mm**
% LESS THAN 2 mm	**60.1%**
% LESS THAN 0.85 mm	**43.9%**

ADDITIONAL NOTES:

Dmax= 74.0 mm
Dmax mass= 444 g

Sample Dry Wt 20480 - Total Processed Wt 20475 = Net Loss: 5.1
% of Sample: 0.02%

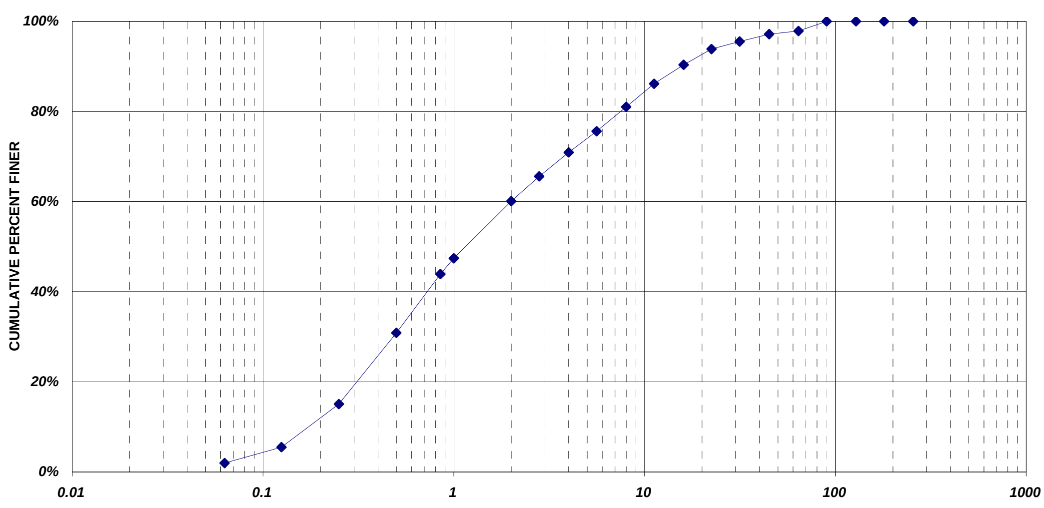

Figure E-8. Sediment size results from the Haskell Canyon 1 sample.

Hydrology | Geomorphology | Stream Restoration

BULK SAMPLE: PARTICLE SIZE ANALYSIS

River:	Newhall Cr	Sample #	STOP- 31
Location (origi	Newhall 0 - 1	Date Collected:	3/13/2010
Crew:	Dusterhoff, Reyman	Method of Collection:	Bulk
Reach	1	Surface/Sub-surface	
Sampler		Bag # of #	1, 2 of 2

Date Processed: 4/15/2010
Processed by: E. Olson
UNITS G

------------------ WEIGHT ------------

Sieve	Finer than	Final Net	%	Cum%<
256		0.0	0.0%	100.0%
180	256	0.0	0.0%	100.0%
128	180	0.0	0.0%	100.0%
90	128	0.0	0.0%	100.0%
64	90	0.0	0.0%	100.0%
45	64	281.0	1.5%	100.0%
31.5	45	895.0	4.6%	98.5%
22.4	31.5	924.5	4.8%	93.9%
16	22.4	743.0	3.8%	89.1%
11.2	16	959.0	5.0%	85.3%
8	11.2	855.5	4.4%	80.3%
5.6	8	994.5	5.1%	75.9%
4	5.6	873.5	4.5%	70.8%
2.8	4	1354.2	7.0%	66.2%
2	2.8	1416.9	7.3%	59.2%
1	2	3351.5	17.3%	51.9%
0.85	1	899.3	4.7%	34.6%
0.5	0.85	2687.5	13.9%	29.9%
0.25	0.5	2159.4	11.2%	16.0%
0.125	0.25	721.5	3.7%	4.8%
0.063	0.125	146.4	0.8%	1.1%
Pan	0.063	68.0	0.4%	0.4%
TOTAL:				

SIZE PARAMETERS

D5	0.3 mm
D16	0.5 mm
D25	0.7 mm
D35	1.0 mm
D50	1.9 mm
D65	3.8 mm
D75	7.5 mm
D84	14.6 mm
D90	23.9 mm
dg	2.4 mm
FREDLE	0.7 mm
T&B STEELHEAD SURVIVAL	-133.7 mm
T&B CHINOOK SURVIVAL	-190.4 mm
% LESS THAN 2 mm	51.9%
% LESS THAN 0.85 mm	29.9%

ADDITIONAL NOTES:

Dmax= 65.0 mm
Dmax mass= 281 g

Sample Dry Wt 19340 - Total Processed Wt 19331 = Net Loss: 9.2
% of Sample: 0.05%

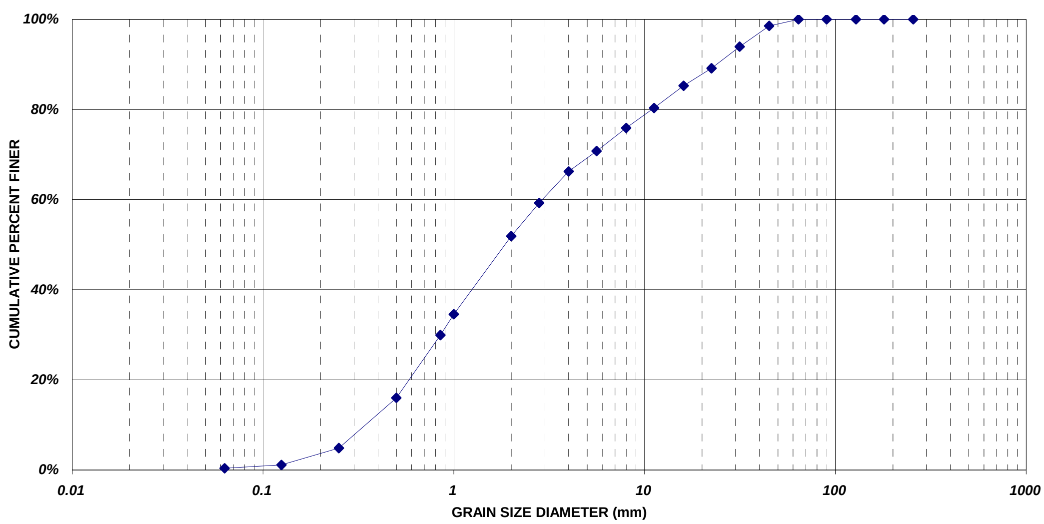

Figure E-9. Sediment size results from the Newhall Creek 1 sample.

GMA
Hydrology | Geomorphology | Stream Restoration

BULK SAMPLE: PARTICLE SIZE ANALYSIS

River:	Newhall Cr	Sample #	STOP- 33
Location (origi	Newhall 3 - 4	Date Collected:	3/13/2010
Crew:	Dusterhoff, Reyman	Method of Collection:	Bulk
Reach	4	Surface/Sub-surface	
Sampler		Bag # of #	1, 2 of 2

Date Processed: 4/15/2010
Processed by: E. Olson
UNITS G

------------------- WEIGHT ------------

Sieve	Finer than	Final Net	%	Cum%<
256		0.0	0.0%	100.0%
180	256	0.0	0.0%	100.0%
128	180	0.0	0.0%	100.0%
90	128	0.0	0.0%	100.0%
64	90	0.0	0.0%	100.0%
45	64	0.0	0.0%	100.0%
31.5	45	69.0	0.3%	100.0%
22.4	31.5	181.0	0.9%	99.7%
16	22.4	312.0	1.5%	98.8%
11.2	16	447.5	2.2%	97.2%
8	11.2	664.0	3.3%	95.0%
5.6	8	845.5	4.2%	91.7%
4	5.6	875.0	4.3%	87.6%
2.8	4	1370.6	6.8%	83.3%
2	2.8	1977.8	9.8%	76.5%
1	2	5781.5	28.5%	66.7%
0.85	1	1352.2	6.7%	38.2%
0.5	0.85	3003.4	14.8%	31.6%
0.25	0.5	2331.9	11.5%	16.7%
0.125	0.25	915.3	4.5%	5.2%
0.063	0.125	115.0	0.6%	0.7%
Pan	0.063	32.2	0.2%	0.2%
TOTAL:				

SIZE PARAMETERS

D5	0.2 mm
D16	0.5 mm
D25	0.7 mm
D35	0.9 mm
D50	1.3 mm
D65	1.9 mm
D75	2.7 mm
D84	4.2 mm
D90	6.9 mm
dg	1.5 mm
FREDLE	0.7 mm
T&B STEELHEAD SURVIVAL	-186.1 mm
T&B CHINOOK SURVIVAL	-288.4 mm
% LESS THAN 2 mm	66.7%
% LESS THAN 0.85 mm	31.6%

ADDITIONAL NOTES:

Dmax= 35.0 mm
Dmax mass= 69 g

Sample Dry Wt 20290 - Total Processed Wt 20274 = Net Loss: 16.0
% of Sample: 0.08%

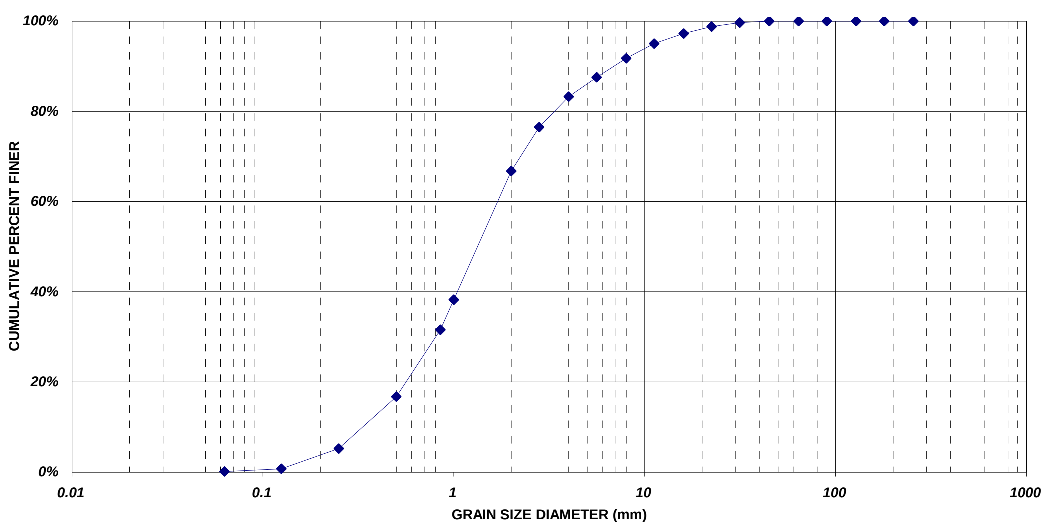

Figure E-10. Sediment size results from the Newhall Creek 4 sample.

GMA
Hydrology | Geomorphology | Stream Restoration

BULK SAMPLE: PARTICLE SIZE ANALYSIS

River:	**Placerita Cr**	**Sample #**	**STOP- 35**
Location (origi	**Placerita 5 - 6**	**Date Collected:**	**3/13/2010**
Crew:	**Dusterhoff, Reyman**	**Method of Collection:**	**Bulk**
Reach	**5**	**Surface/Sub-surface**	
Sampler		**Bag # of #**	**1, 2 of 2**

Date Processed: **4/13/2010**
Processed by: **E. Olson**

UNITS **G**

------------------- WEIGHT ------------

Sieve	Finer than	Final Net	%	Cum%<
256		0.0	**0.0%**	**100.0%**
180	256	0.0	**0.0%**	**100.0%**
128	180	0.0	**0.0%**	**100.0%**
90	128	0.0	**0.0%**	**100.0%**
64	90	0.0	**0.0%**	**100.0%**
45	64	0.0	**0.0%**	**100.0%**
31.5	45	218.0	**1.0%**	**100.0%**
22.4	31.5	248.0	**1.2%**	**99.0%**
16	22.4	523.5	**2.5%**	**97.8%**
11.2	16	697.5	**3.3%**	**95.3%**
8	11.2	992.5	**4.7%**	**91.9%**
5.6	8	1283.5	**6.1%**	**87.2%**
4	5.6	1312.0	**6.3%**	**81.0%**
2.8	4	1704.8	**8.2%**	**74.8%**
2	2.8	2233.6	**10.7%**	**66.6%**
1	2	5188.6	**24.8%**	**55.9%**
0.85	1	1013.0	**4.8%**	**31.1%**
0.5	0.85	2910.6	**13.9%**	**26.3%**
0.25	0.5	1803.7	**8.6%**	**12.4%**
0.125	0.25	632.5	**3.0%**	**3.7%**
0.063	0.125	118.6	**0.6%**	**0.7%**
Pan	0.063	29.6	**0.1%**	**0.1%**
TOTAL:				

SIZE PARAMETERS

D5	**0.3 mm**
D16	**0.6 mm**
D25	**0.8 mm**
D35	**1.1 mm**
D50	**1.7 mm**
D65	**2.7 mm**
D75	**4.0 mm**
D84	**6.6 mm**
D90	**9.8 mm**
dg	**1.9 mm**
FREDLE	**0.9 mm**
T&B STEELHEAD SURVIVAL	**-122.2 mm**
T&B CHINOOK SURVIVAL	**-207.4 mm**
% LESS THAN 2 mm	**55.9%**
% LESS THAN 0.85 mm	**26.3%**

ADDITIONAL NOTES:

Dmax= 46.0 mm
Dmax mass= 106 g

Sample Dry Wt 20930 - Total Processed Wt 20910 = Net Loss: 19.9
% of Sample: 0.10%

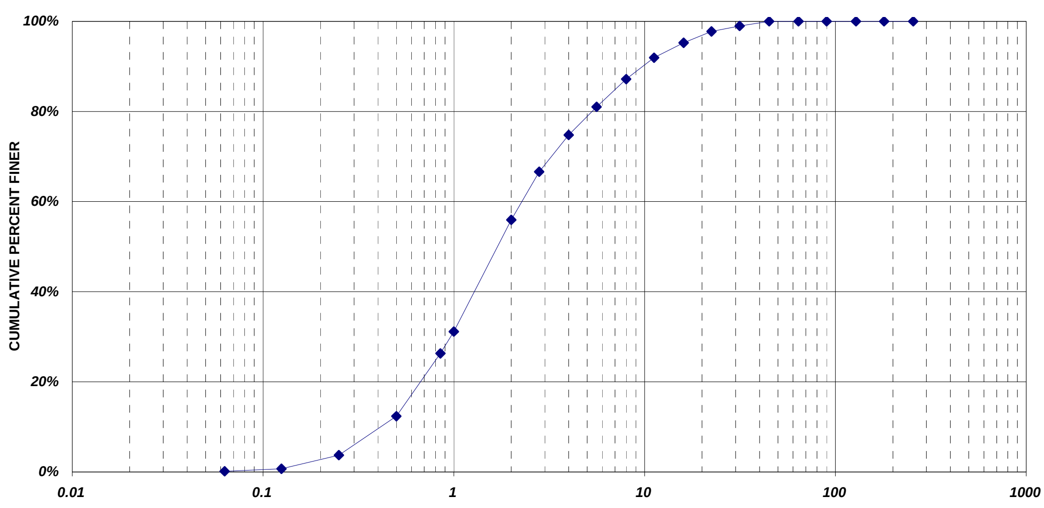

Figure E-11. Sediment size results from the Placerita Canyon 5 sample.

Hydrology | Geomorphology | Stream Restoration

BULK SAMPLE: PARTICLE SIZE ANALYSIS

River:	Vasquez Canyon	Sample #	STOP- 52
Location (origi	Vasquez Canyon 2 - 3	Date Collected:	3/14/2010
Crew:	Dusterhoff, Reyman	Method of Collection:	Bulk
Reach	3	Surface/Sub-surface	
Sampler		Bag # of #	1, 2 of 2

Date Processed: 4/15/2010
Processed by: E. Olson
UNITS G

------------------- WEIGHT ------------

Sieve	Finer than	Final Net	%	Cum%<
256		0.0	0.0%	100.0%
180	256	0.0	0.0%	100.0%
128	180	0.0	0.0%	100.0%
90	128	0.0	0.0%	100.0%
64	90	0.0	0.0%	100.0%
45	64	0.0	0.0%	100.0%
31.5	45	200.0	1.1%	100.0%
22.4	31.5	85.0	0.5%	98.9%
16	22.4	142.0	0.8%	98.5%
11.2	16	295.5	1.6%	97.7%
8	11.2	457.5	2.5%	96.1%
5.6	8	825.5	4.4%	93.7%
4	5.6	974.5	5.2%	89.2%
2.8	4	1416.1	7.6%	84.0%
2	2.8	2047.6	11.0%	76.4%
1	2	4243.5	22.8%	65.4%
0.85	1	1109.9	6.0%	42.5%
0.5	0.85	3195.8	17.2%	36.6%
0.25	0.5	2358.5	12.7%	19.4%
0.125	0.25	784.6	4.2%	6.7%
0.063	0.125	253.6	1.4%	2.5%
Pan	0.063	210.5	1.1%	1.1%
TOTAL:				

SIZE PARAMETERS

D5	0.2 mm
D16	0.4 mm
D25	0.6 mm
D35	0.8 mm
D50	1.3 mm
D65	2.0 mm
D75	2.7 mm
D84	4.0 mm
D90	6.0 mm
dg	1.4 mm
FREDLE	0.6 mm
T&B STEELHEAD SURVIVAL	-244.8 mm
T&B CHINOOK SURVIVAL	-358.5 mm
% LESS THAN 2 mm	65.4%
% LESS THAN 0.85 mm	36.6%

ADDITIONAL NOTES:

Dmax= 42.0 mm
Dmax mass= 119 g

Sample Dry Wt 18610 - Total Processed Wt 18600 = Net Loss: 10.0
% of Sample: 0.05%

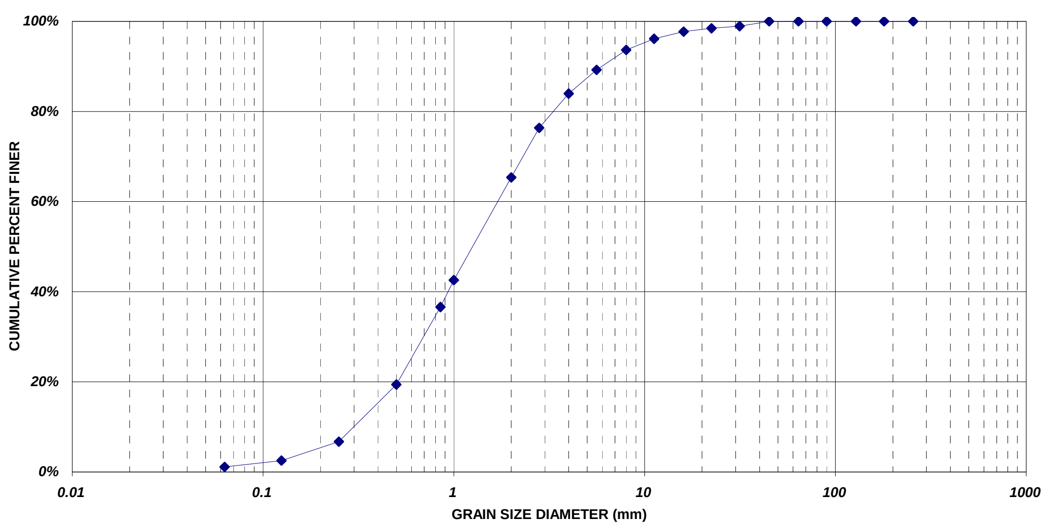

Figure E-12. Sediment size results from the Vasquez Canyon 3 sample.

Hydrology | Geomorphology | Stream Restoration

BULK SAMPLE: PARTICLE SIZE ANALYSIS

River:	Acton Canyon	Sample #	STOP - 88
Location (origi	Acton Canyon	Date Collected:	3/17/2010
Crew:	Wooster, Reyman	Method of Collection:	Bulk
Reach	8	Surface/Sub-surface	
Sampler		Bag # of #	1 of 1

Date Processed: 4/28/2010
Processed by: E. Olson

UNITS G

------------------ **WEIGHT** -----------

Sieve	Finer than	Final Net		%	Cum%<
256		0.0		**0.0%**	**100.0%**
180	256	0.0		**0.0%**	**100.0%**
128	180	0.0		**0.0%**	**100.0%**
90	128	0.0		**0.0%**	**100.0%**
64	90	0.0		**0.0%**	**100.0%**
45	64	252.5		**1.5%**	**100.0%**
31.5	45	223.0		**1.3%**	**98.5%**
22.4	31.5	483.5		**2.8%**	**97.3%**
16	22.4	906.5		**5.2%**	**94.5%**
11.2	16	996.5		**5.8%**	**89.2%**
8	11.2	1164.5		**6.7%**	**83.5%**
5.6	8	1261.0		**7.3%**	**76.8%**
4	5.6	1178.5		**6.8%**	**69.5%**
2.8	4	1355.1		**7.8%**	**62.7%**
2	2.8	1182.1		**6.8%**	**54.9%**
1	2	2130.4		**12.3%**	**48.0%**
0.85	1	486.9		**2.8%**	**35.7%**
0.5	0.85	1688.3		**9.7%**	**32.9%**
0.25	0.5	1954.2		**11.3%**	**23.2%**
0.125	0.25	1239.8		**7.2%**	**11.9%**
0.063	0.125	528.6		**3.1%**	**4.8%**
Pan	0.063	294.7		**1.7%**	**1.7%**
TOTAL:					

SIZE PARAMETERS

D5	**0.1 mm**
D16	**0.3 mm**
D25	**0.6 mm**
D35	**1.0 mm**
D50	**2.2 mm**
D65	**4.5 mm**
D75	**7.3 mm**
D84	**11.6 mm**
D90	**16.8 mm**
dg	**2.1 mm**
FREDLE	**0.6 mm**
T&B STEELHEAD SURVIVAL	**-166.4 mm**
T&B CHINOOK SURVIVAL	**-230.3 mm**
% LESS THAN 2 mm	**48.0%**
% LESS THAN 0.85 mm	**32.9%**

ADDITIONAL NOTES:

Dmax= 48.0 mm
Dmax mass= 143 g

Sample Dry Wt 17340 - Total Processed Wt 17326 = Net Loss: 14.0
% of Sample: 0.08%

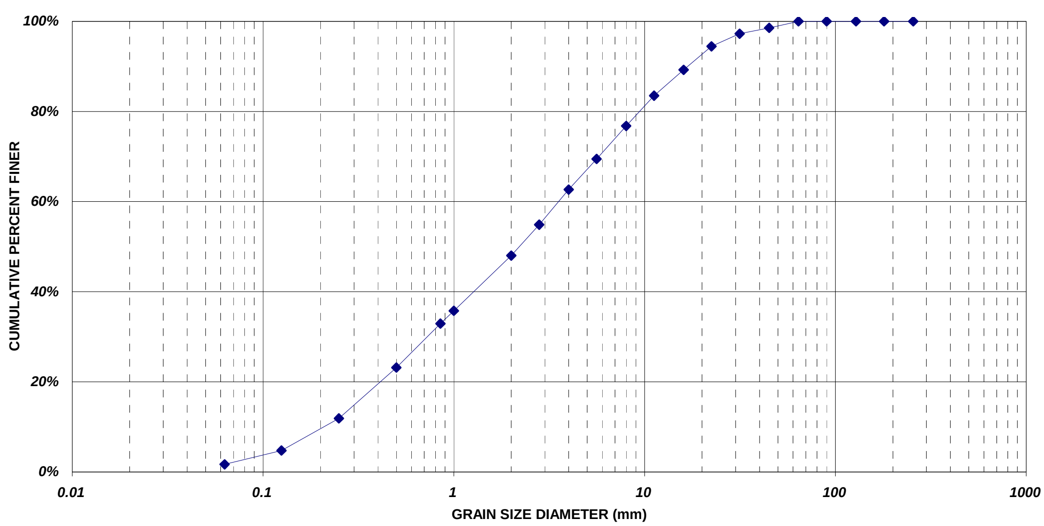

Figure E-13. Sediment size results from the Acton 8 sample.

Hydrology | Geomorphology | Stream Restoration

BULK SAMPLE: PARTICLE SIZE ANALYSIS

River:	Escondido Cr	Sample #	STOP-90
Location (origi	Escondido Canyon Creek	Date Collected:	3/17/2010
Crew:	Wooster, Reyman	Method of Collection:	Bulk
Reach	5	Surface/Sub-surface	
Sampler		Bag # of #	1 of 1

Date Processed: 4/19/2010
Processed by: E. Olson
UNITS G

------------------- WEIGHT ------------

Sieve	Finer than	Final Net	%	Cum%<
256		0.0	0.0%	100.0%
180	256	0.0	0.0%	100.0%
128	180	0.0	0.0%	100.0%
90	128	0.0	0.0%	100.0%
64	90	0.0	0.0%	100.0%
45	64	152.0	0.9%	100.0%
31.5	45	664.5	3.9%	99.1%
22.4	31.5	1332.5	7.8%	95.2%
16	22.4	1080.5	6.3%	87.4%
11.2	16	1117.0	6.5%	81.1%
8	11.2	1009.0	5.9%	74.5%
5.6	8	1040.0	6.1%	68.6%
4	5.6	872.5	5.1%	62.5%
2.8	4	1221.6	7.2%	57.4%
2	2.8	958.8	5.6%	50.3%
1	2	1979.1	11.6%	44.7%
0.85	1	460.6	2.7%	33.1%
0.5	0.85	1347.8	7.9%	30.4%
0.25	0.5	1457.0	8.5%	22.5%
0.125	0.25	1197.7	7.0%	13.9%
0.063	0.125	702.9	4.1%	6.9%
Pan	0.063	481.1	2.8%	2.8%
TOTAL:				

SIZE PARAMETERS

D5	0.1 mm
D16	0.3 mm
D25	0.6 mm
D35	1.1 mm
D50	2.8 mm
D65	6.5 mm
D75	11.5 mm
D84	18.7 mm
D90	25.2 mm
dg	2.6 mm
FREDLE	0.6 mm
T&B STEELHEAD SURVIVAL	-121.7 mm
T&B CHINOOK SURVIVAL	-160.9 mm
% LESS THAN 2 mm	44.7%
% LESS THAN 0.85 mm	30.4%

ADDITIONAL NOTES:

Dmax= 55.0 mm
Dmax mass= 152 g

Sample Dry Wt 17090 - Total Processed Wt 17075 = Net Loss: 15.4
% of Sample: 0.09%

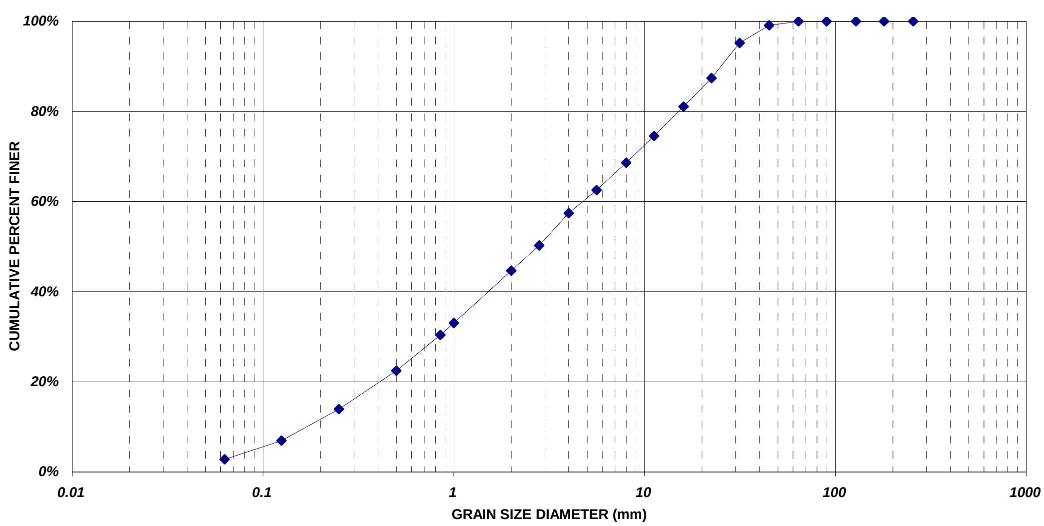

Figure E-14. Sediment size results from the Escondido Canyon 5 sample.

Appendix F

Tributary and River Reach Descriptions

TRIBUTARY AND RIVER REACH DESCRIPTIONS

This appendix provides supplementary information on tributary and mainstem reach descriptions that was introduced in Section 4.3.1 in the main report. These observations are based on an extensive field reconnaissance effort that was conducted in March 2010. As introduced in Section 4.3.1 of the main report, and visually depicted in Figures 1-3 and 4-14 in the main report, we have separated the USCR watershed into three distinct regions: Upper Region (i.e., areas draining into the Action basin), Middle Region (i.e., areas draining into Soledad Canyon reaches, but below the Acton basin), and Lower Region (i.e., areas draining into the Santa Clarita basin, but below the Soledad Canyon reaches). The USCR mainstem and tributary channels within the Feasibility Study subwatersheds (Figure 1-2 in the main report) were further separated into distinct reaches that are relatively geomorphologically homogenous (Figure 4-14 and Table 4-4).

Upper Region (Acton Basin)

The mainstem channel through the Upper Region flows for approximately 5 km and transitions from a wide, depositional reach (M28) to a narrower reach (M27) with a higher reach-average channel gradient and a higher capacity to transport sediment. The reach-average active channel width (i.e., the width of channel that is frequently scoured during storm events) decreases by a factor of 5 from M28 to M27, and the reach-average slope remains relatively moderate but increases by approximately 10%. Soledad Canyon Road is adjacent to the active channel through M28 and confines the channel along the right bank. The river valley within M28 contains a dominant channel with several shallow distributary channels that convey flow and sediment only during high flow events. The channels have little geomorphic structure and essentially lose discrete form towards the downstream end of M28, with a discrete channel reappearing within M27. The channel bed through both reaches is relatively fine-grained (very fine gravel [G_{vf}]) and very poorly sorted (Figure F-1). As these reaches are very geomorphically active, there is a moderate amount of young in-channel vegetation (e.g., there appears to be very few trees >20 years old). The density of floodplain development decreases downstream from the town of Acton as the channel transitions from a depositional basin to a bedrock-controlled canyon reach and the overall floodplain area decreases.

The subwatersheds that are the primary sources of water and sediment to M28 include (from upstream to downstream) Soledad,[1] Aliso, and Trade Post canyons. These subwatersheds contain a relatively expansive developed footprint concentrated primarily within the lower tributary valleys. The degree, extent, and type of development throughout these subwatersheds appear to have an impact on the local morphologic characteristics and sediment connectivity to the mainstem USCR.

The two primary tributary channels within the Soledad subwatershed are Soledad and Kentucky Springs canyons. Soledad Canyon is the dominant tributary channel, with Kentucky Springs Canyon draining into the Soledad Canyon upstream from the M28 confluence. Both tributary channels are ephemeral washes that infiltrate water during dry low-flow conditions and convey water and sediment downstream only during larger storm events. Tributary reach slopes are

[1] Note: the “Soledad Canyon” tributary referenced here is effectively the upstream end of the mainstem river as designated in USGS 1:24,000 topographic quadrangle maps and not the middle-Region reaches that are commonly referred to as Soledad Canyon.

moderately steep (1.5–3.1%) and deliver a fairly fine-grained load to M28 (the bed sediment along the tributary reaches is predominantly sand [S]).

Figure F-1. Mainstem reach M27 (looking downstream).

The Aliso Canyon subwatershed enters from the south and appears to be the dominant source of both flow and coarser sediment to M28 (Figure F-2). Aliso Canyon is a plane-bedded channel that transports a mixed sediment load (sand [S] to fine cobble [C_f][2]) and appears capable of frequently transporting larger sediment (cobbles to boulders) based on the condition of in-channel bars. The coarser sediment appears to be derived from upstream fluvial transport as well as adjacent hillslope sources. The channel appears to have a relatively high capacity for sediment transport in spite of relatively moderate reach slopes (1.5–2.1%). The channel appears to convey some water year-round and was transporting presumably fire-derived fine sediment with approximately 0.1–0.3 $m^3\ s^{-1}$ (5–10 cfs) of flow during the Spring 2010 field survey (burned during the 2009 Station Fire).

Tradepost Canyon contains a combination of both natural and engineered reaches, yet appears disconnected from M28 during most flows. In general, the reach-average channel slopes range from moderate to very steep (1.6–5.1%) and the channel transports a relatively fine sediment load (bed sediment is predominantly S). The most upstream reaches drain a mountain catchment and are the steepest within the study channel. Farther downstream, the channel gradient decreases and the channel becomes poorly defined as it flows through developed areas. Towards the downstream end of the tributary reach where the channel crosses Santiago Road, sediment is frequently deposited on the channel crossing during storm events and reworked in an attempt to maintain channel capacity, which causes considerable channel incision downstream

[2] S = sand (<2 mm), Gvf = very fine gravel (2–4 mm), Gf = fine gravel (4–8 mm), Gm = medium gravel (8–16 mm), Gc = coarse gravel (16–32 mm), Cc = coarse cobble (128–256 mm).

(approximately 4 m). Downstream of the incised reach, the channel definition decreases as the channel enters a historic alluvial fan deposit and flow delivered to this reach is presumed to spread out across the fan and infiltrate rapidly. It therefore appears that most sediment delivered from the upper reaches of Tradepost Canyon is deposited and stored in the lower portion of the tributary before reaching the mainstem river channel.

Figure F-2. Mainstem Aliso Canyon (looking upstream).

The main subwatershed supplying flow and sediment to M27 is the Acton subwatershed, which includes (from upstream to downstream) Escondido Creek, Red Rover Mine Canyon, Acton Canyon, and Acton Canyon 2. Land use within this subwatershed is similar to the adjacent subwatersheds to the east, except that the development density is relatively higher. The Acton subwatershed main tributary channels are all very similar to Tradepost Canyon in that they originate in steep mountain catchments and flow onto the historic alluvial fan (Figure F-3). Downstream of the steeper mountain catchment reaches, channel form and erosion processes are highly influenced by development impacts (e.g., road crossings, road-related confinement) and channel incision is pronounced in some locations. The downstream reaches within the alluvial fan are characterized by a relatively high reach-average slope and limited bank resistance (i.e., fine-grained texture and little vegetation), and have a high degree of lateral mobility. Downstream of the confluence between Acton Canyon and Escondido Creek, the channel empties onto a paved road (Crown Valley Road) and flows along the pavement and dirt shoulders all the way to the railroad culvert about 100 m upstream of the confluence with M27. The sediment load that is transported down the road and makes its way into M27 during storm events appears to be composed primarily of fine sand and silt.

Figure F-3. Mainstem Acton Canyon (looking upstream).

Middle Region (Soledad Canyon)

Along the 23 km of the mainstem USCR channel through the Middle Region (M17-M26), the geomorphic character changes dramatically. The upstream reaches have a fine-grained and alluvial channel. The middle reaches are characterized by a coarse bed and strong bedrock influence. The downstream reaches contain a wide, low-gradient, fine-grained alluvial channel that then transitions to the Lower Region. The upstream alluvial reaches (M23–M26) have a relatively narrow active channel width (14-53 m) and decrease in reach-average slope by almost 40% (from 2.0–1.3%) moving downstream, resulting in an overall decrease in dominant bed sediment size from coarse gravel [G_c] to sand [S] (Figure F-4). The active channel through these reaches has a very mobile bed, as indicated by the lack of discrete channel form and poorly-sorted bed sediments. In M26, a clogged channel-spanning culvert under the Arastre Road bridge crossing acts to control grade, causing localized sediment deposition upstream and channel incision (~5 m) downstream of the culvert and up several small tributaries. The incision subsides downstream and the bed elevation stabilizes (as indicated by the establishment of mature [>10 years old] cottonwood trees). The middle bedrock-influenced section of the mainstem (M20–M22) is relatively short and is characterized by a bedrock-controlled meandering form through a highly confined valley (i.e., Soledad Canyon). The confinement results in relatively narrow active channel widths (13–34 m), a reach-average slope that increases by over 25% moving downstream (from 1.3 to 1.7%), and a relatively coarse channel bed with pool-riffle and step-pool morphology (the coarsest bed facies along the entire USCR occurs in M21). Local tributaries contribute sediment that helps maintain the coarse bed (discussed below). The lowermost alluvial portion of the Middle Region mainstem channel (M17–M19) increases considerably in width (29–128 m) and decreases in slope (1.3–0.7%) going downstream, with in-channel mining having a substantial impact on geomorphic processes. The downstream reaches (e.g., M18–M19) are relatively fine-grained and appear to currently have a stable bed. However, gravel mining within the active channel and floodplain of M17 has caused the mainstem channel to incise up to 20–30 m below the historic bed elevation (as evidenced in part by the hanging culvert that conveys the flow from Tick Canyon into the mainstem USCR). The Lang Station Road crossing within the gravel mining operation has halted the upstream incision migration and caused sediment deposition and decreased channel gradient into M18 (Figure F-5; see Figure 4-10 in the main report).

Figure F-4. Mainstem reach M24 (looking upstream).

Aqua Dulce Canyon, which drains the largest subwatershed in the Middle Region, delivers flow and sediment to the mainstem USCR at the upstream end of reach M22. The channel originates in a steep mountain catchment and then flows through a low-gradient, developed depositional zone before entering a steeper, coarser-bedded reach confined by valley walls near the confluence with M22. From the developed depositional zone to the mouth, the channel gradient ranges by more than a factor of 3 (1.2–4.2%) and the channel bed texture ranges from predominantly sand [S] to very coarse gravel [G_{vc}]. The Study reaches begin in the depositional zone where the channel is very poorly defined before entering a culvert under Sierra Highway that concentrates flow. The reaches in this section are similar in form to the channels in the Acton Canyon subwatershed in that both channels flow through historic valley bottom fill, are prone to disappearing, and are sensitive to modifications such as bank hardening or flow accumulation. Several at-grade channel crossings cause upstream sediment deposition and channel gradient reduction, and downstream channel incision and bank destabilization. An engineered concrete reach connects the depositional section to the lower coarse bedded section and appears to contribute to disconnection in sediment delivery between the upper and lower reaches. The lower, coarse-bedded section begins downstream of the Highway 14 bridge where the channel size, channel confinement, sediment transport capacity, and presence of coarse bed sediment rapidly increase. The bed is organized into a pool-riffle morphology in some sections, with bedrock exposures where bed sediment has been scoured. The coarse bed sediment load through this lower section is derived from adjacent bars and banks as well as from mass failures on adjacent hillslopes. At the confluence with M22, the channel is very coarse-bedded (bed texture is predominantly coarse to very coarse gravel [G_c-G_{vc}]) and has a braided channel form with active bar features (Figure F-6).

Figure F-5. Mainstem reach M17 on the Lang Station Road crossing (looking downstream).

Figure F-6. Lower Agua Dulce Canyon (looking upstream).

Although not an identified Study tributary, Bear Canyon has a considerable impact on geomorphic conditions in the mainstem USCR and therefore requires some description here. Bear Canyon drains a steep, relatively small (~15 km^2), north-facing catchment and contributes a considerable amount of coarse sediment to M21. The large sediment deposit at the confluence is angular, very coarse (i.e., largest particles are boulders) and very poorly sorted. Combined, these characteristics suggest that debris flows may be a primary mechanism by which sediment is transported to the mouth from sources higher in the canyon (i.e., there is little indication of sediment abrasion by fluvial transport prior to deposition at the mouth). The position of the confluence in a narrow, steep bedrock canyon results in rapid evacuation and downstream transport of sediment that enters the mainstem channel (Figure F-7).

Figure F-7. Lower Bear Canyon, significant source of coarse sediment (looking upstream).

Tick Canyon is a relatively small subwatershed whose geomorphic character and sediment delivery dynamics are strongly influenced by channel engineering for flood control purposes. The tributary channel drains to reach M17 and is essentially separated into an upper natural reach and a lower engineered reach. The upper reach is plane-bedded with a moderately steep slope (1.9%), a relatively wide active channel, and a relatively mobile coarse bed (bed texture is very coarse gravel [G_{vc}]) (Figure F-8). In general, the reach appears to receive and store a relatively large amount of sediment. The extent to which the upper reach's sediment load is transported downstream to the mainstem USCR is impacted by the downstream engineered reach. The engineered reach is a moderately steep concrete flood control channel that extends from the mouth approximately 2 km upstream and lies within a flow path that is constricted by a housing development on both banks. Flow constriction at the transition between the engineered reach and the natural reach causes downstream flow acceleration (and subsequent flow and sediment evacuation) and upstream sediment deposition. Therefore, there is currently very little to no sediment storage within the engineered reach and a considerable amount of sediment storage in the upper reach. It appears that the amount of coarse sediment delivery from the upper reach to the mainstem USCR has decreased with the construction of the downstream engineered reach.

Figure F-8. Upper Tick Canyon (looking upstream).

Lower Region (Santa Clarita Basin)

As the mainstem USCR channel exits the Middle Region and enters the Lower Region (spanning M11-B–M16), the amount of in-channel and floodplain development increases and there is a considerable change in overall geomorphic character. The valley of the Lower Region sits within the large Santa Clarita basin, resulting in a mainstem channel that is predominantly depositional in nature. This depositional characteristic results in an active channel width that doubles upon entering the Lower Region and a decrease in both reach-average channel gradient (from 0.9 to 0.5%) and dominant bed particle size (bed facies transitions from medium gravel [G_m] to sand [S]) moving downstream to the County line.

Local channel constrictions from both natural and anthropogenic influences along the 32-km length of the mainstem channel in this region strongly influence reach-scale geomorphic dynamics and sediment transport/deposition processes. Residential and business development and road infrastructure within the historic active channel in the upper reaches (M14–M16) has decreased the effective flow width, resulting in considerable flow constriction and relatively high reach-average slope and coarser-bed compared to downstream reaches (Figure F-9). The channel bed through these reaches is very poorly sorted and contains mostly young vegetation (presumably established after the 2005 flood season). Within the lower reaches, the channel becomes inset below the adjacent terrace and maintains a sinuous planform. Natural channel constrictions from impinging valley walls and large tributary sediment deposits cause a reach-average pattern of sediment deposition, high dominant channel sinuosity, fine bed texture, and relatively low channel slope. At these constrictions, the decreased flow width causes relatively steep channel gradients, resulting in localized pool-riffle morphology and coarse sediment transport (Figure F-10). The in-channel vegetation is more prevalent in these lower reaches compared to upstream, due primarily to the combination of a decrease in overall bed scour frequency and an increase in subsurface water storage. Most vegetation within and near the low-flow channel is fairly young (predominantly post-2005), but there are stands of mature riparian forest (i.e., trees >20 years old) present on the fringe of the active channel.

Figure F-9. Mainstem reach M14 (looking upstream).

Figure F-10. Mainstem reach M13 (looking downstream).

The most upstream of the Study tributaries that drain to the Lower Region are Oak Springs and Sand canyons, both of which are moderately developed and transport a relatively fine sediment load to reach M16. Downstream of its headwaters, Oak Spring Canyon becomes an ephemeral wash that transitions from a moderately confined channel that flows through a golf course to a more confined channel that continues through a residential area before entering the mainstem USCR. The reach-average slope from the golf course downstream ranges over almost a factor of 2 (1.6–2.9%) and the bed texture ranges from very fine to fine gravel [G_{vf}–G_f] (Figure F-11). The Sand Canyon subwatershed is larger and more developed than Oak Springs Canyon, with both Sand Canyon and Iron Springs Canyon (a secondary tributary channel) flowing through or adjacent to residential areas and golf courses. Both tributary channels are highly confined and range in slope by a factor of 8 (from 1.7 to 8.7%) and in bed texture from very fine to medium gravel [G_{vf}–G_m] (Figure F-12). The sediment deposits at the mouths of these subwatersheds are substantial and contribute to the local confinement of the mainstem USCR channel. The extent of channel confinement and subwatershed development has undoubtedly impacted channel stability and sediment delivery within these tributaries. Recent channel realignment, bank protection, and channel gradient modification near the mouth of Sand Canyon provide a good indication of measures taken to counteract such development-induced impacts.

Figure F-11. Lower Oak Springs Canyon (looking upstream).

Figure F-12. Lower Sand Canyon (looking upstream).

The next Study tributary downstream to drain to the main stem is Mint Canyon, which transitions from relatively undeveloped to moderately developed downstream, transporting a relatively fine sediment load to the upstream end of mainstem reach M15. The upstream study reaches are within a relatively narrow valley where the channel is confined by valley walls and by Sierra Highway, which runs the length of the Mint Canyon stream channel. The channel transports a relatively mixed load within these reaches (very fine to very coarse gravel [G_{vf}–G_{vc}]), has a modest reach-average gradient (1.4–1.8%), and appears to be supply-limited and moderately incised. Channel gradient and form are strongly influenced by local bedrock exposures and bridge crossings, causing the local variability in channel incision and sediment storage dynamics. Within the middle reaches, the channel flows adjacent to Sierra Highway and through residential areas where road and bridge crossings act to stabilize the channel gradient. It also appears that channel modification have been constructed in several locations to help mitigate instability and erosion caused by historic channel incision. The channel through the middle reaches has little geomorphic structure, has a moderate channel gradient (reach-average slope ranges from 1.3 to 1.6%), has a poorly sorted fine-grained bed (bed texture is predominantly very fine gravel [G_{vf}]), and appears to be currently quasi-stable within a historically incised channel (Figure F-13). The downstream reaches transition from a straightened, highly-confined channel that is locked in place along developed areas to an engineered channel that flows under a residential development before entering the mainstem USCR. Similar to upstream reaches, the channel upstream of the engineered reach has a relatively fine bed texture, a relatively moderate channel gradient, and is incised yet currently maintains a stable gradient through a bridge-induced grade control. The engineered reaches have a somewhat steeper channel gradient (and higher sediment transport capacity) than the reaches upstream, and the fine-grained bed texture (very fine gravel [G_{vf}]) indicates the dominant sediment size that is delivered from Mint Canyon to the mainstem USCR.

Figure F-13. Middle Mint Canyon (looking upstream).

Bouquet Canyon drains to the mainstem USCR within reach M14 and has the largest effective drainage area (i.e., area downstream of a major dam that contributes flow and sediment to the mainstem USCR) of all the Study subwatersheds. The headwaters of the subwatershed drain to Bouquet Reservoir, which regulates the upper 35 km^2, or approximately 20% of the total subwatershed area, and presumably traps virtually all of the incoming sediment. The watershed transitions from moderately developed to highly developed moving downstream towards the mouth, with the study reaches transitioning from highly confined canyon reaches to moderately confined alluvial reaches to highly confined engineered reaches through dense floodplain residential development. The reach between Bouquet Reservoir and the start of the Study reaches is relatively steep and confined by Bouquet Canyon Road. Approximately 10 km downstream of the reservoir near a U.S. Forest Service station, an undersized road crossing currently results episodic upstream backwatering, sediment deposition upstream, and channel incision downstream. There are plans to improve flow and sediment passage under this crossing through expansion and realignment of the cross-culvert.

At the start of the mainstem Bouquet Canyon Study reaches at the Texas Canyon confluence, the channel continues to be confined by Bouquet Canyon Road, but the channel gradient decreases somewhat compared to upstream. The channel bed is comprised predominantly of very fine to coarse gravel [G_{vf}–G_c] and receives the coarse fraction from Texas Canyon, a study channel that has a relatively steep channel gradient (2.4%) and relatively coarse bed texture (predominantly coarse gravel [G_c]). Continuing downstream, the channel moves away from Bouquet Canyon Road and is located within residential areas where the channel appears to have been redirected and straightened in several sections (Figure F-14). The channel has a moderate gradient throughout these middle reaches and the bed currently appears to be stable due in part to several road crossings acting as grade control. The channel bed also appears very mobile and has a relatively fine texture (predominantly very fine gravel [G_{vf}]), which is supported by the large input of fine sediment from Vasquez Canyon (a relatively steep, incised, channelized study channel whose gradient is currently stabilized by road and bridge crossings). After entering the dense residential development along both floodplains, the channel is confined by concrete banks for approximately 6 km before entering a short natural reach at the confluence with the mainstem USCR. The lower reach at the confluence has a moderate channel gradient (1.9%) and fine bed texture (predominantly sand [S]).

Figure F-14. Middle Bouquet Canyon (looking downstream).

Along the lower reaches of Bouquet Canyon, the channel receives flow and a relatively fine sediment load from several secondary tributary channels included in the Study area. Plum Canyon is a small, engineered channel that drains a housing development and enters Bouquet Canyon approximately 5 km upstream from the mainstem USCR confluence. Haskell Canyon, which enters Bouquet Canyon approximately 1 km downstream of Plum Canyon, drains a larger area than Plum Canyon and transitions from a wash through an undeveloped area to a highly-confined, straightened engineered channel through a residential development. Dry Canyon, which enters Bouquet Canyon approximately 1 km upstream from the USCR confluence, drains an area downstream of the in-filled Dry Canyon reservoir. Downstream of the reservoir, the channel transitions from natural to engineered. The natural channel is extremely unstable and there is currently a 3–4 m knickpoint migrating upstream (Figure F-15). The instability appears to be caused by an adjacent development drainage outfall positioned downstream. The sediment load being eroded from the channel, and subsequently delivered to the mainstem USCR, is predominantly very fine to medium gravel [G_{vf}–G_m].

Figure F-15. Upper Dry Canyon (looking upstream).

The next Study subwatershed downstream that drains to the mainstem USCR is the South Fork SCR, a highly developed, highly impacted catchment that contributes considerable fine sediment to the downstream end of reach M14. The city center of Santa Clarita is located within this subwatershed, resulting in a very high average development density . The channel network has been engineered to convey flood flows rapidly while maintaining a stable channel form and grade. The major tributaries that drain to the mainstem South Fork SCR are (from west to east) Pico Canyon, upper South Fork SCR, Newhall Creek, and Placerita Creek. Pico Canyon, the tributary draining the western portion of the subwatershed, transitions from a culvert pipe under a housing development to a low-gradient concrete channel that passes under a business development and Interstate 5. The tributary then becomes a small quasi-natural channel through a golf course before transitioning to an engineered channel with a fine-grained bed and grade control structures to maintain bed position. Upper South Fork SCR, which drains the southwestern portion of the subwatershed and contains Lyon Canyon, transitions from a small natural channel to a concrete channel and box culvert under Interstate 5. Downstream, the tributary is highly incised (~2–3 m) with a moderate gradient and relatively coarse bed (coarse gravel [G_c]) before becoming an engineered channel through Santa Clarita. Towards the confluence with the main South Fork SCR, the upper South Fork SCR channel widens and grade control structures affix the bed elevation, resulting in a relatively fine bed texture and an overall depositional channel. Newhall Creek, which drains the southeastern portion of the subwaterhsed, starts as wide, low-gradient alluvial channel with relatively fine bed (predominantly very gravel [G_{vf}]) and then becomes and engineered channel through a residential area before transitioning back to a depositional alluvial channel at the South Fork SCR confluence (Figure F-16). Channel gradient within the upstream natural reach is maintained by the bed elevation at the engineered channel transition. Similar to Newhall Creek, Placerita Creek, which drains the eastern portion of the subwatershed, is a low-gradient natural channel with a relatively fine bed (very fine gravel [G_{vf}], though large particles are present) that flows through a residential area before the South Fork SCR confluence . Channel gradient throughout is maintained by at-grade road crossings and bridges, though local incision and channel instability downstream of these grade controls can be very pronounced (Figure F-17).

Figure F-16. Lower Newhall Creek (looking upstream).

Figure F-17. Middle Placerita Creek (downstream of road crossing).

Downstream from the confluence of the four Study tributaries, the mainstem South Fork SCR flows through a relatively wide engineered reach and then enters a narrow engineered reach before draining to the mainstem USCR (Figure F-18). A decrease in channel width between the Magic Mountain Parkway bridge and the Valencia Road bridge crossings, in conjunction with in-channel grade control structures, causes the engineered reach to have a relatively low gradient and act as a sediment trap. The sediment being deposited in the engineered reach is predominantly sand to very fine gravel [S–G_{vf}]. The bed sediment in the reach just upstream of the confluence with the mainstem USCR has coarser sediment patches than is present in the upstream reach, suggesting that coarser sediment from upstream reaches (presumably from Placerita Creek) is indeed transported out of the subwatershed during some storm events.

Figure F-18. South Fork SCR (looking upstream).

Similar to neighboring Bouquet Canyon, San Francisquito Canyon, which enters the mainstem USCR at the upstream end of reach M14, increases in development towards the downstream end of the subwatershed. The channel transitions from canyon reaches confined by valley walls in the upper subwatershed to reaches confined by in-channel infrastructure in the lower subwatershed. The Study channel begins in a canyon reach downstream of the St. Francis Dam-break site. The upstream-most Study reach is moderately steep and bedrock-confined with a relatively coarse, poorly sorted bed that contains large, coarse depositional bars. Local channel gradient and sediment deposition dynamics are controlled by valley-wall constrictions and local bedrock outcropping. The valley walls are composed of colluvium deposits and contribute coarse sediment directly to the tributary channel. Downstream from San Francisquito Reach 1, the degree of channel confinement decreases, the channel gradient decreases, and the channel bed texture becomes finer (see Figures 4-17 and 4-18 in the main report). The middle alluvial reaches maintain a relatively high active width (50–100 m) and relatively low, stable channel gradient (0.9%), with a bed texture that transitions from coarse to very fine gravel [G_c–G_{vf}] (Figure F-19). The channel morphology is somewhat braided (i.e., there appears to be more than one dominant channel in some locations) and the channel bed appears to be very mobile. Most in-channel vegetation appears to be fairly young (<10 years old) and is buried at the base with fresh sediment. The most downstream reach is confined on both banks by residential and commercial development for approximately 1.5 km before the confluence with the mainstem USCR. Although this reach has a higher degree of confinement than the upstream alluvial reaches, it is predominantly depositional with a relatively low reach-average channel slope (0.7%) and fine bed texture (predominantly very fine gravel [G_{vf}]). The relatively low mainstem USCR channel gradient at the San Francisquito Creek confluence promotes sediment deposition and the growth of the mouth bar deposit, which in turn controls the local gradient and promotes sediment deposition within lower San Francisquito Creek.

Figure F-19. Middle San Francisquito Creek (looking downstream).

Lion Canyon is a small, Study subwatershed that drains to the downstream end of M14. The subwatershed has very little developed area, yet has an extensive unpaved road network and several cleared areas for future development. The extent of impervious surfaces throughout the subwatershed most likely results in a channel that is supply-limited compared to historic conditions. The main tributary channel transitions from a small, relatively steep headwater channel draining a mountain catchment to a relatively steep alluvial wash that meanders through a cleared valley before entering the mainstem USCR. Several road crossings act to control the channel gradient, causing upstream sediment deposition and downstream channel incision. The road crossing in the most downstream reach results in a steep incised channel that extends to the mainstem USCR confluence. The bed texture is relatively fine throughout the subwatershed (sand to fine gravel [S–G_f]) and the channel appears to deliver a considerable supply of fine sediment to the lower mainstem channel.

The next Study subwatershed to drain to the mainstem USCR is Castaic Creek, which enters the mainstem USCR at the upstream end of M12 and is a source of finer and coarser sediment within the Lower Region. The regulation of approximately one-quarter of the subwatershed by Castaic Lake has decreased flow (see Figure 4-8 in the main report) and cut off virtually all sediment delivery to downstream reaches. Despite this condition, the mainstem Castaic Creek channel between the dam and the USCR appears to have an overall stable morphology due to a sustained sediment supply and grade control by in-channel structures. The two most upstream study tributaries (Violin Canyon and Violin Canyon 2 [aka: Marple Canyon]) transition from natural to engineered flood control channels through developed areas before converging. The sediment supply from Violin Canyon—a tributary with a high sediment that is constrained by valley walls and contains coarse sediment—to the mainstem Castaic Creek appears to be somewhat reduced compared to historic conditions (Figure F-20). At the confluence of the Violin Canyon engineered reach with mainstem Castaic Creek (approximately 0.75 km downstream of the Castaic Lagoon dam), a large sediment deposit marks the transition from a supply-limited gorge that appears incised by over 10 meter directly downstream of the dam to a mainstem channel that is less incised with a stable gradient and considerable sediment storage. Sediment is derived locally from the eroding left bank bluff downstream of the dam (coarser and finer fraction) and Charlie Canyon (right bank tributary that delivers a fairly fine sediment load).

Figure F-20. Violin Canyon (looking downstream toward engineered reach).

Downstream from the Charlie Canyon confluence, the channel is confined by alluvial terraces and the gradient is controlled by the Tapia Canyon Road bridge crossing (culverts across the active channel) and the Interstate 5 bridge piers and abutments (Figure F-21). The low-flow channel in these reaches meanders through large bar deposits and has a low channel gradient and a bed that is primarily composed of fine to medium gravel [G_f–G_m]. From the Interstate 5 bridge to the confluence with the mainstem USCR, the channel continues to have a considerable amount of sediment storage and the gradient remains relatively low and stable due to the grade control provided by the Commerce Center Drive bridge and Highway 126 bridge. In-channel vegetation is also more established compared to upstream and the bed texture towards the mouth remains predominantly gravel, although coarse cobble [C_c] is present.

Figure F-21. Middle San Castaic Creek (looking upstream).

Hasley Canyon, the dominant tributary to lower Castaic Creek and a Study tributary, enters Castaic Creek just upstream of the Commerce Center Drive bridge and delivers a relatively fine sediment load. Hasley Canyon drains a subwatershed containing a residential development and transitions from a relatively steep wash with a channel inset a few meters below the adjacent floodplain to an engineered channel through a commercial development. Downstream, the channel becomes a lower gradient inset wash with a low-flow channel that meanders around the active channel zone before entering mainstem Castaic Creek underneath Commerce Center Drive. At the confluence with Castaic Creek, the Hasley Canyon bed is predominantly very fine to fine gravel [G_{vf}–G_f].

Similar to Lion Canyon, Long Canyon, which enters the mainstem USCR at the downstream end of M12, is a study subwatershed that drains an area impacted by impervious surfaces and delivers a fine sediment load. The main tributary channel is a steep wash throughout its length that originates on the ridge adjacent to the Pico Canyon headwaters. As it flows downstream, the channel becomes moderately confined within a narrow valley before entering a more broad alluvial valley. The channel has been straightened through an agricultural field for the 0.5 km reach upstream of the confluence with M12. Throughout the length of the channel, natural valley constriction and road crossings act to control channel gradient and cause local lower-gradient depositional zones and higher gradient incised areas. The bed sediment is very fine grained throughout (predominantly sand [S]) and the channel appears to deliver a finer sediment load than Lion Canyon.

The third and final study subwatershed to enter M12 is San Martinez Chiquito Canyon, which is highly impacted by development in the upper reaches and is a considerable source of finer sediment to the Lower Region mainstem channel. The study reaches are located within the town of Val Verde along San Martinez Road and through residential developments. The channel through these reaches is very confined, relatively steep, highly incised, and has a relatively fine bed texture (predominantly sand to fine gravel [S–G_f]). The bed texture remains this fine downstream to the confluence with the mainstem USCR. The channel is incised several meters in some of the upper reaches and there are active restoration efforts aimed at stabilizing channel gradient and channel banks (Figure F-22). Downstream of the upper-most Chiquito Canyon Road crossing, the channel changes from incised and supply-limited to a channel with a stable gradient that stores and transports a considerable sediment load. This change is caused primarily by an increase in sediment production from adjacent hillslopes coupled with bedrock-induced grade control at local valley wall constrictions. A short, steep bedrock reach separates upper and lower reaches with high sediment storage and transport capacity (Figure F-23). As culverts under road crossings are buried on both the upstream and downstream side, the increase in sediment supply and storage downstream of the Chiquito Canyon Road crossing appears somewhat recent. Between the lowermost Chiquito Canyon Road crossing and the Highway 126 bridge crossing, the channel bed elevation drops several meters below the adjacent terrace; however, the bed elevation rises to above the adjacent floodplain downstream of Highway 126 bridge to be at grade with the mainstem USCR confluence. This lowermost reach is channelized and confined by agricultural levees. The mainstem USCR through M12 is very depositional and aggraded, which in turn promotes deposition of the considerable fine sediment load from the subwatershed in the lower reaches of San Martinez Chiquito Canyon.

Figure F-22. Upper San Martinez Chiquito Canyon (looking downstream).

Figure F-23. Middle San Martinez Chiquito Canyon (looking upstream).

San Martinez Grande Canyon is the next Study subwatershed downstream from San Martinez Chiquito Canyon and enters the mainstem USCR at the upstream end of M11-B. Although the subwatershed is similar in many ways to the adjacent San Martinez Chiquito Canyon, differences in local sediment production, degree of channel confinement, and development-induced increase in runoff volume result in a channel that is more supply-limited and relatively inset. The most upstream Study reach contains a small, steep-gradient (3.3%) tributary channel that drains a mountain catchment. Downstream of the confluence with the other primary tributary channel that drains the western subwatershed, the channel is larger yet very confined and the bed is inset several meters below the adjacent terrace. The active channel has little structure, contains relatively mature vegetation and the bed texture is fine-grained (predominantly sand to fine gravel [S–G_f]), however cobbles and boulders are present. As the channel continues downstream along San Martinez Grande Canyon Road, the bed becomes more inset as it flows past an industrial operation on the right bank floodplain with a large developed footprint. The channel bed through this reach is currently stable and the in-channel vegetation is relatively mature (>10 years old), suggesting that the channel has adjusted to the increased runoff and reduced sediment delivery associated with the adjacent road and floodplain development. Several trees in this part of the subwatershed appear to have been recently burned, possibly in the recent 2007 Ranch Fire. Farther downstream, the channel meanders through a reach confined by valley walls. The channel gradient through the meandering reaches is higher than upstream and the bed is very mobile. The bed texture is predominantly sand to very fine gravel [S–Gv_f] and there appears to be a relatively recent influx of a finer sediment load (Figure F-24). The reach between the Highway 126 bridge and the confluence with the mainstem USCR has been channelized and is confined by agricultural levees. The bed texture is very fine (silt to sand [S]) and although the channel bed elevation currently appears to be stable, there is evidence that there has been recent channel down-cutting through a fine-grained alluvial deposit. It is possible that a pulse of fine sediment was transported to the mouth of San Martinez Grande Creek during a storm event after the 2007 Ranch Fire, and that the channel has been eroding through this deposit ever since.

Figure F-24. Middle San Martinez Grande Canyon (looking downstream).

The most downstream Study subwatershed that drains to the mainstem USCR is Potrero Caynon, which enters M11-B approximately 0.75 km downstream from the San Martinez Grande Canyon confluence. Similar to both Lion Canyon and Long Canyon, Potrero Canyon drains an area impacted by development and delivers a fine sediment load. The channel within the upstream study reaches is relatively unconfined and meanders through a cleared alluvial valley, with several road crossings controlling local channel gradient. The channel through these reaches has a moderate gradient (1.8–2.1%) and fine bed texture (predominantly sand to very fine gravel [S–G_{vf}]). As the channel continues downstream, it becomes confined by Pico Canyon Road and appears channelized. Flow confinement has caused the channel to incise and resulted in steep local gradient (up to 4.3%). At the confluence with the mainstem USCR, the channel gradient is very low (0.7%) and the channel bed texture is predominantly very fine gravel [G_{vf}].

Appendix G

Bedload Transport Capacity Analysis
Supporting Materials

BEDLOAD TRANSPORT CAPACITY ANALYSIS SUPPORTING MATERIALS

This appendix provides additional details on the methods employed and results generated from our analysis of bedload transport capacity. As introduced in Section 4.3.2 of the main report, this analysis was conducted at numerous sites throughout the Feasibility Study reaches of the USCR watershed (see site locations in Figure 4-19 of the main report). Here we present the equations used in our analysis along with the generated transport capacity curves. This analysis was performed by our senior hydraulic engineer, Dr. Yantao Cui, who is internationally recognized for his many years of research in sediment transport modeling, including the authorship of several customized models.

Bedload Transport Capacity Analysis Equations

Transport capacity modeling required the use of two equations whose application depended on relative bed texture. The Brownlie (1982) equation was used to determine sediment transport capacity for the finer-bedded reaches (D_{50} <4 mm) and the Parker and Klingman (1982) equation for the coarser-bedded reaches (D_{50} >4 mm). The Brownlie (1982) equation is one of the most reliable equations for rivers with relatively finer bed material particles (i.e., sand or slightly coarser), due in large part to the extensive amount of field data used to develop the equation. The Parker and Klingman (1982) equation is widely used to calculate transport capacity for coarser-grained sediment load based on surface bed particle size and has been shown to perform very well in many sediment transport investigations (e.g., Sutherland et al. 2002, Cui et al. 2008, Shvidchenko and Pender 2008).

The form of the Brownlie (1982) equation used in this analysis can be expressed as

$$Q_s = 7.115 \times 10^{-3} \frac{1.268}{R+1} Q_w \left(F_g - F_{go}\right)^{1.978} S_f^{\ 0.6601} \left(\frac{R_h}{D_{50}}\right)^{-0.3301} \tag{G.1}$$

in which Q_s denotes volumetric sediment transport rate; R denotes submerged specific gravity of sediment particles; Q_w denotes river discharge rate; S_f denotes local friction slope, and in this study, approximated with surveyed local bed slope or water surface slope; R_h denotes hydraulic radius; D_{50} denotes bed material median size; and

$$F_g = \frac{Q_w}{A\sqrt{RgD_{50}}} \tag{G.2}$$

$$F_{go} = 4.596\tau_{*o} S_f^{\ -0.1405} \sigma_g^{\ -0.1606} \tag{G.3}$$

$$\tau_{*o} = 0.22Y + 0.06^{(-17.73Y)} \tag{G.4}$$

$$Y = \left(\sqrt{RR_g}\right)^{-0.6} \tag{G.5}$$

$$R_g = \frac{\sqrt{gD_{50}^{\ 3}}}{\nu} \tag{G.6}$$

in which *A* denotes flow area; *g* denotes acceleration of gravity; σ_g denotes bed material geometric standard deviation; R_g denotes grain Reynolds number; ν denotes kinematic viscosity of water; and all other parameters are intermediate parameters to make the expression more readable (e.g,. F_g and F_{go} effectively represent the downward pull on a settling sediment particle).

Hydraulic radius (R_h) was calculated with the Brownlie (1982) resistance relations combined with a known friction slope (S_f) value:

$$S_f = 0.02054 R^{1.286} F_g^{\ 2.572} \left(\frac{R_h}{D_{50}}\right)^{-1.361} \sigma_g^{\ 0.4130} \text{ for lower flow regime} \tag{G.7a}$$

$$S_f = 0.01252 R^{1.086} F_g^{\ 2.172} \left(\frac{R_h}{D_{50}}\right)^{-1.304} \sigma_g^{\ 0.2785} \text{ for upper flow regime} \tag{G.7b}$$

When $S_f > 0.006$, the flow was considered to be upper regime and equation (G.7a) was used. For $S_f < 0.006$, an additional computation was needed to determine whether the flow was upper regime or lower regime. The first step in the additional computation involved determining the values for the following parameters:

$$F_g' = 1.74 S_f^{\ -1/3} \tag{G.8}$$

$$u_*' = \sqrt{g R_h' S_f} \tag{G.9}$$

$$\delta = \frac{11.6\nu}{u_*'} \tag{G.10}$$

where F_g' effectively represents the submerged weight of the settling sediment particle, u_*' denotes shear velocity, δ effectively represents an eddy length scale, R_h' (effective hydraulic radius) in equation (G.9) had to be calculated with equation (G.7b) (i.e., with the upper flow regime assumption).

The lower limit of upper regime flow was determined using the following equation:

$$\ell og_{10}\left(\frac{F_g}{F_g'}\right) = \begin{cases} -0.02469 + 0.1517\,\ell og_{10}\left(\frac{D_{50}}{\delta}\right) + 0.838\,\ell og_{10}^2\left(\frac{D_{50}}{\delta}\right) \ for\ \frac{D_{50}}{\delta} < 2 \\ \ell og_{10}(1.25)\ for\ \frac{D_{50}}{\delta} \geq 2 \end{cases} \tag{G.11a}$$

If the value of $log_{10}(F_g/F_g')$ using equations (G.2) and (G.8) was greater than that given in equation (G.11a), the flow was determined to be in upper regime and equation (G.7b) was used.

The upper limit of lower regime flow was determined using the following equation:

$$\ell \mathrm{og}_{10}\left(\frac{\mathrm{F_g}}{\mathrm{F_g}'}\right) = \begin{cases} -0.2026 + 0.07026\,\ell \mathrm{og}_{10}\left(\frac{\mathrm{D}_{50}}{\delta}\right) + 0.933\,\ell \mathrm{og}_{10}^2\left(\frac{\mathrm{D}_{50}}{\delta}\right) \text{ for } \frac{\mathrm{D}_{50}}{\delta} < 2 \\ \ell \mathrm{og}_{10}(0.8) \text{ for } \frac{\mathrm{D}_{50}}{\delta} \geq 2 \end{cases} \tag{G.11b}$$

If the value of $log_{10}(F_g/F_g')$ using equations (2) and (8) was less than that given by (11b), the flow was determined to be in lower regime.

If $log_{10}(F_g/F_g')$ using equations (2) and (8) was less than calculated with equation (11a) and higher than calculated in equation (11b), then flow the flow was considered to be in transition, and hydraulic radius (R_h) was assumed to be the average of that calculated with equations (G.7a) and (G.7b).

The form of the Parker and Klingman (1982) equation used was derived from the BAGS computer program (Pitlick et al. 2009, Wilcock et al. 2009) and can be expressed as

$$\phi_i = \frac{\tau_{50}^*}{\tau_{r50}^*}\left(\frac{D_i}{D_{50}}\right)^{-\beta} \qquad \text{(G.12a)}$$

$$\frac{p_i R Q_s}{f_i A S_f u_*} = \begin{cases} 11.2\left[1-\dfrac{0.853}{\phi_i}\right]^{4.5}, & \phi_i > 0.95 \\ 0.00243\phi_i^{35.714}, & \phi_i \le 0.95 \end{cases} \qquad \text{(G.12b)}$$

in which ϕ_i is normalized Shields stress for the i-th size group; τ^*_{50} denotes substrate D_{50}-based Shields stress; $\tau_r{}^*{}_{50}$ denotes substrate D_{50}-based reference Shields stress; D_i denotes the mean grain size of the i-th size group; D_{50} denotes substrate median grain size; β is a hiding coefficient, p_i denotes the volumetric fraction of the i-th size group in bedload; and f_i denotes the volumetric fraction of the i-th size group in the substrate. Shields stress was calculated by the following relationship:

$$\tau_{50}^* = \frac{\tau}{\rho R g D_{50}} \qquad \text{(G.13)}$$

in which ρ denotes the density of water. The hiding coefficient (β) value used was 0.018 and the reference Shields stress (τ^*_{50}) value used was 0.0876.

Hydraulic radius (R_h) and flow area (A) were calculated from Keulegan resistance relation:

$$\frac{Q_w}{Au_*} = 2.5\ell n\left(11\frac{R_{hc}}{k_s}\right) \qquad \text{(G.14)}$$

in which roughness (k_s) is assumed to be 10.7 times D_{50}.

Bedload Transport Capacity Curves

The bedload transport capacity curves are presented here in order that the modeled sites are listed in Tables 4-6 (tributaries) and 4-7 (mainstem river) of the main report, which are generally organized in an upstream to downstream order.

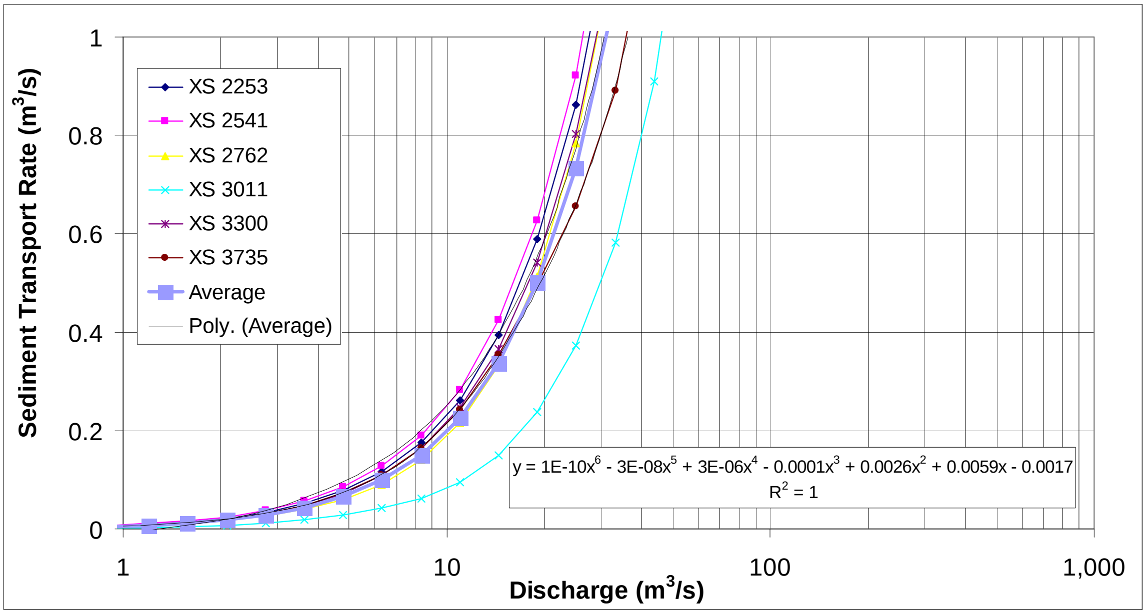

Figure G-1. Bedload transport capacity curves generated for Site 2-1 (Acton Canyon, Escondido Creek reach 3).

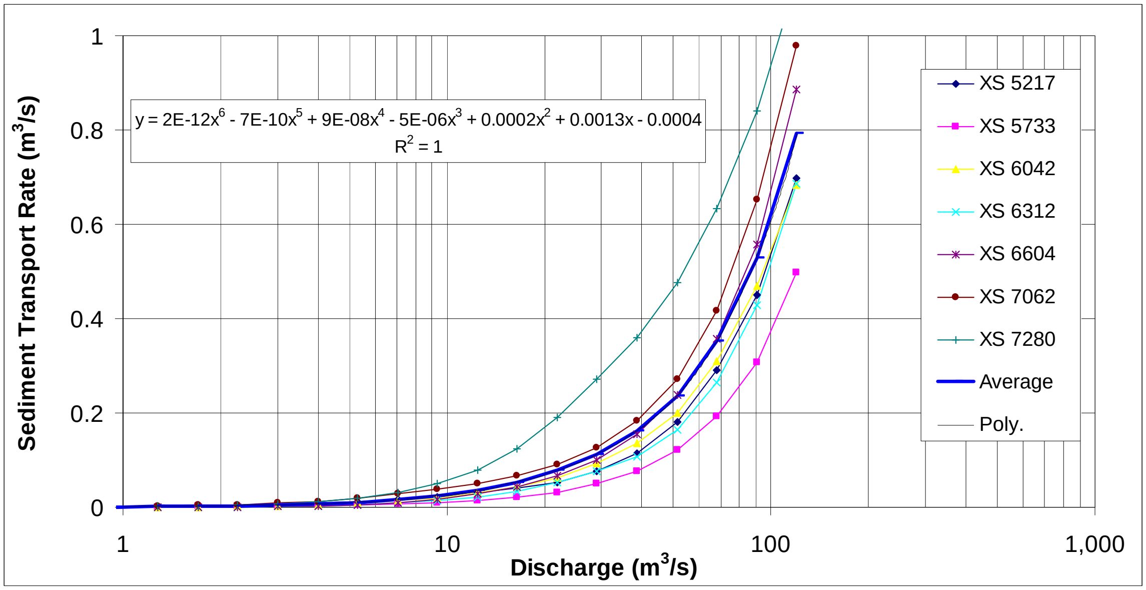

Figure G-2. Bedload transport capacity curves generated for Site 2-2 (Acton Canyon, reach 8).

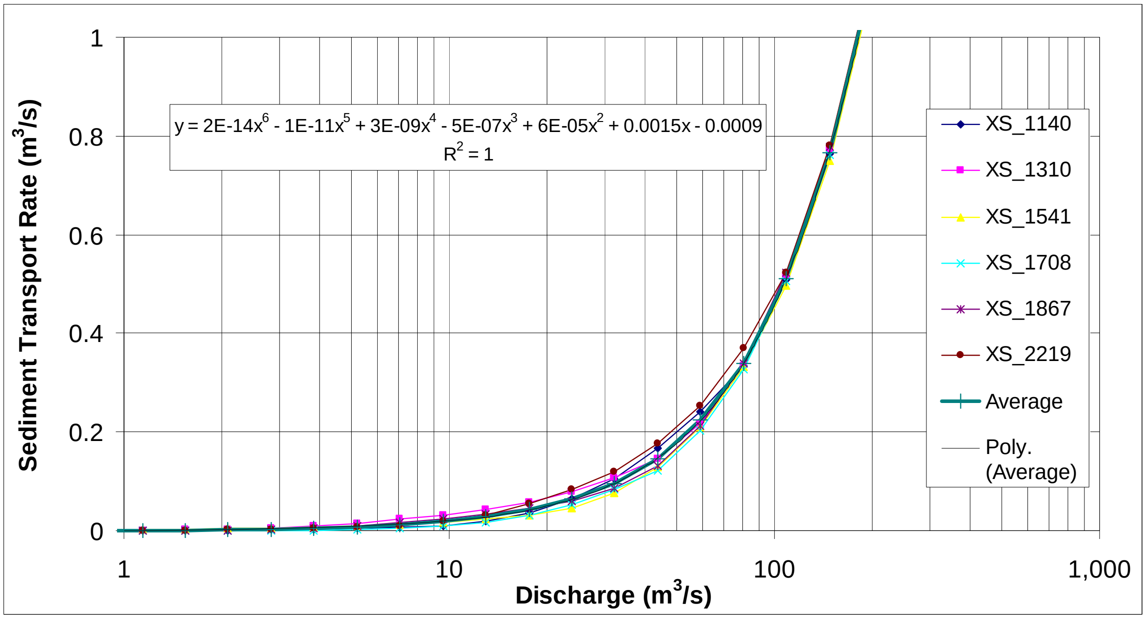

Figure G-3. Bedload transport capacity curves generated for Site 5-1 (Agua Dulce Canyon, reach 10).

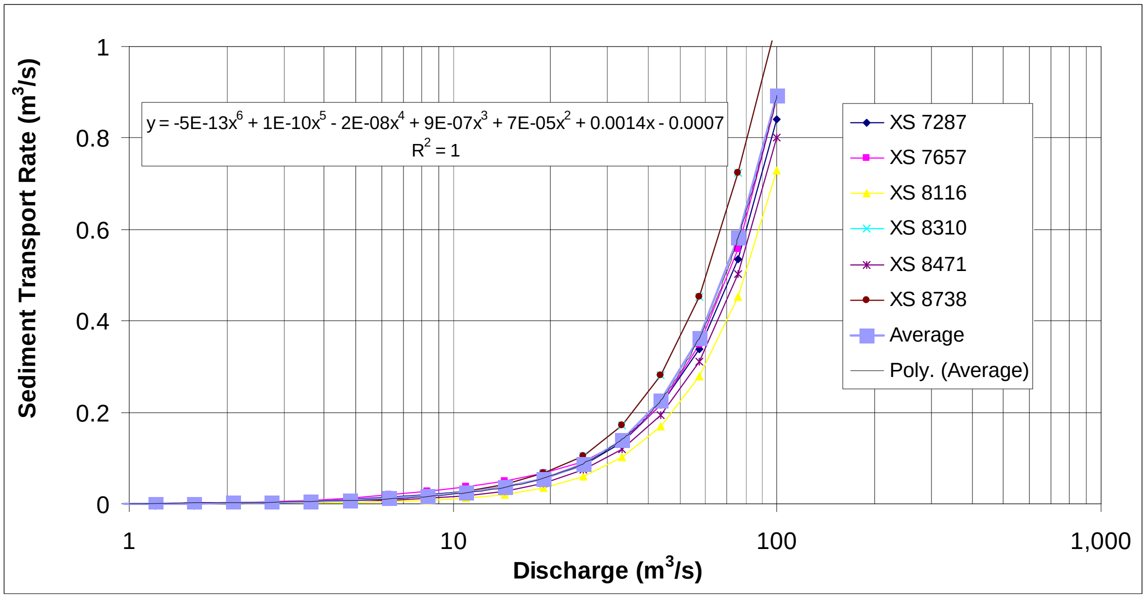

Figure G-4. Bedload transport capacity curves generated for Site 7-1 (Tick Canyon, reach 1).

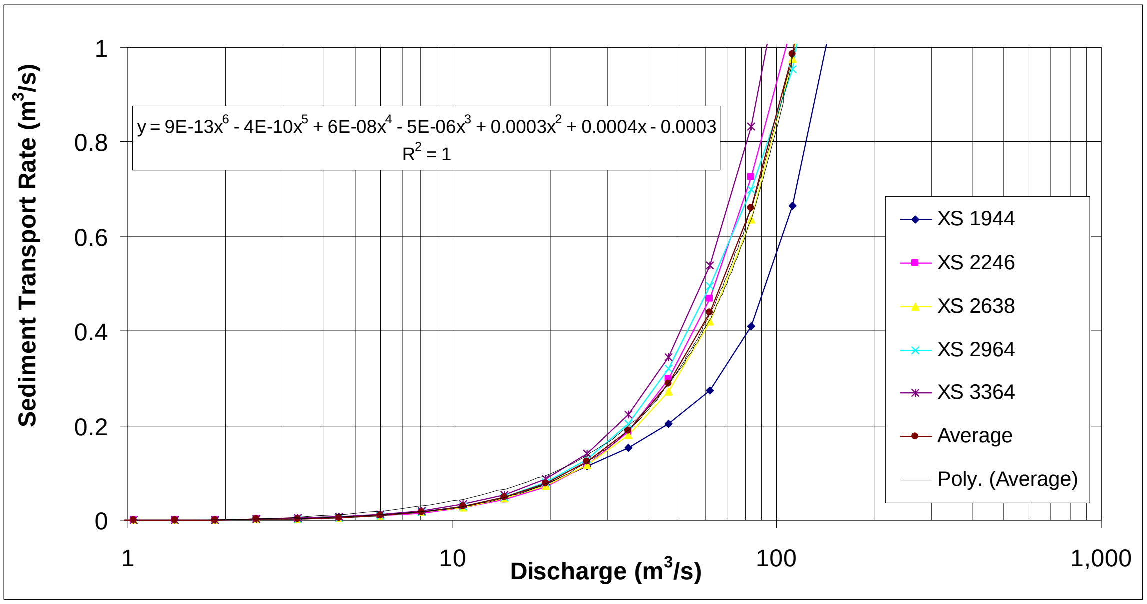

Figure G-5. Bedload transport capacity curves generated for Site 7-2 (Sand Canyon, reach 4).

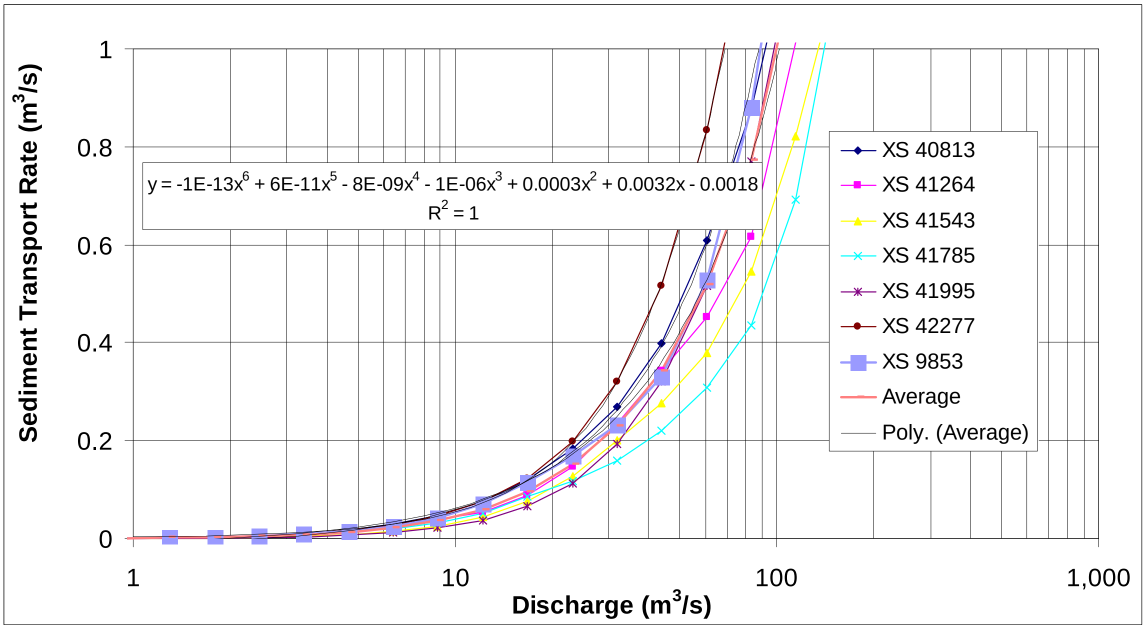

Figure G-6. Bedload transport capacity curves generated for Site 8-1 (Mint Canyon, reach 3).

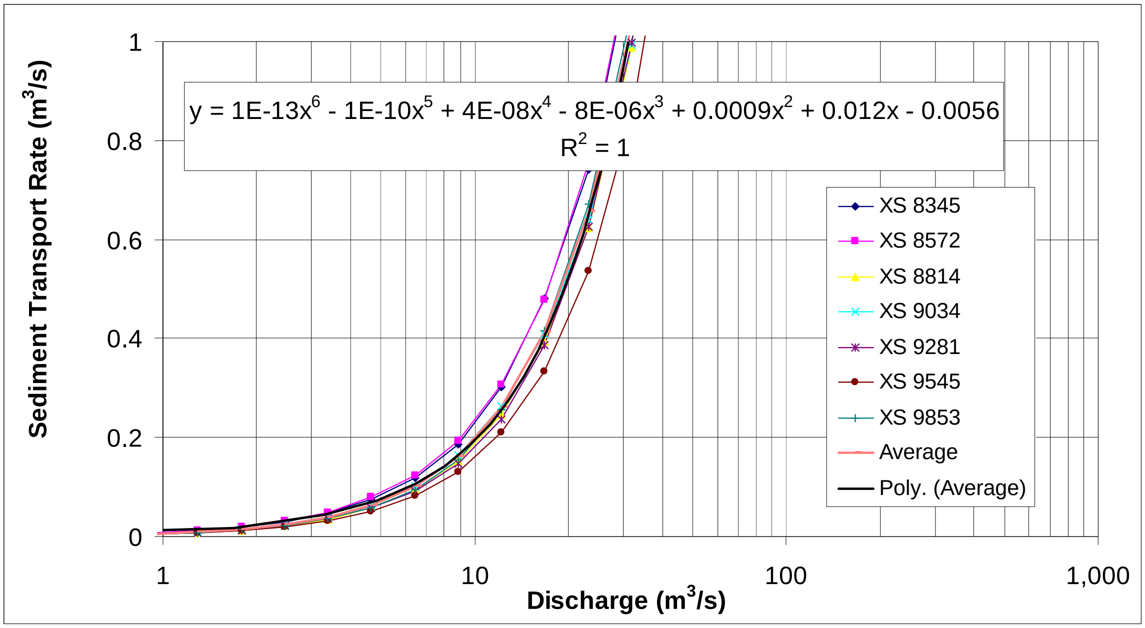

Figure G-7. Bedload transport capacity curves generated for Site 8-2 (Mint Canyon, reach 9).

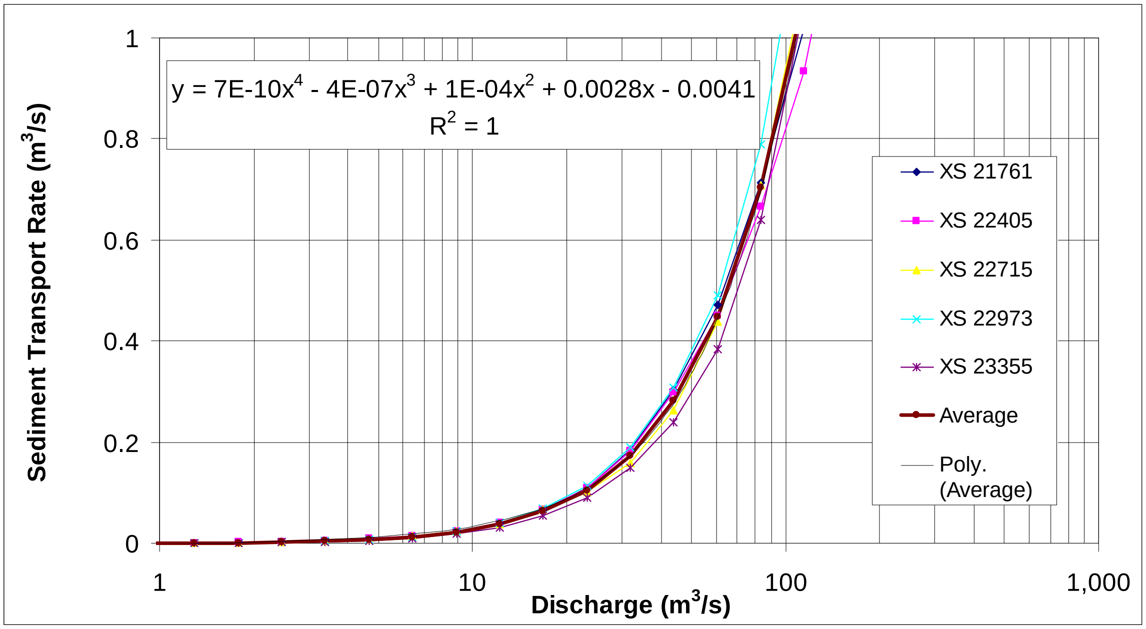

Figure G-8. Bedload transport capacity curves generated for Site 9-1 (Bouquet Canyon, reach 5).

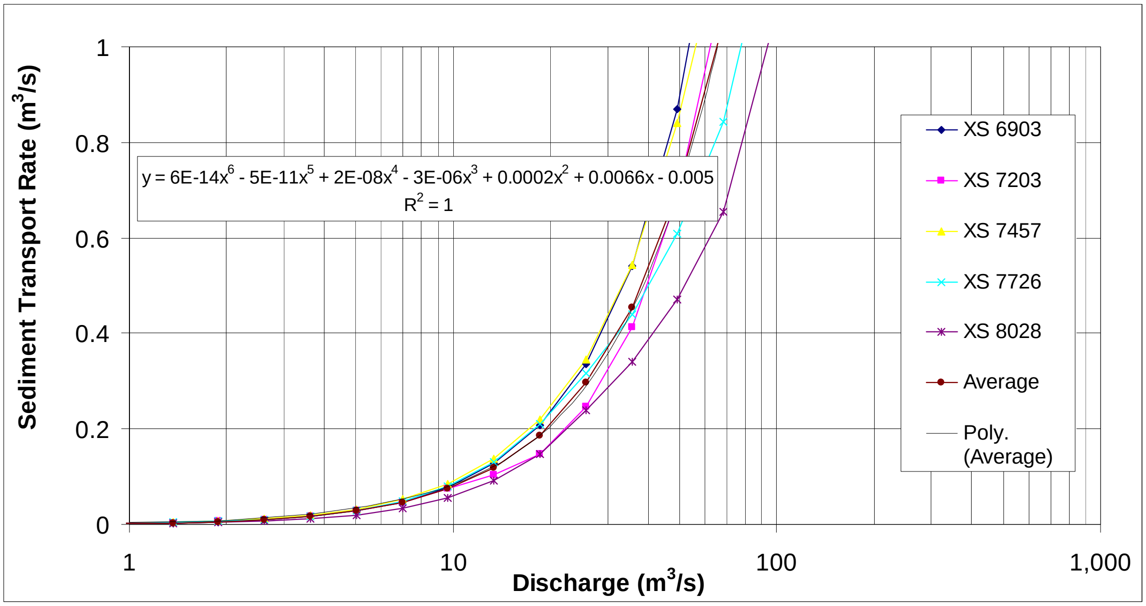

Figure G-9. Bedload transport capacity curves generated for Site 9-2 (South Fork Santa Clara River, reach 5).

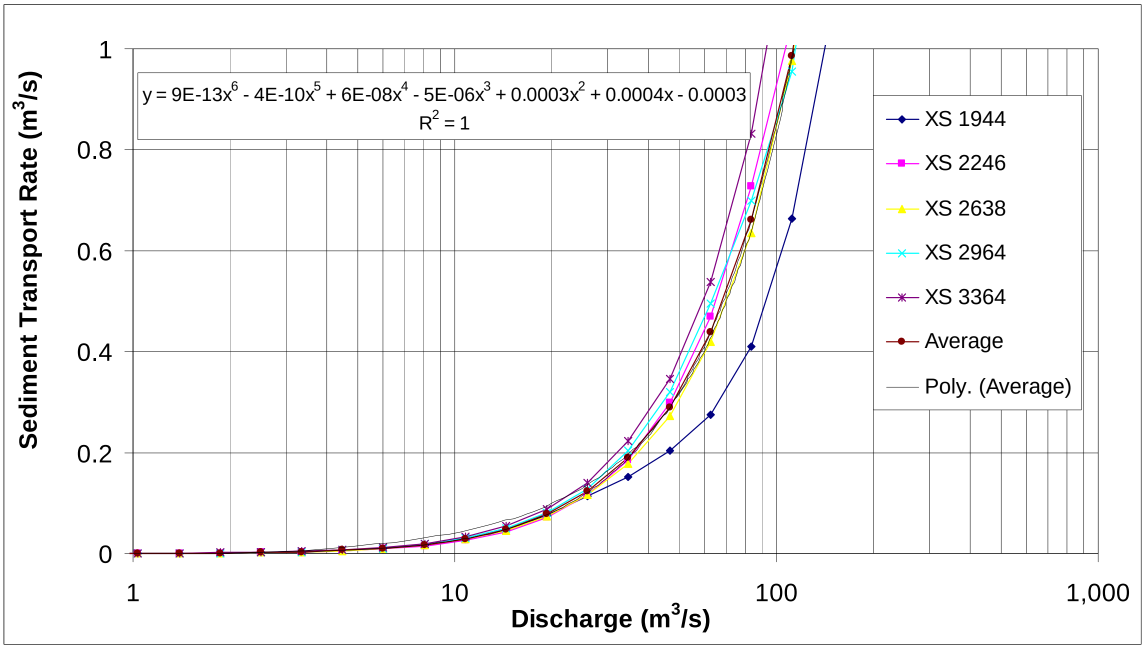

Figure G-10. Bedload transport capacity curves generated for Site 9-3 (South Fork Santa Clara River, Placerita Canyon, reach 4).

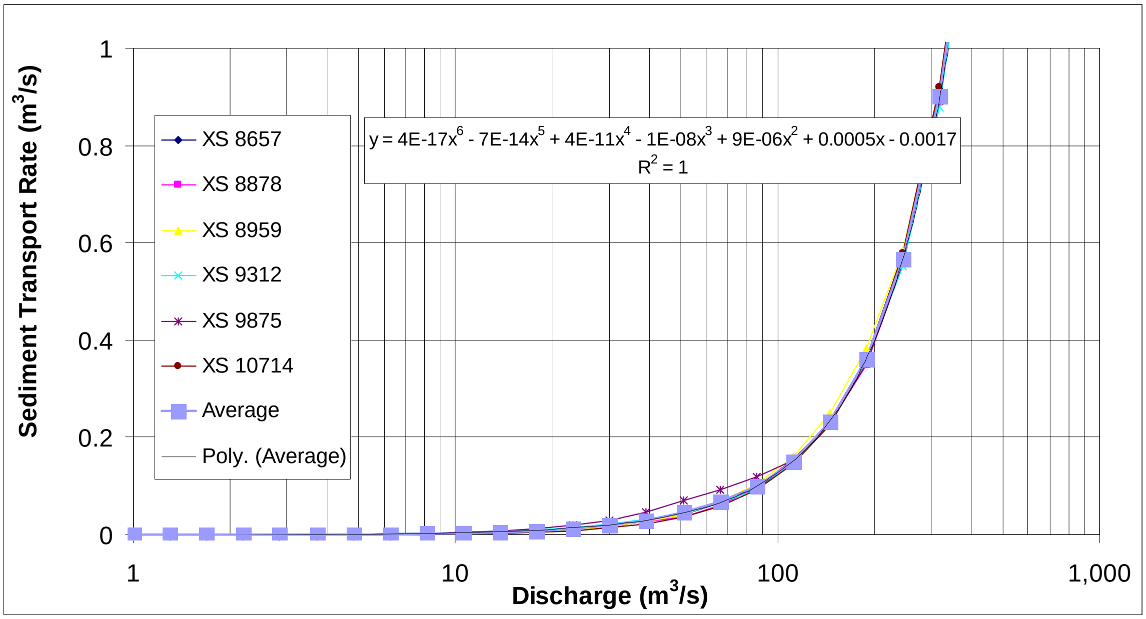

Figure G-11. Bedload transport capacity curves generated for Site 9-4 (South Fork Santa Clara River, reach 10).

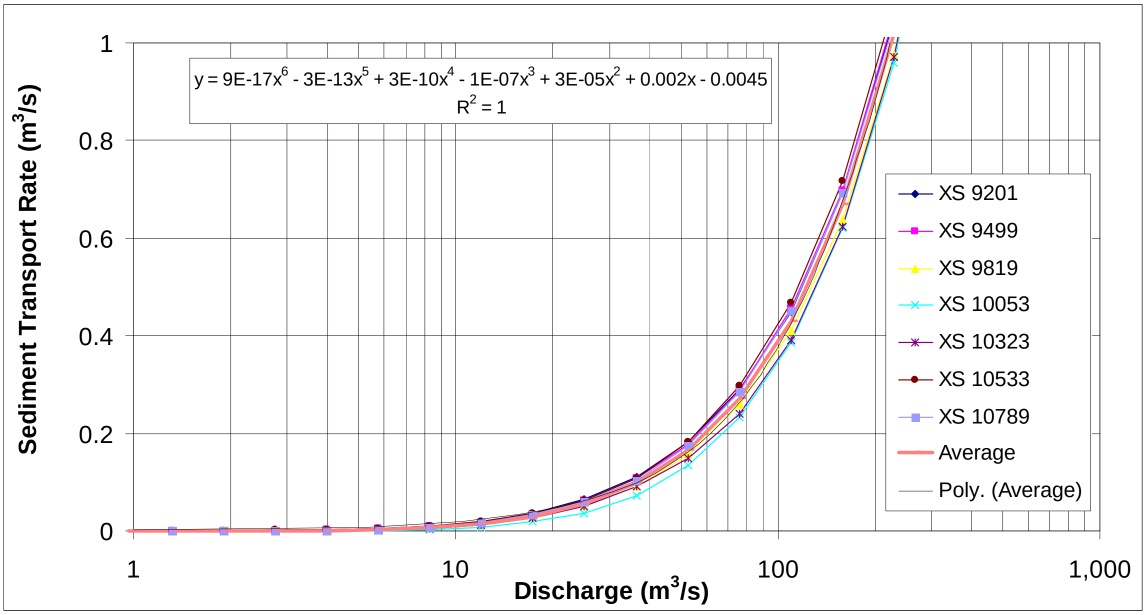

Figure G-12. Bedload transport capacity curves generated for Site 10-1 (San Francisquito Canyon, reach 1).

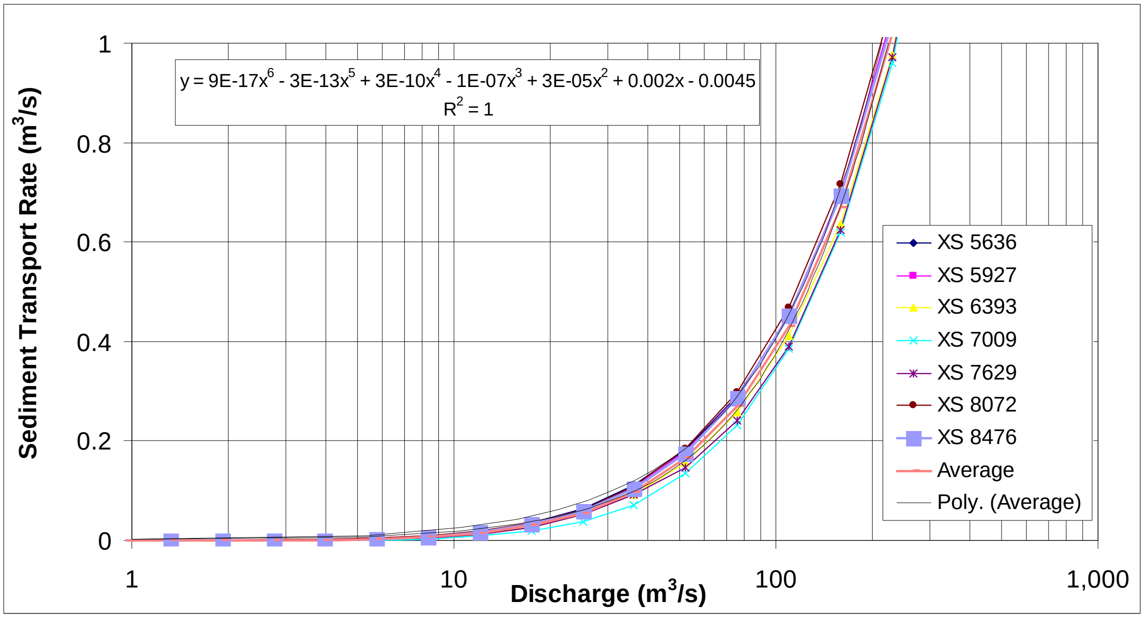

Figure G-13. Bedload transport capacity curves generated for Site 10-2 (San Francisquito Canyon, reach 3).

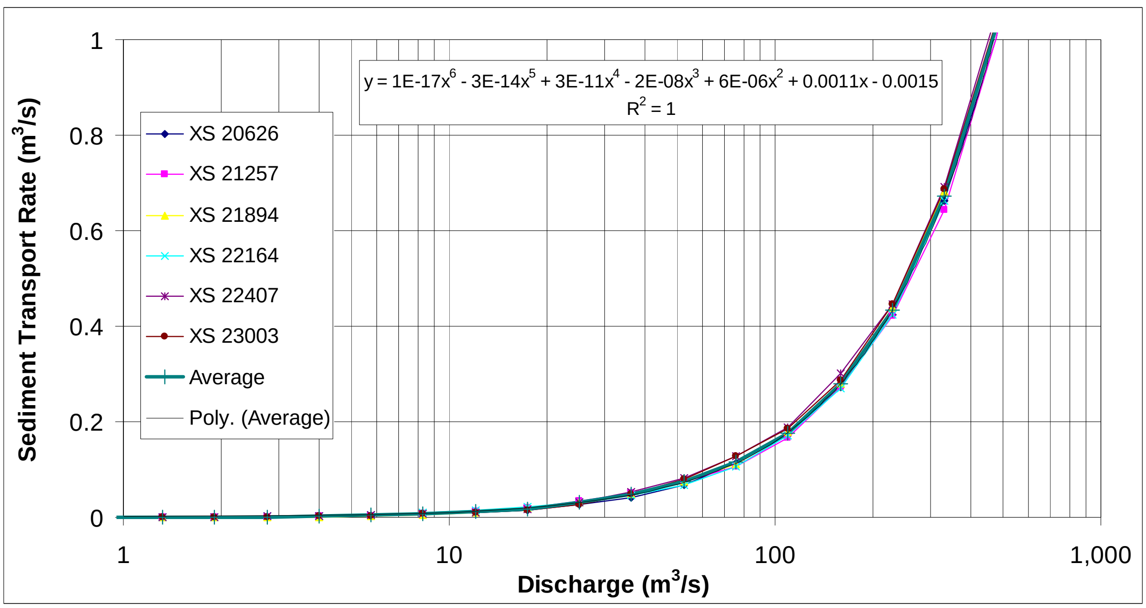

Figure G-14. Bedload transport capacity curves generated for Site 11-1 (Castaic Creek, reach 7).

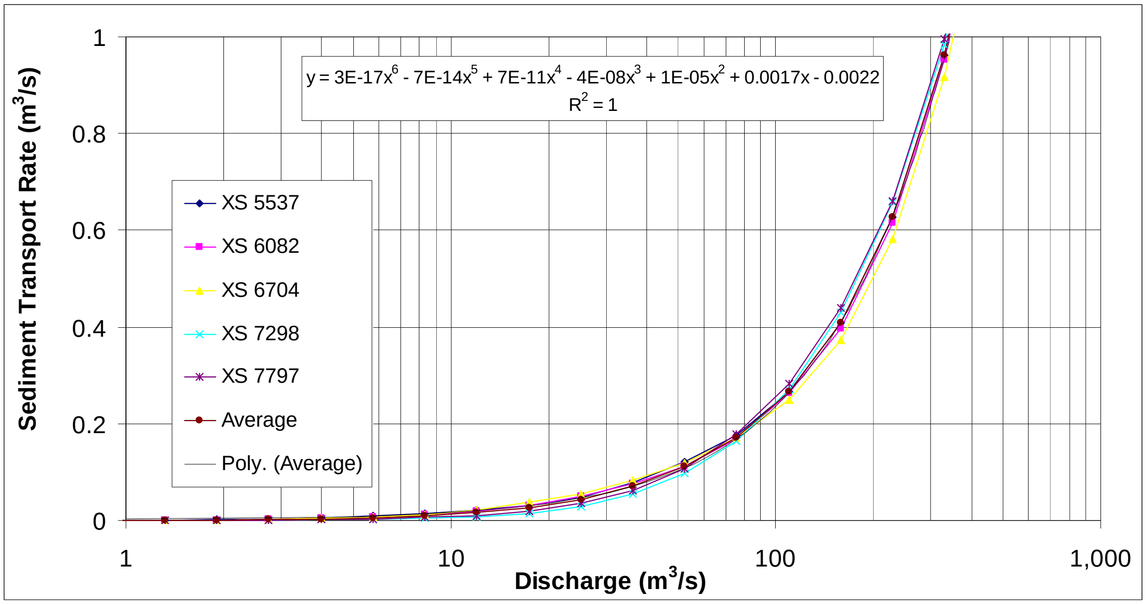

Figure G-15. Bedload transport capacity curves generated for Site 11-2 (Castaic Creek, reach 8).

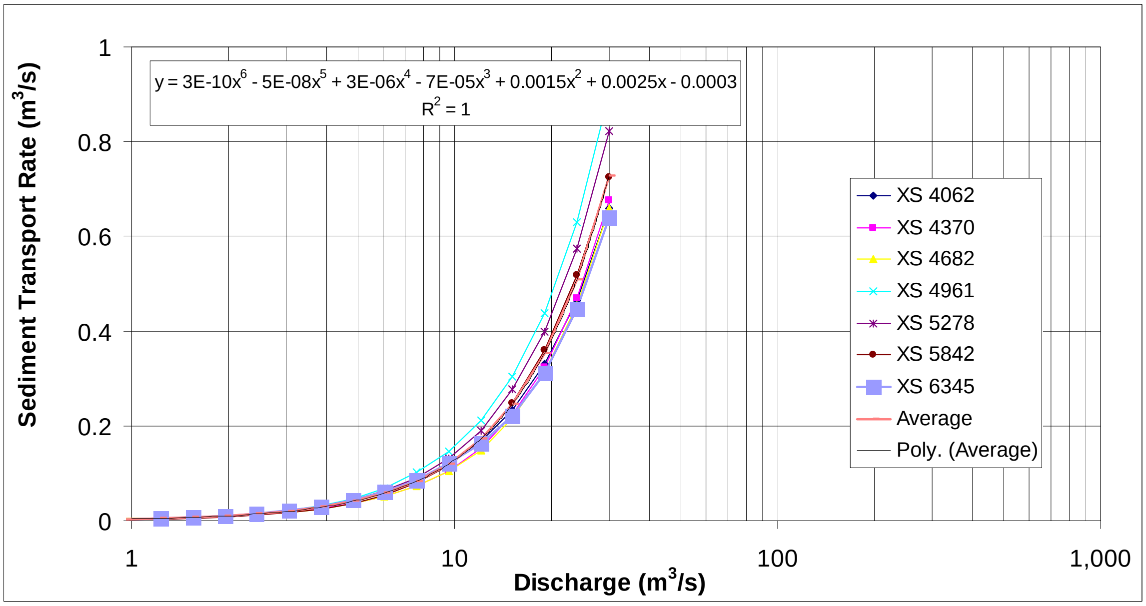

Figure G-16. Bedload transport capacity curves generated for Site 11-3 (San Martinez Chiquito Canyon, reach 3).

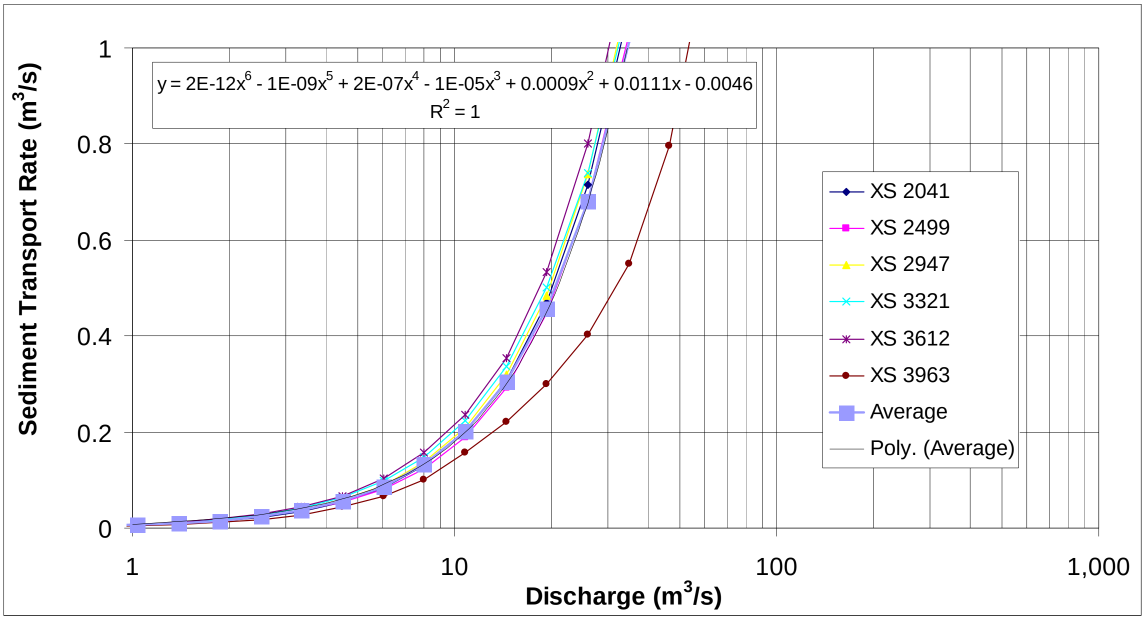

Figure G-17. Bedload transport capacity curves generated for Site 11-4 (San Martinez Grande Canyon, reach 4).

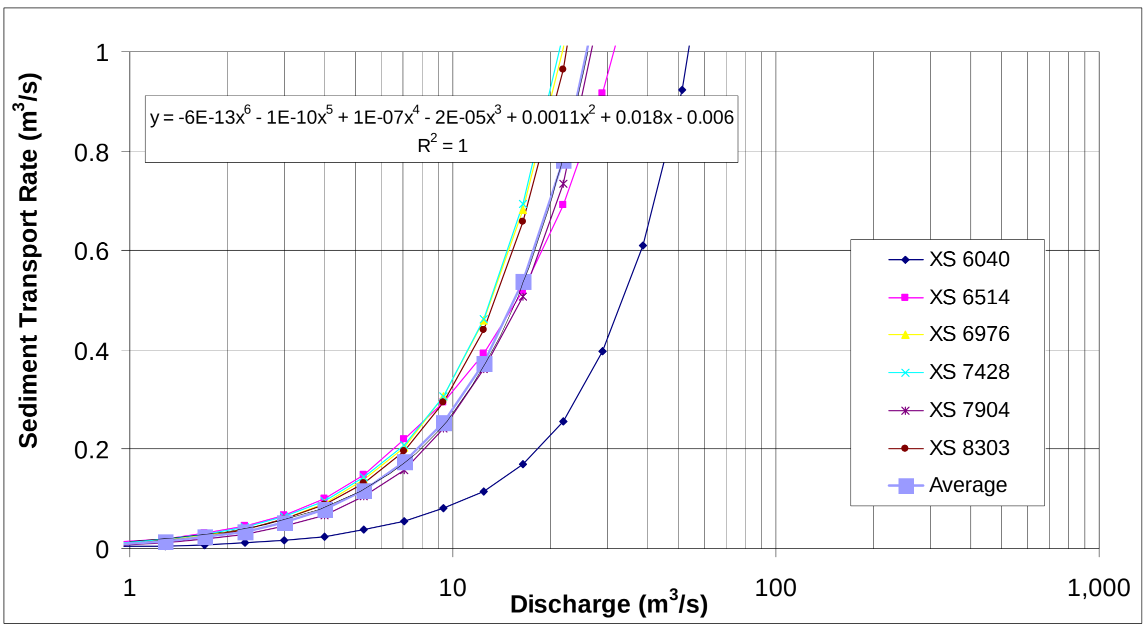

Figure G-18. Bedload transport capacity curves generated for Site 11-5 (Potrero Canyon, reach 6).

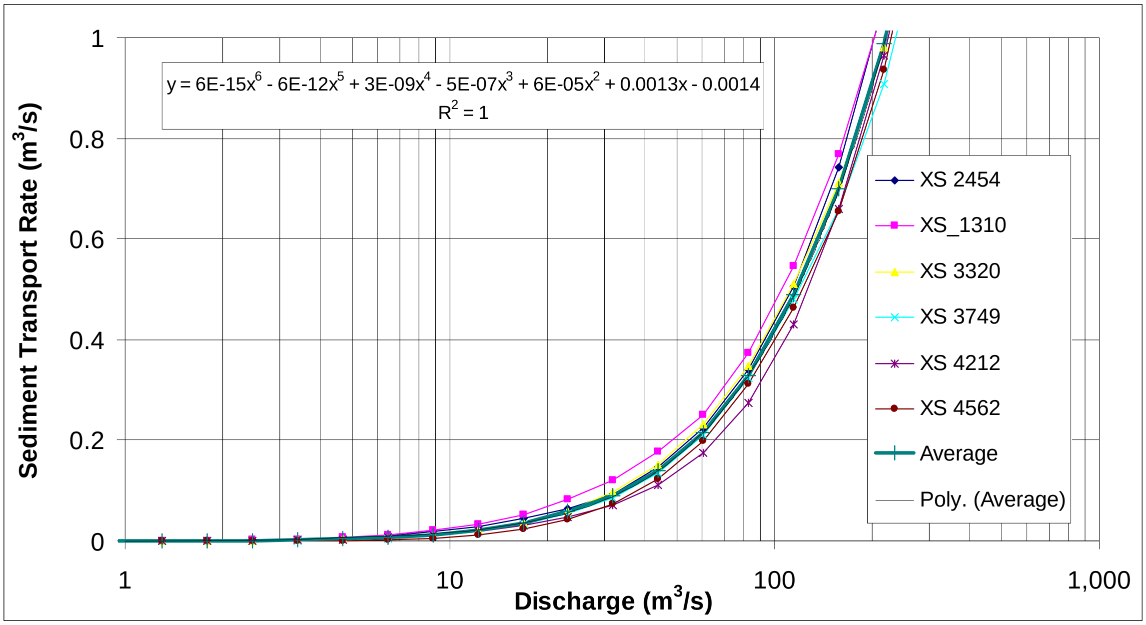

Figure G-19. Bedload transport capacity curves generated for Site 1-1 (USCR, reach M29).

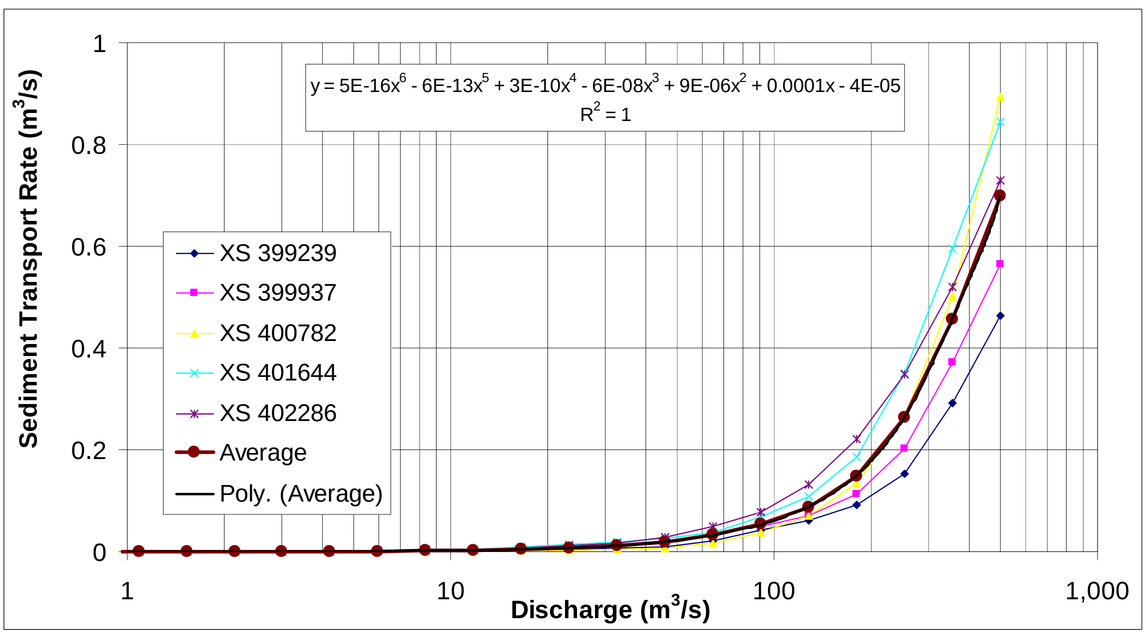

Figure G-20. Bedload transport capacity curves generated for Site 1-2 (USCR, reach M28).

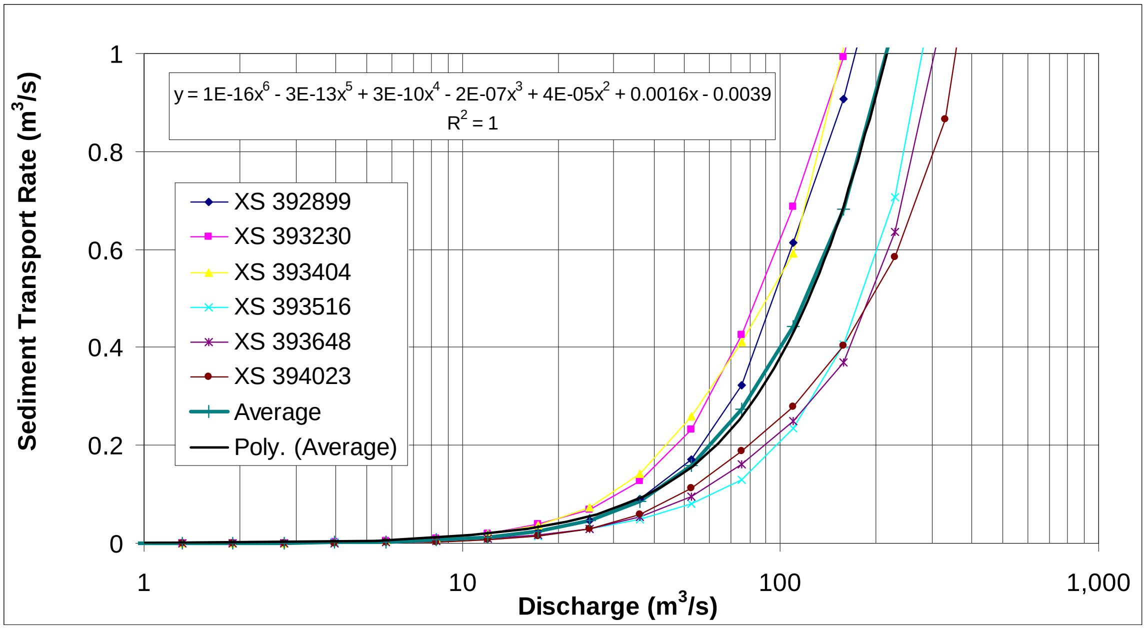

Figure G-21. Bedload transport capacity curves generated for Site 2-3 (USCR, reach M27).

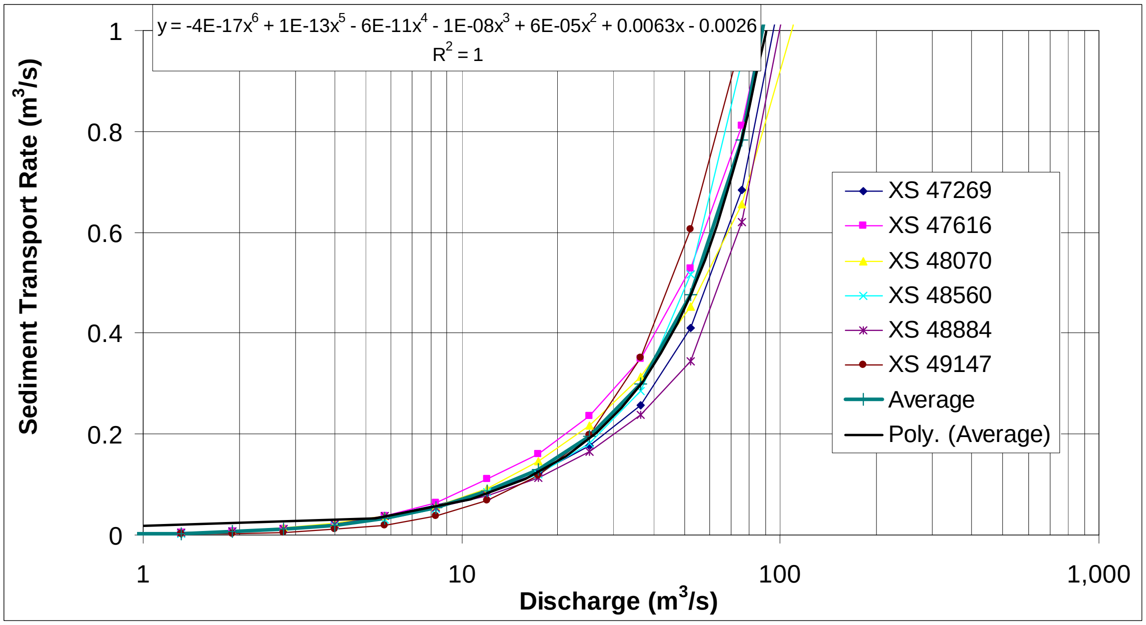

Figure G-22. Bedload transport capacity curves generated for Site 3-0 (USCR, reach M24).

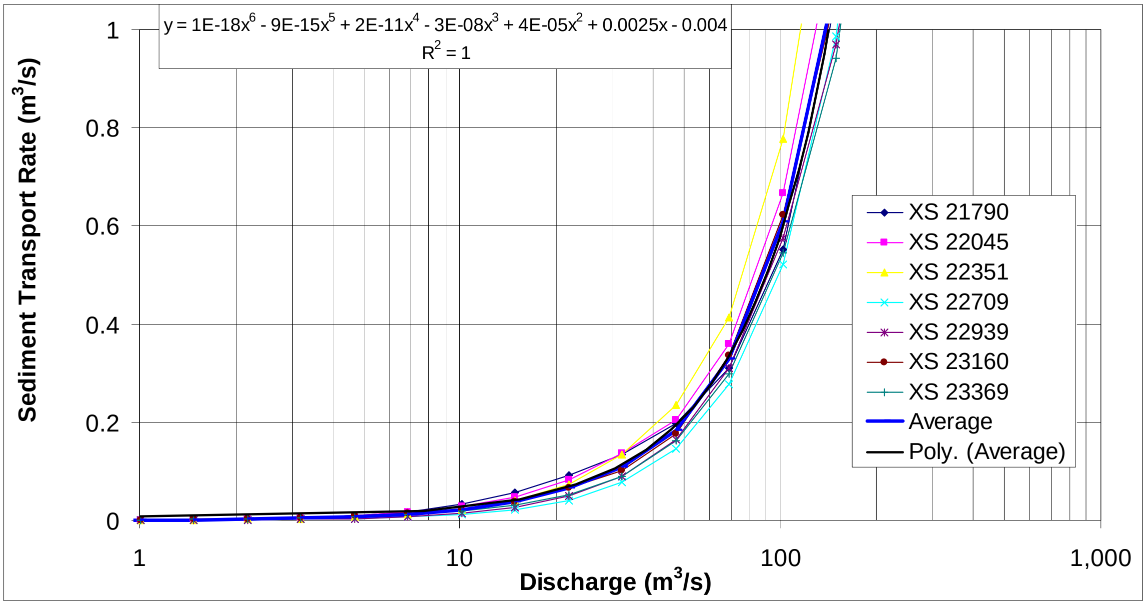

Figure G-23. Bedload transport capacity curves generated for Site 4-0 (USCR, reach M23).

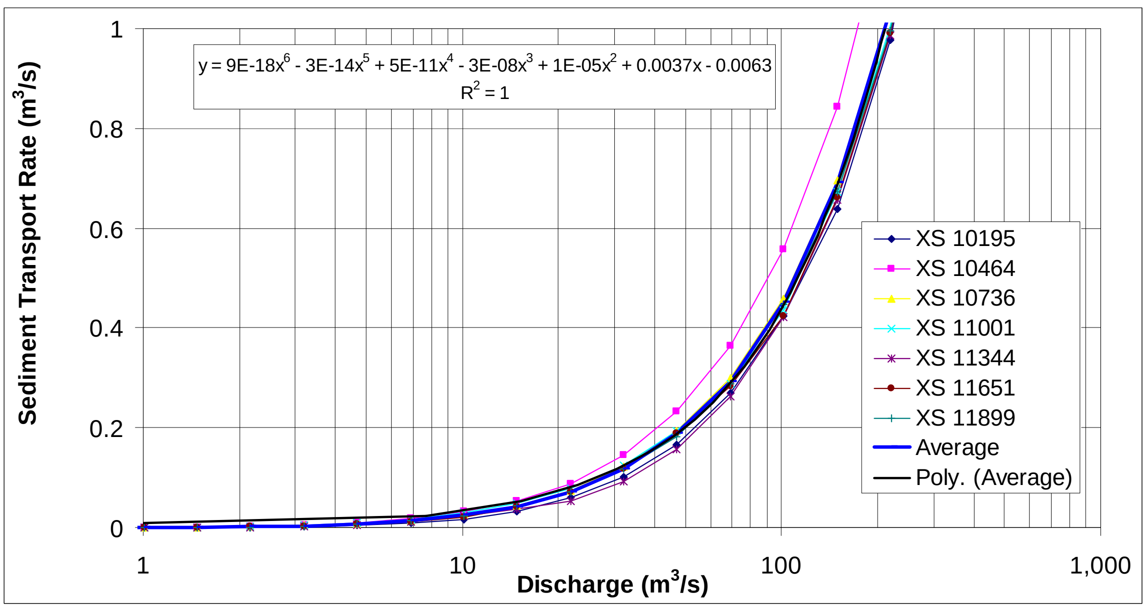

Figure G-24. Bedload transport capacity curves generated for Site 5-2 (USCR, reach M22).

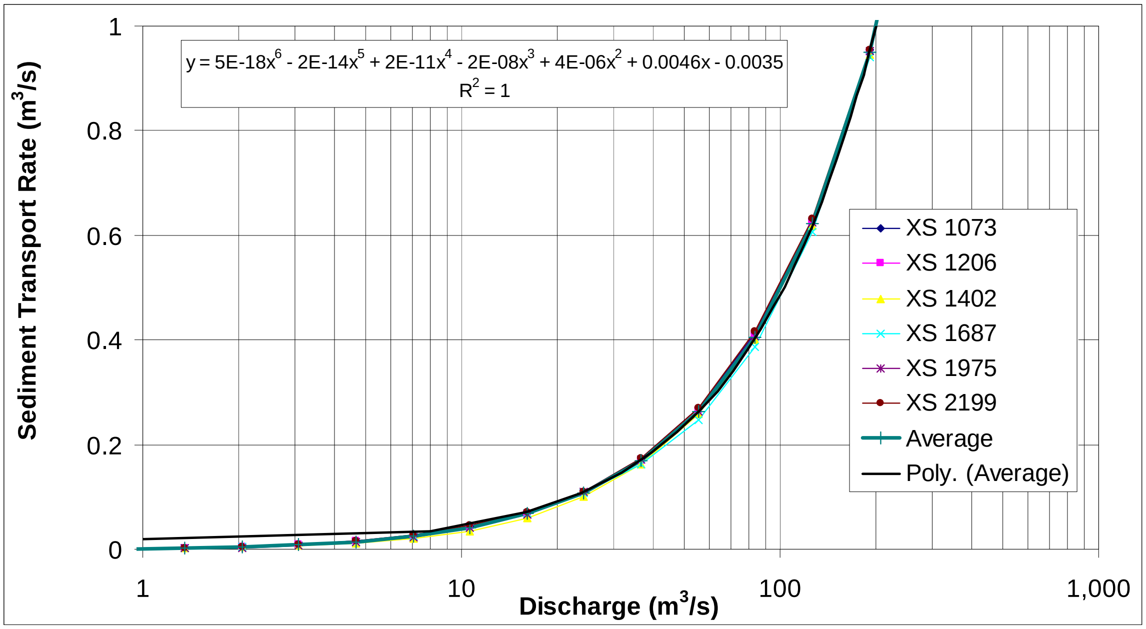

Figure G-25. Bedload transport capacity curves generated for Site 6-0 (USCR, reach M19).

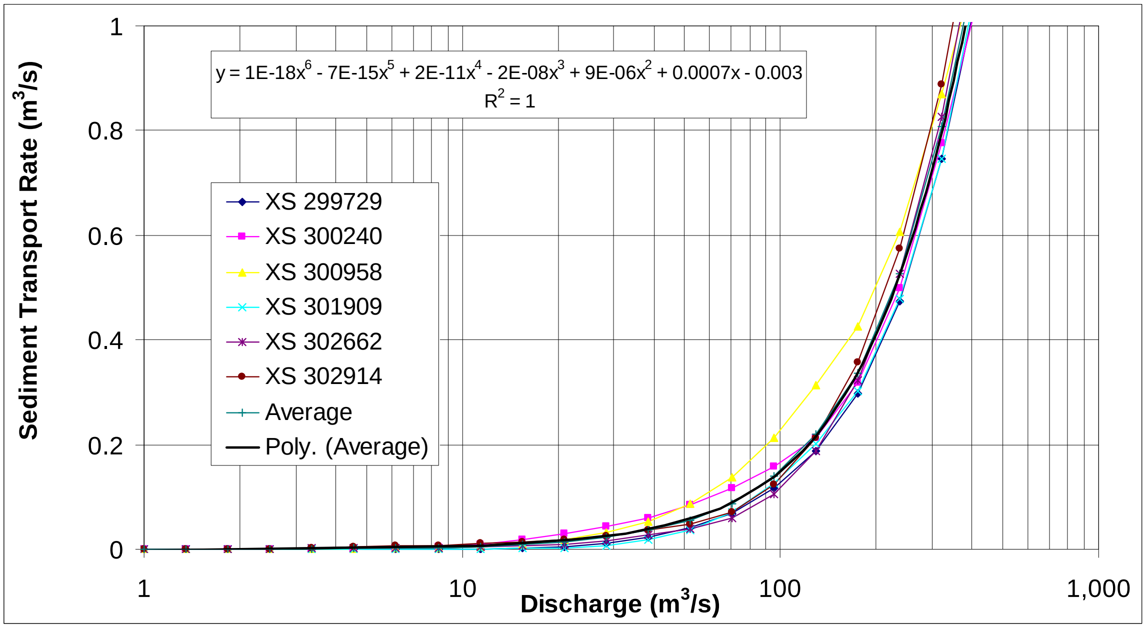

Figure G-26. Bedload transport capacity curves generated for Site 7-3 (USCR, reach M16).

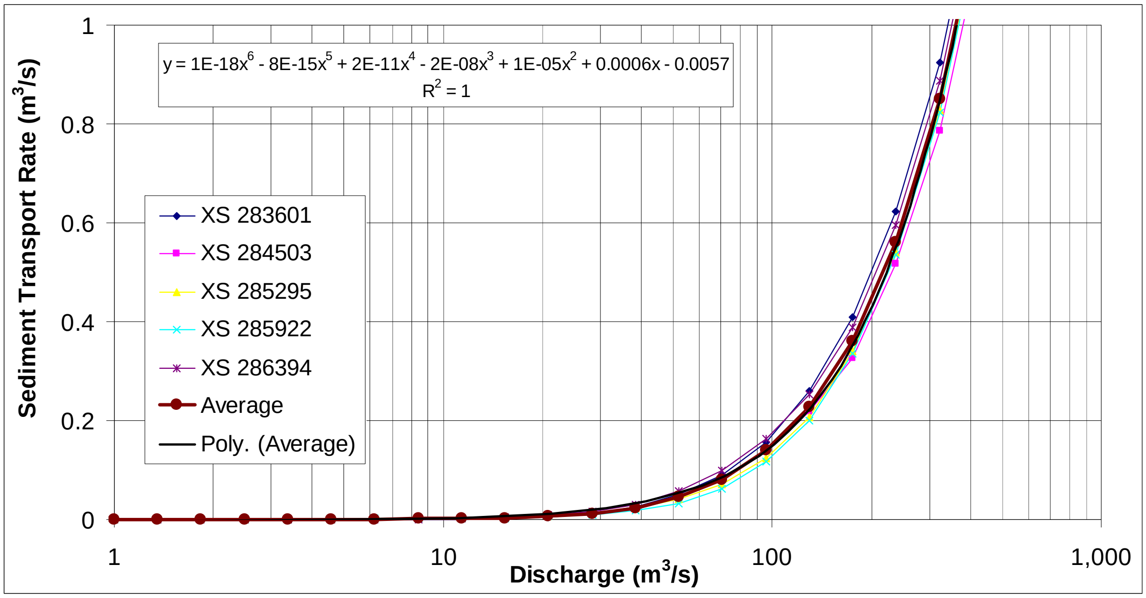

Figure G-27. Bedload transport capacity curves generated for Site 8-3 (USCR, reach M15).

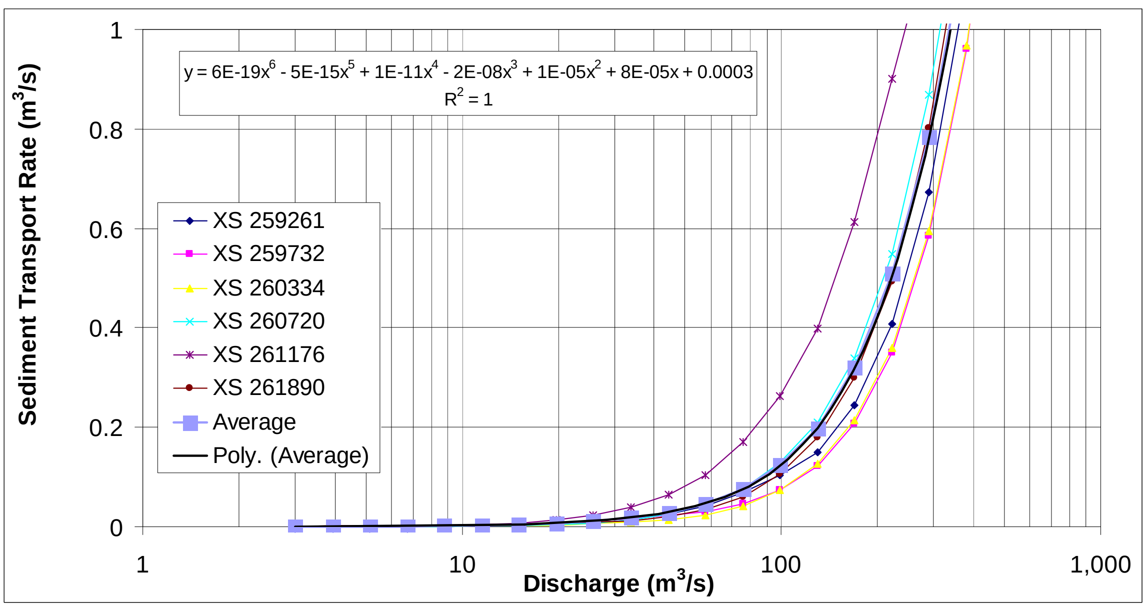

Figure G-28. Bedload transport capacity curves generated for Site 9-5 (USCR, reach M14).

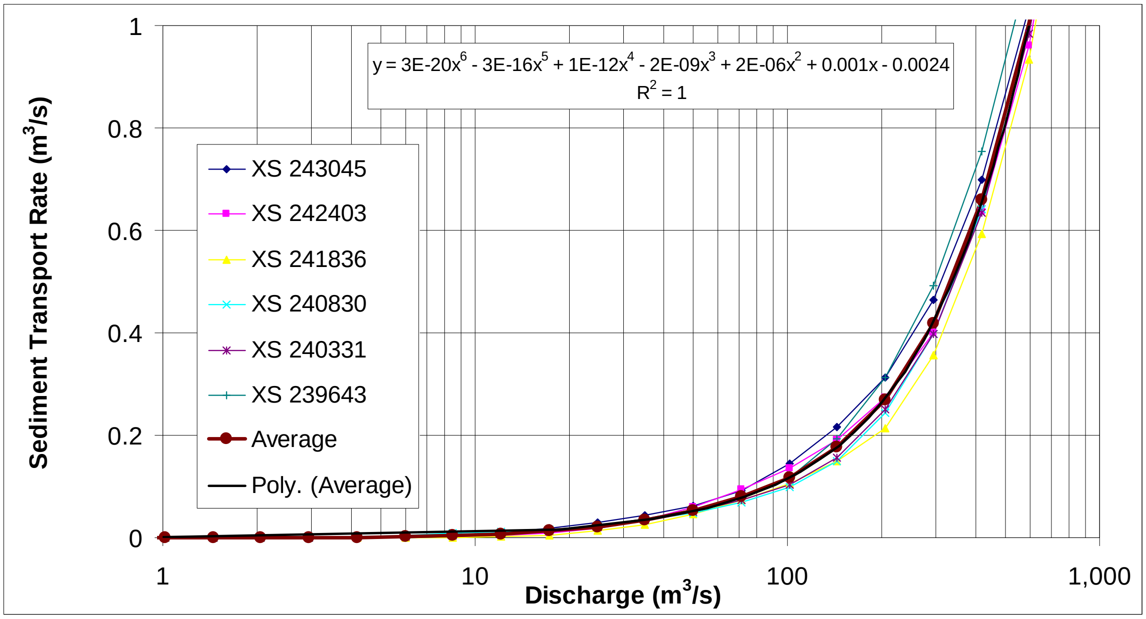

Figure G-29. Bedload transport capacity curves generated for Site 10-3 (USCR, reach M13).

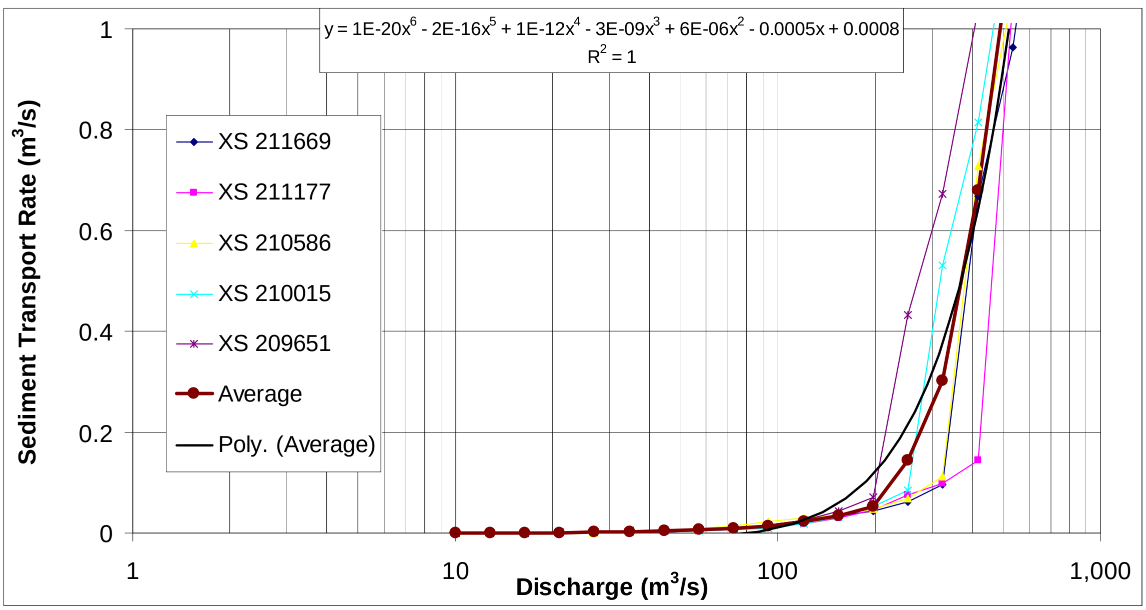

Figure G-30. Bedload transport capacity curves generated for Site 11-6 (USCR, reach M11B).

REFERENCES

Brownlie, W. 1982. Prediction of flow depth and sediment discharge in open channels. Doctoral thesis, California Institute of Technology, Pasedena, California.

Cui, Y., J. K. Wooster, J. G. Venditti, S. R. Dusterhoff, W. E. Dietrich, and L.S. Sklar. 2008 Simulating sediment transport in a flume with forced pool-riffle morphology: examinations of two one-dimensional numerical models. Journal of Hydraulic Engineering 134: 892–904.

Parker, G., P. C. Klingeman, and D. L. McLean. 1982. Bedload and size distribution in paved gravel bed streams. Journal of Hydraulics Division, ASCE. 108: 544–571.

Pitlick, J., Y. Cui, and P. Wilcock. 2009. Manual for computing bedload transport using BAGS (Bedload Assessment for Gravel-bed Streams) Software. Gen. Tech. Rep. RMRS-GTR-223. U.S. Department of Agriculture, Forest Service, Rocky Mountain Research Station, Fort Collins, Colorado.

Shvidchenko, A and G. Pender. 2008. Computer modeling of graded sediments in rivers. Water Management 161: 281–297.

Sutherland, D. G., M. Hansler-Ball, S. J. Hilton, T. E. and Lisle. 2002. Evolution of a landslide-induced sediment wave in the Navarro River, California. Geological Society of America Bulletin 114: 1036–1048.

Wilcock, P.R., J. Pitlick, and Y. Cui, Y. 2009. Sediment transport primer: estimating bed-material transport in gravel-bed rivers. Gen. Tech. Rep. RMRS-GTR-226. U.S. Department of Agriculture, Forest Service, Rocky Mountain Research Station, Fort Collins, Colorado.

Appendix H

Methods for Assessing Planform Channel Dynamics of the Upper Santa Clara River: 1928–2005

INTRODUCTION

Historical aerial photography was utilized in a geographic information system (GIS) to delineate areas of flood disturbance for 5 selected historical floods (1928, 1964, 1980/81, 1994, and 2005) along the entire length of the Upper Santa Clara River (USCR) within Los Angeles County, California. Many aspects of this analysis were modeled on similar work done by Graf (2000), Tiegs et al. (2005), and Tiegs and Pohl (2005).

PHOTO ACQUISITION

Imagery was acquired from a number of sources, including the Los Angeles Department of Public Works (LADPW), U.C. Santa Barbara, and the U.S. Geological Survey (USGS). Historically, much of the aerial photography flown over the lower Santa Clara River Valley was commissioned by Los Angeles County to document flood damage (including damage caused by the 1928 Saint Francis Dam disaster), and so was particularly well suited to analyzing the effects of major floods along the USCR. For this analysis, photo sets were chosen to represent the effects of 5 major floods of interest (see Table H-1 and Figure H-1). Although suitable aerial photography exists to document major floods in 1980, 1983, and 1998, funding was not available to process these photo sets. The extent of coverage each aerial photo set provided was not uniform, as some photography, particularly early sets, were flown only to assess effects on the major towns in the valley.

Aerial photography was acquired in one of two different formats, depending upon availability and age: non-georeferenced digital images or orthorectified imagery[1]. The non-georeferenced photography was typically scanned by the supplier at resolutions ranging from 600 dots per square inch (dpi) to 1200 dpi.

[1] Georeferencing refers to the process of “rubber-sheeting” or matching features in an image to a “real-world” coordinate system. Georeferencing typically only considers horizontal referencing, whereas an orthorectified image will be referenced using both horizontal and vertical components, resulting in a more accurate representation of earth’s surface.

Table H-1. Aerial photography sets used in the mainstem USCR channel processes analyses. [a, b]

Photography year(s)	Most recent significant flood date(s)	Estimated peak discharge (cfs) at County Line gauge [a]	Coverage extent [b]	Resolution/ scale	Photo source [c]	Use in analysis
1928	N/A [d]	N/A	SCR – county line to Acton	1:18,000	UCSB	Digitize active channel areas and facies
1964	2/11/62	9,100	SCR – county line to Soledad Canyon	1:1,200 (from matching topographic maps)	LADPW	Digitize active channel areas and facies
1980/1981	2/9/78 2/16/80	22,800 13,900	SCR – county line to	1:6,000	LADPW	Digitize active channel areas and facies
1994	1/12/92 2/18/83	12,300 10,700	Entire watershed	0.3 m (1-ft) resolution	USGS	Digitize active channel areas and facies
2005	1/10/05	32,000	Entire watershed	0.3 m (1-ft) resolution	LADPW	Digitize active channel areas and facies
2009	1/2/06 1/25/08	12,500 3,130	Entire watershed	1 m (3.3 ft) resolution	NAIP	Used this high-resolution aerial photograph set to guide active channel areas in other aerial photograph years

[a] County line flow gauge represented by USGS 11108500 (Santa Clara River at L.A.-Ventura Co. Line; 1952-1996) and USGS 11109000 (Santa Clara River near Piru; 1997-present).
[b] SCR = Santa Clara River mainstem.
[c] UCSB = U.C. Santa Barbara M.I.L. Davidson Library, LADPW = L.A. County Department of Public Works, USGS = U.S. Geological Survey, NAIP = National Agriculture Imagery Program.
[d] No flow records in USCR watershed prior to 1930. The 1928 aerial photos are potentially useful to the analysis by providing the oldest condition of the active channel area. Prior to 1928, two recorded high rainfall events occurred: 1914 precipitation at Santa Paula rain gauge of 28 inches was same as precipitation during known flood year of 1938; and 1917 precipitation at Santa Paula rain gauge of 23 inches.

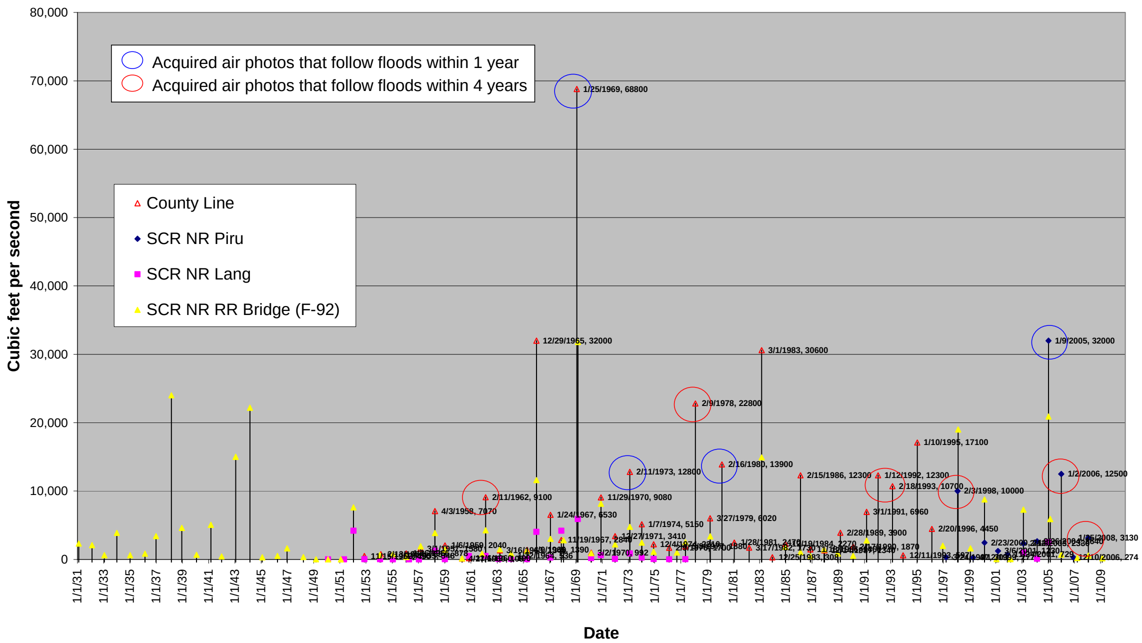

Figure H-1. Historical peak flows at stream gauges on USCR shown in comparison to known air photo imagery acquisition dates.

GEOREFERENCING

In order to extract and accurately compare river planform data from the acquired aerial photography, a common spatial context was necessary. The methodology described here is based mostly upon the methodology used to assess active channel areas along the lower Santa Clara River (Stillwater Sciences 2007), although some deviations to this methodology were needed due to inherent differences between data quality (e.g., photo resolution and density of reference points). Using a GIS, all imagery was georeferenced to a single spatial projection (UTM Zone 11N, NAD 83). Aerial photographs taken following significant flood events were obtained for several years: 1928, 1964, 1980/81, 1994, and 2005 (Table H-1; Figure H-1). The aerial photographs from 1994 and 2005 were orthophotographs and arrived GIS-ready. The remaining aerial photograph years were acquired as non-georeferenced digital images scanned by third parties from hard-copy photos. The ESRI ArcGIS georeferencing toolset was utilized to georeference the scanned hardcopy contact prints and digital imagery to the high-resolution 2009 orthophotography also acquired for this project, thus providing a highly accurate standard control point source for the entire photographic record. Control points were typically located using old buildings, bridges, intersections, and other features that appeared unchanged between photos sets. Georeferencing methods utilized at least 10 control points per photograph; thin plate splines were used to produce a smooth (continuous and differentiable) surface. Orthorectified imagery was acquired at pixel resolutions ranging from 0.3 to 1 m (1 to 3.3 ft) (see Table H-1). The 1964 image rectification methodology differed from the lower Santa Clara River rectification methodology: 1964 topographical maps associated with the photos included high-accuracy coordinate tick-marks, which were used to rectify the 1964 topographic maps, which were then, in turn, used to rectify the 1964 photos.

Spatial error in certain portions of photo sets due to imagery registration errors were occasionally significant, as high as 35 m. These errors were typically associated with image distortion at the outer edges of older photos, due to sub-standard aerial photography techniques, standard lens distortion, or oblique camera angles. However, spatial errors between most photo sets generally ranged between 3 and 15 m, and sometimes as low as 1 m. For the rectification of the 1964 images, errors generally ranged between 1 and 8 m, with errors for the topographic maps generally ranged between 1 and 4 m. Additionally, some photographs within the 1980/1981 photo set contained visual artifacts from scanning, which consequently offered lower image quality.

FLOOD SCOUR DIGITIZING

Each set of spatially referenced photography (each representing a particular flood) was used in a GIS to interpret two levels of flood-caused disturbance in the channel and floodplain areas. In addition, areas of low-disturbance or areas apparently retaining natural riparian vegetation coverage[2] after the flood were also mapped. For purposes of photo interpretation, these areas were defined as follows:

High disturbance: These areas are characterized by distinct channel and floodplain areas severely disturbed by flow (i.e. scoured to bare substrate), typically with 10% or less apparent remaining riparian vegetative cover. This category may include agricultural or developed lands with a high level of apparent disturbance by flood flows, thus identification of this type is not always based upon vegetative cover, sometimes relying on patterns of obvious scour. Additionally, certain channel-adjacent areas surrounded by scour were classified as high disturbance, despite having high coverage of herbaceous or nascent vegetation; this characterization was assigned when vegetation appeared to have grown post-flood and prior to the aerial photograph date.

Medium disturbance: This class is characterized by distinct areas of low to moderate apparent disturbance by flow, typically defined as areas with more than 10% but less than 80% apparent riparian vegetative cover. This type includes agricultural or developed lands with low to moderate apparent disturbance by flood flows, thus identification of this type is not always based upon vegetative cover, as with the high disturbance class.

Low disturbance (riparian vegetation): These areas were characterized by distinct zones of apparently natural riparian vegetation with little to no apparent disturbance by flood, typically containing more than 80% riparian vegetation. Areas in this class may have been inundated by floodwaters, but did not show significant signs of scouring or other disturbance that removed vegetation.

In addition to flood disturbance level, all polygons were classified as being either within or outside of the active channel. Polygons within the active channel were those that appeared to have been directly affected by the river during the prior flood event and/or subsequent flows (i.e., most areas of medium to high disturbance). Areas of riparian or non-riparian vegetation with no apparent disturbance were excluded, unless bounded by the active channel on three or more sides. Particular areas of medium to high disturbance were nonetheless excluded from the active

[2] In the context of the floodplain vegetation communities of the USCR, “riparian vegetation” may include types more typical of upland communities, such as coastal sage scrub, or non-native plant species which in some cases includes non-native species. Agricultural lands within the river's floodplain/terraces were also included as Low Disturbance, but were excluded from the active channel area.

channel when these areas appeared to have been affected by flows from tributaries at their confluence with the river, or by runoff from surrounding land, rather than the river itself.

To record these areas, polygons were delineated around features within each flood year photo set using heads-up digitizing at a scale of 1:4500 in the GIS; in certain upstream canyon areas, shadow or dense vegetation made it necessary to sometimes digitize at scales of 1:2500 or, in cases of extremely low visibility, 1:1500. For the 2005 dataset, orthophotographs and associated 2005 LiDAR data were used to delineate the active channel and classify areas of disturbance. While methods for digitizing generally followed those described by Tiegs and Pohl (2005), the data generated in this study were not converted to a raster format for analysis, but rather kept as polygons in an ESRI shapefile format (.shp), as originally digitized. All subsequent analyses were conducted using the polygon representation, which allowed for a finer scale of resolution in analysis output.

In addition to spatial error related to georeferencing, polygon delineation likely resulted in unknown spatial errors due to difficulties in interpreting features of interest. These types of error are most likely to occur with older images (e.g., 1928, 1964) used in this study, as well as the low quality images from the 1980/1981 set. Older photographic film typically had a coarser grain than more modern films resulting in lower feature resolution once the image was scanned and georeferenced, making interpretation of floodplain features more difficult. The grayscale color spectrum of older imagery (1928, 1964, 1980/81, and 1994) made interpretation of residual riparian vegetation more difficult in certain cases as well.

QUALITY CONTROL

Each flood year polygon data set was checked for spatial and interpretive accuracy by a GIS analyst that was not associated with the digitization process for that particular year. This process ensured that the data sets were consistent and accurate between and across years. Assessments of spatial error were conducted by a GIS analyst not directly involved in georeferencing or digitization processes.

ANALYSES

The planform data digitized from the aerial photography sets were used to conduct a number of spatial analyses to support understanding of fluvial dynamics in the USCR. These analyses included calculation of historical flood disturbance probability, “last flood” spatial analyses, and average reach width calculations for each historical flood.

Locational Probability Model

The methods and nomenclature discussed below have been modeled on those of Graf (2000) and Tiegs et al. (2005). For this analysis, we define a locational probability model as a graphical representation of the historical probability that any particular area within the floodplain and channel of the USCR was scoured (i.e. the “high disturbance” and “medium disturbance” categories described above) by a major flood. As discussed above, aerial photographs chosen for use in this study were taken after major floods (see Table H-1 and Figure H-1) and thus represent the post-flood channel configuration for a particular flood.

Because the USCR is a flood event dominated system (see Chapter 4 of the main report) and each set of photography was taken shortly after a major flood event, it can be assumed that each photo set represents the dominant planform configuration of the channel until the next large flood documented by aerial photography. This approach differs from that of Graf (2000), Tiegs et al. (2005), and Tiegs and Pohl (2005), who assume that each photo set is representative of general channel conditions for a period of time from one photo set to the previous photo set. Thus, their approach does not appear to explicitly consider whether the photo is representative of the effects of particular floods, but rather describes general channel conditions over time.

There are numerous caveats to our assumption discussed above, the most important being that smaller floods occur between the photograph sets and likely result in reworking of the channel; however, it remains that major changes to the channel and floodplain of the USCR are accomplished by large floods. For this analysis, another significant caveat is the lack of aerial photographic coverage for two major floods in 1938 and 1969; although partial aerial photography exists to document these floods, funding limited the number of aerial photograph sets that could be processed.

To derive a disturbance probability model, the study area was divided into 11 reaches which were distinguished primarily by differences in stream power (see Chapter 4 of the main report for further discussion). A separate disturbance probability model was calculated for each of 18 reaches. In order to build the disturbance probability model, the photo sets needed to be weighted based on the amount of time each represented in the overall study period[3] (1928-2010), on a reach basis. The weighting values were calculated for each flood year and reach using the following equation:

$$\text{Weighting value } (W_n) = \frac{\text{years represented by given photograph } (t_n)}{\text{total number of years in photographic record } (m)}$$

The value of t_n is the number of years between the documented flood of interest and the next photo documented flood. The value of m is the total number of years documented by aerial photography for a particular reach, from earliest photography set to most recent. Working through the equation for each flood year and reach gave the results displayed in Tables F-2 and F-3 below.

[3] Photography was acquired for selected floods between 1928 and 2005, thus this period represents the photographic record. For the purposes of calculating probability of disturbance, the "study period" was 1928–2010, since no major floods had occurred between 2005 and the year this study was completed, 2010.

Table H-2. Years represented by individual flood photography and total number of years in the photographic record, by reach.

Reach	Number of years represented by given flood photography (t_n)					Number of years in photographic record (m)
	1928	1964	1980/81	1994	2005	
M1	36	16/17	14/13	11	4	81
M2	36	16/17	14/13	11	4	81
M3	36	16/17	14/13	11	4	81
M4	36	16/17	14/13	11	4	81
M5	36	16/17	14/13	11	4	81
M6	36	16/17	14/13	11	4	81
M7	36	16/17	14/13	11	4	81
M8	36	16/17	14/13	11	4	81
M9	36	16/17	14/13	11	4	81
M10	36	16/17	14/13	11	4	81
M11	36	16/17	14/13	11	4	81
M12	36	16/17	14/13	11	4	81
M13	36	16/17	14/13	11	4	81
M14	36	16/17	14/13	11	4	81
M15	36	16/17	14/13	11	4	81
M16	36	16/17	14/13	11	4	81
M17	36	16/17	14/13	11	4	81
M18	36	16/17	14/13	11	4	81
M19	36	16/17	14/13	11	4	81

Table H-3. Weighting values for individual floods photography and reaches.

Reach	Weighting value (W_n)				
	1928	1964	1980/81	1994	2005
M1	0.44	0.20/0.21	0.17/0.16	0.14	0.05
M2	0.44	0.20/0.21	0.17/0.16	0.14	0.05
M3	0.44	0.20/0.21	0.17/0.16	0.14	0.05
M4	0.44	0.20/0.21	0.17/0.16	0.14	0.05
M5	0.44	0.20/0.21	0.17/0.16	0.14	0.05
M6	0.44	0.20/0.21	0.17/0.16	0.14	0.05
M7	0.44	0.20/0.21	0.17/0.16	0.14	0.05
M8	0.44	0.20/0.21	0.17/0.16	0.14	0.05
M9	0.44	0.20/0.21	0.17/0.16	0.14	0.05
M10	0.44	0.20/0.21	0.17/0.16	0.14	0.05
M11	0.44	0.20/0.21	0.17/0.16	0.14	0.05
M12	0.44	0.20/0.21	0.17/0.16	0.14	0.05
M13	0.44	0.20/0.21	0.17/0.16	0.14	0.05

Reach	Weighting value (W_n)				
	1928	1964	1980/81	1994	2005
M14	0.44	0.20/0.21	0.17/0.16	0.14	0.05
M15	0.44	0.20/0.21	0.17/0.16	0.14	0.05
M16	0.44	0.20/0.21	0.17/0.16	0.14	0.05
M17	0.44	0.20/0.21	0.17/0.16	0.14	0.05
M18	0.44	0.20/0.21	0.17/0.16	0.14	0.05
M19	0.44	0.20/0.21	0.17/0.16	0.14	0.05

Weighting values were assigned to flood year and reach polygon layers in the GIS. All of the flood year layers were then combined in the GIS (using the "union" function), resulting in numerous smaller polygons, all of which retained their original assigned probability for each year and reach. For each individual polygon, all the years weighting values were summed, resulting in a probability of scour for each (Table H-4). The probability field was then used to illustrate locational probability in a map (see Figures 4-23 a–i in the main report) for each reach.

Table H-4. Example of GIS data table with summed weighting values or probability of scour ("SumProb") for each polygon.

Polygon	1938	1969	1978	1992	1995	2005	Sum prob	Shape area
1	0.45	0	0	0	0	0	0.45	1459947.254
2	0	0.13	0	0	0	0	0.13	1710181.258
3	0	0.13	0	0	0	0	0.13	825.8837909
4	0	0.13	0	0	0	0	0.13	321.74415
5	0.45	0.13	0	0	0	0	0.58	1037.485881
6	0	0.13	0	0	0	0	0.13	1777.786451
7	0	0.13	0.2	0	0	0	0.53	181.1416506
8	0	0.13	0.2	0	0	0	0.53	113.8613641
9	0	0.13	0.2	0	0	0	0.53	5636.241047
10	0	0	0	0.04	0	0	0.04	46170.7421
11	0	0	0	0.04	0	0	0.04	435.8034547
12	0	0	0	0.04	0	0	0.04	2020.878413
13	0	0	0	0	0.14	0	0.14	327800.4409
14	0	0	0	0	0.14	0	0.14	40539.56361
15	0	0	0	0	0	0.03	0.03	222838.8706
16	0	0	0	0	0	0.03	0.03	66320.23549

Width of Active Channel Bed in Successive Floods

Knowledge of the last known flood disturbance for any particular area of the floodplain is critical to understanding the age of geomorphic surfaces and thus the approximate age of riparian vegetation growing there. The flood scour layers were manipulated in the GIS to derive a map of "last flood" scour areas for the entire study reach. All flood year layers were combined in a GIS using the "union" command, resulting in numerous smaller polygons each retaining information on the years in which the particular polygon was inundated. Using a "max number" algorithm, the most recent year was chosen from the GIS data and copied to a new field; the value in the new field (the "last flood" field) now contained the date of the most recent scour event for any particular polygon. The value of the "last flood" field was then used to produce a map of last flood scour for the entire study reach (see Figures 4-24 a–i in the main report).

Reach Width Analysis

In order to help inform an understanding of the behavior of the USCR, a geomorphological analysis was undertaken using the "active channel width" (i.e. the scoured area or "high disturbance" and "medium disturbance" classifications) of each documented flood (see Chapter 4). In order to facilitate the analysis, reach average widths were calculated for each documented flood based upon the area of scour documented for each flood (as calculated in the GIS). A channel centerline was established as the basis for reach length, then width was derived from the simple relationship between length, width and area:

Width = Area/Length

Reach-based areas for each documented flood were exported from the GIS and imported to Microsoft Excel, where the calculations were completed using the Pivot Tables function.

REFERENCES

Graf, W. L. 2000. Locational probability for a dammed, urbanizing stream: Salt River, Arizona, USA. Environmental Management 25: 321–335.

Simons, Li & Associates. 1983. Hydraulic, erosion and sedimentation study of the Santa Clara River Ventura County, California. Prepared for Ventura County Flood Control District, Ventura, California.

Tiegs, S. D., J. F. O'Leary, M. M. Pohl, and C. L. Munill. 2005. Flood disturbance and riparian diversity on the Colorado River Delta. Biodiversity and Conservation 14: 1175–1194.

Tiegs, S. D. and M. Pohl. 2005. Planform channel dynamics of the lower Colorado River: 1976-2000. Geomorphology 69: 14–27.